Aplicación de la Tecnología de Adhesivos en Estructuras Multimaterial: Empleo de Adhesivos Tenaces

Pedro Gálvez Villarino

Tesis depositada en cumplimiento parcial de los requisitos para el grado de Doctor en

Ciencia e Ingeniería de Materiales

Universidad Carlos III de Madrid

Director/es:

Juana Abenojar Buendía
Miguel Ángel Martínez Casanova

Tutor/a:

Miguel Ángel Martínez Casanova

Enero 2020

A todas esas personas que algún día creyeron en mí

AGRADECIMIENTOS

No será fácil, pero merecerá la pena…

Recuerdo haber escuchado esta frase al tiempo de empezar esta aventura, y es verdad que no ha sido fácil, pero sin duda ha merecido la pena.

No sería justo empezar estos agradecimientos sin mencionar a las dos personas que hicieron posible que hoy haya escrito estas líneas, mis padres en la ciencia, Juani y Miguel Ángel. Grandes jefes y mejores amigos. ¡Gracias!.

Como no continuar con Sara, después de tanta ayuda y esfuerzo, mi hermana en la ciencia. Esta tesis también debería llevar tu nombre. María, gran apoyo, amiga en mayúsculas, conciertos para superar los malos momentos. Morena, de esas personas que a veces tienes la suerte de encontrar, y que pese a la distancia sabes que nada cambiará. Belén, hermana mayor, siempre con una sonrisa. El mundo sería un lugar mucho mejor con más gente como vosotras.

Y el despacho 1.1A11D. Gracias Susana y Mariola por todos vuestros consejos, y por tantas conversaciones de despacho. Nieves, siempre dispuesta a ayudar desinteresadamente cuando fuera necesario. Andrea, un espejo en el que mirarse, al final las cosas sí que salieron bien.

Guille, amigo y compañero de laboratorio. Eric, tanto tiempo juntos. Alberto, dispuesto siempre a ayudar. Andrea PH, Segundo, Carmen, Teresa, Mariu, Fran, Asun…

Pichi, amigo y apoyo.

A mi familia, por convertirme en la persona que soy. A ti mamá, por comprenderme mejor que nadie. A ti Angelita, debería llamarte mamá en vez de abuela. A ti papá, por animarme a empezar esta aventura y cuidar de mí siendo el mejor padre posible. A ti Iván, qué suerte tenerte como primo. A ti Raúl, siempre pendiente de mí, siempre orgulloso de ti.

Delia, que llegaste como un soplo de aire fresco para poner todo del revés, amiga y compañera de vida.

A todas aquellas personas que aunque no estén aquí citadas, sin duda algo dejaron en mí. Y por último a ti, abuela, desde arriba siempre cuidando de mí.

Pedro

CONTENIDOS PUBLICADOS Y PRESENTADOS

Esta tesis se ha realizado por compendio de trabajos previamente publicados en revistas del JCR, cuyas referencias bibliográficas se citan a continuación:

Galvez P, Quesada A, Martinez MA, Abenojar J, Boada MJL, Diaz V. Study of the behaviour of adhesive joints of steel with CFRP for its application in bus Structures. Composites Part B 2017; 129: 41-6. DOI: doi.org/10.1016/j.compositesb.2017.07.018.

Galvez P, Abenojar J, Martinez MA. Durability of steel-CFRP structural adhesive joints with polyurethane adhesives. Composites Part B 2019; 165: 1-9. DOI: doi.org/10.1016/j.compositesb.2018.11.097.

Galvez P, Abenojar J, Martinez MA. Effect of moisture and temperature on the thermal and mechanical properties of a ductile epoxy adhesive for use in steel structures reinforced with CFRP. Composites Part B 2019; 176: 107194. DOI: doi.org/10.1016/j.compositesb.2019.107194.

Galvez P, Noda N, Takaki R, Sano Y, Miyazaki T, Abenojar J, Martinez MA. Intensity of singular stress field (ISSF) variation as a function of the Young's modulus in single lap adhesive joints. International Journal of Adhesion and Adhesives 2019; 95: 102418. DOI: doi.org/10.1016/j.ijadhadh.2019.102418.

También se ha incluido el siguiente trabajo publicado en una revista no perteneciente al JCR:

Galvez P, Carbas RJC, Campilho RDSG, Abenojar J, Martinez MA, da Silva LFM. Fracture toughness in Mode I (G_{IC}) for ductile adhesives. Journal of Physics: Conference Series 2017; 843: 012008. DOI: 10.1088/1742-6596/843/1/012008.

Así mismo se han incluido los siguientes trabajos presentados para su publicación en revistas del JCR, y que actualmente se encuentran en proceso de revisión:

Galvez P, López de Armentia S, Abenojar J, Martinez MA. Effect of moisture and temperature on thermal and mechanical properties of structural polyurethane adhesive joints. Composite Structures, acceptance pending.

Quesada A, Galvez P, Boada MJL, Martinez MA, Garcia-Pozuelo D, Abenojar J. Designing, manufacturing and testing of a new 3D steel-CFRP node bonded by adhesives for its use in bus Structures. Journal of Materials Science & Technology, acceptance pending.

OTROS MÉRITOS DE INVESTIGACIÓN

Publicaciones científicas:

Noda N, Takaki R, Shen Y, Inoue A, Sano Y, Akagi D, Takase Y, Galvez P. Strain rate concentration factor for flat notched specimen to predict impact strength for polymeric materials. Mechanics of Materials 2019; 131: 141-57. DOI: doi.org/10.1016/j.mechmat.2019.01.011.

Abenojar J, López de Armentia S, Galvez P, Martínez MA. Tribological and Mechanical Properties of Polyester Based Composites with SiC Particles. In: Wahab MA, editor. Proceedings of the 7th International Conference on Fracture Fatigue and Wear. FFW 2018. Lecture Notes in Mechanical Engineering. Springer, Singapore; 2019.

Contribuciones a congresos nacionales e internacionales:

Congreso Nacional de Materiales 2016 (Gijón).

Congreso Internacional de Adhesivos 2016 (Madrid).

AB2017 (Porto).

FFW2017 (Porto).

EAEC 2017 (Leganés).

Congreso Internacional de Adhesivos 2017 (Barcelona).

WCARP2018 (San Diego).

FFW2018 (Gante).

Congreso Internacional de Adhesivos 2018 (Madrid).

JSMS2018 (Kumamoto).

MatComp2019 (Vigo).

AB2019 (Porto).

ÍNDICE

RESUMEN

En esta Tesis Doctoral se ha estudiado la problemática actual existente en estructuras de acero utilizadas tanto en el ámbito del transporte de pasajeros como en aplicaciones de ingeniería civil. Este tipo de estructuras están sometidas durante su vida útil a un proceso de fatiga mecánica que desencadenará en fallos indeseados y problemas de seguridad.

Los métodos de fabricación actuales, basados principalmente en la soldadura, hacen que las estructuras sean muy rígidas, y por tanto que su comportamiento frente a la fatiga mecánica no sea el adecuado. Se propone una solución basada en el uso de adhesivos estructurales elásticos y materiales compuestos de matriz polimérica reforzados con fibra de carbono (CFRP). El problema ha sido resuelto en superestructuras de autobús mediante el diseño y fabricación de un nuevo nodo de CFRP unido mediante un adhesivo de poliuretano elástico a la estructura. Por otro lado, en estructuras de ingeniería civil se propone el uso de piezas de CFRP unidas a la estructura mediante un adhesivo epoxi elástico.

La resistencia de las nuevas uniones frente a los esfuerzos a los que estará sometida ha sido garantizada de forma experimental y por medio de análisis de elementos finitos, estudiando las singularidades mediante el "Intensity of Singular Stress Field" (ISSF). Los resultados obtenidos son excelentes, mostrando las nuevas uniones valores de resistencia ampliamente superiores a las solicitaciones requeridas. Del mismo modo, se ha dotado al conjunto de la elasticidad suficiente, mejorando el comportamiento a fatiga de las estructuras estudiadas.

ABSTRACT

In this Doctoral Thesis the current problems in steel structures used both in the fields of passenger transport and civil engineering applications are studied. These types of structures are subjected to mechanical fatigue during their useful life that will lead to unwanted failures and safety problems.

Current manufacturing methods, based mainly on welding, make the structures very rigid, and therefore their behavior against mechanical fatigue is not adequate. A solution based on the use of ductile structural adhesives and carbon fiber reinforced polymers (CFRP) is proposed. The problem has been solved in bus superstructures by designing and manufacturing a new CFRP node joined by a ductile polyurethane adhesive to the structure. On the other hand, in civil engineering structures the use of CFRP pieces attached to the structure by means of a ductile epoxy adhesive is proposed.

The resistance of the new joints against the stresses to which they will be subjected has been guaranteed experimentally and through finite element analysis, studying the singularities by means of the “Intensity of Singular Stress Field” (ISSF). The results obtained are excellent, and the new joints show resistance values far superior to the system requirements. Likewise, the structure has enough elasticity, and therefore fatigue behavior has been improved.

Capítulo 1:

MOTIVACIONES Y OBJETIVOS

Índice

Capítulo 1:

MOTIVACIONES Y OBJETIVOS

1.1 MOTIVACIONES

Esta Tesis Doctoral está enmarcada dentro de un proyecto del Plan Nacional de I+D+I del Ministerio de Economía y Competitividad del Gobierno de España (con número de proyecto TRA2014-56471-C4-2-R). El principal objetivo del proyecto es encontrar una solución a los problemas de fatiga existentes en las superestructuras de acero actualmente utilizadas en la fabricación de vehículos de pasajero. Este problema puede ser extrapolado a cualquier estructura civil de acero, en la que sea necesario unir mecánicamente dos componentes iguales (acero-acero) o disimilares (acero-material compuesto). Por lo tanto, esta Tesis Doctoral busca resolver los problemas existentes tanto en estructuras de acero de vehículos de pasajeros como en estructuras de acero diseñadas para aplicaciones civiles (edificios, puentes…).

Normalmente en la fabricación de estructuras de autobús o de ingeniería civil, se utilizan vigas de acero que son unidas unas a otras mediante soldadura. Esta tecnología presenta varias ventajas bien conocidas: costes de producción moderados, desarrollos ampliamente utilizados en la industria, facilidad de operación y buena accesibilidad tanto a mano de obra cualificada como a los materiales necesarios. Sin embargo, también presentan una lista de desventajas que aconsejan en muchos casos el uso de nuevas tecnologías capaces de reemplazar las soldaduras en ciertas aplicaciones. Los principales inconvenientes están asociados a un ciclo de vida no sostenible del conjunto. La soldadura aporta rigidez a la estructura, y junto a las vibraciones derivadas de las condiciones de servicio, resultará en problemas de fatiga mecánica a lo largo del ciclo de vida (especialmente en áreas frágiles cerca de las zonas soldadas de la estructura). Este problema se agrava por el hecho de que en cualquier soldadura hay zonas afectadas por el calor, donde a menudo se producen cambios micro-estructurales que debilitan el material. Además, los cambios micro-estructurales producen pilas galvánicas, y por tanto corrosión. Después de un proceso de fatiga la estructura colapsa por las zonas afectadas por el calor, ayudado por las áreas sujetas a corrosión.

Para resolver este problema, en esta Tesis Doctoral se propone el uso de otro tipo de materiales y uniones híbridas formadas por adhesivos y materiales compuestos (CFRP-Carbon

Fiber Reinforced Polymer). Los recientes desarrollos en el campo de los adhesivos hacen posible su uso en aplicaciones estructurales, siendo capaces de aportar elasticidad, evitando la corrosión, y reduciendo en gran medida los problemas derivados de un proceso de fatiga mecánica. Por otro lado, el uso de materiales compuestos y más específicamente el uso de polímeros reforzados con fibra de carbono (CFRP) está muy extendido en la industria hoy en día. Sus propiedades son bien conocidas, destacando la baja densidad para altos valores de resistencia.

1.2 OBJETIVOS

Esta Tesis Doctoral se divide en tres objetivos principales:

1. Resolver los problemas de fatiga mecánica existentes en superestructuras soldadas de autobús mediante el uso de adhesivos y materiales compuestos.

2. Resolver los problemas ocasionados por fatiga mecánica en estructuras civiles de acero, utilizando para ello adhesivos y materiales compuestos.

3. Garantizar la resistencia de las nuevas uniones frente a los esfuerzos a los que estará sometida por medio de análisis de elementos finitos, estudiando las singularidades mediante el Intensity of Singular Stress Field (ISSF) por sus siglas en inglés.

Cada uno de los objetivos principales se divide en objetivos secundarios. De esta forma, el primer objetivo, resolver los problemas de fatiga existentes en superestructuras soldadas de autobús mediante el uso de adhesivos, fue dividido de la siguiente manera:

-Calcular las zonas o puntos de concentración de tensiones, propensas a sufrir problemas de fatiga a lo largo del ciclo de vida del autobús.

-Calcular el tipo y valor de los esfuerzos que actúan en la unión.

-Diseñar y fabricar un nuevo nodo de CFRP, para ser instalado en los puntos de concentración de tensiones, capaz de soportar las tensiones que hasta ahora recaían sobre los nodos de acero soldados.

-Estudiar diferentes tipos de adhesivos capaces de ser utilizados para el problema planteado: caracterización mecánica y térmica.

-Optimizar las uniones adhesivas planteadas mediante programas basados en los elementos finitos.

-Estudiar el comportamiento de las uniones adhesivas frente a ambientes agresivos, tratando de simular las condiciones de servicio a las cuales estará sometida la unión.

-Encontrar el adhesivo apropiado para unir el nodo de CFRP a la estructura de acero de forma fiable y eficiente. Este adhesivo debe ser capaz de soportar los esfuerzos calculados y comportarse de forma adecuada después de sufrir degradación por exposición a medios agresivos externos.

-Fabricar prototipos a escala real de los nuevos nodos para su implementación en la superestructura de autobús, y así poder compararlos de manera fiable con los nodos de acero actuales.

El segundo objetivo, resolver los problemas de fatiga existentes en estructuras civiles de acero mediante el uso de adhesivos, fue dividido de la siguiente manera:

-Estudiar la viabilidad del uso de uniones adhesivas acero-CFRP en aplicaciones de ingeniería civil, con diferentes adhesivos y tratamientos superficiales.

-Adaptar la solución planteada en el primer objetivo al refuerzo de estructuras metálicas usando elementos de CFRP.

-Desarrollar nuevas uniones adhesivas acero-CFRP, usando adhesivos epoxi elásticos que sean válidos para el problema planteado.

-Estudiar el comportamiento de las uniones bajo ambientes agresivos.

-Caracterizar mecánica y térmicamente tanto los adhesivos como las uniones adhesivas.

El tercer objetivo, garantizar la resistencia de las nuevas uniones frente a los esfuerzos a los que estará sometida por medio de análisis de elementos finitos, estudiando las singularidades mediante el Intensity of Singular Stress Field (ISSF), fue dividido de la siguiente manera:

-Desarrollar modelos de elementos finitos de uniones adhesivas simples y mixtas entre dos sustratos de acero, con adhesivos epoxi elásticos.

-Estudiar el campo de singularidades (ISSF) en los modelos desarrollados.

-Optimizar los modelos para alcanzar el valor mínimo de ISSF en cada caso.

-Comparar los modelos análogos de acuerdo a los valores de ISSF.

Capítulo 2:

ESTADO DEL ARTE

Índice

Capítulo 2:

ESTADO DEL ARTE

2.1 INTRODUCCIÓN

El uso de adhesivos en uniones con materiales compuestos en estructuras ha crecido de forma significativa en las últimas décadas. Los materiales compuestos presentan una serie de ventajas respecto a otro tipo de materiales comúnmente usados como los materiales metálicos o los cerámicos. Quizás la principal ventaja de los materiales compuestos radica en la posibilidad de poder crear materiales dentro de un muy amplio rango de características técnicas, simplemente modificando la matriz o los refuerzos a utilizar. Gracias a esto es posible conseguir materiales en los que se ha reforzado una o varias de sus características, como dar alta resistencia, larga vida a fatiga, alta rigidez, bajo coeficiente de expansión térmica, baja densidad y bajo peso. Sin embargo, lo que hace especialmente atractivos a los materiales compuestos en términos de rendimiento estructural son la alta resistencia y rigidez específicas, y las propiedades anisotrópicas y heterogéneas del material. Además, dentro de una elección particular de matriz y refuerzo, la orientación de los refuerzos, el método de fabricación, las condiciones de procesado, y las posibles combinaciones con otros materiales aportan una variedad adicional en términos de propiedades mecánicas [1]. En esta Tesis solo los materiales compuestos de matriz polimérica (PMC's – por sus siglas en inglés) van a ser tenidos en cuenta. Los refuerzos usados pueden ser de diferente naturaleza: partículas (nano o micrométricas) o fibras (cortas o largas). Sallal et al. [2] introducen nano-partículas (Al_2O_3-CaO) como refuerzo en una mezcla polimérica (4% epoxi y 96% poliéster) buscando mejorar las propiedades mecánicas del polímero. Los nuevos materiales muestran una mejora de la resistencia a tracción del 24%, una mejora de la resistencia a flexión del 23.5%, y un aumento de la dureza del 25%. Otros autores como Batista y Drzal [3] utilizan nano-cristales de celulosa para modificar materiales compuestos de matriz epoxi reforzados con fibra de carbono, mejorando las propiedades en la interfase matriz-fibra.

En cuanto al uso de fibras como refuerzo, está sobradamente documentado en la literatura y ampliamente extendido el uso de estos refuerzos sobre todo en matrices epoxi [3] y matrices de poliéster [4]. De acuerdo con esta naturaleza, la Tesis está centrada en PMC con fibra larga de carbono, llamado por sus siglas en inglés CFRP (Carbon Fiber Reinforced Polymer). Una estimación en el año 2014 (Figura 1) [5] ya indicaba la tendencia creciente del uso de los CFRP.

La creciente demanda en los sectores como el aeroespacial [6] y el automovilístico [7] hace de los CFRP uno de los materiales compuestos más usados hoy en día. Junto al desarrollo de los PMC's han tenido que desarrollarse técnicas de unión diferentes a la unión mecánica o la soldadura para estos materiales [8]. Del mismo modo, el uso de estructuras híbridas formadas por materiales disimilares, como por ejemplo un PMC y un metal se está extendiendo cada vez más en la industria [9]. En muchos casos no es posible el uso de técnicas tradicionales de unión, requiriendo por tanto el desarrollo de nuevas técnicas [10]. Los adhesivos han resultado ser una solución ideal para esta problemática, aumentando su uso de forma exponencial en las últimas décadas, tal y como documentan algunos autores como Van-Straalen y Van-Tooren [11] o Ebnesajjad [12].

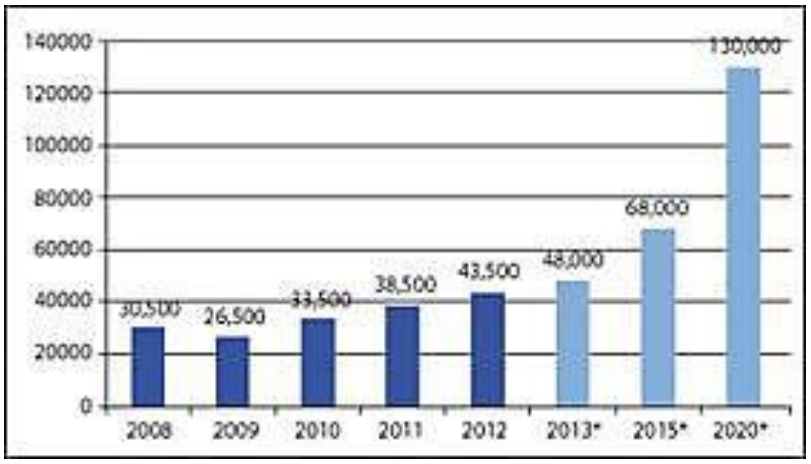

Figura 1. Estimación de demanda global de fibra de carbono (en toneladas) entre los años 2008 y 2020 [5].

Otras fuentes dan también cifras del mercado de la fibra de carbono un poco más baja [13], como se muestra en la Figura 2, aunque la tendencia es la misma. Los adhesivos se usan para unir un amplio rango de materiales similares y disimilares. De esta forma es posible unir tanto materiales metálicos como no metálicos, además de materiales compuestos y componentes con diferentes formas, tamaños y espesores. Todos los desarrollos llevados a cabo en el campo de los adhesivos han hecho posible, que hoy en día, las ventajas de las uniones adhesivas frente a las técnicas tradicionales de unión (uniones mecánicas) estén ampliamente aceptadas [14]. Los adhesivos son capaces de aportar una mayor flexibilidad en el diseño, permiten obtener una mejor distribución de las cargas, reducen la concentración de tensiones, e incrementan la resistencia a fatiga y frente a la corrosión. Además, permiten reducir el peso de toda la estructura [15], pudiendo unir diferentes materiales [10].

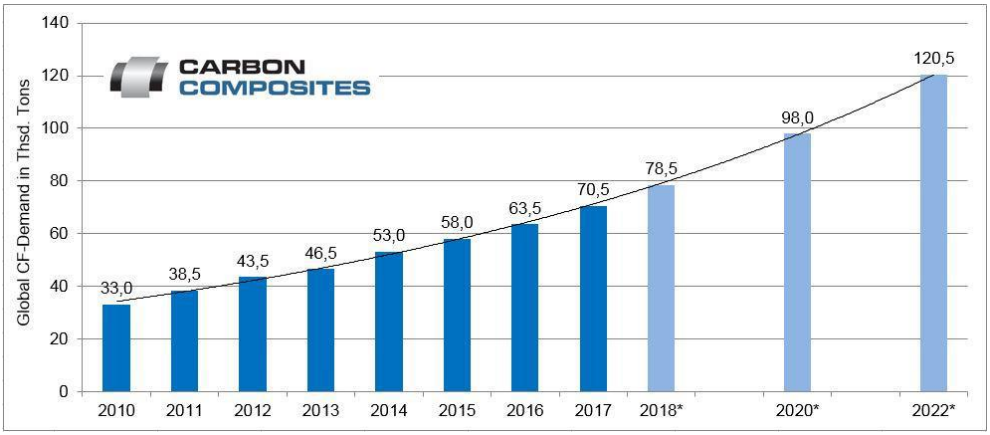

Figura 2. Evolución de la demanda global de fibra de carbono (en miles de toneladas) hasta el año 2022 [13].

En el sentido más amplio, se puede considerar como adhesivo a cualquier sustancia capaz de unir las superficies de diferentes objetos resistiendo a la separación de los mismos. El proceso de unir dos o más estructuras usando adhesivos es comúnmente conocido como "adhesive bonding" por sus palabras en inglés. Las partes que son unidas se denominan adherentes o sustratos dependiendo del contexto. Aunque hay que saber que un adherente puede estar formado por diferentes capas o sustratos, por ejemplo un material compuesto laminado y pintado estará compuesto por la pintura y cada una de las capas que lo forman serán sustratos.

Los adhesivos estructurales se han vuelto de vital importancia en cualquier campo ingenieril porque son capaces de crear uniones resistentes y permanentes entre una gran cantidad de sustratos. En el rendimiento de la unión, es de vital importancia el proceso de curado, cuando tienen lugar reacciones químicas de endurecimiento del adhesivo haciendo que las partes se unan mediante una fuerza interna (o fuerza de cohesión) y una adherencia superficial (o fuerza de adhesión). Hu et al. [16] investigan el efecto del curado en la resistencia y en las propiedades cohesivas de estructuras tipo sándwich corrugadas unidas mediante adhesivos estructurales. El estudio muestra que el aumento gradual de la temperatura y la duración del curado puede mejorar el rendimiento mecánico y la resistencia de estas estructuras unidas mediante adhesivos estructurales. Han et al. [17] estudian el efecto del post-curado en la tenacidad a fractura en modo II de un adhesivo epoxi estructural, concluyendo que el post-curado afecta de forma efectiva al comportamiento en modo II del adhesivo alcanzando una mayor resistencia a la fractura.

Los adhesivos estructurales de alto rendimiento son cada vez más comunes en sectores como el aeroespacial [18], automovilístico [19], marino [20], médico [21] y de la construcción [22]. Es importante remarcar que los adhesivos estructurales avanzados no solo son utilizados como método de unión (aunque en este caso en forma de resina), ya que pueden ser empleados en la fabricación de materiales compuestos, como es el caso de las resinas epoxis o las resinas de poliéster. Un ejemplo de este uso es el "Glare", formado por aluminio y fibra de vidrio y ampliamente utilizado en estructuras primarias de aviones.

A pesar de la gran cantidad de ventajas existentes en el uso de uniones adhesivas en materiales compuestos, comprender y cuantificar la durabilidad a largo plazo en este tipo de uniones bajo condiciones de servicio es un área de interés que debe recibir la atención adecuada por parte de los investigadores, ya que hasta el momento no hay mucha información accesible. Por esta razón, en esta tesis doctoral se han realizado diferentes ensayos acelerados con el objetivo de determinar el comportamiento de las uniones adhesivas planteadas frente a las posibles condiciones de servicio. Bowditch [23] estudia la durabilidad de uniones adhesivas en presencia de agua. El agua afecta tanto a las propiedades físicas como a las propiedades mecánicas del adhesivo, además de a la naturaleza de la intercara o interfase que existe entre el adhesivo y el sustrato. Viana et al. [24] realizan una completa revisión bibliográfica sobre el efecto de la temperatura y la humedad en la degradación de uniones adhesivas (principalmente con adhesivos epoxi). Por otro lado, Korta et al. [25] estudian el efecto de procesos acelerados de degradación por humedad (95% de humedad relativa) y temperatura (entre -40°C y 180°C). Los resultados muestran que incluso bajo ambientes moderadamente agresivos se pueden producir roturas indeseadas aunque no se apliquen fuerzas externas. Además, identifican el coeficiente de expansión térmica como un factor crucial en el rendimiento de uniones adhesivas de materiales disimilares. Agarwal et al. [26] estudian la influencia de cargas mecánicas y ambientales combinadas en el comportamiento de estructuras de acero reforzadas con CFRP. Los resultados experimentales muestran un descenso de la resistencia del 16% en probetas sometidas a ciclos térmicos entre 10°C y 50°C durante 21 días. Costa et al. [27] investigan los efectos del agua sobre el comportamiento a fatiga de uniones adhesivas con aluminio. Este trabajo afirma que el aumento del contenido de agua reduce la resistencia a fatiga de las uniones adhesivas planteadas. A su vez, se producen cambios en las curvas de la ley de Paris, principalmente provocados por la iniciación de grieta a umbrales más bajos que los del adhesivo sin envejecer.

Algunos trabajos existentes en la literatura como los de Matthews et al. [28], y Banea y da Silva [14] presentan sendas revisiones bibliográficas sobre la resistencia de uniones adhesivas en estructuras de material compuesto. En el primer caso los autores se centran principalmente en el estudio de la resistencia en plásticos reforzados con fibras. En el segundo trabajo, se profundiza más exhaustivamente en distintos aspectos como la preparación superficial, la configuración de la unión, las propiedades del adhesivo o los factores ambientales.

2.2 TIPOS DE ADHESIVOS EN UNIONES CON MATERIALES COMPUESTOS

La gran cantidad de adhesivos existentes y los continuos desarrollos que se están realizando en este campo hacen posible su uso para infinidad de aplicaciones. Sin embargo, esto puede llegar a suponer un problema en cuanto a la selección del adhesivo adecuado. Por tanto será necesario conocer detalladamente las propiedades del adhesivo a emplear y los requerimientos o solicitaciones bajo los que va a tener que trabajar la unión adhesiva. La selección del adhesivo no es un proceso sencillo porque no existe un adhesivo universal que pueda trabajar bajo cualquier condición o aplicación. La selección del adhesivo incluye numerosas variables, como el tipo y la naturaleza de los sustratos que deben ser unidos, el proceso de curado, el método de aplicación del adhesivo, y sobre todo las condiciones de servicio (ambiente y esfuerzos) a los que estará sometida la unión adhesiva durante su vida útil. Identificar correctamente todas las cargas (de impacto, quasi-estáticas, y de alto/bajo ciclo de fatiga) es básico para poder trabajar en condiciones de seguridad adecuadas. El coste es otro factor fundamental en el proceso de selección de un adhesivo, sobre todo dentro de un proceso de producción complejo. Las propiedades más importantes a tener en cuenta en el proceso de selección de un adhesivo para una aplicación particular son las siguientes:

-Resistencia (a cizalla y a pelado).

-Resistencia a fluidos y productos químicos.

-Habilidad para el mojado de las superficies que deben ser unidas.

-Dureza.

-Resistencia a degradación medio ambiental (incluyendo calor y humedad).

-Fluencia.

-Fatiga.

Las propiedades de los adhesivos son muy diferentes dependiendo de la familia a la que pertenezcan, así como las aplicaciones donde pueden ser usados. Por ejemplo las resinas epoxi tienen una doble función en los CFRP; ellas son comúnmente utilizadas para unir las capas de fibra de carbono y a la vez son usadas como adhesivo estructural. Se puede decir que prácticamente todos los CFRP son fabricados con resina epoxi, lo que a la vez favorece usar un adhesivo epoxi para sus uniones adhesivas. Aparte de las resinas epoxi, existen muchos otros tipos de adhesivos capaces de ser utilizados en muy diversas aplicaciones estructurales. La Figura 3 muestra la clasificación de adhesivos realizada por Van-Straalen y Van-Tooren [11] en función de la deformación y la resistencia.

Anes et al. [29] analizan la selección de adhesivos para unir materiales disimilares que van a trabajar a muy baja temperatura. Los autores estudian factores como el rango de temperatura, las condiciones de contorno, la variación del coeficiente de expansión térmica con la temperatura, y las grietas entre las intercaras adhesivo-sustrato. Los resultados muestran que cuando las uniones planteadas trabajan a baja temperatura, se crean estados tensionales en la unión que pueden llegar a ser incluso superiores a la resistencia a cizalla del adhesivo. Así a la hora de seleccionar el adhesivo más adecuado para trabajar a bajas temperaturas se deben tener en cuenta tres factores fundamentales:

-Coeficiente de expansión térmica: debe ser bajo (para garantizar mayores esfuerzos marginales) y cercano al coeficiente de expansión térmica de los sustratos.

-Resistencia a cizalla: debe ser lo más alta posible, para garantizar el correcto funcionamiento de la unión incluso ante cargas elevadas.

-Capacidad de deformación: debe ser elevada, para garantizar la adaptabilidad del adhesivo a los sustratos cuando se produzcan cambios en los mismos (al tener distintos coeficientes de expansión térmica).

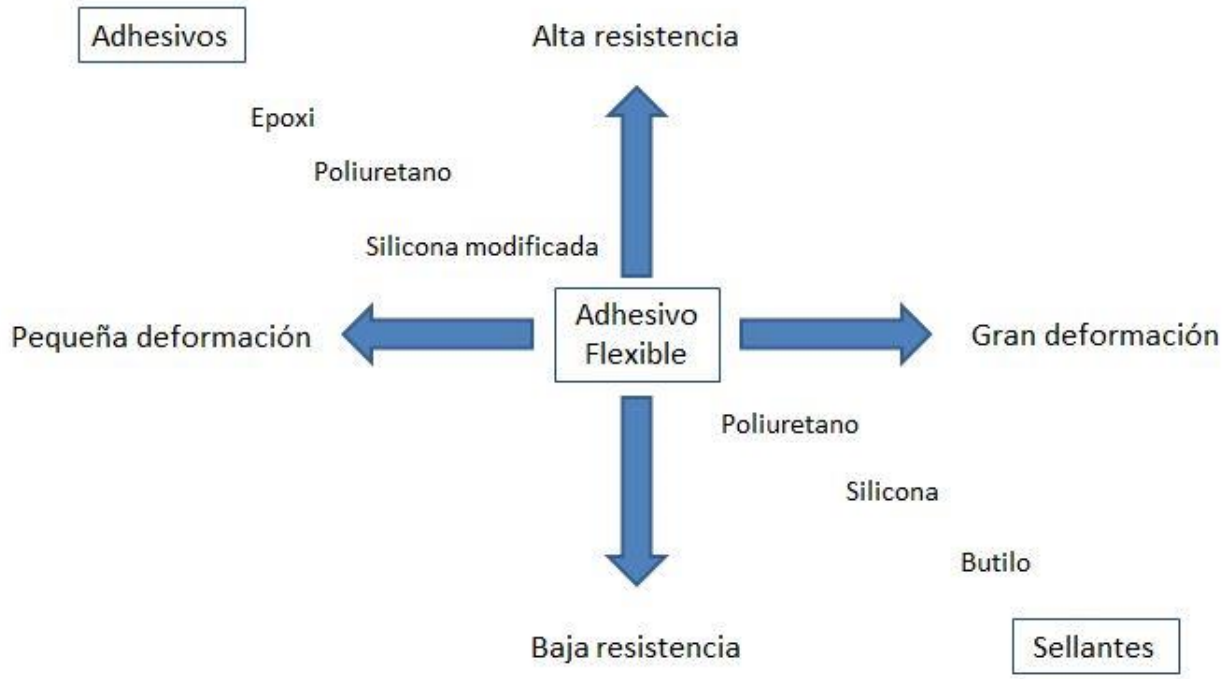

Figura 3. Características mecánicas de los adhesivos [11].

2.2.1 CONFIGURACIONES DE UNIONES ADHESIVAS Y MODOS DE FALLO

El ensamblaje de la unión adhesiva es una fase crítica en la que se requiere del máximo cuidado posible por parte del operario. Los principales tipos de uniones adhesivas utilizadas en estructuras ingenieriles ya sea para metales o materiales compuestos se muestran en la Figura 4 [30]. Desde un punto de vista puramente mecánico, la combinación de cargas de pelado y de cizalla, que a su vez influyen en el valor de la resistencia, varían de una geometría a otra. Esto es importante para poder comprender las condiciones que llevan al fallo de la unión.

De acuerdo a la norma ASTM D5573 [31] existen siete tipos de fallo en uniones adhesivas con materiales compuestos: fallo adhesivo, fallo cohesivo, fallo cohesivo mediante una fina capa de adhesivo, fallo por desgarro de la fibra, fallo por desgarro de la fibra cerca de la zona adhesiva, fallo por rotura total del sustrato de material compuesto, y fallo mixto. En la mayoría de los casos el fallo adhesivo es el factor limitante, ya que se trata del peor tipo de fallo posible para cualquier unión adhesiva. Este tipo de fallo suele ser debido a una mala preparación superficial o a un curado incompleto del adhesivo. En otras aplicaciones donde los sustratos sean

muy finos o incluso con determinados tipos de material compuesto, el fallo por sustrato puede ser motivo de preocupación y estudio. Sin embargo, algunos autores como Ebnesajjad [32] consideran que el modo de fallo no debe ser usado como único criterio para seleccionar una unión útil. Algunas combinaciones de adhesivo y sustrato pueden fallar siempre de forma adhesiva, y a la vez tener mayores resistencias que otras uniones similares con fallo cohesivo en las que se han utilizado adhesivos más débiles. La resistencia última de la unión es un criterio más importante que el modo de fallo.

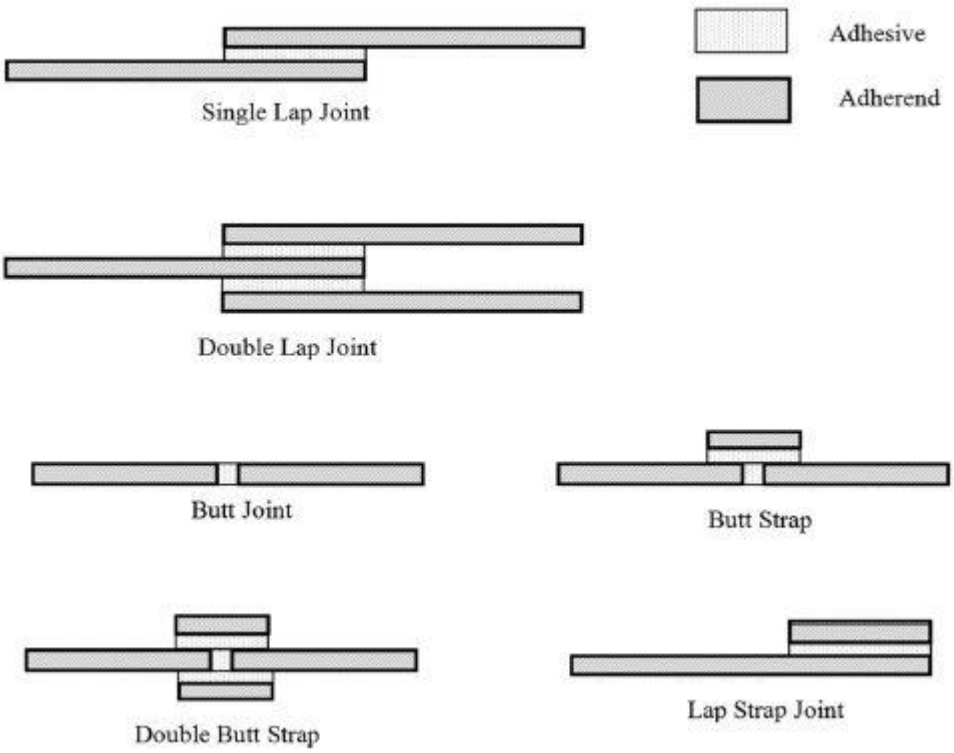

Figura 4. Configuraciones de unión adhesiva más comunes en ingeniería [30].

En algunas ocasiones puede ser complicado distinguir entre un fallo cohesivo o un fallo adhesivo (o por la intercara). Un ejemplo claro de esta circunstancia se muestra en uno de los trabajos realizados durante esta Tesis Doctoral [33], donde los autores tuvieron que realizar micrografías mediante un microscopio electrónico de barrido (SEM) para caracterizar como fallo cohesivo (fina capa de adhesivo) lo que a simple vista parecía un fallo adhesivo. Otros autores se basan en estudios numéricos o en elementos finitos para predecir el fallo en uniones adhesivas. Ye et al. [34] desarrollan y validan experimentalmente un modelo integrado para analizar el fallo a tracción y el diseño del solape en uniones adhesivas con materiales compuestos. Los autores utilizan dos criterios en este modelo:

-Para el fallo por la matriz y por las fibras: modelo 3D basado en el criterio de Tsai-Wu introduciendo factores de modo y una evolución de daño exponencial y progresiva.

-Para delaminación y separación de sustratos: modelo 3D basado en el modelado de la zona cohesiva (CZM - Cohesive zone model) introduciendo nuevos componentes tangenciales.

Liu et al. [35] desarrollan un modelo cohesivo visco-elástico robusto e independiente del tamaño de malla para analizar el fallo en uniones adhesivas de materiales compuestos. Mediante elementos finitos obtienen los parámetros cohesivos (resistencia) y predicen el comportamiento frente al fallo de las uniones adhesivas. Tosun y Çalık [36] presentan un modelo basado en redes neuronales artificiales para predecir el fallo en uniones adhesivas a solape simple, siendo capaces de realizar predicciones eficientes y con un error aceptable respecto a los resultados obtenidos experimentalmente.

2.3 LIMITACIONES DE LAS UNIONES ADHESIVAS CON MATERIALES COMPUESTOS

A pesar de que el uso de uniones adhesivas está aumentando rápidamente, sigue habiendo importantes consideraciones que deben ser tenidas en cuenta en términos de análisis de la unión, diseño, y durabilidad. El estudio de uniones adhesivas implica considerar diferente variedad de geometrías de unión, los materiales a emplear, las condiciones de carga, los modos de fallo y los efectos del ambiente al que van a estar sometidas. Por tanto, el análisis de cualquier unión con adhesivos requiere del uso de las herramientas adecuadas para obtener de forma fiable el valor de los esfuerzos, deformaciones y parámetros de fractura. Pantelakis y Tserpes [37] estudian los retos a los que se enfrentan las uniones adhesivas de materiales compuestos en estructuras de avión, identificando cinco limitaciones básicas: durabilidad de las uniones adhesivas, contaminación previa a la realización de la unión, diseño efectivo de la unión, desarrollo de técnicas no destructivas capaces de detectar todo tipo de defectos en las zonas de unión y fatiga. Ciupack et al. [38] evalúan los retos a los que se enfrentan las uniones adhesivas en estructuras de acero aplicadas a la ingeniería civil. Estos autores identifican el diseño de la unión, la capacidad de deformación, los métodos de fabricación, el diseño de las uniones y el comportamiento frente a cargas cíclicas como los puntos críticos de las uniones adhesivas en este tipo de estructuras.

Los PMCs son estructuralmente más eficientes que los metales y no sufren de corrosión galvánica [39]. Sin embargo, los metales tienen una mejor tolerancia al daño, siendo más sencilla la predicción de fallos. Además, los materiales metálicos de forma general, presentan buen comportamiento frente al efecto de solventes y temperatura, factores que para el caso de los polímeros, son muy negativos provocando un proceso de degradación [33].

A pesar de las numerosas ventajas existentes en las uniones adhesivas, su uso es todavía muy limitado. Algunos autores como Wahab et al. [40] sostienen que esto es debido principalmente a la baja durabilidad de estas uniones cuando la estructura está sometida a condiciones ambientales hostiles. El efecto de la humedad en la resistencia de uniones adhesivas es muy significativo debido al deterioro del adhesivo y de la intercara adhesivo-sustrato. La resistencia de la unión decrece rápidamente cuando es envejecida en ambientes calientes y húmedos, como ha sido demostrado en numerosos trabajos [33,41,42].

La dificultad a la hora de encontrar el adhesivo ideal para cada aplicación es otra limitación a tener en cuenta al trabajar con adhesivos, ya que no existe un adhesivo universal, y en el mercado hay una gran variedad de opciones disponibles. Algunos factores a tener en cuenta a la hora de elegir un adhesivo son:

I. Los adhesivos son productos químicos, y en algunos casos dentro de su formulación contienen elementos peligrosos para la salud, por lo que si su uso va a ser continuado, habrá que tomar medidas de seguridad e higiene en el trabajo [43].

II. Por otro lado, la mayoría de los adhesivos industriales no son estables por encima de 180°C. En general a altas temperaturas (por encima de los 100ºC) pierden propiedades si se trabaja de forma continua. A 180ºC casi todos los polímeros termoplásticos estarán trabajando muy por encima de la temperatura de transición vítrea (Tg) provocando ablandamiento del mismo e incluso la fusión de las zonas cristalinas. En el caso de los polímeros termoestables, a estas temperaturas tendrá lugar un proceso de rotura de enlaces químicos y en consecuencia la descomposición del material [24].

III. Los diferentes coeficientes de expansión térmica existentes en todo el conjunto de la unión adhesiva (sustratos y adhesivo) van a fomentar la aparición de tensiones residuales. Por lo que hay que realizar cálculos para saber el grosor de adhesivo que se puede poner y en consecuencia que adhesivo elegir dependiendo de los requerimientos de la unión [29].

IV. Algunos adhesivos son muy sensibles a la presencia de grasa, aceite o humedad en las superficies que deben ser unidas. Por lo tanto la rugosidad y las condiciones de mojado (tensión superficial en el adhesivo y energía superficial en el sustrato) deben ser minuciosamente controladas [44].

V. La dificultad de la unión para ser reemplazada es otro hándicap a tener en cuenta al trabajar con adhesivos. Esto es debido a que todavía no hay un método para separar los sustratos, aunque ya se está trabajo en ello [45].

VI. Además, los tiempos de ensamblaje pueden llegar a ser mayores que en métodos de unión tradicionales, al depender cada adhesivo de su mecanismo de curado. En ocasiones, estos mecanismos de curado requerirán de altas temperaturas o incluso de equipos especializados, como prensas, autoclaves y hornos para el correcto curado y fabricación de la unión adhesiva [46,47].

VII. En cuanto al diseño de la unión, este estará limitado por el espesor del adhesivo, siendo el tipo de esfuerzo más adecuado el de cizalla, ya que otros esfuerzos como el de pelado son muy perjudiciales en uniones adhesivas [48].

VIII. En cuanto al comportamiento a impacto, la fragilidad de la mayoría de adhesivos estructurales (sobre todo las resinas epoxi) de alta resistencia hace que su uso no sea aconsejable para este tipo de aplicaciones. La tenacidad de una unión adhesiva puede decrecer considerablemente bajo cargas de impacto [49].

IX. Continuando con las limitaciones, realizar el tratamiento superficial adecuado es fundamental para obtener rotura cohesiva y por tanto los resultados esperados [50].

X. Por último, es muy complicado determinar la calidad de una unión adhesiva mediante técnicas no destructivas, a pesar del desarrollo de nuevos métodos de inspección [51,52].

2.4 PROPIEDADES ADHESIVAS DE MATERIALES COMPUESTOS DE MATRIZ EPOXI

Las características de la superficie van a influir de forma decisiva en procesos que incluyen la unión con adhesivos, el pintado, el barnizado o el sellado [53]. La adhesión es un fenómeno que tiene lugar en la superficie y que consiste en la unión de las capas superficiales de

dos cuerpos en contacto debido a las fuerzas de atracción existentes entre ellos [54]. Por esta razón, para que la adhesión pueda llegar a ocurrir debe haber mucha proximidad entre los sustratos a unir.

Las propiedades adhesivas de la superficie pueden ser descritas con diferentes parámetros físicos [55,56,57]: el ángulo de contacto (θ) y los fenómenos de mojado de la superficie relacionados, el trabajo termodinámico de adhesión (Wa) y la energía libre de la superficie.

El ángulo de contacto es un indicador de la mojabilidad. De esta forma una buena mojabilidad está relacionada con un ángulo de contacto pequeño (θ < 90°) (Figura 5a) mientras que una mala mojabilidad se relaciona con un ángulo de contacto grande (θ > 90°) (Figura 5b) [58,59]. En el punto triple C (Figura 6), donde las interfases sólido-líquido-vapor están en contacto, el equilibrio termodinámico se expresa por la ecuación de Young: γ_LV cosθ=γ_SV-γ_SL. Siendo γLV, γSV y γSL los valores de tensión superficial líquido-vapor, la energía superficial del sustrato, y la tensión superficial sólido-líquido, respectivamente [60].

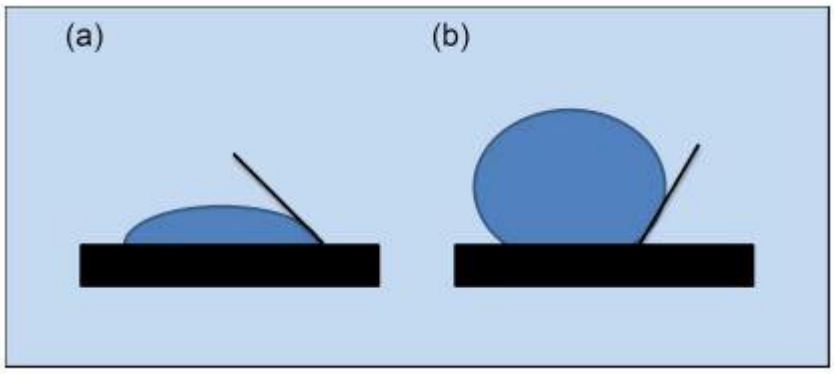

Figura 5. Ángulo de contacto de una gota de agua en la superficie de un sólido. θ < 90° indica una buena mojabilidad (a) mientras que θ > 90° (b) indica una mala mojabilidad [58].

El trabajo de adhesión (Wa) es la suma de todas las interacciones intermoleculares requeridas para construir un área unitaria separando dos fases en equilibrio durante un proceso isotérmico reversible. Muchos investigadores sostienen que las propiedades adhesivas pueden ser determinadas con la energía libre de la superficie. Este valor termodinámico describe el estado energético de la superficie y es una característica particular de sólidos o líquidos (donde se denomina tensión superficial). Existen diferentes formas para calcular la energía libre de la superficie, destacando los trabajos realizados por Fowkes, Zisman, Owens-Wendt, Van Oss-Chaudhury-Good, Neumann y Wu [61,62].

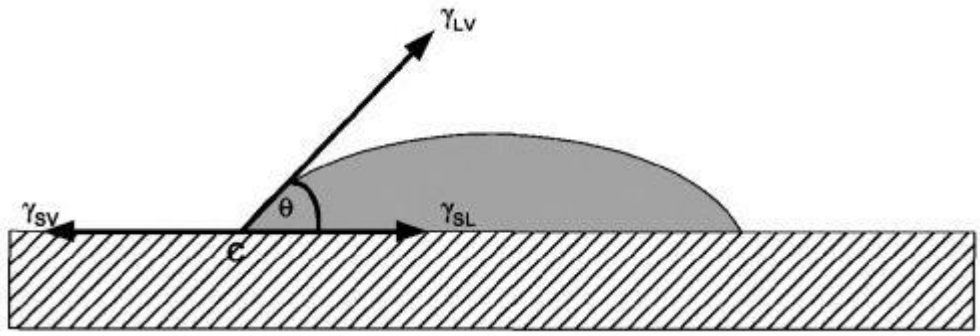

Figura 6. Ángulo de contacto (θ) de una gota de líquido depositada en la superficie de un sólido. Representación del equilibrio termodinámico en el punto triple C [60].

Otra característica de la superficie que tiene una gran influencia sobre la resistencia de la unión es la rugosidad superficial [63,64]. Sin embargo, la magnitud de esta influencia no ha sido definida completamente debido a la complejidad del fenómeno. Autores como Uehara y Sakurai [63] dedujeron que el valor óptimo de rugosidad superficial existe al calcular la resistencia a tracción de la adhesión. Por otro lado, no encuentran una relación clara entre la resistencia a pelado y la rugosidad superficial.

2.5 TRATAMIENTOS SUPERFICIALES

2.5.1 DEFINICIÓN Y OBJETIVOS

La capacidad de unión entre dos superficies está influenciada por las características superficiales de los materiales que deben ser unidos. Mediante el uso de tratamientos superficiales se asegura que los sustratos son capaces de ser unidos y la durabilidad de la unión [33,65]. Los objetivos principales del uso de tratamientos superficiales son:

- Optimizar el contacto intermolecular entre el adhesivo y el sustrato, mejorando de esta manera la mojabilidad [66].

-Eliminar o prevenir la formación de capas de baja cohesión producidas por la migración de plastificantes a la superficie del sustrato. Estas capas son un potencial punto de inicio para el fallo adhesivo de la unión [67].

-Facilitar la reproducibilidad de los resultados. El objetivo es homogeneizar las superficies para aumentar la reproducibilidad de los resultados y evitar fallos aleatorios durante la vida útil de las piezas [68].

-Activadores e imprimaciones funcionan no solo como tratamientos superficiales. Los activadores pueden facilitar la reticulación del adhesivo; mientras que las imprimaciones pueden proteger la superficie del sustrato, especialmente en el caso de metales, más propensos a sufrir corrosión galvánica [69].

-Estos tratamientos permiten asegurar que la adhesión es debida a las fuerzas adhesivas y no solo al anclaje mecánico, y de esta forma obtener una alta capacidad inicial de pegado así como buena durabilidad a largo plazo en la unión adhesiva. Las propiedades de los materiales deben ser mejoradas a nivel molecular, para de esta forma incrementar la resistencia y durabilidad de los adhesivos [70].

2.5.2 TIPOS DE TRATAMIENTO

2.5.2.1 LIMPIEZA DE LA SUPERFICIE

Los tratamientos de limpieza van a ser necesarios en todos los materiales. La limpieza de la superficie consiste en eliminar la suciedad o contaminación de un sustrato o adherente sin llegar a causar alteraciones físicas o químicas en él.

Los productos de limpieza generalmente usados para metales consisten en una combinación de compuestos decapantes y desengrasantes, como hidróxidos de sodio [71] y potasio [72], fosfatos y poli-fosfatos [73], ácidos [74], carbonatos de sodio y bicarbonatos [75]. Sin embargo, para polímeros y materiales compuestos, el uso de solventes orgánicos es más común. Existen varios procedimientos de limpieza usando solventes: desengrase por medio de vapor, tratamiento de baño con ultrasonidos, fregado, inmersión y pulverización.

2.5.2.2 TRATAMIENTOS ABRASIVOS

Los tratamientos abrasivos tienen la misión de aumentar la rugosidad del sustrato [76]. Las siguientes cuestiones deben ser tenidas en cuenta con este tipo de tratamiento:

-La profundidad de la abrasión, o la medida en que el espesor del sustrato va a ser reducido.

-Las posibles deformaciones de la superficie.

-La idoneidad de llevar a cabo un proceso en seco o en húmedo.

-El aspecto cinético, es decir, la velocidad a la que ocurre todo el proceso.

-El control de la presión ejercida sobre los sustratos.

Con estos tratamientos es esencial evitar dañar la superficie del material, especialmente cuando se trabaja con materiales compuestos reforzados con fibra. Un tratamiento excesivamente agresivo puede llevar a que aparezcan las fibras en la superficie. Este efecto es indeseable en cualquier material compuesto ya que cambia las propiedades superficiales del material. Sin embargo, para materiales compuestos reforzados con fibra de vidrio, la existencia de fibras en la superficie del material puede hacer que la mojabilidad de la superficie aumente debido a su rápida oxidación. Esta oxidación es responsable del incremento de la energía superficial y por tanto de la mejora de la adhesión [77].

Los tratamientos abrasivos más comúnmente utilizados son el granallado y el lijado, además también se puede emplear un láser para aumentar la rugosidad [78,79]. Aunque estos métodos pueden llegar a ser muy agresivos para materiales poliméricos y compuestos, si el material de abrasión y la presión aplicada son elegidos de forma minuciosa, es posible evitar daños. La superficie debe ser limpiada inmediatamente después del proceso de abrasión para eliminar restos de arena y material desprendido.

2.5.2.3 TRATAMIENTOS QUÍMICOS

Los tratamientos químicos cambian la naturaleza de la superficie para mejorar sus propiedades adhesivas. Se crean grupos funcionales [59] en la superficie de los sustratos, que van a permitir obtener uniones adhesivas de mayor duración. Es necesario realizar siempre una limpieza de la superficie antes de cualquier tratamiento químico, y en muchas ocasiones también es necesario realizar limpiezas intermedias dentro del proceso.

La mayoría de las matrices poliméricas utilizadas para el desarrollo de materiales compuestos tienen baja polaridad [80], lo que hace más difícil el mojado de la superficie por el adhesivo; consecuentemente, solo será posible generar enlaces intermoleculares de baja energía. Por esta razón, es necesario activar la superficie mediante el uso de imprimaciones (que mejoran la unión química) o mordentados con ácido o bases (oxidación superficial), creando grupos funcionales polares tipo –COOH, OH….

2.5.2.3.1 IMPRIMACIONES

Uno de los tratamientos químicos más comúnmente utilizados son las imprimaciones. Estas sustancias se utilizan como producto intermedio entre el adhesivo y el sustrato. El proceso consiste en aplicar una única capa de imprimación sobre la superficie del sustrato. Esta capa actúa como un puente entre el sustrato y el adhesivo.

Estos tratamientos son relativamente sencillos de llevar a cabo ofreciendo una gran flexibilidad operacional, y por tanto siendo fáciles de aplicar manteniéndose activos durante largos periodos de tiempo [81]. La forma ideal de aplicación de estos productos es mediante spray, brochas o hisopos. Una vez aplicada la capa de imprimación, el solvente se evapora, dejando el compuesto activo debajo, que es lo que actúa de puente químico entre el sustrato y el adhesivo.

Las imprimaciones pueden ser utilizadas en todo tipo de materiales; de este modo es posible encontrar productos para metales y para polímeros, siendo también un factor fundamental el tipo de adhesivo. Entre sus funciones principales se incluyen:

1. Protección de la superficie del sustrato.

2. Mejora de la interacción entre el adhesivo y el sustrato, incrementando el tiempo de vida útil de la unión adhesiva.

3. Generación de características específicas como:

-Reducir la penetración de humedad dentro del área adhesiva.

-Sellar superficies con alta porosidad.

-Ayudar a prevenir la corrosión (imprimaciones inhibidoras de la corrosión).

-Eliminar o reducir la rugosidad superficial, incrementando los puntos de contacto entre el adhesivo y el sustrato.

-Proteger la intercara del adhesivo de la radiación ultravioleta.

-Proteger la superficie del adherente de la oxidación, pudiendo aumentar el tiempo máximo entre la realización del tratamiento superficial y la aplicación del adhesivo.

-Hacer de recubrimiento-barrera para prevenir reacciones indeseables entre el adhesivo y el sustrato.

Por regla general imprimaciones acuosas que no contienen solventes agresivos suelen ser las más utilizadas, debido principalmente a la sensibilidad de algunos sustratos frente a determinados solventes. La formulación más utilizada en imprimaciones son los silanos [82], los cuales ya suelen estar incluidos en las formulaciones. Los silanos son moléculas con una parte orgánica y otra inorgánica, lo que permite que se unan de forma covalente tanto al sustrato (parte inorgánica) como al adhesivo (parte orgánica) [83].

2.5.2.3.2 OXIDACIÓN SUPERFICIAL

Tratar polímeros con disoluciones oxidantes es conocido como mordentado, así por ejemplo una disolución de ácido sulfúrico saturada con trióxido de cromo a 80°C permite mejorar las propiedades adhesivas del material [77], por aumento de la rugosidad y la creación de grupos funcionales polares que aumentan la energía superficial.

Estos tratamientos siguen unos procedimientos específicos, algunos de los cuales están disponibles en la bibliografía, pero en muchos casos se encuentran bajo patente o son confidenciales.

Otra técnica de tratamiento químico es la oxidación de superficies poliméricas usando ozono [84]. Sin embargo, se trata de un sistema relativamente caro. Esto es debido a que es necesario eliminar el exceso de ozono de forma rápida y segura para evitar la contaminación atmosférica de la zona de trabajo. Por otro lado este sistema presenta la ventaja de no requerir del uso de productos químicos.

Por regla general, el tratamiento con ozono sólo se aplica a films plásticos, y suelas de calzado de caucho. Esta oxidación suele ir combinada con otros procesos como el tratamiento de corona de plasma atmosférico o el uso de imprimaciones (para mejorar el anclaje de las imprimaciones al sustrato) [77].

En los materiales metálicos se suelen usar procesos de conversión que permiten quitar la capa de óxido de baja cohesión y crear otra capa con mejor unión al sustrato y con una buena rugosidad para aumentar el anclaje con el adhesivo. Un ejemplo es el anodizado usado en el aluminio [85]. En el caso del acero se suelen hacer tratamientos químicos de fosfatado [86], siempre que el acero no esté ya galvanizado.

Los materiales cerámicos no necesitan en principio tratamiento químico ya que ellos ya están oxidados, teniendo una alta energía superficial [87]. En algunos casos para hacerlos más compatibles con el adhesivo y rebajar su energía superficial se tratan con silanos.

2.5.2.4 TRATAMIENTOS FÍSICOS

La principal ventaja de usar procesos físicos es que se elimina la necesidad de utilizar productos químicos. Todos estos procesos físicos incluyen el uso de plasma. Se define como plasma a una sustancia gaseosa ionizada formada por cargas eléctricas positivas y negativas libres, radicales, fotones, iones y moléculas excitadas [88]. Se le conoce como el cuarto estado de la materia. Si se aplica energía a un gas, ya sea por medio de descarga eléctrica, calentamiento o mediante inyección de ondas electromagnéticas, tendrá lugar una ionización, volviéndose eléctricamente conductor. Las partículas de gas empiezan a moverse rápidamente en las tres dimensiones del espacio como consecuencia de la energía aplicada al sistema, adquiriendo mayor energía rotacional y vibracional. Cuando el plasma entra en contacto con la superficie de cualquier material, su energía se libera y se transmite a esa superficie. El principio del proceso está basado en las interacciones entre las partículas del plasma y la superficie del material. Por tanto, el `bombardeo' de la superficie del material con partículas cargadas va a producir cambios físicos y químicos. En exposiciones de baja energía típicamente usadas para tratamientos superficiales, las interacciones sólo cambian la superficie del material; los efectos sólo afectan a una pequeña región formada por unas pocas capas moleculares de profundidad, y no cambian las propiedades intrínsecas del material. Los cambios superficiales resultantes dependen de la composición de la superficie y del gas usado.

Existen diferentes tipos de plasma, variando uno de otro sobre todo en función de su temperatura; plasmas calientes (el sol, la llama de una vela) y plasmas fríos (como la aurora boreal). Los plasmas también pueden ser clasificados de acuerdo a la presión existente en la zona donde ha sido generado, existiendo plasmas de baja presión y plasmas de presión atmosférica. Tendero et al. [89] estudiaron ambos tipos de plasma, concluyendo que en ambos casos se trata de plasmas que no están en equilibrio. Waters et al. [90] estudiaron el efecto del tratamiento superficial de plasma sobre la permeabilidad de compuestos farmacéuticos. Los resultados muestran que el tratamiento de plasma reduce la permeabilidad en la mayoría de los compuestos estudiados, apareciendo el efecto contrario en algunos compuestos (como la cafeína). Esto es indicativo de que la polaridad juega un papel muy importante en la permeabilidad, pudiendo ser

observado incluso a simple vista. Los principales efectos que pueden ser obtenidos gracias al tratamiento de plasma son:

-Limpieza (superficie libre de solvente y contaminantes) [91].

-Activación superficial (introduciendo funcionalidades, incrementando la mojabilidad) [88].

-Erosión superficial (pudiendo obtener resultados similares a decapados con ácido) [92].

-Recubrimientos superficiales (usando gases especiales como hexametildisiloxano-HMDSO, hexametildisilazano-HMDSN, o C2F6) [93].

Los tratamientos de plasma también son ampliamente utilizados en aplicaciones biomédicas [94], para esterilizar equipamientos quirúrgicos (bisturís, fórceps, u otros instrumentos metálicos). También son ampliamente utilizados para aumentar la mojabilidad de catéteres y materiales poliméricos desechables).

2.5.2.4.1 FLAMEADO

El tratamiento de flameado es el más antiguo de los tratamientos físicos. Incluye el uso de plasma caliente y es muy común en la industria; se usa principalmente para tratar poliolefinas [95]. El equipo consiste en un quemador de gas, generalmente de butano, aunque en algunos casos se pueden usar sopletes de acetileno con oxígeno que proporciona temperaturas más altas (entre 1000°C y 2000°C). Suelen ser equipos portátiles y son usados en el mismo lugar en el que se requiere el tratamiento. Su efecto no solo se debe a la alta temperatura de la llama, sino a las reacciones que van a generar numerosas especies excitadas. Para prevenir la combustión de sustancias contaminantes, el material tratado debe ser previamente limpiado y desengrasado. La llama a alta temperatura se obtiene mediante la combustión de una mezcla de gas inflamable y el oxígeno del aire. Los mejores resultados se obtienen con un exceso de oxígeno en la mezcla de la combustión. Los gases normalmente utilizados son el acetileno (es el más caro), butano y el propano.

Los parámetros que deben ser controlados en este tratamiento son: la proporción aire/gas de la llama, la distancia entre la superficie del material y la punta de la llama, y la duración y velocidad del tratamiento. La mayor desventaja de este tratamiento es que un mal uso en materiales poliméricos puede provocar un sobrecalentamiento y una posterior deformación del material. Pijpers and Meier [96] estudiaron el comportamiento adhesivo del polipropileno

después de un tratamiento de flameado utilizando para ello espectroscopía XPS (X-ray photoelectron spectroscopy). Los autores concluyen que la composición del gas (relación aire/propano) es el parámetro más importante respecto a la química de la superficie en el tratamiento de flameado de piezas de polipropileno. También determinan que la distancia entre la muestra y la llama influye en la química de la superficie. Además, otros factores como la presencia de ciertos aditivos en el polímero pueden causar problemas de adhesión inesperados.

2.5.2.4.2 TRATAMIENTO DE PLASMA DE BAJA PRESIÓN

Este tratamiento utiliza plasma frío y se realiza en una cámara de vacío, donde el gas es introducido después de alcanzar baja presión, estando la presión de trabajo en torno a 300 mbar. Este gas puede ser aire, oxígeno, nitrógeno, un gas noble o incluso metano, dependiendo del tipo de funcionalidades que la superficie final debe tener. En este tratamiento se genera un campo electromagnético producido por una bobina de inducción, donde las propias paredes de la cámara son los electrodos, produciéndose la ionización del gas [77].

Este proceso permite trabajar de forma segura y obtener resultados más precisos que al trabajar con tratamientos de flameado. Sin embargo, existe una limitación muy importante en el tamaño del reactor donde las piezas deben ser depositadas. Otra limitación radica en el hecho de que el equipo no puede ser instalado como parte de un sistema de producción continuo. Una solución existente en la industria para tratar más zonas en determinadas piezas es el uso de un tambor rotativo que permite activar toda la superficie de las muestras.

En este tratamiento los parámetros que deben ser controlados son principalmente el tiempo que está la muestra dentro de la cámara de vacío (o tiempo de residencia) y la potencia aplicada. Si el tiempo de residencia y/o la potencia aplicada en la cámara de vacío son muy altos, ceras u otros compuestos existentes en el material pueden migrar de la superficie. Esto va a provocar una disminución de la energía superficial del material tratado.

Sanchis et al. [97] modificaron la superficie de films de polietileno de baja densidad (LDPE) mediante plasma atmosférico de baja presión. Los autores utilizan el tratamiento de plasma para aumentar la mojabilidad del polímero, mejorando las propiedades adhesivas de la superficie y haciendo posible su uso para aplicaciones técnicas. Bajos tiempos de exposición al tratamiento resultan en la formación de especies polares en la superficie. Mientras que mayores tiempos de exposición provocan abrasiones en el polímero y una mayor rugosidad superficial. Nitschke et al. [98] modificaron la superficie de films de poli(3-hidroxibutirato) mediante un

tratamiento de plasma atmosférico de baja presión obteniendo una superficie hidrofílica con buena estabilidad a largo plazo.

2.5.2.4.3 TRATAMIENTO DE PLASMA ATMOSFÉRICO

En estos tratamientos se utilizan plasmas fríos que no están en equilibrio y que operan a presión atmosférica. Existen dos tipos de tratamientos con plasma atmosférico: descarga de corona y antorcha de plasma atmosférico.

2.5.2.4.3.1 DESCARGA DE CORONA

El tratamiento de descarga de corona consiste en la generación de plasma a partir de aire a presión atmosférica mediante la aplicación de alta frecuencia y alto voltaje eléctricos entre dos electrodos. Se utiliza principalmente para films de poliolefinas [99], aunque existen otros trabajos en la literatura en los que se ha utilizado esta técnica para tratar materiales compuestos de matriz epoxi [100].

Dentro de las características generales del tratamiento, una de las más importantes es la velocidad a la cual el tratamiento debe ser realizado (hasta 1600 m/min). Solo es posible tratar films, siendo posible su procesado por ambos lados. Este tratamiento es uniforme y fácil de usar. Es muy efectivo, creando grupos polares (carboxilos y carbonilos) en la superficie, promoviendo la adhesión mediante el aumento de la energía superficial del polímero o material compuesto a través del aumento de su componente polar. Puede también aplicarse en materiales compuestos de matriz termoplástica.

El mayor problema de este sistema radica en que el electrodo que emite la descarga tiene que situarse muy cerca de la superficie a tratar. Sin embargo, tiene la ventaja de permitir el control de las áreas donde la descarga es producida, pudiendo así realizar el tratamiento en partes específicas del film. La distancia entre el electrodo y el cilindro donde se coloca el film suele rondar los 1.5 mm. Esta distancia puede variar en films con mayores espesores, siendo posible utilizar espesores de hasta 6 mm.

2.5.2.4.3.2 ANTORCHA DE PLASMA ATMOSFÉRICO

Este tratamiento utiliza plasma frío que no está en equilibrio. El plasma se genera igual que en el tratamiento de corona. Se pueden utilizar diferentes tipos de gas para producir el plasma, entre los que se incluye el aire, oxígeno y los gases nobles. El plasma se genera mediante un campo magnético oscilante, usando placas capacitivas o inducción magnética. Al

colocar el gas a alta presión dentro de un campo eléctrico oscilante, los electrones de los átomos y las moléculas son aceleradas debido al efecto del aumento de la energía cinética y al calentamiento. Si el calentamiento alcanza niveles suficientemente altos, los electrones se liberan de los átomos y las moléculas, y el gas se ioniza.

Por medio de este sistema es posible crear una antorcha de plasma frío. La boquilla (o tobera) del plasma se fabrica con una muy alta precisión de contorno y está libre de potencial eléctrico (no transfiere voltaje al material). La llama tiene unos pocos centímetros de longitud, siendo suficiente para tratar las superficies del material. Dependiendo de la capacidad de la tobera, un solo haz de plasma puede alcanzar dimensiones de hasta 50 mm de longitud y 25 mm de ancho. Dependiendo de los requerimientos del tratamiento, el chorro de plasma puede recorrer desde 1 mm hasta 60 mm de longitud a una velocidad entre 0.1 y 600 m/min.

En aplicaciones donde una mayor superficie tiene que ser tratada, es posible instalar varias toberas en paralelo. Para el tratamiento de superficies más complicadas, existen toberas con más grados de libertad capaces de alcanzar toda la superficie del material.

Todas las técnicas de plasma modifican la superficie del material, incrementando la energía superficial. Estas técnicas también modifican la rugosidad; generalmente se reduce la micro-rugosidad pero se incrementa la nano-rugosidad [77,101].

Un ejemplo de aplicación de esta técnica es el trabajo de Encinas et al. [102]. Los autores tratan mediante antorcha de plasma la superficie de tres poliolefinas (HDPE, LDPE y PP) buscando mejorar la mojabilidad de las superficies. Los resultados muestran que el tratamiento aumenta las componentes total y polar de la energía superficial, siendo estable durante más de ocho meses frente a condiciones extremas de durabilidad.

Algunas técnicas con las que es posible observar estas modificaciones superficiales (incluso analizar los cambios de grupos funcionales) son SEM (Scanning Electron Microscopy) [103], AFM (Atomic Force Microscopy) [104], ATR-FTIR (Attenuated Total Reflection Fourier Transform Infrared Spectroscopy) [105], y XPS (X-ray Photoemission Spectroscopy) [106].

2.6 DISEÑO DE UNIONES ADHESIVAS

El diseño de la unión, junto la elección del adhesivo y el tratamiento superficial son los factores más importantes en una unión adhesiva. Los parámetros más importantes en el diseño de uniones adhesivas son:

-Solicitaciones o factores de carga [107]: es fundamental tener en cuenta la geometría de la unión, determinando el tipo y magnitud de los esfuerzos mecánicos a los cuales va a estar sometida la unión (torsión, compresión, cizalla, tensión, desgarro o pelado). También es importante conocer la forma en la que estos esfuerzos van a ser aplicados (esfuerzos estáticos, esfuerzos de fatiga o esfuerzos de impacto por ejemplo). Del mismo modo, es fundamental conocer el comportamiento mecánico del adhesivo y de los sustratos.

-Factores geométricos [108]: hay que estudiar la resistencia de los sustratos en relación con el tipo de adhesivo empleado y con las dimensiones de la unión (espesor del adhesivo y superficie adhesiva), así como la distribución de esfuerzos de la unión.

-Factores físico-químicos [109]: es necesario conocer los detalles del proceso de curado (velocidad, presión y temperatura) para diseñar el proceso de pegado adecuadamente.

-Factores de comportamiento en servicio [33,42,110]: es fundamental conocer las condiciones de servicio a las que va a estar sometida la unión durante su vida útil. Determinar el comportamiento frente a la temperatura, humedad, agentes químicos o ambientes que provoquen envejecimientos de la unión será siempre necesario.

De acuerdo a estos factores, cada unión adhesiva debe ser diseñada pensando en la aplicación específica en la que va a ser utilizada. De forma ideal ese diseño debe permitir que la unión trabaje principalmente a cizalla, evitando en todo momento que trabaje a pelado [111]. Es importante remarcar que utilizar diseños previos con origen en otros tipos de uniones (como soldaduras o remaches) no siempre es posible al trabajar con uniones adhesivas, siendo necesario realizar un estudio previo que valide el uso de adhesivos [107].

Además, incrementar el espesor del sustrato puede conducir a un aumento no deseado de la rigidez [112]. Mediante sistemas de mecanizado se puede reducir el espesor de los sustratos, y por tanto la rigidez de la unión [113].

Dada la complejidad de los mecanismos que envuelven a las uniones adhesivas, es extremadamente difícil y costoso identificar todas las características mecánicas y por tanto los factores de seguridad que deben ser tenidos en cuenta [114]. Sin embargo, cuanto mayor sea el número de datos conocidos sobre el sistema, menor será la incertidumbre existente, y menores medidas de seguridad será necesario tener en cuenta, lo que al final repercutirá en menores costes [115].

Para realizar un diseño correcto de uniones adhesivas, el procedimiento normal y más adecuado consiste en desarrollar modelos de simulación por elementos finitos [116,117,118]. Para ello es necesario conocer todas las propiedades mecánicas de los materiales (sustratos y adhesivos) e introducirlas en los modelos desarrollados [119]. Entre los programas más utilizados tanto académica como industrialmente se encuentran ANSYS, ABAQUS o MARC MENTAT. En muchas aplicaciones, particularmente aquellas que requieren del uso de uniones de alto rendimiento, es necesario realizar un elevado número de ensayos para validar los resultados. Del mismo modo, también será necesario analizar los resultados mediante distintos métodos estadísticos, como el test de Grubbs (para detectar outliers) o la distribución de Weibull (para calcular la fiabilidad de la unión) [33,120].

Actualmente la falta de seguridad que provocan los adhesivos, lleva a sobre-dimensionar las uniones, incrementando los costes sin necesidad, e incluso en algunas industrias se están realizando uniones hibridas [121,122]. La elección del diseño y la simulación de la unión pueden dar seguridad en esta técnica de unión.

2.7 SELECCIÓN DEL ADHESIVO

La selección del adhesivo debe ser acorde al tipo de sustrato a unir y a la aplicación en que va a estar localizada la unión. Por tanto, factores como la capacidad de adhesión del sustrato [123,124] (dependiente principalmente de características intrínsecas de la superficie como la energía superficial y la rugosidad), condiciones de servicio de la unión adhesiva [107] (tipo y magnitud de los esfuerzos), restricciones relacionadas con el proceso de producción [125] (método de aplicación, estabilidad), y requerimientos especiales de servicio [33] (factores químicos y ambientales) deben ser tenidos en cuenta.

A la hora de seleccionar un adhesivo, también son importantes las condiciones bajo las que la unión adhesiva va a ser formada o fabricada. Por ello es necesario estudiar la necesidad o

no de usar tratamientos superficiales [126], siendo también de vital importancia conocer otros factores como son:

-Si es necesario aplicar presión y/o calor durante el proceso de curado.

-Si el ambiente de curado tiene que ser en un medio inerte o puede ser al aire.

-El tiempo que puede estar el envase del adhesivo abierto, condiciones de almacenamiento y el intervalo de tiempo entre la aplicación del adhesivo sobre los sustratos y la unión de las dos partes que deben ser pegadas, es decir el tiempo abierto (EN 923:1998). Todos estos datos deben ser proporcionados por el proveedor en la ficha técnica correspondiente.

-Si es necesario utilizar sistemas de dosificación automáticos.

-Factores de salud y seguridad del proceso de fabricación en el sistema de producción. El proveedor debe de proporcionar una ficha de seguridad e higiene en el trabajo del adhesivo correspondiente.

-El precio del producto debe ser el primer factor a tener en cuenta y debe incluir los costes de adquisición y transporte del adhesivo, su vida útil, los costes de la preparación superficial, imprimaciones, equipos de dosificación del adhesivo, mantenimiento y reparación, cálculos de aplicación y tiempos de curado. Este coste está relacionado directamente con el coste del producto final.

Para el caso de materiales compuestos de matriz polimérica, y siempre que sea posible, se debe utilizar un adhesivo con la misma base química que la matriz. Al compartir la misma base química, es menos necesario utilizar tratamientos superficiales complejos, ya que la energía superficial del sustrato y la tensión superficial del adhesivo serán similares [127], y el adhesivo será capaz de mojar el material compuesto de forma adecuada. Sin embargo, para garantizar la durabilidad de la unión y su reproducibilidad, siempre será recomendable utilizar tratamientos superficiales (aunque sean relativamente complejos).

2.8 UNIONES MATERIAL COMPUESTO-METAL

La ciencia y tecnología de materiales compuestos ha crecido de forma exponencial durante los últimos años. La industria cada vez confía más en este tipo de materiales gracias a su

buen comportamiento a largo plazo y al alto rendimiento de los mismos. Estos materiales surgen de la necesidad de reemplazar las estructuras convencionales fabricadas con metales como el acero o el aluminio por estructuras más ligeras (y con mejores relaciones fuerza-peso y rigidez-peso) [128,129]. Sin embargo, los sistemas de materiales compuestos pueden ser utilizados para la fabricación de estructuras solo si se conocen la mayoría de las especificaciones (cargas, medio ambiente, inspección y coste). Un ejemplo del uso de materiales compuestos junto a metales son las superficies de control (como los alerones o flaps) de modelos de avión como el Airbus A380. El reto en este caso es establecer las metodologías adecuadas para el diseño y análisis de las uniones entre dos materiales disimilares (material compuesto-metal) [10,33,42,107,130]. Este campo está atrayendo la atención de numerosos investigadores e ingenieros de diseño, ya que es ampliamente conocido que la unión es considerada la parte más crítica en un conjunto ensamblado porque un fallo de este componente pondría en peligro la integridad de todo el conjunto [131].

En este contexto, existen diversos métodos capaces de unir materiales disimilares [10]. De forma genérica, se pueden dividir en dos categorías: uniones mecánicas [132] y uniones adhesivas [107]. Se conoce como uniones mecánicas a aquellas que involucran el uso de tornillos y remaches. Existen numerosas ventajas en este tipo de uniones que favorecen su elección por parte de los ingenieros de diseño. Es posible encontrar numerosas herramientas de análisis (tanto numéricas como empíricas) que pueden ser utilizadas para el estudio del rendimiento a medio y largo plazo permitiendo el desarrollo de diseños seguros. A su vez, debido a la gran cantidad de tiempo que estas técnicas llevan siendo utilizadas, existe numerosa regulación y normativa aprobada por importantes organizaciones internacionales [131,133,134,135]. Del mismo modo, los sistemas de producción son cada vez más automatizados. Otra ventaja muy importante es la capacidad de des-ensamblaje que las uniones mecánicas son capaces de ofrecer, pudiendo reemplazar las partes conectadas en caso de daño de forma más o menos rápida y sencilla.

Entre las desventajas de este tipo de uniones, está el hecho de tener que realizar modificaciones en las piezas (como taladros) que acabarán por convertirse en zonas de concentración de tensiones [136,137]. En componentes metálicos esta situación no es crítica, sin embargo en materiales compuestos puede dar lugar a una gran cantidad de problemas. Realizar un taladro en un material compuesto reforzado con fibra rompe la continuidad de las mismas, disminuyendo la resistencia del material drásticamente [138,139]. Esto hace necesario estudiar y optimizar el tipo y colocación del tejido de fibra en las zonas cercanas al taladro. Al realizar la

unión mecánica se produce un daño local debido a la concentración de tensiones antes comentada. Este hecho se vuelve mucho más relevante cuando la unión se somete a fatiga, pudiendo producirse roturas ante esfuerzos muy inferiores a los nominales [140].

La industria cada vez demanda el uso de estructuras más ligeras que sean capaces de mantener la rigidez y la resistencia de sus predecesoras [107], realizadas principalmente con metales. Esto solo es posible con el uso y desarrollo de nuevas técnicas de unión. Por ello, el campo de los adhesivos estructurales ha evolucionado con el desarrollo de un amplio rango de adhesivos provenientes de la industria química. Las razones por las que las uniones adhesivas son más adecuadas que otras uniones mecánicas tradicionales fueron estudiadas por Adams et al. [141]. Es muy común encontrar en la industria aeronáutica actual numerosas aplicaciones de uniones adhesivas con materiales compuestos. Así los últimos modelos de Airbus (A350 XWB) y Boeing (787 Dreamliner) contienen más del 50% de materiales compuestos unidos mediante adhesivos en su estructura. Otro modelo de Airbus, el A380 presenta alrededor del 25% de uniones basadas en adhesivos. Es incluso frecuente encontrar este tipo de uniones en aviación militar, así tanto el F-18 como el F-20 poseen zonas fabricadas con materiales compuestos y unidas mediante adhesivos en las alas y en las superficies de control. Toda esta tecnología ha sido adaptada a otras industrias con el paso de los años. Hoy en día es muy común encontrar este tipo de materiales y uniones adhesivas en barcos, edificios y automóviles [142,143,144]. Además, es posible reparar estructuras fabricadas en material compuesto gracias a la buena compatibilidad que en muchos casos tienen las matrices con los nuevos adhesivos estructurales disponibles [145,146].

2.8.1 GEOMETRÍAS DE LA UNIÓN

El diseño de la unión adhesiva está basado en la resistencia, fiabilidad y durabilidad de la superficie adhesiva. Un diseño basado en la aplicación a la que va a estar sometida la unión depende de las condiciones de carga aplicadas y en las propiedades mecánicas de los sustratos y del adhesivo. Por tanto, una unión bien diseñada debe ser capaz de soportar todas las cargas existentes en condiciones de servicio, con un grado de confianza y seguridad aceptables [147]. Dado que las tensiones se transfieren de un sustrato al otro a través de la capa adhesiva, generalmente se obtiene una mayor resistencia cuanto mayor es la superficie de adhesivo [148].

-Butt Joint o uniones a tope: este diseño se basa en la capacidad del adhesivo para soportar tensiones desarrolladas por los sustratos. El principal inconveniente del uso de este tipo de uniones es su incapacidad para resistir momentos de flexión, ya que harían que el adhesivo

sufriera esfuerzos de pelado. Además, este tipo de unión no puede ser utilizada cuando los sustratos no tienen el mismo espesor, ya que incluso para cargas axiales puras, su desequilibrio geométrico conducirá a concentraciones de tensiones no deseadas [131].

-Lap Joint o uniones a solape: este tipo de geometría es la más utilizada para el ensamblaje de materiales disimilares (como por ejemplo metales y materiales compuestos) o similares, porque son simples de fabricar, pueden ser utilizadas en sustratos finos, y por encima de todo, hacen trabajar al adhesivo de forma que la carga y la fractura ocurren principalmente bajo esfuerzos de cizalla. Dentro de este tipo de uniones, la unión a solape simple (Single Lap Joint – SLJ) [149] y la unión a solape doble (Double Lap Joint – DLJ) [150] son las configuraciones más estudiadas en la bibliografía. Desde el punto de vista teórico, su geometría simple ha motivado a muchos investigadores a realizar investigaciones de todo tipo (tanto de forma experimental, como de forma analítica o numérica) [151,152] respecto a la deformación de la unión, a las distribuciones de esfuerzos, a la rigidez y a la resistencia. Estos estudios están impulsados por la necesidad de vincular las condiciones de fabricación, las características geométricas y las propiedades de los materiales con la resistencia de las uniones.

El diseño correcto y eficiente de juntas implica la combinación de las configuraciones geométricas anteriormente mencionadas (y de otras configuraciones más complejas) con el objetivo de que el diseño final sea capaz de soportar todas las cargas aplicadas. Sin embargo, hay que tener en cuenta otros factores como el espesor de los sustratos, que afectará al modo de fallo y a la resistencia de la unión. Con sustratos más gruesos, es posible obtener mayores desalineaciones de la carga durante el ensayo de cizalla por tracción, dando como resultado el desarrollo de mayores tensiones de pelado que van a actuar en los bordes de la unión adhesiva, disminuyendo por tanto la resistencia de la misma. Sin embargo, si la alineación de la carga durante el ensayo es la adecuada, el pelado se reduce con el incremento del espesor del sustrato, manteniéndose constantes los valores de este esfuerzo a partir de un valor determinado de espesor [116].

2.9 TRANSPORTE PÚBLICO

Las principales formas de transporte público incluyen desde autobuses, taxis o metro, hasta trenes, tranvías o ferris. Sin embargo, el transporte público entre ciudades está dominado sin duda alguna por el uso de autocares, dejando el autobús al medio urbano [153].

El transporte público mejora la calidad de vida y provee importantes ventajas respecto del transporte privado, entre las que se encuentran: ahorro de combustible y reducción de emisión de gases de efecto invernadero [154,155]. Durante años, los materiales compuestos han sido ampliamente utilizados en la industria aeroespacial gracias a sus buenas características, entre las que destacan su baja densidad y alta resistencia específica. Del mismo modo, el uso de materiales compuestos en la fabricación de componentes para el sector del transporte terrestre está creciendo de forma significativa en los últimos años. Chehroudi [156] muestra cómo ha cambiado el uso de materiales en la fabricación de automóviles desde el año 1970 hasta la actualidad. En la década de los 70 el uso de materiales compuestos en automoción era prácticamente nulo, excepto para alguno modelos más exclusivos como el Chevrolet Corvette, que ya en la década de los 50 incorporó piezas fabricadas con fibra de vidrio. En el año 2000 ya se observa un uso generalizado de componentes de materiales compuestos, sobretodo en fibra de vidrio. Si se comparan estos modelos con aquellos fabricados a partir del año 2010, se observa un incremento del uso de elastómeros del 6%, del uso de plásticos en general del 19%, del uso de magnesio del 300%, y del uso de aluminio del 36%. Mientras que se reduce el uso de acero un 10%.

Sin embargo, estas tendencias aún están siendo adaptadas en la fabricación y diseño de autobuses y autocares. La falta de mano de obra cualificada, unido a la necesidad de realizar inversiones en I+D+I por parte de las empresas constructoras, ha llevado a que la mayoría de ellas aún opte por técnicas y materiales más tradicionales durante el proceso de fabricación de autobuses y autocares. Al reducir el peso de una estructura metálica, es necesario rediseñar el conjunto, implementando nuevas técnicas de fabricación dentro del proceso de producción.

Sin embargo, el uso de materiales compuestos en el sector transporte permitiría mejorar el rendimiento de los sistemas:

-Reduciendo el peso el 50% para aplicaciones estructurales y el 75% para aplicaciones no estructurales.

-Reduciendo el consumo de combustible.

-Reduciendo la inercia del vehículo.

-Disminuyendo el desgaste de la carretera.

-Permitiendo transportar mayores cargas, para consumos iguales de combustible.

Los materiales compuestos tienen un gran nicho de aplicación en el sector del transporte público por sus excelentes propiedades estructurales y su estética mejorada [157]. Así autobuses, autocares o vagones de tren más ligeros son fundamentales para lograr una mayor velocidad, con un menor consumo de combustible. Otro aspecto de vital importancia en los vehículos de pasajeros es la capacidad de la estructura para absorber la energía del impacto y mejorar la capacidad de supervivencia por parte de los pasajeros [158,159]. La resistencia al choque está relacionada con la capacidad de absorción de energía del conjunto, siendo necesario conocer los posibles mecanismos y modos de fallo a los que va a estar expuesta la estructura. Las características de los materiales compuestos hacen posible su aplicabilidad como buenos amortiguadores de energías de choque. Además en el transporte eléctrico no solo hay que proteger el habitáculo, sino que hay que proteger la batería ya que un golpe en ella produciría un incendio [160].

Es conocido que los materiales compuestos son capaces de absorber más energía por unidad de masa que los metales. Los polímeros reforzados con fibra suelen presentar modos de fallo frágiles en los que se ven involucrados mecanismos de absorción de energía muy eficientes [161]. Por tanto, aquellas estructuras de vehículos fabricadas con materiales compuestos son capaces de disipar mayor cantidad de energía que las estructuras metálicas convencionales [107].

El uso de materiales compuestos junto con otros materiales en estructuras, es un proceso de re-ingeniería dentro del diseño de procesos de unión. Las uniones adhesivas estructurales (aquellas en las que se utilizan adhesivos estructurales) son una alternativa viable a procesos de unión como la soldadura o el remachado, ya que son capaces de aportar numerosas ventajas sobre estos medios tradicionales (menor peso de la estructura, menores costes de fabricación y mejor tolerancia al daño) [107,162]. La aplicación de adhesivos para unir materiales compuestos reforzados con fibras a otros materiales ha crecido significativamente en los últimos años, tal y como explica Banea et al. [14].

El mayor uso de materiales compuestos ha dado como resultado un aumento de la variedad y formas de producción de los mismos [163]. Estas novedades representan múltiples desafíos para las uniones con adhesivos, ya que en muchos casos será necesario modificar los procesos de unión, o incluso rediseñar las partes o el modo de fabricación del conjunto. Esto puede suponer la necesidad de introducir cambios en los equipos, modificar los tiempos de aplicabilidad o manejo, desarrollar nuevos tratamientos superficiales, etc. Todo esto es posible gracias a la buena eficiencia y flexibilidad intrínseca en las uniones con adhesivos, que son

capaces de dotar de flexibilidad al proceso de producción (pudiendo reducir por tanto los tiempos de fabricación), y resultando finalmente en un aumento de la competitividad de las compañías que usan esta tecnología [164].

La forma ideal para fabricar cualquier estructura de material compuesto es como un componente integral (o monolítico). Sin embargo, las limitaciones existentes hoy en día en los procesos de fabricación de materiales compuestos impiden que esto pueda realizarse así siempre [165]. Por ello, las uniones adhesivas resultan fundamentales para resolver esta problemática.

Los materiales compuestos tienen propiedades diferentes a aquellos materiales tradicionalmente utilizados, por tanto se deberán tener en cuenta otras variables en el diseño. En muchos casos se puede dar la circunstancia de tener que unir materiales disimilares, con lo que algunas consideraciones como los diferentes coeficientes de expansión térmica las distintas tenacidades a fractura deben ser tenidas en cuenta [166].

Finalmente, para poder obtener los resultados óptimos, se debe integrar la aplicación del adhesivo dentro del proceso de fabricación. Esto supone conocer los costes de operación, los tiempos de producción, la fiabilidad y la calidad del producto (entre otras consideraciones). La reducción del peso en estructuras metálicas ha supuesto un reto importante para diseñadores e ingenieros en los últimos años [167,168]. Por tanto, el uso de nuevos materiales e innovaciones en los procesos de producción abren un gran abanico de posibilidades con las que ser capaces de superar este reto.

Otro reto en el uso de adhesivos para aplicaciones estructurales es el comportamiento de estas uniones a largo plazo cuando están expuestas a diferentes medios y condiciones ambientales [33,42]. Así por ejemplo, la unión adhesiva empleada en el AVE que conecta las ciudades de Medina La Meca debe ser capaz de resistir las altas y bajas temperaturas del desierto durante los trayectos diurnos y nocturnos respectivamente, así como soportar el efecto abrasivo de la arena al impactar sobre las mismas a velocidades de hasta 450 km por hora [169].

Baldan [146] dedujo que la forma más efectiva para poder obtener altas resistencias y buenas durabilidades en uniones adhesivas con materiales compuestos es modificando las condiciones de la superficie. De este modo, un buen tratamiento superficial permite obtener uniones estables y robustas entre el adhesivo y el sustrato. Existen numerosas referencias en la literatura en las que se detallan diferentes tratamientos superficiales sobre materiales compuestos. Encinas et al. [170] desarrollan modificaciones superficiales mediante abrasión y

tratamientos de plasma atmosférico para realizar uniones adhesivas con polipropileno. También se ha estudiado cómo afecta la modificación de la rugosidad superficial a la mojabilidad de distintos polímeros como el polietileno de alta y baja densidad (HDPE y LDPE), el polipropileno (PP) y la silicona [102]. Las modificaciones de la superficie de materiales compuestos de matriz epoxi reforzados con fibras de vidrio y de carbono han sido estudiadas después de un tratamiento de plasma atmosférico, encontrando que la eficacia del tratamiento depende del método de preparación del material compuesto [171].

2.9.1 AUTOBUSES Y AUTOCARES

El principal reto al que se enfrenta la industria del transporte colectivo mediante autobuses y autocares es el de la reducción del consumo de combustible, haciendo más eficientes los vehículos. El modo más lógico de lograr este reto es mediante la reducción del peso utilizando para ello materiales más ligeros como los PMC's [107].

El autobús/autocar tiene una superestructura montada sobre un chasis. Sobre ella se panela suelo, techo, laterales, lunas, etc. Aunque la superestructura de los autobuses y/ o autocares es de acero, los fabricantes utilizan una gran variedad de materiales y procesos en el ensamblaje del vehículo. Por ello, existe una gran cantidad de posibles aplicaciones de adhesivos estructurales y no estructurales en ellos. En la Figura 7 se muestran seis aplicaciones actuales en autobuses y autocares de uniones adhesivas de PMC [172]: suelo (1), módulo frontal (2), techo (3), paneles laterales y puertas de equipaje (4), paneles del arco de rueda (5) y módulo trasero (6). Todas las aplicaciones mencionadas son panelados sobre la superestructura, de acero. Estos panelados no se pueden considerar como parte de la superestructura, aunque aportan rigidez torsional, resistencia a impactos, etc.

Una de las aplicaciones más importantes de los adhesivos en el panelado de autobuses es el pegado de los paneles del techo (fabricados con materiales compuestos reforzados con fibra de vidrio). El conjunto está sometido a condiciones de servicio en las que se deben soportar cambios de temperatura continuos. Por otro lado, los diferentes materiales empleados poseen diferentes coeficientes de expansión térmica, con lo que el sistema de unión debe ser capaz de compensar todos estos desajustes y movimientos; el espesor de adhesivo es un factor fundamental para compensar las expansiones diferenciales que se producen [173]. Las uniones mecánicas tradicionales no son capaces de solventar esta problemática, ya que son rígidas [174]. Estas uniones suponen un riesgo para el conjunto, y por tanto para el vehículo, al ser zonas preferenciales de concentración de tensiones.

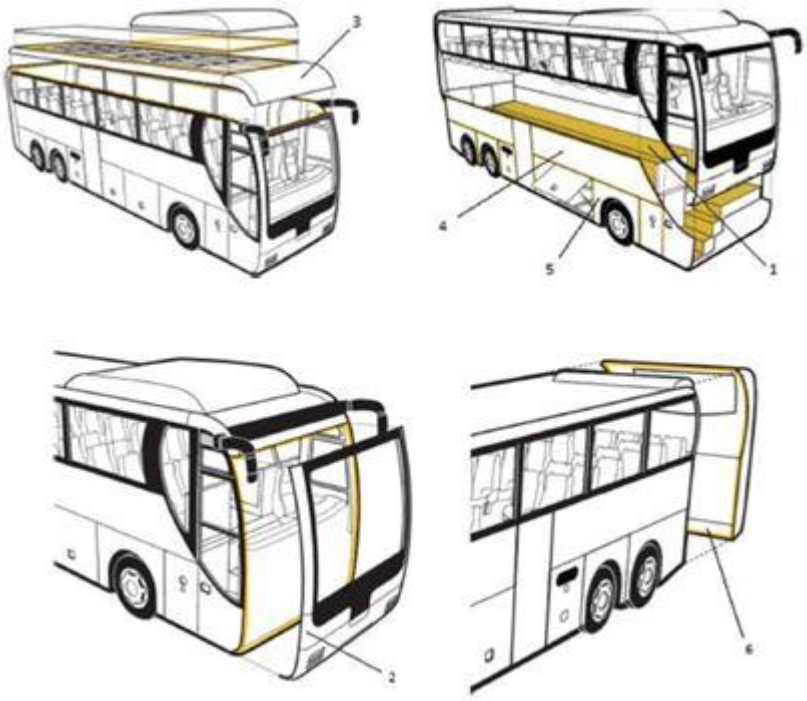

Figura 7. Ejemplos de aplicación actual de uniones adhesivas de materiales compuestos en autobuses y autocares [172].

En los últimos años, se han producido grandes avances en la parte aerodinámica y estética tanto en autobuses como en autocares. Esto ha sido posible en gran medida gracias al avance de los PMC's [175]. Un ejemplo claro de estas mejoras son los módulos frontal y trasero, fabricados con materiales compuestos de matriz polimérica reforzados con fibra de vidrio (GFRP). En general, el uso de PMC's en la fabricación de componentes de todo tipo es una práctica común en la industria y ha ayudado a que las mejoras expuestas anteriormente hayan sido posibles. Además, estos materiales tienen buena durabilidad [176] y resistencia a impacto [177].

Junto con las aplicaciones anteriormente descritas, la industria está centrando sus esfuerzos en ampliar el uso de los PMC's y más en con concreto los GFRP y los CFRP a partes de la superestructura del vehículo, lo cual llevaría asociado un mayor uso de uniones adhesivas.

Un ejemplo práctico del uso de PMC's y adhesivos en la industria de los autobuses/autocares es el de la empresa Optare PLC cuyo modelo Metrocity ha sido fabricado de una sola pieza con un cuerpo de material compuesto dentro del cual se ha incorporado (durante el proceso de moldeo) un marco de acero inoxidable. La unión entre el cuerpo de material compuesto y el marco de acero inoxidable se realiza mediante un adhesivo de metacrilato

bicomponente, desarrollado por ITW Performance Polymers cuyo nombre comercial es ITW Plexus® [153].

Otro ejemplo es el modelo desarrollado por North American Bus Industries Inc. que ha desarrollado un autobús con todo el cuerpo de material compuesto. La estructura del autobús consiste en un material compuesto híbrido formado por una piel externa de material termoplástico sin reforzar (fabricada mediante tecnología de termoformado de bajo coste), y una parte estructural formada por compuestos termoplásticos de baja densidad (fabricados por moldeo por compresión a baja presión). Los componentes de material compuesto son ensamblados mediante uniones adhesivas usando cintas adhesivas sensibles a la presión de la compañía 3M (3M VHB Tape 5952) [153].

2.10 INGENIERÍA CIVIL: REFUERZO DE ESTRUCTURAS CON MATERIALES COMPUESTOS

El uso de materiales compuestos reforzados con fibra (FRP) unidos externamente con adhesivos en estructuras civiles ha crecido exponencialmente en los últimos años [178,179,180,181]. De esta forma ha sido posible reforzar, reparar y reequipar eficientemente estructuras antiguas de muy diferentes materiales (acero, aluminio, cemento, etc.) [167,168,182].

Esto ha sido posible gracias a las propiedades intrínsecas de los FRP: resistencia frente a la corrosión, bajo peso, fácil aplicación en espacios pequeños, muy altos valores de resistencia a la tracción, gran capacidad de deformación, y prácticamente ilimitada disponibilidad en términos de tamaños, geometrías, y dimensiones. Sin embargo, la principal desventaja de estos composites es que el comportamiento mecánico es generalmente elástico lineal hasta rotura sin mostrar signo alguno de límite elástico o deformación plástica [183].

Por ejemplo, las estructuras de cemento necesitan ser reforzadas cuando la resistencia o rigidez de los miembros existentes es insuficiente [184,185]. El incremento de las cargas, los errores de construcción o de diseño pueden provocar que la resistencia de la estructura sea menor de lo esperado. Un método de refuerzo actualmente utilizado consiste en adherir piezas o partes de CFRP laminado a la superficie de las vigas metálicas o de cemento con el objetivo de repararlas o incrementar su capacidad [186,187]. Los materiales normalmente utilizados para realizar estos refuerzos son adhesivos estructurales (poliuretanos y epoxis) y laminados de CFRP.

En la década de los 80, los FRP empezaron a utilizarse en aplicaciones de ingeniería civil [188,189,190,191,192]. Los elementos preformados de FRP resultaron ser ideales como refuerzo externo de miembros de acero y cemento. Hasta ese momento, se empleaban elementos de acero como refuerzo [193], siendo más pesados y difíciles de instalar que los elementos de material compuesto reforzado con fibras [181]. Además, las piezas fabricadas en FRP no se oxidan como si ocurre con las equivalentes de acero por formación de pilas de concentración [194].

Ghafoori et al. [167] presentan un nuevo criterio de diseño para el refuerzo frente a la fatiga de un puente metálico de 120 años de antigüedad en Suiza. Del mismo modo, también desarrollan un nuevo sistema de refuerzos pre-tensados de CFRP. Este método permite disminuir el tiempo requerido para la instalación del refuerzo, ya que no es necesario realizar preparación superficial en la superficie metálica del puente. Hosseini et al. [168] estudian el refuerzo de un puente metálico del siglo XIX usando elementos de CFRP pre-tensados y no pre-tensados (unidos a la estructura mediante adhesivos). Ellos demuestran que los esfuerzos de tracción en las vigas del puente son reducidos un 15% utilizando refuerzos no pre-tensados y alrededor de un 44% utilizando refuerzos pre-tensados. Ghafoori et al. [182] muestran otra aplicación de refuerzos pre-tensados de CFRP en otro puente metálico de más de 120 años de antigüedad, pero esta vez situado en Australia. En este caso utilizan una red de sensores inalámbricos para monitorizar el comportamiento del puente una vez aplicado el refuerzo. Los resultados muestran que el nuevo sistema es muy eficiente de cara al fortalecimiento de las vigas del puente frente al comportamiento a flexión y fatiga.

La introducción de FRP supone también la necesidad del uso de nuevos tratamientos superficiales. Tal y como se explica anteriormente en esta introducción (ver 1.6), los polímeros en general, y los materiales compuestos en particular, poseen bajos valores de energía superficial. Por tanto requerirán de tratamientos superficiales especiales para lograr una unión adhesiva óptima (plasma atmosférico, imprimaciones, etc.). Además, al tratarse de uniones de materiales disimilares, hay que tener en cuenta las diferentes propiedades de los sustratos (sobre todo en cuanto a los diferentes coeficientes de expansión térmica).

Además, la capa de adhesivo aplicada entre el refuerzo y la estructura puede presentar problemas por el comportamiento de los miembros reforzados. Pueden aparecer esfuerzos de pelado (los más perjudiciales para uniones adhesivas) en las zonas inicial y final de instalación de los refuerzos, induciendo a la separación de la pieza de PMC de la estructura principal. Si estos esfuerzos de pelado son mayores que la resistencia del adhesivo, todo el miembro de PMC

se despegará de la estructura, provocando un problema grave de seguridad por la caída de miembros suspendidos y por la pérdida de resistencia debido a la desaparición del refuerzo [195].

Del mismo modo, el adhesivo puede sufrir complicaciones debido a la aparición de grietas en la estructura principal. Esto es especialmente preocupante cuando la capa de adhesivo se sitúa entre las dos partes de la grieta, haciendo que la misma entre en contacto con el adhesivo. La viga o estructura reforzada puede llegar a perder resistencia de manera crítica, dando lugar a fallos catastróficos inesperados [196].

Pese a los inconvenientes o complicaciones mostradas, las vigas reforzadas con FRP tal y como se plantea en este apartado muestran un incremento importante de los valores de resistencia, además de mejorar la capacidad de carga y la rigidez, y el comportamiento a flexión de toda la estructura [197].

2.10.1 PROCESO DE IMPLANTACIÓN DE LOS REFUERZOS

El refuerzo de estructuras metálicas mediante el uso de FRP está ampliamente extendido en la industria. La clave para obtener un refuerzo de calidad se encuentra en obtener la mejor adherencia posible entre el sustrato metálico y el PMC. El comportamiento mecánico de la estructura reforzada va a depender principalmente de las características superficiales de la estructura metálica, de la resistencia del material de esta estructura, las medidas de los refuerzos de PMC y la resistencia del adhesivo.

La resistencia de la unión adhesiva entre el acero y el FRP depende tanto de las características superficiales de ambos sustratos [198] como del rendimiento del adhesivo [199]. El procedimiento básico para la aplicación de estos refuerzos de composite en estructuras de acero consiste en tres fases:

-Preparación de la superficie de acero: es fundamental realizar los tratamientos superficiales adecuados para optimizar la unión adhesiva. Entre los tratamientos más utilizados en sustratos de acero se encuentra el lijado, el granallado, el decapado con ácido o el uso de imprimaciones.

-Preparación de la superficie del FRP: al igual que para la superficie del acero, es fundamental realizar el tratamiento superficial adecuado. Al tratarse de un polímero, los bajos valores de energía superficial intrínsecos de este material hacen necesario optimizar el

tratamiento superficial. Entre los tratamientos más comunes se encuentra el plasma atmosférico o las imprimaciones. Dentro de todo el conjunto acero-adhesivo-FRP, la intercara relativa al FRP será la parte más compleja y delicada, requiriendo por tanto de un mayor control de calidad [200].

-Selección del adhesivo: por regla general en este tipo de aplicaciones se utilizan adhesivos epoxi o adhesivos de poliuretano, ambos estructurales. Los adhesivos epoxi son materiales bicomponentes que curan por polimerización al entrar en contacto el componente A (resina) y el componente B (catalizador), necesitando en muchos casos un curado con temperatura o un post-curado. Los epoxis estructurales tienen alta resistencia pero también alta rigidez. En cuanto a los adhesivos de poliuretano, su principal diferencia respecto a los epoxis es la mayor capacidad de deformación y mejor comportamiento frente a agentes externos como la humedad, con altos valores de resistencia, aunque menores que la de los epoxis estructurales. El problema de estos poliuretanos estructurales es actualmente el tiempo de curado, aunque se han empezado a fabricar poliuretanos de curado rápido. El adhesivo seleccionado debe ser capaz de asegurar la calidad de la unión entre ambos sustratos durante toda la vida útil del refuerzo [33,42].

2.11 ESTUDIO DE SINGULARIDADES EN UNIONES ADHESIVAS

Tal y como se explica en profundidad en varios de los apartados de esta introducción (o estado del arte), los adhesivos son capaces de aportar diversas ventajas respecto a otras técnicas tradicionales de unión. Entre estas ventajas cabe destacar la baja densidad y costes de estos materiales [201], distribución homogénea de cargas [202] y habilidad para proteger frente a la corrosión entre otros [203].

El gran aumento del uso de adhesivos en los últimos años hace necesario desarrollar nuevas técnicas capaces de evaluar con precisión el comportamiento y habilidad de las uniones adhesivas. Los métodos basados en elementos finitos (FEM - Finite Elements Method) han demostrado ser una herramienta muy efectiva para realizar los cálculos en este tipo de uniones. En la literatura existen numerosos trabajos basados en elementos finitos en los que se realizan muy diversos cálculos de uniones adhesivas. Xará y Campilho [204] demostraron, usando diferentes criterios de iniciación, que los elementos finitos son una herramienta precisa y apropiada para predecir la resistencia en uniones adhesivas tanto con adhesivos rígidos como con

adhesivos elásticos. Por otro lado, Li et al. [205] y Noda et al. [206] dedujeron que la resistencia del adhesivo puede ser controlada en la parte final de la intercara por el campo de singularidades (ISSF – Intensity of Singular Stress Field). Del mismo modo, la resistencia en uniones a solape simple puede ser dada como Kσc = constante, donde Kσc son los valores críticos de intensity of singular stress. Por su parte, Mintzas and Nowell [207] comprobaron que la resistencia de la unión adhesiva puede ser expresada como Hcr = constante. Por lo tanto, existen métodos lógicos y eficientes basados en el ISSF que pueden ser aplicados para evaluar la resistencia del adhesivo. Wang y Rose [208] desarrollaron un trabajo novedoso en el cual muestran soluciones compactas para las singularidades situadas en las esquinas de las intercaras adhesivo-sustrato en uniones a solape simple. Estos autores utilizan un método numérico de expansión asintótica para el caso particular de sustratos rígidos. La idoneidad de las soluciones analíticas está demostrada ya que son capaces de ofrecer buenos resultados en cuanto a singularidades se refiere con respecto a los resultados obtenidos por elementos finitos usando una malla fina en la esquina adhesivo/sustrato. Goglio y Rossetto [209] calcularon la relación existente entre el factor de intensidad de tensiones y las tensiones estructurales máximas en el adhesivo en el extremo del solape. Estos autores proponen un procedimiento para estimar el factor de intensidad de tensiones sin necesidad de un análisis detallado de las uniones por elementos finitos. Las ecuaciones del problema se resuelven mediante un procedimiento numérico válido. La validez de este procedimiento es evaluada para uniones adhesivas a solape simple mediante la combinación de diferentes valores de los parámetros de la unión, y estableciendo el tipo de esfuerzo que debe ser considerado para obtener la definición correcta del factor de intensidad de tensiones.

La configuración de unión adhesiva elegida de manera mayoritaria en esta tesis doctoral es a solape simple (o single lap joint por sus siglas en inglés). UNE-EN 1465 detalla cómo calcular la resistencia adhesiva en uniones a solape simple. Sin embargo, es importante remarcar que las posibles variables existentes en cuanto a configuración se refiere afectan de manera significativa a la resistencia promedio de la unión (τave), y por lo tanto esta fuerza no puede expresarse como τave = constante tal y como dedujeron Li et al. [192].

De forma ideal, los ensayos de probetas de solape simple se deben realizar bajo cargas puramente de cizalla, pero la existencia de otras cargas es bien conocida en la literatura, estando esto asociado a la aparición de otros esfuerzos como el pelado [33]. El esfuerzo de pelado máximo está localizado dentro de la unión adhesiva cerca de la intercara adhesivo sustrato en el

borde de la esquina (Figura 8), tal y como es explicado por da Silva y Adams [111] y Martinez et al. [210] en sus trabajos.

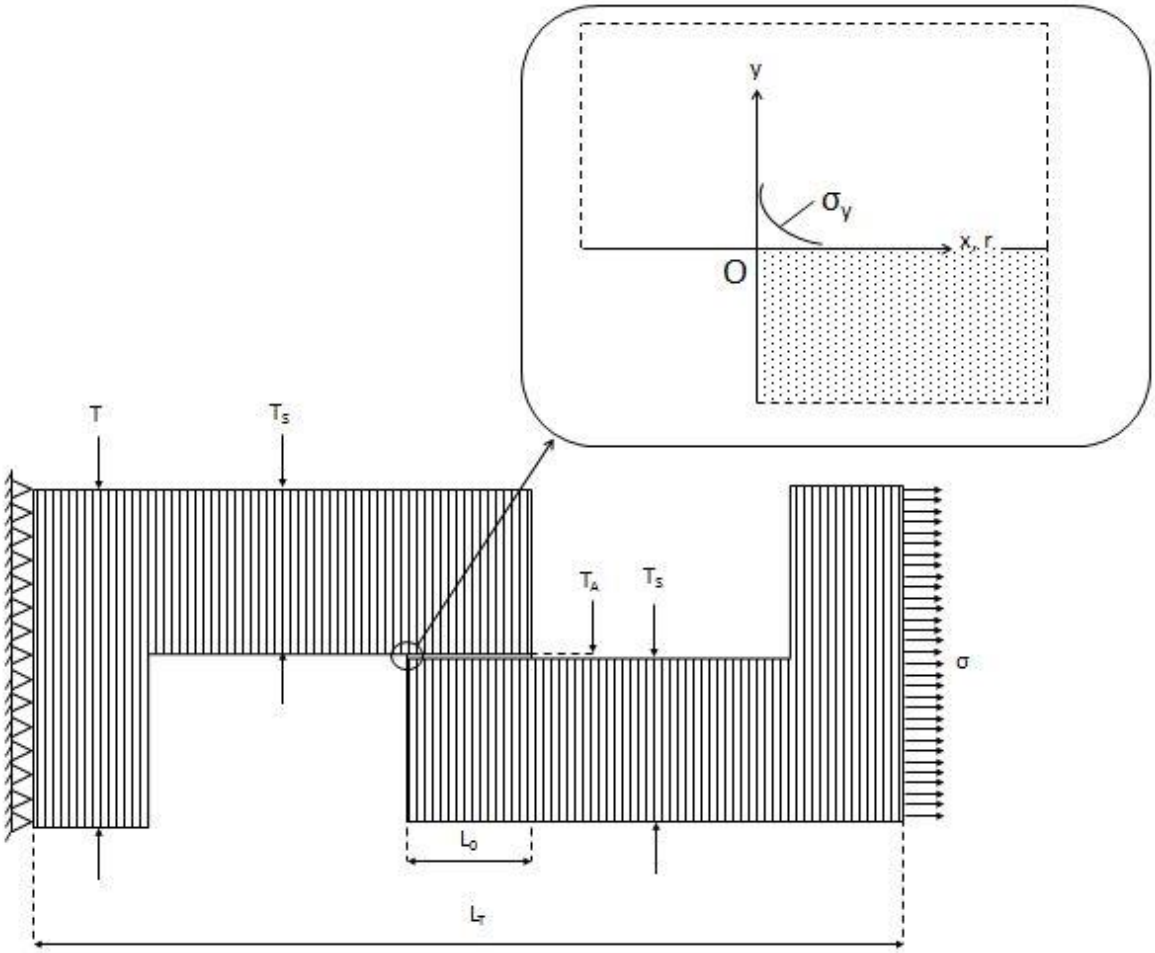

Figura 8. Localización del punto (O) donde se encuentran los esfuerzos máximos de pelado en uniones adhesivas a solape simple [116], siendo T el espesor total de la probeta, T_S el espesor de cada uno de los sustratos de acero, T_A el espesor de adhesivo, L_0 la longitud de solape del adhesivo y σ el esfuerzo de cizalla.

Li et al. [211] dedujeron que el ISSF en el punto O (Figura 4) está relacionado con el esfuerzo de pelado, y del mismo modo, este esfuerzo depende directamente de la rigidez y espesor del adhesivo. Una solución válida y aceptada para reducir estos esfuerzos de pelado, es el uso de uniones adhesivas mixtas [116]. Incorporar diferentes adhesivos (con diferentes propiedades mecánicas) puede mejorar la distribución de tensiones y también reducir estos esfuerzos. En la literatura existen numerosos trabajos que ahondan en este tipo de uniones, incluyendo alguna de las investigaciones desarrolladas en esta tesis doctoral [116], donde se estudian cuatro modelos diferentes de uniones adhesivas, logrando reducir los esfuerzos de

pelado en uniones a solape simple. Para ello, se utiliza un adhesivo más elástico en las esquinas y un adhesivo más rígido en la zona central. Chiminelli et al. [212] utilizan uniones adhesivas mixtas, y muestran que es posible incrementar la carga última alrededor del 70% respecto a configuraciones en las que se utiliza un solo adhesivo. Breto et al. [213] estudian el impacto de las singularidades por medio de dos metodologías independientes, para poder seleccionar el material intermedio entre dos bandas de adhesivo en uniones mixtas. Fitton et al. [214] muestran el efecto de utilizar uniones adhesivas a solape simple con módulos variables, concluyendo que este tipo de uniones son capaces de reducir la concentración de tensiones, incrementar la resistencia de la unión, reducir las dispersiones e incluso cambiar el modo de fallo. Da Silva et al. [215] comparan uniones adhesivas mixtas con uniones fabricadas con un único adhesivo rígido, obteniendo mayores resistencias en uniones adhesivas mixtas. Carbas et al. [216] han creado un método de calentamiento por inducción para fabricar uniones adhesivas funcionalmente graduadas obteniendo una mejora del rendimiento cercana al 70%.

2.12 BIBLIOGRAFÍA

[1] Strong AB. Fundamentals of composites manufacturing, materials, methods, and applications. Society of Manufacturing Engineers, USA; 2008.

[2] Sallal HA, Abdul-Hamead AA, Othman FM. Effect of nano powder (Al2O3-CaO) addition on the mechanical properties of the polymer blend matrix composite. Defence Technology 2019. DOI: https://doi.org/10.1016/j.dt.2019.07.013.

[3] Batista MDR, Drzal LT. Carbon fiber/epoxy matrix composite interphases modified with cellulose nanocrystals. Composites Science and Technology 2018; 164: 274-81.

[4] Monteiro SN, Terrones LAH, Lopes FPD, d'Almeida JRM. Mechanical strength of polyester matrix composites reinforced with coconut fiber wastes. Revista Matéria 2005; 10: 571-6.

[5] Holmes M. Carbon fibre reinforced plastics market continues growth path (Part 1). Reinforced Plastics 2013; 57: 24-9.

[6] Morioka K, Tomita Y, Takigawa K. High-temperature fracture properties of CFRP composite for aerospace applications. Materials Science and Engineering 2001; A319-321: 675-8.

[7] Adam H. Carbon fibre in automotive applications. Materials & Design 1997; 18: 349-55.

[8] Kluke M. The joining of composite materials: the best of both worlds. Reinforced Plastics 2018; 62: 79-81.

[9] Botelho EC, Silva RA, Pardini LC, Rezende MC. A review on the development and properties of continuous fiber/epoxy/aluminum hybrid composites for aircraft structures. Materials Research 2006; 9: no.3. DOI: http://dx.doi.org/10.1590/S1516-14392006000300002.

[10] Kah P, Suoranta R, Martikainen J. Techniques for joining dissimilar materials: metals and polymers. Reviews on Advanced Materials Science 2014; 36(2): 152-64.

[11] Van Straalen IJJ, Van Tooren MJL. Building and construction – steel and aluminium. In: Adams RD, editor. Adhesive Bonding. Science, Technology and Applications. Woodhead Publishing, United Kingdom; 2005.

[12] Ebnesajjad S. Appendix A - Safety, environmental, and economic aspects and future trends. In: Handbook of Adhesives and Surface Preparation. p.387-93. William Andrew Publishing, USA; 2011.

[13] Witten E, Mathes V, Sauer M, Kühnel M. Market developments, trends, outlooks and challenges. Composites Market Report 2018 [Online]. Disponible: https://www.avk-tv.de/files/20181115_avk_ccev_market_report_2018_final.pdf [Accessed 23-09-2019].

[14] Banea MD, da Silva LFM. Adhesively bonded joints in composite materials: an overview. Proceedings of the institution of Mechanical Engineers, Part L: Journal of Materials Design and Applications 2009; 223(1): 1-18.

[15] Haraga K, Taguchi K, Yoda K, Nakashima Y. Assembly technique for control panel enclosures with the combined use of adhesive and rivets and the reduction of energy consumption. International Journal of Adhesion & Adhesives 2003; 23: 371-6.

[16] Hu P, Akhmet G, Wu CW, Han X, Chao YX, Yu Y, Orazbayeva A. Characterisation on the influence of curing history on the mechanical performance of adhesively bonded corrugated sandwich structures. Thin-Walled Structures 2019; 142: 37-51.

[17] Han X, Chao Y, Zhang W, Chao Y, Wu C. Study on the effect of post curing on the mode II fracture energy of structural adhesive using a parameter identification approach. International Journal of Adhesion & Adhesives 2019; 95: 102398.

[18] Marques EAS, da Silva LFM, Flaviani M. Testing and simulation of mixed adhesive joints for aerospace applications. Composites Part B: Engineering 2015; 74: 123-30.

[19] Fessel G, Broughton JG, Fellows NA, Durodola JF, Hutchinson AR. Evaluation of different lap-shear joint geometries for automotive applications. International Journal of Adhesion & Adhesives 2007; 27: 574-83.

[20] Alia C, Arenas JM, Suarez JC, Pinilla P. Mechanical behavior of polyurethane adhesive joints used in laminated materials for marine structures. Ocean Eng 2016;113: 64-74.

[21] Zdrahala RJ, Zdrahala IJ. Biomedical Applications of Polyurethanes: a review of past promises, present realities, and a vibrant future. Journal of Biomaterials Applications 1999;14: 67-90.

[22] Mays GC. Structural applications of adhesives in civil engineering. Materials Science and Technology 1985; 1: 937-43.

[23] Bowditch MR. The durability of adhesive joints in the presence of water. International Journal of Adhesion & Adhesives 1996; 16: 73-9.

[24] Viana G, Costa M, Banea MD, da Silva LFM. A review on the temperature and moisture degradation of adhesive joints. Proceedings of the Institution of Mechanical Engineers, Part L: Journal of materials: Design and applications 2016; 0(0): 1-14.

[25] Korta J, Mlyniec A, Uhl T. Experimental and numerical study on the effect of humidity-temperature cycling on structural multi-material adhesive joints. Composites Part B: Engineering 2015; 79: 621-30.

[26] Agarwal A, Foster SJ, Hamed E. Testing of new adhesive and CFRP laminate for Steel-CFRP joints under sustained loading and temperature cycles. Composites Part B: Engineering 2016; 99: 235-47.

[27] Costa M, Viana G, da Silva LFM, Campilho RDSG. Effect of humidity on the fatigue behaviour of adhesively bonded aluminium joints. Latin American Journal of Solids and Structures 2017; 14: 174-87.

[28] Matthews FL, Kilty PPF, Godwin EW. A review of the strength of joints in fibre-reinforced plastics 2: adhesively bonded joints. Composites 1982; 13(1): 29-37.

[29] Anes V, Pedro R, Henriques E, Freitas M, Reis L. Bonded joints of dissimilar adherends at very low temperatures – An adhesive selection approach. Theoretical and Applied Fracture Mechanics 2016; 85: 99-112.

[30] Ali HT, Wahab MA. History of adhesive composite joints. In: Wahab MA, editor. Joining Composites with Adhesives: Theory and Applications. DEStech Publications Inc., USA; 2015.

[31] ASTM D5573 – 99 (2019). Standard practice for classifying failure modes in fiber-reinforced-plastic (FRP) joints. ASTM International, West Conshohocken, PA, 2019.

[32] Ebnesajjad S. Theories of adhesion. In: Surface treatment of materials for adhesive bonding. p.77-91. William Andrew Publishing, USA; 2014.

[33] Galvez P, Abenojar J, Martinez MA. Durability of steel-CFRP structural adhesive joints with polyurethane adhesives. Composites Part B: Engineering 2019; 165: 1-9.

[34] Ye J, Yan Y, Hong Y, Guo F. An integrated constitutive model for tensile failure analysis and overlap design of adhesive-bonded composite joints. Composite Structures 2019; 223: 110986.

[35] Liu PF, Peng XQ, Guo ZY, Leng JX, Jiao L. Viscoelastic bilinear cohesive model and parameter identification for failure analysis of adhesive composite joints. Composite Structures 2019; 224: 111016.

[36] Tosun E, Çalık A. Failure load prediction of single lap adhesive joints using artificial neural networks. Alexandria Engineering Journal 2016; 55: 1341-6.

[37] Pantelakis S, Tserpes KI. Adhesive bonding of composite aircraft structures: Challenges and recent developments. Science China Physics, Mechanics & Astronomy 2014; 57: 2-11.

[38] Ciupack Y, Pasternak H, Mette C, Stammen E, Klaus D. Adhesive bonding in steel construction - Challenge and innovation. Procedia Engineering 2017; 172: 186-93.

[39] Wahab MA. Aerospace: application to aircraft structures. In: Wahab MA, editor. Joining Composites with Adhesives: Theory and Applications. DEStech Publications Inc., USA; 2015.

[40] Wahab MA, Crocombe AD, Beevers A, Ebtehaj K. Coupled stress-diffusion analysis for durability study in adhesively bonded joints. International Journal of Adhesion & Adhesives 2002; 22(1): 61-73.

[41] Hart-Smith LJ. A peel-type durability test coupon to assess interfaces in bonded, co-bonded, and co-cured composite structures. International Journal of Adhesion & Adhesives 1999; 19(2–3): 181-91.

[42] Galvez P, Abenojar J, Martinez MA. Effect of moisture and temperature on the thermal and mechanical properties of a ductile epoxy adhesive for use in steel structures reinforced with CFRP. Composites Part B: Engineering 2019; 176: 107194.

[43] BTI Bond Tech Industries Inc. Safety Tips for Working with Industrial Adhesive. Blog 2014 [Online]. Disponible: https://www.bond-tech-industries.com/about-us/blog/safety-tips-working-industrial-adhesive/ [Accessed 24-09-2019].

[44] Wegman RF, Van Twisk J. Surface preparation techniques for adhesive bonding. William Andrew Publishing, USA; 2013. DOI: https://doi.org/10.1016/C2012-0-02158-8.

[45] Banea MD, da Silva LFM, Carbas RJC. Debonding on command of adhesive joints for the automotive industry. International Journal of Adhesion & Adhesives 2015; 59: 14-20.

[46] Matsui K. Effects of curing conditions and test temperatures on the strength of adhesive-bonded joints. International Journal of Adhesion & Adhesives 1990; 10: 277-84.

[47] Park SY, Choi WJ, Choi CH, Choi HS. The effect of curing temperature on thermal, physical and mechanical characteristics of two types of adhesives for aerospace structures. Journal of Adhesion Science and Technology 2018; 32: 1200-23.

[48] Banea MD, da Silva LFM, Campilho RDSG. The effect of adhesive thickness on the mechanical behavior of a structural polyurethane adhesive. The Journal of Adhesion 2015; 91: 331-46.

[49] Machado JJM, Marques EAS, da Silva LFM. Adhesives and adhesive joints under impact loadings: An overview. The Journal of Adhesion 2018; 94: 421-52.

[50] Martínez-Landeros VH, Vargas-Islas SY, Cruz-González CE, Barrera S, Mourtazov K, Ramírez-Bon R. Studies on the influence of surface treatment type, in the effectiveness of structural adhesive bonding, for carbon fiber reinforced composites. Journal of Manufacturing Processes 2019; 39: 160-6.

[51] Adams RD, Cawley P, Guyott CCH. Non-destructive inspection of adhesively-bonded joints. The Journal of Adhesion 1987; 21: 279-90.

[52] Palumbo D, Tamborrino R, Galietti U, Aversa P, Tatì A, Luprano VAM. Ultrasonic analysis and lock-in thermography for debonding evaluation of composite adhesive joints. NDT & E International 2016; 78: 1-9.

[53] Rudawska A. Surface free energy and 7075 aluminium bonded joint strength following degreasing only and without any prior treatment. Journal of Adhesion Science and Technology 2012; 26: 1233-47.

[54] Żenkiewicz M. Adhesion and modification of the high-molecular materials surface layer. Warsaw: Scientific and Technical Publishers, USA; 2000.

[55] Comyn J. Contact angles and adhesive bonding. International Journal of Adhesion & Adhesives 1992; 12: 145-9.

[56] Bayer IS, Megaridis CM, Hang J, Gamota D, Biswas A. Analysis and surface energy estimation of various model polymeric surfaces using contact angle hysteresis. Journal of Adhesion Science and Technology 2007; 29: 1439-67.

[57] Good RJ. Contact angle, wetting, and adhesion: a critical review. Journal of Adhesion Science and Technology 1992; 6: 1269-302.

[58] Kulkarni VS, Shaw C. Chapter 2 - Surfactants, Lipids, and Surface Chemistry. In: Kulkarni VS and Shaw C editors. Essential Chemistry for Formulators of Semisolid and Liquid Dosages. Academic Press, Netherlands; 2016.

[59] Encinas N, Pantoja M, Abenojar J, Martinez MA. Control of wettability of polymers by surface roughness modification. Journal of Adhesion Science and Technology 2010; 24: 1869-83.

[60] Kanezashi M, Tsuru T. Chapter 6 - Gas permeation properties of helium, hydrogen, and polar molecules through microporous silica membranes at high temperatures: correlation with silica network structure. Membrane Science and Technology 2011; 14: 117-36.

[61] Della Volpe C, Siboni S. Some reflections on acid-base solid surface free energy theories. Journal of Colloid and Interface Science 1997; 195: 121-36.

[62] Białopiotrowicz T. Influence of erroneous date on the results of calculations from acid-base surface free energy theories. I. Simulations for a small input data set. Journal of Adhesion Science and Technology 2007; 21: 1539-56.

[63] Uehara K, Sakurai M. Bonding strength of adhesives and surface roughness of joined parts. Journal of Materials Processing Technology 2002; 127: 178-81.

[64] Aydin S, Solmaz MY, Turgut A. The effects of adhesive thickness, surface roughness and overlap distance on joint strength in prismatic plug-in joints attached with adhesive. International Journal of the Physical Sciences 2012; 7(17): 2580-6.

[65] Prolongo SG, Ureña A. Effect of surface pre-treatment on the adhesive strength of epoxy–aluminium joints. International Journal of Adhesion & Adhesives 2009; 29: 23-31.

[66] Kasalkova NS, Slepicka P, Kolska Z, Svorcik V. Wettability and other surface properties of modified polymers. In: Aliofkhazraei M, editor. Wetting and Wettability. IntechOpen, United Kingdom; 2015.

[67] Aronsson BO, Lausmaa J, Kasemo B. Glow discharge plasma treatment for surface cleaning and modification of metallic biomaterials. Journal of Biomedical Materials Research 1997; 35: 49-73.

[68] Li Q, Kim K. Micromechanics of rough surface adhesion: a homogenized projection method. Acta Mechanica Solida Sinica 2009; 22: 377-90.

[69] Schauer T, Joos A, Dulog L, Eisenbach CD. Protection of iron against corrosion with polyaniline primers. Progress in Organic Coatings 1998; 33: 20-7.

[70] Kang ET, Zhang Y. Surface modification of fluoropolymers via molecular design. Advanced Materials 2000; 12(20): 1481-94.

[71] Panesar D, Leung R, Sain M, Panthapulakkal S. The effect of sodium hydroxide surface treatment on the tensile strength and elastic modulus of cellulose nanofiber. In: Junior HS, Fiorelli J, dos Santos SF editors. Sustainable and nonconventional construction materials using inorganic bonded fiber composites. Woodhead Publishing, United Kingdom; 2017.

[72] Okumura H, Takahagi T, Nagai N, Shingubara S. Depth profile analysis of polyimide film treated by potassium hydroxide. Journal of Polymer Science: Part B: Polymer Physics 2003; 41: 2071-8.

[73] Zhou W, Shan D, Han E, Ke W. Structure and formation mechanism of phosphate conversion coating on die-cast AZ91D magnesium alloy. Corrosion Science 2008; 50: 329-37.

[74] Chaiyabutr Y, McGowan S, Phillips KM, Kois JC, Giordano RA. The effect of hydrofluoric acid surface treatment and bond strength of a zirconia veneering ceramic. The Journal of Prosthetic Dentistry 2008; 100: 194-202.

[75] Fiore V, Scalici T, Valenza A. Effect of sodium bicarbonate treatment on mechanical properties of flax-reinforced epoxy composite materials. Journal of Composite Materials 2017; 0(0): 1-12.

[76] Skienhe H, Habchi R, Ounsi H, Ferrari M, Salameh Z. Evaluation of the effect of different types of abrasive surface treatment before and after zirconia sintering on its structural

composition and bond strength with resin cement. BioMed Research International 2018; Article ID 1803425.

[77] Abenojar J. Composite to composite adhesion. In: Wahab MA, editor. Joining Composites with Adhesives: Theory and Applications. DEStech Publications Inc., USA; 2015.

[78] Gnanamuthu DS. Laser surface treatment. Optical Engineering 1980; 19(5): 195783.

[79] Bizi-Bandoki P, Benayoun S, Valette S, Beaugiraud B, Audouard E. Modifications of roughness and wettability properties of metals induced by femtosecond laser treatment. Applied Surface Science 2011; 257: 5213-18.

[80] Paul SA, Joseph K, Mathew GDG, Pothen LA, Thomas S. Influence of polarity parameters on the mechanical properties of composites from polypropylene fiber and short banana fiber. Composites Part A: Applied Science and Manufacturing 2010; 41: 1380-7.

[81] Molitor P, Barron V, Young T. Surface treatment of titanium for adhesive bonding to polymer composites: a review. International Journal of Adhesion & Adhesives 2001; 21: 129-36.

[82] Lima RBW, Barreto SC, Alfrisany NM, Porto TS, De Souza GM, De Goes MF. Effect of silane and MDP-based primers on physico-chemical properties of zirconia and its bond strength to resin cement. Dental Materials 2019; In Press. DOI: https://doi.org/10.1016/j.dental.2019.07.008.

[83] Xie Y, Hill CAS, Xiao Z, Militz H, Mai C. Silane coupling agents used for natural fiber/polymer composites: A review. Composites: Part A 2010; 41: 806-19.

[84] Mathieson I, Bradley RH. Improved adhesion to polymers by UV/ozone surface oxidation. International Journal of Adhesion & Adhesives 1996: 16; 29-31.

[85] He T, Wang Y, Zhang Y, Iv Q, Xu T, Liu T. Super-hydrophobic surface treatment as corrosion protection for aluminum in seawater. Corrosion Science 2009; 51: 1757-61.

[86] Morks MF. Magnesium phosphate treatment for steel. Materials Letters 2004; 58: 3316-9.

[87] Król P, Król B. Determination of free surface energy values for ceramic materials and polyurethane surface-modifying aqueous emulsions. Journal of the European Ceramic Society 2006; 26: 2241-8.

[88] Hegemann D, Brunner H, Oehr C. Plasma treatment of polymers for surface and adhesion improvement. Nuclear Instruments and Methods in Physics Research Section B: Beam Interactions with Materials and Atoms 2003; 208: 281-6.

[89] Tendero C, Tixier C, Tristant P, Desmaison J, Leprince P. Atmospheric pressure plasmas: A review. Spectrochimica Acta Part B 2006; 61: 2-30.

[90] Waters LJ, Finch CV, Bhuiyan AKMMH, Hemming K, Mitchell JC. Effect of plasma surface treatment of poly(dimethylsiloxane) on the permeation of pharmaceutical compounds. Journal of Pharmaceutical Analysis 2017; 7: 338-42.

[91] Rodríguez-Villanueva C, Encinas N, Abenojar J, Martínez MA. Assessment of atmospheric plasma treatment cleaning effect on steel surfaces. Surface and Coatings Technology 2013; 236: 450-6.

[92] Cvelbar U, Pejovnik S, Mozetiè M, Zalar A. Increased surface roughness by oxygen plasma treatment of graphite/polymer composite. Applied Surface Science 2003; 210: 255-61.

[93] Zanini S, Riccardi C, Orlandi M, Esena P, Tontini M, Milani M, Cassio V. Surface properties of HMDSO plasma treated polyethylene terephthalate. Surface and Coatings Technology 2005; 200: 953-7.

[94] Yasuda H, Gazicki M. Biomedical applications of plasma polymerization and plasma treatment of polymer surfaces. Biomaterials 1982; 3: 68-77.

[95] Farris S, Pozzoli S, Biagioni P, Duó L, Mancinelli S, Piergiovanni L. The fundamentals of flame treatment for the surface activation of polyolefin polymers – A review. Polymer 2010; 51: 3591-605.

[96] Pijpers AP, Meier RJ. Adhesion behaviour of polypropylenes after flame treatment determined by XPS(ESCA) spectral analysis. Journal of Electron Spectroscopy and Related Phenomena 2001; 121: 299-313.

[97] Sanchis MR, Blanes V, Blanes M, Garcia D, Balart R. Surface modification of low density polyethylene (LDPE) film by low pressure O2 plasma treatment. European Polymer Journal 2006; 42: 1558-68.

[98] Nitschke M, Schmack G, Janke A, Simon F, Pleul D, Werner C. Low pressure plasma treatment of poly(3-hydroxybutyrate): Toward tailored polymer surfaces for tissue engineering scaffolds. Journal of Biomedical Materials Research 2002; 59: 632-8.

[99] Sutherland I, Popat RP, Brewis DM, Calder R. Corona discharge treatment of polyolefins. The Journal of Adhesion 1994; 46: 79-88.

[100] Gassan J, Gutowski VS. Effects of corona discharge and UV treatment on the properties of jute-fibre epoxy composites. Composites Science and Technology 2000; 60: 2857-63.

[101] Park S, Kim J, Park CH. Influence of micro and nano-scale roughness on hydrophobicity of a plasma-treated woven fabric. Textile Research Journal 2016; 87(2): 193-207.

[102] Encinas N, Díaz-Benito B, Abenojar J, Martínez MA. Extreme durability of wettability changes on polyolefin surfaces by atmospheric pressure plasma torch. Surface and Coatings Technology 2010; 205: 396-402.

[103] Valian A, Moravej-Salehi E. Surface treatment of feldspathic porcelain: scanning electron microscopy analysis. The Journal of Advanced Prosthodontics 2014; 6: 387-94.

[104] Salerno M, Giacomelli L, Derchi G, Patra N, Diaspro A. Atomic force microscopy in vitro study of surface roughness and fractal character of a dental restoration composite after air-polishing. BioMedical Engineering OnLine 2010; 9: 59.

[105] Junior MSO, Diniz MF, Dutra RCL, Massi M, Otani C. Applicability of FT-IR techniques and goniometry on characterization of carbon fiber surfaces. Journal of Aerospace Technology and Management 2016; 8: 1.

[106] Gardner SD, Singamsetty CSK, Booth GL, He G, Pittman CU. Surface characterization of carbon fibers using angle-resolved XPS and ISS. Carbon 1995; 33: 587-95.

[107] Galvez P, Quesada A, Martinez MA, Abenojar J, Boada MJL, Diaz V. Study of the behaviour of adhesive joints of steel with CFRP for its application in bus structures. Composites Part B: Engineering 2017; 129: 41-6.

[108] Adams RD, Harris JA. The influence of local geometry on the strength of adhesive joints. International Journal of Adhesion & Adhesives 1987; 7: 69-80.

[109] Aydın MD, Temiz Ş, Özel A. Effect of curing pressure on the strength of adhesively bonded joints. The Journal of Adhesion 2007; 83: 553-71.

[110] da Silva LFM, Dillard DA, Blackman B, Adams RD. Testing adhesive joints: best practices. Wiley-VCH Verlag, USA; 2012.

[111] da Silva LFM, Adams RD. Techniques to reduce the peel stresses in adhesive joints with composites. International Journal of Adhesion & Adhesives 2007; 27: 227-35.

[112] Duan K, Hu X, Mai Y. Substrate constraint and adhesive thickness effects on fracture toughness of adhesive joints. Journal of Adhesion Science and Technology 2004; 18: 39-53.

[113] Davim JP, editor. Machining, Fundamentals and recent advances. Springer-Verlag, United Kingdom; 2008.

[114] Moreno MCS, Cela JJL, Vicente JLM, Vecino JAG. Adhesively bonded joints as a dissipative energy mechanism under impact loading. Applied Mathematical Modelling 2015; 39: 3496-505.

[115] Arenas JM, Alía C, Cañizo C, Ocaña R, Narbón JJ. Technical and economic evaluation of adhesive, screwed and hybrid joints for bonding metallic materials in industrial applications. Procedia Manufacturing 2017; 13: 1447-54.

[116] Galvez P, Noda N, Takaki R, Sano Y, Miyazaki T, Abenojar J, Martinez MA. Intensity of singular stress field (ISSF) variation as a function of the Young's modulus in single lap adhesive joints. International Journal of Adhesion & Adhesives 2019; 95: 102418.

[117] Santos MAS, Campilho RDSG. Experimental and numerical analysis of the fracture envelope of composite adhesive joints. Science and Technology of Materials 2018; 30: 131-37.

[118] Campilho RDSG, Banea MD, Neto JABP, da Silva LFM. Modelling of single-lap joints using cohesive zone models: effect of the cohesive parameters on the output of the simulations. The Journal of Adhesion 2012; 88: 513-33.

[119] Banea MD, da Silva LFM. Mechanical characterization of flexible adhesives. The Journal of Adhesion 2009; 85: 261-85.

[120] Arenas JM, Narbón JJ, Alía C. Optimum adhesive thickness in structural adhesives joints using statistical techniques based on Weibull distribution. International Journal of Adhesion & Adhesives 2010; 30: 160-5.

[121] Fu M, Mallick PK. Fatigue of hybrid (adhesive/bolted) joints in SRIM composites. International Journal of Adhesion & Adhesives 2001; 21: 145-59.

[122] Sadowski T, Kneć M, Golewski P. Experimental investigations and numerical modelling of steel adhesive joints reinforced by rivets. International Journal of Adhesion & Adhesives 2010; 30: 338-46.

[123] Comyn J. Contact angles and adhesive bonding. International Journal of Adhesion & Adhesives 1992; 12: 145-9.

[124] Wanga YY, Lia CJ, Ohmorib A. Influence of substrate roughness on the bonding mechanisms of high velocity oxy-fuel sprayed coatings. Thin Solid Films 2005; 485: 141-7.

[125] Davis M, Bond D. Principles and practices of adhesive bonded structural joints and repairs. International Journal of Adhesion & Adhesives 1999; 19: 91-105.

[126] Comyn J. Surface treatment and analysis for adhesive bonding. International Journal of Adhesion & Adhesives 1990; 10: 161-5.

[127] Orowan E. Surface energy and surface tension in solids and liquids. Proceedings of the Royal Society A: Mathematical, Physical and engineering sciences 1970; 316: 473-91.

[128] Uddin N, editor. Developments in Fiber-reinforced polymer (FRP) composites for civil engineering. Woodhead Publishing, United Kingdom; 2013.

[129] Mangalgiri PD. Composite materials for aerospace applications. Bulletin of Materials Science 1999; 22: 657-64.

[130] Lee M, Kim H, Oh S. Crushing test of double hat-shaped members of dissimilar materials with adhesively bonded and self-piercing riveted joining methods. Thin-Walled Structures 2006; 44: 381-6.

[131] Anyfantis KN. Composite to metal. In: Wahab MA, editor. Joining Composites with Adhesives: Theory and Applications. DEStech Publications Inc., USA; 2015.

[132] Darwish M. Analysis of weld-bonded dissimilar materials. International Journal of Adhesion & Adhesives 2004; 24: 347-54.

[133] Kah P, Martikainen MSJ. Trends in joining dissimilar metals by welding. Applied Mechanics and Materials 2014; 440: 269-76.

[134] UNE-EN ISO 15614:2018. Especificación y cualificación de los procedimientos de soldeo para los materiales metálicos.

[135] ISO 13469:2014. Mechanical joining. Form-fit blind rivets and (lock) bolt joints. Specifications and qualification of testing procedures.

[136] Harsha HK, Rokade RP, Anandan S. Studies on stress concentration at bolt hole location in lap joints using finite element analysis. International Journal of Civil Engineering and Technology 2014; 5: 333-9.

[137] Caliskan M. Evaluation of bonded and bolted repair techniques with finite element method. Materials & Design 2006; 27: 811-20.

[138] Khashaba UA, El-Sonbaty IA, Selmy AI, Megahed AA. Machinability analysis in drilling woven GFR/epoxy composites: Part I – Effect of machining parameters. Composites Part A: Applied Science and Manufacturing 2010; 41: 391-400.

[139] Karataş MA, Gökkaya H. A review on machinability of carbon fiber reinforced polymer (CFRP) and glass fiber reinforced polymer (GFRP) composite materials. Defence Technology 2018; 14: 318-26.

[140] Persson E, Eriksson I, Zackrisson L. Effects of hole machining defects on strength and fatigue life of composite laminates. Composites Part A: Applied Science and Manufacturing 1997; 28: 141-51.

[141] Adams RD, Comyn J, Wake WC. Structural adhesive joints in engineering. Chapman & Hall, United Kingdom; 1997.

[142] Neşer G. Polymer based composites in marine use: history and future trends. Procedia Engineering 2017; 194: 19-24.

[143] Flaga K. Advances in materials applied in civil engineering. Journal of Materials Processing Technology 2000; 106: 173-83.

[144] Friedrich K, Almajid AA. Manufacturing aspects of advanced polymer composites for automotive applications. Applied Composite Materials 2013; 20: 107-28.

[145] Campilho RDSG, de Moura MFSF, Domingues JJMS. Modelling single and double-lap repairs on composite materials. Composites Science and Technology 2005; 65: 1948-58.

[146] Baldan A. Adhesively-bonded joints and repairs in metallic alloys, polymers and composite materials: adhesives, adhesion theories and surface pretreatment. Journal of Materials Science 2004; 39: 1-49.

[147] Malysheva GV. Problems of the reliability of machines with adhesive joints. Polymer Science Series D 2008; 1: 51-6.

[148] Fernández-Cañadas LM, Ivañez I, Sanchez-Saez S, Barbero EJ. Effect of adhesive thickness and overlap on the behavior of composite single-lap joints. Mechanics of Advanced Materials and Structures 2019; In Press. DOI: https://doi.org/10.1080/15376494.2019.1639086.

[149] Harris JA, Adams RA. Strength prediction of bonded single lap joints by non-linear finite element methods. International Journal of Adhesion & Adhesives 1984; 4: 65-78.

[150] Campilho RDSG, Banea MD, Pinto AMG, da Silva LFM, de Jesus AMP. Strength prediction of single- and double-lap joints by standard and extended finite element modeling. International Journal of Adhesion & Adhesives 2011; 31: 363-72.

[151] Grant LDR, Adams RD, da Silva LFM. Experimental and numerical analysis of single-lap joints for the automotive industry. International Journal of Adhesion & Adhesives 2009; 29: 405-13.

[152] You M, Yan Z, Zheng X, Yu H, Li Z. A numerical and experimental study of adhesively bonded aluminium single lap joints with an inner chamfer on the adherends. International Journal of Adhesion & Adhesives 2008; 28: 71-6.

[153] del Real JC. Public transport service. In: Wahab MA, editor. Joining Composites with Adhesives: Theory and Applications. DEStech Publications Inc., USA; 2015.

[154] Beirão G, Cabral JAS. Understanding attitudes towards public transport and private car: A qualitative study. Transport Policy 2007; 14: 478-89.

[155] McShane WR, Bloch AJ, Ihlo W. The energy advantages of public transportation. US Urban Mass Transportation Administration Office of Policy Research University Research and Training Program 1980; Vol. 1.

[156] Chehroudi B. Composite materials and their uses in cars. Part II: Applications. Advanced Technology Consultants 2017 [Online]. Disponible: https://advtechconsultants.com/CompositeMaterial.htm. [Accessed 09-10-2019].

[157] McGeehin P. Composites in transportation: Design and current developments. Materials & Design 1982; 3: 378-87.

[158] Jacob GC, Fellers JF, Simunovic S, Starbuck JM. Energy absorption in polymer composites for automotive crashworthiness. Journal of Composite Materials 2002; 36: 813-50.

[159] Di Benedetto RM, Raponi OA, Junqueira DM, Junior ACA. Crashworthiness and impact energy absorption study considering the CF/PA commingled composite processing optimization. Materials Research 2017; 20: 792-9.

[160] Singh KV, Bansal HO, Singh D. A comprehensive review on hybrid electric vehicles: architectures and components. Journal of Modern Transportation 2019; 27: 77-107.

[161] Hadavinia H, Ghasemnejad H. Effects of Mode-I and Mode-II interlaminar fracture toughness on the energy absorption of CFRP twill/weave composite box sections. Composite Structures 2009; 89: 303-14.

[162] Barbosa NGC, Campilho RDSG, Silva FJG, Moreira RDF. Comparison of different adhesively-bonded joint types for mechanical structures. Applied Adhesion Science 2018; 6: 15.

[163] Hoa SV. Principles of the Manufacturing of Composite Materials. DEStech Publications Inc., USA; 2009.

[164] Pomykala M. Benefits of adhesive bonding for any industry. Industrial Manufacturing and Engineering Blog 2016 [Online]. Disponible: http://henkeladhesivesna.com/blog/adhesive-bonding-benefits/. [Accessed 09-10-2019].

[165] Kim BC, Hazra K, Weaver P, Potter K. Limitations of fibre placement techniques for variable angle tow composites and their process-induced defects. 18th International Conference on Composite Materials 2011.

[166] Willis B. Composites challenges. Adhesives & Sealant Industry 2012; 2: 17-9.

[167] Ghafoori E, Motavalli M, Nussbaumer A, Herwig A, Prinz GS, Fontana M. Design criterion for fatigue strengthening of riveted beams in a 120-year-old railway metallic bridge using pre-stressed CFRP plates. Composites Part B: Engineering 2015; 68: 1-13.

[168] Hosseini A, Ghafoori E, Al-Mahaidi R, Zhao X, Motavalli M. Strengthening of a 19th-century roadway metallic bridge using nonprestressed bonded and prestressed unbonded CFRP plates. Construction and Building Materials 2019; 209: 240-59.

[169] Patentes Talgo SL. Alta velocidad La Meca-Medina. Proyecto Haramain [Online]. Disponible: https://www.talgo.com/es/proyectos/arabia-saudi/haramain/. [Accessed 09-10-2019].

[170] Encinas N, Abenojar J, Martinez MA. Development of improved polypropylene adhesive bonding by abrasion and atmospheric plasma surface modifications. International Journal of Adhesion & Adhesives 2012; 33: 1-6.

[171] Encinas N, Oakley BR, Belcher MA, Blohowiak KY, Dillingham RG, Abenojar J, Martinez MA. Surface modification of aircraft used composites for adhesive bonding. International Journal of Adhesion & Adhesives 2014; 50: 157-63.

[172] Sika AG. Bus & coach innovative technology for customer solutions. Sika transportation tecnhical information 2012. Disponible en: http://bel.sika.com/dms/getdocument.get/d0413141-6e8a-3f97-90cf-f9663302830f/bro-cmi-bus-coach.pdf.

[173] Miravete A. Los nuevos materiales en la construcción. Editorial Reverté, España; 2008.

[174] Suga T, Elssner G, Schmauder S. Composite parameters and mechanical compatibility of material joints. Journal of Composite Materials 1988; 22(10): 917-34.

[175] Njuguna J, editor. Lightweight composite structures in transport: design, manufacturing, analysis and performance. Woodhead Publishing, United Kingdom; 2016.

[176] Shin KB. Ageing of composites in transport applications. In: Martin R, editor. Ageing of Composites. Woodhead Publishing, United Kingdom; 2008.

[177] Agrawal S, Singh KK, Sarkar PK. Impact damage on fibre-reinforced polymer matrix composite – A review. Journal of Composite Materials 2013; 48: 317-332.

[178] Oller E, Pujol M, Marí A. Contribution of externally bonded FRP shear reinforcement to the shear strength of RC beams. Composites Part B: Engineering 2019; 164: 235-48.

[179] Colangelo F, Russo P, Cimino F, Cioffi R, Farina I, Fraternali F, Feo L. Epoxy/glass fibres composites for civil applications: comparison between thermal and microwave crosslinking routes. Composites Part B: Engineering 2017; 126: 100-7.

[180] Ribeiro F, Sena-Cruz J, Branco FG, Júlio E. Hybrid effect and pseudo-ductile behaviour of unidirectional interlayer hybrid FRP composites for civil engineering applications. Construction and Building Materials 2018; 171: 871-90.

[181] Teng JG, Yu T, Fernando D. Strengthening of steel structures with fiber-reinforced polymer composites. Journal of Constructional Steel Research 2012; 78: 131-43.

[182] Ghafoori E, Hosseini A, Al-Mahaidi R, Zhao X, Motavalli M. Prestressed CFRP strengthening and long-term wireless monitoring of an old roadway metallic bridge. Engineering Structures 2018; 176: 585-605.

[183] Li A, Assih J, Delmas Y. Civil engineering: strengthening RC structures. In: Wahab MA, editor. Joining Composites with Adhesives: Theory and Applications. DEStech Publications Inc., USA; 2015.

[184] Justo J, París F. Experimental mechanical characterization of composite-concrete joints. Composites Part B: Engineering 2018; 154: 148-56.

[185] Shash AA. Repair of concrete beams – a case study. Construction and Building Materials 2005; 19: 75-9.

[186] D'Aniello M, Portioli F, Landolfo R. Lap shear tests on hot-driven steel riveted connections strengthened by means of C-FRPs. Composites Part B: Engineering 2014; 59: 140-52.

[187] Danilov AI. Some aspects of CFRP steel structures reinforcement in civil engineering. Procedia Engineering 2016; 153: 124-30.

[188] Swamy RN, Jones R, Bloxham JW. Structural behavior of reinforced concrete beams strengthened by epoxy bonded steel plates. Structural Engineering 1987; 65(2):59-68.

[189] Saadatmanesh H, Ehsani MR. RC beams strengthened with GFRP plates. I: Experimental study. Journal of Structural Engineering 1991; 117(11): 3417-33.

[190] Triantafillou TC, Plevris N. Strengthening of RC beams with epoxy-bonded fibre-composite materials. Materials and Structures 1992; 25: 201-11.

[191] Meier U. Strengthening of structures using carbon fibre/epoxy composites. Construction and Building Materials 1995; 9(6): 341-51.

[192] Li A, Assih J, Delmas Y. Shear strengthening of RC beams with externally bonded CFRP sheets. Journal of Structural Engineering 2001; 127(4): 374-80.

[193] Medina E, Medina JM, Cobo A, Bastidas DM. Evaluation of mechanical and structural behavior of austenitic and duplex stainless steel reinforcements. Construction and Building Materials 2015; 78: 1-7.

[194] Schnerch D, Dawood M, Rizkalla S, Sumner E, Stanford K. Bond behavior of CFRP strengthened steel structures. Advances in Structural Engineering 2006; 9: 805-17.

[195] Maalej M, Bian Y. Interfacial shear stress concentration in FRP-strengthened beams. Composite Structures 2001; 54: 417-26.

[196] Yu QQ, Zhao XL, Chen T, Gu XL, Xiao ZG. Crack propagation prediction of CFRP retrofitted steel plates with different degrees of damage using BEM. Thin-Walled Structures 2014; 82: 145-58.

[197] Bonacci JF, Maalej M. Externally bonded fiber-reinforced polymer for rehabilitation of corrosion damaged concrete beams. ACI Structural Journal 2001; 97(5)5: 703-11.

[198] Toutanji H, Ortiz G. The effect of surface preparation on the bond interface between FRP sheets and concrete members. Composite Structures 2001; 53: 457-62.

[199] Wu C, Zhao X, Duan WH, Al-Mahaidi R. Bond characteristics between ultra high modulus CFRP laminates and steel. Thin-Walled Structures 2012; 51: 147-57.

[200] Luccioni B, Rougier VC. Shear behaviour of brick–mortar interface in CFRP retrofitted or repaired masonry. International Journal of Mechanical Sciences 2010; 52: 602-11.

[201] Bell S. Structural adhesives deliver lighter structures with performance and costs benefits. Reinforced Plastics 2012; 56: 34-7.

[202] Cognard JY, Créac'hcadec R, Sohier L, Davies P. Analysis of the nonlinear behavior of adhesives in bonded assemblies - Comparison of TAST and Arcan tests. International Journal of Adhesion & Adhesives 2008; 28: 393-404.

[203] Gonzalez-Rodriguez JG, Lucio-García MA, Nicho ME, Cruz-Silva R, Casales M, Valenzuela E. Improvement on the corrosion protection of conductive polymers in pemfc environments by adhesives. Journal of Power Sources 2007; 168: 184-90.

[204] Xará JTS, Campilho RDSG. Strength estimation of hybrid single-L bonded joints by the extended finite element method. Composite Structures 2018; 183: 397-406.

[205] Li R, Noda NA, Takaki R, Sano Y, Takase Y, Miyazaki T. Most suitable evaluation method for adhesive strength to minimize bend effect in lap joints in terms of the intensity of singular stress field. International Journal of Adhesion & Adhesives 2018; 86: 45-58.

[206] Noda NA, Li R, Miyazaki T, Takaki R, Sano Y. Convenient adhesive strength evaluation method in terms of the intensity of singular stress field. International Journal of Computational Methods 2018; 15(1). 1850085: 01-30.

[207] Mintzas A, Nowell D. Validation of an Hcr-based fracture initiation criterion for adhesively bonded joints. Engineering Fracture Mechanics 2012; 80: 13-27.

[208] Wang CH, Rose LRF. Compact solutions for the corner singularity in bonded lap joints. International Journal of Adhesion Adhesives 2000; 20: 145–54.

[209] Goglio L, Rossetto M. Evaluation of the singular stresses in adhesive joints. Journal of Adhesion Science and Technology 2009; 23: 1441–57.

[210] Martinez MA, Velasco F, Abenojar J, Pantoja M, Del Real JC. Analytical solution to calculate the stress distribution in pin-and-collar samples bonded with anaerobic adhesives (following ISO 10123 standard). International Journal of Adhesion & Adhesives 2008; 28: 405-10.

[211] Li G, Lee-Sullivan P, Thring RW. Nonlinear finite element analysis of stress and strain distributions across the adhesive thickness in composite single-lap joints. Composite Structures 1999; 46: 395-403.

[212] Chiminelli A, Breto R, Izquierdo S, Bergamasco L, Duvivier E, Lizaranzu M. Analysis of mixed adhesive joints considering the compaction process. International Journal of Adhesion & Adhesives 2017; 76: 3-10.

[213] Breto R, Chiminelli A, Lizaranzu M, Rodríguez R. Study of the singular term in mixed adhesive joints. International Journal of Adhesion & Adhesives 2017; 76: 11–6.

[214] Fitton MD, Broughton JG. Variable modulus adhesives: an approach to optimized joint performance. International Journal of Adhesion & Adhesives 2005; 25: 329-36.

[215] da Silva LFM, Lopes MJCQ. Joint strength optimization by the mixed-adhesive technique. International Journal of Adhesion & Adhesives 2009; 29: 509-14.

[216] Carbas RJC, da Silva LFM, Critchlow GW. Adhesively bonded functionally graded joints by induction heating. International Journal of Adhesion & Adhesives 2014; 48: 110-8.

Capítulo 3:

UNIDAD TEMÁTICA

Índice

Capítulo 3:

UNIDAD TEMÁTICA

3.1 UNIDAD TEMÁTICA

A lo largo de estos años, el doctorando ha participado en el desarrollo de nueve publicaciones científicas, estando siete de ellas enmarcadas dentro de esta tesis doctoral, perteneciendo las otras dos a colaboraciones realizadas en otros trabajos dentro de la misma área.

Tal y como se explica en las motivaciones que han llevado al desarrollo de esta tesis doctoral, los problemas de fatiga existentes en las estructuras de acero soldadas suponen un inconveniente a resolver tanto en la industria del transporte, como en otras aplicaciones de la ingeniería civil.

En la Publicación 1 (Study of the behaviour of adhesive joints of steel with CFRP for its application in bus Structures. Composites Part B, 129 (2017) 41-46), se introduce el problema existente en las superestructuras de acero de autobuses y se propone una solución basada en el uso de adhesivos. Estas superestructuras sufren fatiga debido a la rigidez de las uniones soldadas utilizadas, siendo muy evidentes los problemas de grietas debidos a la fatiga en determinadas zonas del autobús situadas cerca de la puerta trasera. Miembros del Departamento de Ingeniería Mecánica de la Universidad Carlos III de Madrid han participado en esta publicación, siendo su función la de desarrollar el modelo de elementos finitos de la estructura de autobús, obteniendo las fuerzas que trabajan en el nodo de referencia (zonas de la superestructura de acero con mayores concentraciones de tensiones). A partir de estos valores, el doctorando calculó los valores y tipos de esfuerzos en el nodo de referencia.

A continuación fue necesario seleccionar el adhesivo, de acuerdo a los esfuerzos en el nodo de referencia, teniendo en cuenta que el objetivo era fabricar el nodo de CFRP. Para esta selección, se han realizado tres publicaciones en las que se estudia el comportamiento de distintos adhesivos frente a esfuerzos de cizalla y su durabilidad, es decir después de ser sometidas las uniones a condiciones agresivas (Publicaciones 2, 3 y 4).

Así, en la Publicación 2 (Durability of steel-CFRP structural adhesive joints with polyurethane adhesives. Composites Part B, 165 (2019) 1-9) se estudia el comportamiento de

uniones adhesivas acero-CFRP frente a condiciones de humedad y temperatura. En este trabajo se realizó un planteamiento genérico de las uniones adhesivas, de tal forma que las uniones no solo sean útiles para su uso en estructuras de autobús, sino que también puedan ser adaptadas a otro tipo de estructuras metálicas de ingeniería civil.

Para este estudio, se seleccionaron dos adhesivos de poliuretano estructurales, uno de ellos convencional y el otro híbrido (con silanos en su formulación). Los adhesivos de poliuretano son ampliamente aceptados industrialmente gracias a las buenas propiedades de este material frente a agentes externos y a los altos valores de resistencia que son capaces de aportar a la unión.

El objetivo de la publicación 2 era realizar un estudio completo de uniones adhesivas acero-CFRP para poder comparar después con los estudios realizados con otros adhesivos, y de esta forma poder seleccionar al final de todo el proceso el adhesivo que mejor se adaptase a la problemática planteada.

Este trabajo fue realizado en su totalidad por el doctorando bajo la supervisión de sus directores de tesis. El nuevo concepto de nodo de CFRP permite que la unión adhesiva trabaje a cizalla. Por ese motivo se realizaron ensayos de cizalla por tracción siguiendo la norma UNE-EN 1465. Con estos ensayos se evaluaron las propiedades mecánicas de la unión: esfuerzos de cizalla, deformación y rigidez. Para poder seleccionar el mejor adhesivo posible, no solo se deben tener en cuenta los resultados obtenidos después de curar las uniones en condiciones de laboratorio. Es necesario someter a la unión a condiciones extremas. De esta forma se descartan adhesivos que a priori puedan presentar buenas propiedades, pero cuyo comportamiento frente a agentes externos sea deficiente.

La durabilidad de los adhesivos de poliuretano se evaluó mediante las propiedades mecánicas antes y después de ser sometidas las uniones a 100h y 500h de degradación bajo condiciones extremas (70°C y 80% de humedad relativa). Al ser elementos diseñados para una función estructural, se realizaron estudios estadísticos para evaluar la fiabilidad de los mismos antes y después de ser sometidos a degradación. Para ello se obtuvieron los datos anómalos mediante el test de Grubbs y se implementó un modelo simple de Weibull mediante el que se estudiaba la fiabilidad de la unión durante todo el proceso.

De forma complementaria al estudio mecánico de las uniones, se realiza la caracterización térmica de las mismas durante todo el proceso de degradación mediante

calorimetría diferencial de barrido (DSC - Differential Scanning Calorimetry). También se realizaron ensayos FTIR-ATR (Fourier Transform Infrared Spectroscopy by Attenuated Total Reflectance). Finalmente se evaluó el modo de fallo de las uniones adhesivas mediante microscopía óptica y mediante microscopía electrónica de barrido (SEM - Scanning Electron Microscope).

Gracias, tanto a los estudios mecánicos, como a los ensayos DSC, FTIR-ATR y de microscopía fue posible estudiar exhaustivamente el fenómeno de degradación de las uniones adhesivas planteadas. Cada adhesivo presenta un comportamiento diferente ante condiciones adversas de humedad y temperatura debido a sus diferentes composiciones químicas. El adhesivo de poliuretano convencional presenta un mejor comportamiento frente a la humedad y la temperatura, ya que ambos factores inducen un post-curado del adhesivo, incrementando tanto la resistencia como la rigidez y la fiabilidad de la unión. Por otro lado, el adhesivo de poliuretano híbrido alcanza todas sus propiedades antes de ser sometida la unión a condiciones adversas, por lo que no se observa post-curado y la degradación tiene lugar desde los primeros tiempos de exposición. Ambos adhesivos fueron descartados (a pesar de que los valores mostrados eran suficientes para el problema planteado) buscando otras formulaciones con mejores propiedades mecánicas.

En la Publicación 3 (Effect of moisture and temperature on the thermal and mechanical properties of a ductile epoxy adhesive for use in steel structures reinforced with CFRP. Composites Part B, 176 (2019) 107194) se planteó el uso de un adhesivo epoxi elástico para reforzar estructuras de acero mediante componentes de CFRP. El adhesivo epoxi usado tiene alta deformación por lo que podría absorber las vibraciones. Esto es algo básico, ya que como se plantea en las motivaciones de esta tesis doctoral, las actuales estructuras de acero soldadas presentan altos valores de rigidez, que derivan en problemas de fatiga durante el ciclo de vida del conjunto. Las uniones adhesivas fueron sometidas a condiciones de durabilidad y envejecimiento térmico, estudiando el proceso de degradación en cada caso. El desarrollo de este trabajo fue realizado íntegramente por el doctorando, bajo la supervisión de sus directores de tesis.

El adhesivo epoxi fue caracterizado mecánicamente siguiendo la norma francesa NF T 76–142, obteniendo los valores de tensión de rotura, elongación y Módulo de Young. Del mismo modo que en las publicaciones 1 y 2, se ha planteado una unión sometida principalmente a esfuerzos de cizalla. Por ello se han realizado ensayos de cizalla por tracción siguiendo la norma UNE-EN 1465. Con estos ensayos se evaluaron las propiedades mecánicas de la unión: esfuerzos

de cizalla, deformación y rigidez. Las probetas fueron fabricadas después de optimizar los tratamientos superficiales tanto en la superficie de acero como en la superficie de CFRP. De esta forma los ensayos fueron realizados tras asegurar las mejores propiedades mecánicas de la unión.

Tal y como se explica anteriormente, es fundamental conocer o al menos intuir cuál es el comportamiento de las uniones frente a condiciones adversas. Por ello, se sometió a las uniones a condiciones de durabilidad (60°C y 95% de humedad relativa) y a condiciones de envejecimiento térmico.

Al tratarse de un adhesivo epoxi elástico, distinto a los adhesivos epoxi convencionales, se estudiaron sus cinéticas de curado mediante los modelos de Kissinger y free kinetics (MFK) utilizando para ello un equipo de DSC. Con el mismo equipo se calcularon las temperaturas de transición vítrea en cada fase de degradación para cada ambiente adverso. Las probetas también fueron analizadas mediante FTIR-ATR.

Cualquier componente cuyo uso se plantee para aplicaciones estructurales debe ser sometido a estudios de fiabilidad. Por ese motivo, en este trabajo se ha calculado como varía la fiabilidad de las uniones durante el proceso de durabilidad y durante el proceso de envejecimiento térmico. Para ello se ha desarrollado un modelo simple de la distribución de Weibull, junto con estudios estadísticos que permitieron descartar los valores anómalos (Test de Grubbs). Por último, las superficies de rotura de las uniones fueron estudiadas mediante microscopía SEM y mediante espectroscopía de rayos X (Energy-dispersive X-ray spectroscopy Analysis).

Las propiedades térmicas del adhesivo, pese a tratarse de un adhesivo epoxi no convencional y con mayor capacidad de deformación, son similares a las de otros adhesivos epoxi convencionales. En cuanto a los procesos de durabilidad y fatiga térmica, ambos van a afectar de forma muy negativa a las propiedades mecánicas de la unión, incluso para tiempos cortos de exposición, siendo más perjudicial para la integridad de la unión el efecto combinado de la temperatura y la humedad del proceso de durabilidad.

La publicación 4 (Effect of moisture and temperature on thermal and mechanical properties of structural polyurethane adhesive joints. Composite Structures, pendiente de aceptación, pasada la primera revisión) es el último trabajo en el que se ha estudiado el comportamiento de adhesivos para evaluar su idoneidad para ser utilizados en uniones acero-CFRP. Una vez estudiado el comportamiento de todos los adhesivos planteados en esta Tesis

Doctoral fue posible seleccionar el más adecuado para unir elementos de CFRP a estructuras de acero. Este trabajo ha sido realizado por el doctorando con la ayuda de Sara López de Armentia Hernández y bajo la supervisión de sus directores de tesis.

Esta vez se han seleccionado dos adhesivos de poliuretano estructurales, uno mono-componente y otro bi-componente. Ambos adhesivos han sido sometidos a condiciones de durabilidad (72°C y 82% de humedad relativa) y a fatiga térmica.

Al igual que en las Publicaciones 2 y 3, se han realizado ensayos de cizalla por tracción siguiendo la norma UNE-EN 1465. Con estos ensayos se evaluaron las propiedades mecánicas de la unión: esfuerzos de cizalla, deformación y rigidez. Los objetivos son poder comparar todos los adhesivos disponibles de forma correcta y eficaz, y bajo condiciones similares, además de adaptar los ensayos a escala de laboratorio de la forma más precisa a las solicitaciones de las uniones reales.

Al igual que en las Publicaciones 2 y 3, se trata de adhesivos de carácter estructural, por lo tanto deben ser sometidos a estudios de fiabilidad. Del mismo modo que en anteriores trabajos, se ha desarrollado un modelo simplificado de Weibull, y mediante estadística (Test de Grubbs) se han descartado los valores anómalos.

Los adhesivos de las uniones fueron caracterizados químicamente mediante DSC y FTIR-ATR. De esta forma fue posible encontrar los fenómenos de degradación que afectan a cada adhesivo tanto en condiciones de durabilidad como de fatiga térmica.

A pesar de tratarse de dos adhesivos de poliuretano, las diferencias existentes en su composición química hacen que el comportamiento sea distinto frente a las condiciones estudiadas. El adhesivo bi-componente no alcanza todas sus propiedades mecánicas sólo con la mezcla de ambos componentes, y la exposición a humedad y temperatura producen un post-curado que induce a una mejora sustancial de las mismas. En el caso del adhesivo mono-componente, el efecto combinado de la humedad y la temperatura resulta ser perjudicial una vez que el adhesivo ha curado, no apreciándose en ningún caso signos de post-curado. En cuanto a la fatiga térmica, los dos adhesivos presentan comportamientos similares, ya que en ambos casos se observa un proceso de post-curado.

A partir de los resultados obtenidos en este trabajo, fue posible seleccionar el adhesivo más adecuado para ser aplicado en uniones acero-CFRP en superestructuras. Se seleccionó un

adhesivo de poliuretano mono-componente, el Sikatack® Drive, ya que aunaba una serie de ventajas por encima del resto de adhesivos estudiados (Publicación 4):

-Valores de resistencia muy superiores a las solicitaciones existentes en el nodo de referencia, en el caso de la superestructura del autobús.

-Buen comportamiento frente a la degradación por condiciones agresivas (durabilidad y fatiga térmica).

-Altos valores de deformación, permitiendo mejorar el comportamiento a fatiga de la estructura.

-Valores más altos de tenacidad a fractura en modo I (GIC). Tal y como se observa en la Publicación 5.

-Preparación superficial relativamente sencilla. Siendo más fiable su implantación en procesos industriales.

-Alta disponibilidad del adhesivo, al ser normalmente utilizado para el pegado de las lunas a las carrocerías de los coches.

De forma paralela se introdujo un nuevo concepto de nodo fabricado en CFRP. Este nodo se une mediante un adhesivo elástico a la estructura metálica del autobús. El doctorando participó tanto en la fase de diseño, como en la fase de fabricación tanto del nodo de CFRP, como de la unión adhesiva nodo-estructura (tal y como se explica en la Publicación 6). El nuevo diseño de nodo se realiza de tal forma que permite obtener mayoritariamente esfuerzos de cizalla en la unión adhesiva. Por este motivo, todas las uniones adhesivas fueron caracterizadas siguiendo la norma UNE-EN 1465. A la hora de seleccionar el Sikatack® Drive para la fabricación del nodo no solo se han tenido en cuenta los aspectos puramente mecánicos, si no que otras consideraciones como el comportamiento frente a agentes externos, la fiabilidad de la unión, y la complejidad de los tratamientos superficiales necesarios fueron considerados.

Al trabajar con adhesivos se debe asegurar que la rotura sea cohesiva (a través del adhesivo). Para ello el doctorando desarrolló diferentes tratamientos superficiales hasta lograr optimizar este proceso, siendo diferentes estos tratamientos dependiendo del adhesivo.

Las nuevas uniones adhesivas planteadas muestran valores de resistencia un orden de magnitud superior a las solicitaciones del nodo, con una capacidad de deformación superior al 30%, minimizando por tanto los problemas de fatiga mecánica.

En la Publicación 5 (Fracture toughness in Mode I (GIC) for ductile adhesives. Journal of Physics: Conference Series, 843 (2017) 012008), se calculó el valor de GIC en los adhesivos más adecuados (Sikatack Drive® y Sikaforce® 7720) para el problema planteado. Al trabajar con adhesivos pensados para aplicaciones estructurales, es necesario conocer todas las propiedades de los mismos. De esta forma, y sabiendo las solicitaciones a las que van a estar sometidos, es posible predecir el funcionamiento en servicio. Durante esta tesis doctoral se han caracterizado todos los materiales empleados en su desarrollo. Para ello se fabrican probetas de adhesivo en masa con forma de hueso de perro, que después fueron ensayadas a tracción. A partir de estos ensayos se obtienen los siguientes parámetros relativos a cada material: tensión máxima, tensión de rotura, elongación máxima y rigidez (o Módulo de Young).

Estos valores son básicos en cualquier caracterización de materiales. Conocer otros parámetros como la tenacidad a fractura en Modo I (GIC) y Modo II (GIIC) también puede llegar a ser necesario para según qué aplicaciones. Para el caso particular de esta tesis doctoral, fue necesario calcular el GIC, ya que los modelos de elementos finitos desarrollados durante el proyecto requerían conocer este valor, siendo GIIC calculado mediante métodos inversos. Estos cálculos fueron realizados por el doctorando durante su estancia pre-doctoral en el Departamento de Ingeniería Mecánica de la Facultad de Ingeniería de la Universidad de Oporto (FEUP) - Portugal. Para realizar los cálculos, se realiza el ensayo DCB (Double Cantilever Beam por sus siglas en inglés), obteniendo los valores de fuerza y desplazamiento, y las curvas de resistencia (R-Curve) de cada adhesivo. Análogamente se mide el crecimiento de la grieta durante todo el ensayo por medios ópticos. Los datos obtenidos experimentalmente fueron analizados utilizando tres métodos diferentes:

-Compliance Calibration Method (CCM).

-Corrected Beam Theory (CBT).

-Compliance-Based Beam Method (CBBM).

Los métodos más comúnmente utilizados para el cálculo de GIC se basan en la mecánica de fractura lineal elástica (Linear Elastic Fracture Mechanics - LEFM), esto incluye tanto el CCM como el CBT. Sin embargo, el CBBM está basado en lo que en inglés se denomina crack

equivalent concept, y solo depende de los parámetros de fuerza y desplazamiento obtenidos directamente de la máquina universal de ensayos, siendo un método sencillo y válido.

En la Publicación 6 (Designing, manufacturing and testing of a new 3D steel-CFRP node bonded by adhesives for its use in bus Structures. Journal of Materials Science & Technology, pendiente de aceptación) se ha fabricado el nodo de CFRP a tamaño real, y ha sido unido mediante el adhesivo seleccionado (Sikatack® Drive) a las vigas de acero que simulan la estructura del autobús. Esta publicación ha sido realizada en colaboración con miembros del Departamento de Ingeniería Mecánica de la Universidad Carlos III de Madrid.

Este trabajo se compone de una parte experimental (realizada por el doctorando) y una parte de simulación y optimización por elementos finitos realizada por los miembros del Departamento de Ingeniería Mecánica de la Universidad Carlos III de Madrid.

En lo que respecta a la parte puramente experimental, se ha fabricado el nodo de CFRP mediante un proceso denominado hand-lay up. Para ello, se parte de un núcleo de PLA (ácido poliláctico), fabricado por impresión 3D, al que se van añadiendo capas de tejido de fibra de carbono unidas una a una con resina epoxi. La fabricación del nodo fue realizada íntegramente por el doctorando.

Posteriormente, el nodo de fibra de carbono se une a los perfiles de acero que simulan la estructura de autobús utilizando para ello el adhesivo previamente seleccionado y estudiado en la Publicación 4. Para que la unión sea óptima, se aplican los tratamientos superficiales desarrollados también en la Publicación 4. La unión del nodo a los perfiles también fue realizada por el doctorando.

Se fabricaron tres prototipos completos (nodo de CFRP + adhesivo + vigas de acero). Todos ellos fueron ensayados a flexión en cuatro puntos, y a la máxima velocidad permitida por la máquina. El motivo por el que se realizan ensayos de flexión en cuatro puntos es porque se trata del ensayo que mejor reproduce las solicitaciones a las que está sometido el nodo durante las condiciones de servicio del autobús. Este último punto fue llevado a cabo por el equipo del Departamento de Ingeniería Mecánica de la UC3M con la ayuda del doctorando.

Los resultados muestran la capacidad de los nuevos prototipos de nodo de CFRP para ser utilizados en superestructuras de autobuses. Al estar el método de fabricación elegido muy extendido en la industria, es viable y sencilla su implementación a gran escala. El uso de un adhesivo elástico para realizar la unión entre el nodo de CFRP y la superestructura de acero

permitirá mejorar el comportamiento a fatiga del vehículo haciéndolo más eficiente. Este último apartado es un proyecto a futuro y no es un objetivo de esta tesis doctoral.

La Publicación 7 (Intensity of singular stress field (ISSF) variation as a function of the Young's modulus in single lap adhesive joints. International Journal of Adhesion and Adhesives, 95 (2019) 102418) fue desarrollada durante la estancia pre-doctoral que el doctorando realizó en el Departamento de Ingeniería Mecánica del Instituto de Tecnología de Kyushu (Kyutech) - Japón. Se trata de un trabajo de simulación desarrollado íntegramente por el doctorando bajo la supervisión de los miembros del grupo de investigación de acogida en Japón.

Este trabajo surgió buscando nuevos adhesivos para pegar el nodo a la superestructura de acero. En este estudio se planteó una unión graduada o mixta, siempre pensado en alta resistencia y deformación. Esto permite utilizar un adhesivo epoxi más rígido y con más alta resistencia, junto con otro epoxi más dúctil; de esta forma se pueden repartir los esfuerzos en toda la unión adhesiva. A pesar de que existen numerosos estudios sobre uniones adhesivas mixtas (o graduadas) y uniones adhesivas simples en la literatura, ninguno de ellos ha estudiado el efecto del módulo de Young en ambos tipos de uniones en términos del Intensity of Singular Stress Field (ISSF). Por esta razón, en este trabajo se han desarrollado cuatro modelos diferentes, combinando dos adhesivos epoxi con distintas propiedades mecánicas, estudiando el comportamiento del ISSF de cada modelo. De cara a facilitar al lector la comprensión del ISSF, indicar que es un parámetro proporcional al esfuerzo de pelado, y que se calcula en los bordes de la probeta. De este modo, el objetivo será conseguir el menor valor posible de ISSF.

La geometría seleccionada para las uniones mecánicas es la misma que la utilizada en el resto de la tesis doctoral, es decir a solape simple. Sin embargo, se ha utilizado un espesor de sustrato de 25 mm (muy superior a lo normalmente utilizado). Esto es debido a que trabajos previos desarrollados por el grupo de investigación de Japón, habían deducido que el valor de ISSF decrece paulatinamente hasta llegar a 25 mm, cuando se mantiene constante. Para poder comparar dos modelos, estos deben tener la misma combinación de material en la zona de estudio. Es decir, el sustrato y el adhesivo deben ser los mismos. Por tanto, se han comparado los modelos que tienen el mismo adhesivo en los bordes de la probeta.

La mejor combinación encontrada es aquella en la que el adhesivo con menor módulo de Young es colocado en los bordes, mientras que la zona central está cubierta con un adhesivo más rígido. La combinación de un adhesivo más rígido en las esquinas y más flexible en la zona central trabaja peor que aplicar una única capa del adhesivo rígido.

Este artículo abre una línea de futuro, en la que ya ha sido una parte desarrollada. Esta línea consiste en hacer los ensayos experimentalmente y comparar los resultados con los obtenidos mediante simulación en el Artículo 7. Los resultados son contradictorios ya que los ensayos muestran mejor deformación cuando el epoxi rígido está situado en el centro y el dúctil en los bordes. Esto puede estar producido porque el ISSF solo estudia los puntos singulares en una zona muy limitada en la unión. El trabajo futuro consistirá en simular el ensayo completo y así poder comparar los trabajos experimental y de simulación de forma eficaz.

3.2 PUBLICACIONES DE LA TESIS

Publicación 1

Galvez P, Quesada A, Martinez MA, Abenojar J, Boada MJL, Diaz V. Study of the behaviour of adhesive joints of steel with CFRP for its application in bus Structures. Composites Part B 2017; 129: 41-6. DOI: doi.org/10.1016/j.compositesb.2017.07.018.

Publicación 2

Galvez P, Abenojar J, Martinez MA. Durability of steel-CFRP structural adhesive joints with polyurethane adhesives. Composites Part B 2019; 165: 1-9. DOI: doi.org/10.1016/j.compositesb.2018.11.097.

Publicación 3

Galvez P, Abenojar J, Martinez MA. Effect of moisture and temperature on the thermal and mechanical properties of a ductile epoxy adhesive for use in steel structures reinforced with CFRP. Composites Part B 2019; 176: 107194. DOI: doi.org/10.1016/j.compositesb.2019.107194.

Publicación 4

Galvez P, López de Armentia S, Abenojar J, Martinez MA. Effect of moisture and temperature on thermal and mechanical properties of structural polyurethane adhesive joints. Composite Structures, acceptance pending.

Publicación 5

Galvez P, Carbas RJC, Campilho RDSG, Abenojar J, Martinez MA, da Silva LFM. Fracture toughness in Mode I (GIC) for ductile adhesives. Journal of Physics: Conference Series 2017; 843: 012008. DOI: 10.1088/1742-6596/843/1/012008.

Publicación 6

Quesada A, Galvez P, Boada MJL, Martinez MA, Garcia-Pozuelo D, Abenojar J. Designing, manufacturing and testing of a new 3D steel-CFRP node bonded by adhesives for its use in bus Structures. Journal of Materials Science & Technology, acceptance pending.

Publicación 7

Galvez P, Noda N, Takaki R, Sano Y, Miyazaki T, Abenojar J, Martinez MA. Intensity of singular stress field (ISSF) variation as a function of the Young's modulus in single lap adhesive joints. International Journal of Adhesion and Adhesives 2019; 95: 102418. DOI: doi.org/10.1016/j.ijadhadh.2019.102418.

Capítulo 4:

PUBLICACIONES

Índice

CONTENIDO PUBLICADO EN EL JOURNAL CITATION REPORTS (JCR)

PUBLICACIÓN 1

Composites Part B 129 (2017) 41–46

Contents lists available at ScienceDirect

Composites Part B

journal homepage: www.elsevier.com/locate/compositesb

Study of the behaviour of adhesive joints of steel with CFRP for its application in bus structures

Pedro Galvez [a], Alejandro Quesada [b, *], Miguel Angel Martinez [a], Juana Abenojar [a], Maria Jesus L. Boada [b], Vicente Diaz [b]

[a] Materials Science and Engineering and Chemical Engineering Department, University Carlos III de Madrid, Avda. de la Universidad, 30, 28911 Leganes, Madrid, Spain
[b] Mechanical Engineering Department, University Carlos III de Madrid, Avda. de la Universidad, 30, 28911 Leganes, Madrid, Spain

ARTICLE INFO

Article history:
Received 12 May 2017
Received in revised form
6 June 2017
Accepted 13 July 2017
Available online 16 July 2017

Keywords:
Adhesion
Mechanical testing
Surface treatments
Joints/Joining
Multi-material dissimilar materials
Multi-materials
Adhesive structural joints
Steel-CFRP joints
Buses

ABSTRACT

In recent years, the use of adhesives in structural applications is growing, achieving a great current implementation in the industry, due to the benefits that this technology is capable of providing to complex-shaped structures, both in aerospace and automotive applications. Adhesive joints show many advantages in comparison with other traditional joints such as welded joints, because they offer a continuous joint with homogeneous stress distribution, they are able to joint dissimilar materials (such metals and composite materials) and they do not require large investments. Current bus steel structures present fatigue problems due to the rigidity of the commonly used welded joints. Crack problems due to fatigue are evident in the areas of the bus structure closest to the rear door, being the joint between the side vertical pillars and the waist rail the most critical. A finite element model (FEM) of a bus steel structure is developed, in order to obtain the forces that work on the reference node. From the obtained force values, the value and type of stress at the reference node are calculated. A new carbon fiber reinforced polymer (CFRP) node is developed, replacing the existing welded joint by steel-CFRP adhesive joint. The new node design allows to obtain mainly shear stress. Because of that, single lap joint specimens are developed to carry out the experimental procedure. This work is focused on the study of a structural adhesive for its application in this new type of joint taking also into consideration manufacturing criteria (mounting periods, costs, etc.). This new adhesive joint shows strength values an order of magnitude higher than the requests at the node, and higher than 30% of strain values, minimizing fatigue problems.

1. Introduction

Nowadays, there is a high demand for the design of lightweight energy efficient and safe structures for transport applications [1]. Vehicles for passenger transport in general, and coaches and buses in particular are under a great pressure, due to high competition, safety regulations and user preferences. The most common material employed is still the high strength steel, due to its good mechanical properties at a reasonable cost.

The bus body is typically made of beams with hollow rectangular cross sections joined together by means of welding technique. The main advantages of using welding technique are that the joining process is faster, robust and cheap, no filler material is required, and dimensional accuracy is better preserved during welding with local heating [2,3]. Nevertheless, the welding requires high temperatures which cause the formation of a brittle layer of intermetallic compound at the joint interface, making it difficult to obtain the desired joint strength [4]. It also presents premature fails due to corrosion, needing more frequent inspections. On the other hand, bus body is subjected to different dynamic loads which are transmitted from the pavement to the structure leading also to crack problems, principally in certain welded joints due to fatigue [5,6].

For these reasons, new concept designs, materials and assembly methods have to be developed and applied by bus and coaches manufacturers. Various research works have been carried out in

* Corresponding author.
E-mail addresses: pgalvez@ing.uc3m.es (P. Galvez), alejandro@ing.uc3m.es (A. Quesada), mamc@ing.uc3m.es (M.A. Martinez), mjboada@ing.uc3m.es (M.J.L. Boada), vdiaz@ing.uc3m.es (V. Diaz).

http://dx.doi.org/10.1016/j.compositesb.2017.07.018

order to study the introduction of different types of materials such as aluminium alloys [7–9] and composite [10,11], for bus and coach body manufacturing in order to optimize fuel consumption by reducing vehicle weight without compromising strength or safety. While fiber-reinforced composites have showed potential for automobile parts in the past several decades, the application has yet to be realized on a mass production scale due to several drawbacks including low production, automation rates, and significant costs [12,13].

Multi-materials design strategies are being adopted in many field of transportation not only in aeronautic and aerospace but also in automotive [14–16]. Structures built in that manner consist not only of regular steel parts, but contain also a mix of components made from various lightweight materials like aluminum alloys or composites, which allow for significant reduction in vehicle curb weight. However, due to the differences in mechanical characteristics that are especially evident in the case of laminates, the material substitution is not a straightforward task [17]. New assembly approaches with different materials are now possible thanks to the use of structural adhesives.

Structural adhesive joints are increasingly being used in the manufacturing of hybrid [15,18] and complex [19,20] structures for civil, automotive and aerospace applications. They present important advantages against other type of joints because it is a simple and flexible technique, it offers a continuous joint with a homogeneous stress distribution during loading, ability to join dissimilar materials (such as metals with composite materials), less corrosion problems (avoiding the formation of galvanic corrosion batteries) and does not require great inversions [21].

Recently, a number of works have been undertaken to study the behaviour of multi-material structural adhesives. In Ref. [22] the effect of the humidity-temperature cycling on mechanical performance of adhesively bonded joints is investigated. Agarwal et al. in Ref. [23] study the effects of thermo-mechanical loading in both wet and dry conditions on steel-CFRP (Carbon Fiber Reinforced Polymer) single lap-joints. In Ref. [24] the characteristics of the dissimilar adhesive joint of the mild steel and aluminium sheets as a function of the mechanical and chemical surface treatment of the substrates is investigated. Flow characteristics and wettability of the epoxy based nanocomposite adhesive containing different amount of TiO_2 with substrate are also taken into account. The effect of bond line thickness of the adhesive in lap joints of the differently treated faying surfaces of the dissimilar metals on lap shear strength of the joints is also studied.

In order to solve the issue of fatigue crack in welded joints of steel bus structures, a new concept of joint made with CFRP is proposed. The aim of this work is to redesign the joint achieving higher flexibility to redistribute the stress field towards adjacent joints. This joint is connected to the steel structure by means of an elastic-plastic adhesive bond. This work is focused on the study of a structural adhesive for its application in this new type of joint taking also into consideration manufacturing criteria (mounting periods, costs, etc.). To select the most critical joint of the bus, a 3D FEM model of a bus structure is developed. This model is also used to calculate the loads that the joint needs to resist. With the value of the estimated loads and the size of the overlap area, the adhesive is selected. The steel-CFRP adhesive joint has been characterized by means of stress-strain curves obtained from shear tests, showing the suitability of the proposal for the raised problem.

2. Bus FEM model

The experience has shown that the welded joints which more commonly suffer crack problems in bus structures are closer to the rear door and more specifically those welded joints which joint side

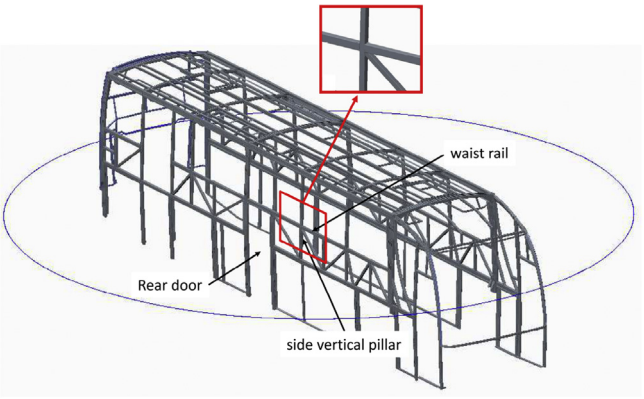

Fig. 1. Selected node.

vertical pillars with the waist rail. In order to confirm such assumption a finite element model (FEM) of a bus steel structure is used. The finite element analysis was carried out using ANSYS® code. This model allows to find the areas of the structure with higher stress problems, and gives the value of loads (in terms of forces and moments) needed to design an adhesive joint of steel with CFRP. Taking the results into account, authors decided to focus the study in the node depicted in Fig. 1 to provide an alternative solution.

The bus model has been built from the 3D geometry given by the manufacturer in STEP format. For this problem, a conventional "tridimensional solid elements" model is inappropriate, because of the high computational cost it can represent. A beams model could be adequate taking into account the geometric profile of the problem, but will not be good enough to calculate properly the stress distribution near to the joints and weldings, which are the most problematic areas in terms of stress values and fatigue resistance. A shell model has been selected, generating the mid-plane geometry model meshed with four nodes shell elements of 20 mm size.

The model has the following main characteristics:

- Number of nodes: 474.000
- Number of degrees of freedom per node: 6 (ux, uy, uz, rotx, roty, rotz)

The used material is structural steel whose properties are summarized in Table 1. A linear elastic isotropic model has been considered for the steel behaviour. The structure is expected to work under elastic conditions by the action of the considered loads. If the Yield Stress is found to be overcome in the model results, loads should be reconsidered, so linear elastic behaviour is an appropriate hypothesis since the loads do not take the material out of the linear elastic working range.

Solving the model for conventional load states that simulate conventional situations for a bus (braking, accelerating, curve passing, etc.) reasonable results have been found, with correct deformed shape and stress values always under 150 MPa.

Torsional loading cases have been studied because they generally result in large stress in the bus body. Displacements have been

Table 1
Properties of structural steel.

Property	Value
Density	7850 kg/m^3
Elastic modulus	210 GPa
Poisson's ratio	0.29
Yield strength	400 MPa

restricted adequately in the suspension connection points, depending on the load state solved in each case. For example, to simulate the torsion state, vertical displacement was restricted in each wheel connection point, with 0 value for three of them and a value of 5 cm for one of them (right front wheel). Longitudinal displacement, transversal displacement and vertical rotation was also zeroed in one point to avoid rigid body motion. Fig. 2 shows the stress distribution due to this torsional loading case. For the studied node, internal forces in each beam of the node are given in Table 2. Values are displayed respect to the reference system established by SAE J670e standard for motor vehicles (see Fig. 3).

Table 2
Forces in each beam of the node due to the torsional loading case.

Beam	F_x [N]	F_y [N]	F_z [N]
6	−452.7	−79.0	−518.5
11	2361.2	−38.2	23.1
37	−4323.7	20.1	168.0
39	−306.5	100.5	−1999.5
44	2721.7	−3.5	2326.8

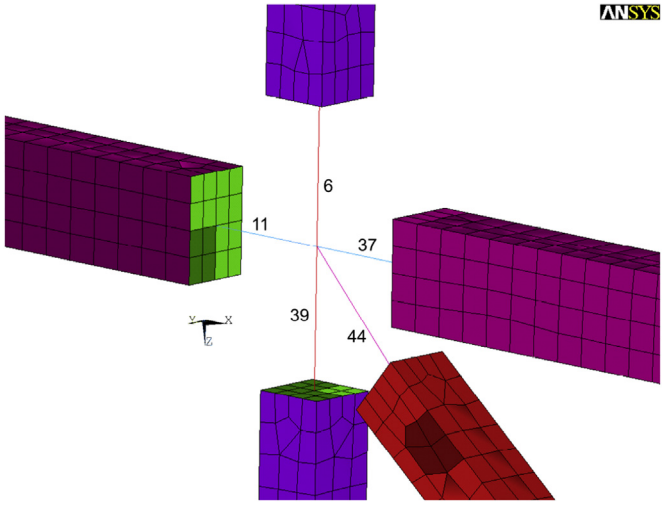

Fig. 3. Coordinate system in the bus FEM model.

3. Proposal of a new concept of node

The new node design to substitute the welded steel node must satisfy some requirements.

- The new design have to purchase strength enough to resist the previously calculated forces and moments.
- Dimensions must keep the geometry under the limits that the original structure sets.
- Stiffness must be adjusted to the optimized value that lets the designer to properly distribute the stress in the surroundings of the bus structure. To get this requirement it is important that the node design has some variable parameters capable to control the stiffness of the system by changing the design value.
- Another expected requirement is that the node design should facilitate the modular manufacturing of the bus structure. Expert welders are needed to build bus structures by the present technology. The new design should facilitate the building of the structure by assembling pre-manufactured parts without the needing of welding.

The geometric concept of the proposed design is shown in Fig. 4.

A composite material with epoxy polymer matrix and fiber reinforcement will be used because of the adequate balance of weight and strength that characterize such materials, being able to satisfy all the established requirements.

The adhesive must be found capable to resist the stresses generated by the node forces calculated from the bus FEM model. Axial forces act on the node, causing mainly shear stresses in the adhesive joint:

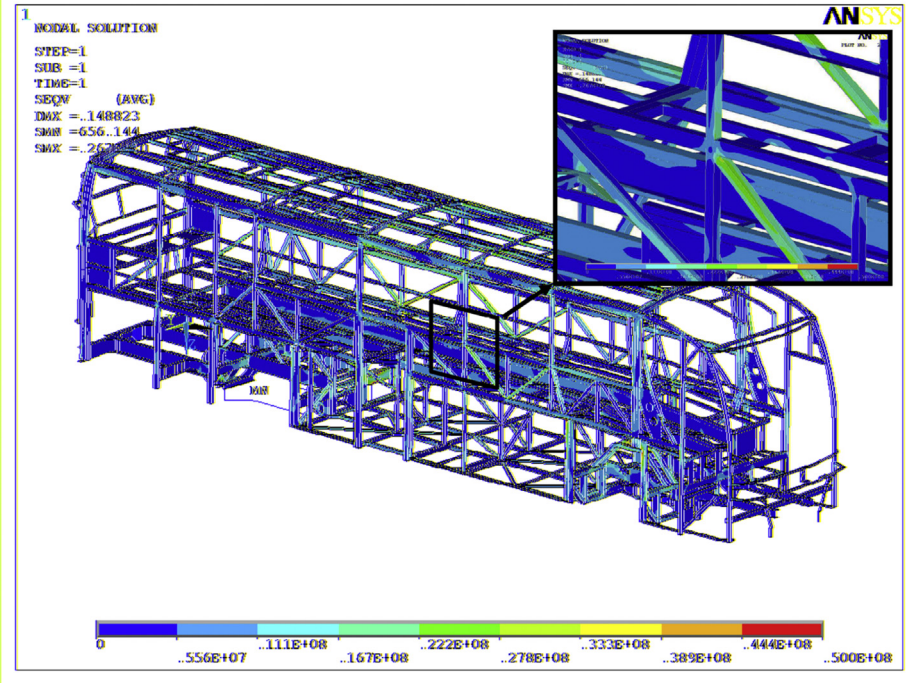

Fig. 2. Stress distribution, in Pa, due to a torsional loading case.

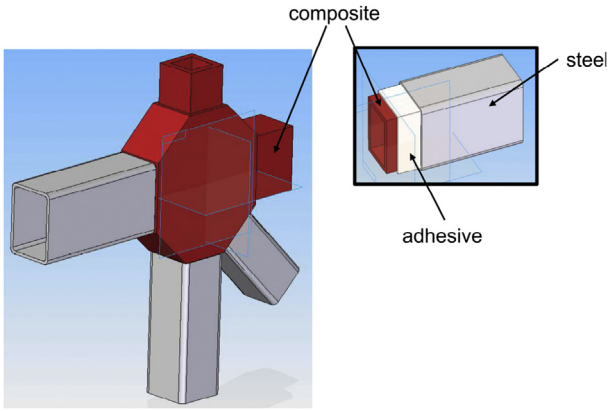

Fig. 4. Proposed new design of CFRP node adhesively bonded to steel beams of the bus structure.

$$\tau = \frac{F}{A} \tag{1}$$

where F is the axial force acting in each beam and A is the adhesive overlap area.

Adhesives work efficiently facing traction-compression or pure shear stresses, nevertheless, peel stresses caused by torques are the most harmful stress for any adhesive bonding. The design of our bond minimizes peel stresses to practically negligible values. Degrees of freedom between beams and composite part have been decreased, avoiding the relative movement between both elements by confined adhesive design [25]. The majority stresses of the bonding perform over the steel beam and the composite part.

The reference node is formed by 5 beams, thus 5 Steel-Adhesive-CFRP contact zones appear. To ensure that the bending will be avoided by geometrical interference of the beams meeting in the node and taking into account their averaged dimensions, an adhesive overlap of 50 mm is used.

From the developments exposed in the experimental procedure, the value of the stresses that the adhesive bonding should resist are calculated. Shear stress components are distributed along the coordinate axes as is shown in Fig. 3.

Table 3 shows the shear stress values obtained for each studied beam. These values have been calculated taking into account the most demanding service conditions for the adhesive joint. Under these conditions the adhesive joint of each beam will be responsible for resisting the resulting force F in its axial direction. Real confined adhesive design allows obtaining lower stress request, as it is explained above. From the most unfavorable case, we can get an idea of the safety margin in the obtained solution for the raised problem.

In terms of the adhesive selection, it is important to remark that this project allows for reducing the effects of fatigue caused by welded joints. Thus, it will be necessary to diminish the rigidity of the structure. This factor is essential in order to choose the adhesive. The selected adhesive must be sufficiently elastic-plastic, so that the stresses of fatigue in the structure of the bus are attenuated. In this paper the main objective is to study the viability of

Table 3
Shear stress values due to the torsional loading case.

Beam	F [N]	A [mm^2]	τ [MPa]
6	518.5	8400	0.06
11	2361.2	10800	0.22
37	4323.7	10800	0.40
39	1999.5	8400	0.24
44	3564.4	8400	0.42

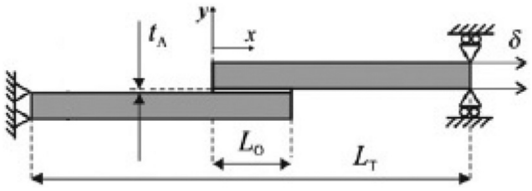

Fig. 5. Geometry and dimensions of studied Single Lap Joint specimens [28].

using a polyurethane based adhesive for the multi-material joint in the new concept of node. Previous works [26] reveal that for ductile adhesives like polyurethanes, 2 mm thickness leads to a better compromise between fracture toughness against traction and shear loads. The same adhesive thickness of 2 mm is used in single lap joints specimens and in the final node design to reproduce as accurately as possible the work conditions of the node.

4. Experimental tests to characterize the adhesive for the multi-material joint

4.1. Specimens

SikaTack Drive®, provided by SIKA SAU SPAIN, is selected as adhesive. It is a very elastic-plastic structural adhesive. Currently, this adhesive is used for bonding windshields of cars. As it is a structural adhesive, it has enough capacity to support the stresses that the node will be subjected to, providing the structure with the necessary elasticity to absorb fatigue stresses. On the other hand, as

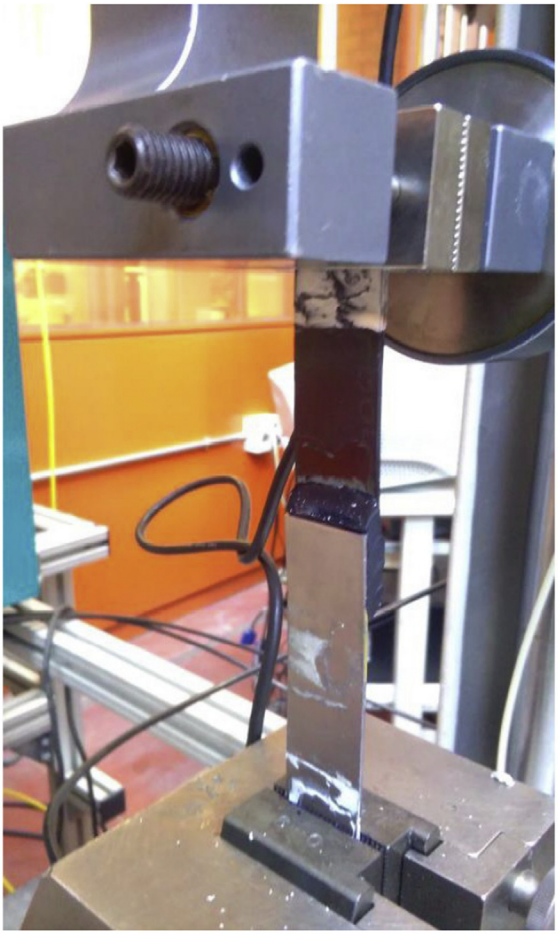

Fig. 6. Shear tests on specimens.

Table 4
Obtained values of shear tests for 5 tested single lap joint specimens.

	τ_{max} [MPa]	$\delta_{\tau max}$ [%]	$\gamma_{\tau max}$ [%]	Stiffness [MPa]	Type of break
Specimen 1	4.3	33	76	13.0	Cohesive
Specimen 2	4.1	33	76	12.5	Cohesive
Specimen 3	4.1	35	73	11.6	Cohesive
Specimen 4	4.8	38	76	12.5	Cohesive
Specimen 5	4.6	38	76	12.0	Cohesive
Average	4.4±0.3	35±2	75±1	12.3±0.5	

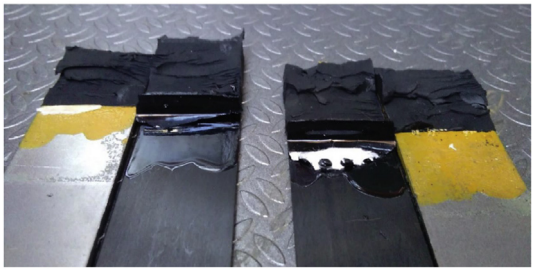

Fig. 7. Cohesive break.

it is polyurethane based adhesive, it has adequate behaviour against external agents, such as humidity and temperature. So it is suitable for the raised problem.

The new design of the joint was made in order to achieve the most favorable conditions for the adhesive bonds, minimizing peel stress and obtaining mainly shear stress.

For this study, five adhesive joint specimens of composite material and steel were manufactured. The composite used in the tests is Sika Carbodur ®, provided by SIKA SAU SPAIN. The other adherent is structural steel which is widely used in bus body structure manufacturing. Measurements for steel specimens are: length $L_S = 100$ mm, width $W_S = 25$ mm and thickness $T_S = 1.6$ mm. CFRP specimens have been manufactured through a pultrusion process. Specimens are cut with the following measurements: length $L_{CFRP} = 100$ mm, width $W_{CFRP} = 25$ mm and thickness $T_{CFRP} = 1.2$ mm.

Single Lap Joint specimens have been developed for carrying out shear tests. Geometry and characteristic dimensions of Single Lap Joint specimens are shown in Fig. 5. The following measures are used: adhesive thickness $t_A = 2$ mm, total specimen length $L_T = 175$ mm and adhesive overlap $L_0 = 25$ mm. Although EN 1465:2009 standard [27] establishes an adhesive overlap of 12.5 mm, previous works reveal that 25 mm overlap length is more appropriate for ductile adhesives [26].

4.2. Surface treatments

It is necessary to ensure a cohesive breaking (inside the adhesive) of the joint working with adhesives, being adhesive breaking (in the substrate-adhesive interfaces) undesirable. Therefore, the right surface treatments on the bonded substrates must be developed. For this work, different tests have been carried out, with the objective of determining the best possible surface treatment for the raised joint.

For steel substrate, the surface treatment consists in a 3 steps process. Step 1, is a sanding process with P180 sandpaper. Step 2, is a cleaning process with Ethanol solvent. And Step 3 consists of the application of a thin layer of a primer, Sika Primer 204 N®. Primers are products that favor the bond forming chemical bonds between the interfaces substrate-adhesive. Another benefit of primers is that it allows to protect the joint against corrosion problems.

For CFRP substrate, firstly, a cleaning process with Ethanol solvent is carried out. Then, an atmospheric pressure plasma treatment (APPT) is done. In the APPT process, an ionized gas is applied on the surface of the material through a torch. This treatment can be used for both polymers and metals, introducing polar groups on the surface of the material, increasing the surface energy value, making possible a better bond with the adhesive or with the primer [29]. The treatment has been used to activate the surface of the polymer (CFRP), with 3 m per minute of torch speed and 6 mm of torch-specimen distance. Finally, a thin layer of primer (Sika Primer 215 ®) is applied on the activated CFRP surface.

4.3. Shear tests

The shear tests were carried out, according to EN 1465:2009 standard [27]. These tests allow to accurately evaluate the suitability of the adhesive and surface treatment used for the considered problem. Shear tests are carried out in a Microtest ® universal testing machine, see Fig. 6, with 2 mm/min of test speed.

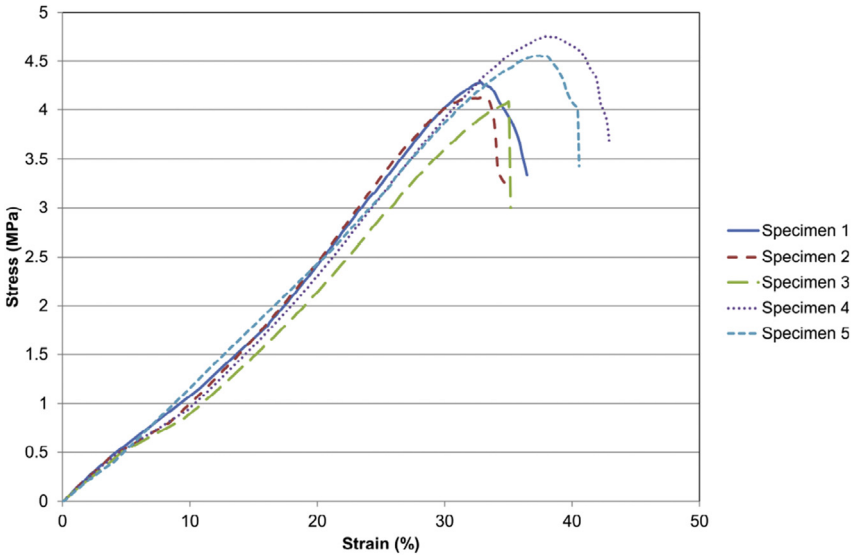

Fig. 8. Stress-Strain curves of the studied single lap joint specimens.

5. Results and discussion

Table 4 shows maximum stress (τ_{max}), normal strain for maximum stress ($\delta_{\tau max}$), shear strain for maximum stress ($\gamma_{\tau max}$) and stiffness values for each specimen. Likewise the type of break is shown too. Fig. 7 shows a cohesive break for one of the specimens used in the shear tests.

Stress-Strain curves of Fig. 8 show the comparison in terms of behaviour of the five studied specimens. The slope of the curve is directly related to the stiffness of the joint, and due to the cohesive failure, dispersion is minimal among the different specimens. This low dispersion can also be appreciated in Table 4 in the Stiffness column.

The selected adhesive shows deformation values higher than 30% for maximum shear stress. This is interesting for the raised problem, so that the rigidity of this part of the structure will be decreased compared to adjacent nodes, and consequently stress will be redistributed towards the surroundings and fatigue problems will also be reduced in the critical area. Maximum shear stress values are also enough, just like the resulting stresses as has been previously shown in Table 3.

6. Conclusions

The present study has analyzed the viability of using a polyurethane based adhesive to connect a new proposed concept of joint made with CFRP to the steel bus structure. From the performed lab test it was possible to conclude that:

- The raised adhesive joint shows values far superior to the stresses that it must bear, an order of magnitude higher than the most unfavorable service condition posed.
- The new raised adhesive joint allows to obtain greater elasticity at the reference node, decreasing the relative rigidity of the surroundings and minimizing mechanical fatigue.
- By replacing welded joints by new CFRP components, it is possible to decrease the weight of the structure, allowing greater efficiency by reducing fuel consumption.

Acknowledgements

This research was supported by Ministerio de Economia y Competitividad, Spain, under grants TRA2014-56471-C4-1-R and TRA2014-56471-C4-2-R. The authors gratefully acknowledge the collaboration of Castrosua S. A. who provided with the CAD information and let making tests over a manufacturing specimen and Sika S.A.U. España for supplying the adhesives.

References

[1] SAFEJOINT. Enhancing structural efficiency through novel dissimilar material joining techniques. European Project FP7-NMP-2012-SMALL-6. 2017. http://cordis.europa.eu/result/rcn/185066_en.html.
[2] Ertas AH, Vardar O, Sonmez FO, Solim Z. Measurement and assessment of fatigue life of spot-weld joints. J Eng Mater Technol 2008;131(1). 011011–011011–11.
[3] Dost I, Khan SA, Aziz M. Mechanical evaluation of joining methodologies in multi material car body. Int J Adv Eng Technol 2012;5(1):259–68.
[4] Sakiyama T, Murayama G, Naito Y, Saita K, Miyazaki Y, Oikawa H, et al. Dissimilar metal joining technologies for steel sheet and aluminum alloy sheet in auto body. Nippon Steel Tech Rep 2013;103:91–8.
[5] Perez JA, Badea F, Arribas D. Experimental characterization of the strain concentration factor in welded junctions of rectangular tube beam using digital image correlation. Procedia - Soc Behav Sci 2014;160:440–8. http://dx.doi.org/10.1016/j.sbspro.2014.12.156.
[6] Branco CM, Ferreira JA. Fatigue analysis of bus structures. In: Proceedings ong the european conference on fracture, ECF5; 1984. p. 643–58.
[7] Muttana SB, Sardar A, Mubashir S. Lightweighting of public transport buses in India: an impact analysis. In: SAE technical papers; 2011. http://dx.doi.org/10.4271/2011-28-0054.
[8] Espezua S, Baptista C, Laurito D, da Silva A. Influence of intermetallics and precipitates on the fatigue crack: nucleation and propagation in aluminum alloys 6005-T6, 6063–T6 and 6351-T6. In: SAE technical papers; 2012. http://dx.doi.org/10.4271/2012-36-0520.
[9] Constellium. World leader in aluminium manufacturing. 2017. http://www.constellium.com/markets/transportation/bus.
[10] LITEBUS. Modular lightweight sandwich bus concept. European Project. FP6-SUSTDEV. project ID: 31321. 2017. http://cordis.europa.eu/project/rcn/79972_en.html.
[11] Colombo C, Vergani L. Experimental and numerical analysis of a bus component in composite material. Compos Struct 2010;92(7):1706–15. http://dx.doi.org/10.1016/j.compstruct.2009.12.012.
[12] Song YS, Youn JR, Gutowski TG. Life cycle energy analysis of fiber-reinforced composites. Compos Part A Appl Sci Manuf 2009;40(8):1257–65. http://dx.doi.org/10.1016/j.compositesa.2009.05.020.
[13] Rocky Mountain Institute. Comparison of carbon fiber vs steel manufacturing costs. 2011. URL http://www.rmi.org/RFGraph-carbonfiber_vs_steel_manufacturing.
[14] Coutellier D, Rozycki P. Multi-layered multi-material finite element for crashworthiness studies. Compos Part A Appl Sci Manuf 2000;31(8):841–51. http://dx.doi.org/10.1016/S1359-835X(00)00022-1.
[15] Lauter C, Troster T, Reuter C. Hybrid structures consisting of sheet metal and fibre reinforced plastics for structural automotive applications. Advanced composite materials for automotive applications. John Wiley & Sons Ltd; 2013. p. 149–74. http://dx.doi.org/10.1002/9781118535288.ch7.
[16] Ocana R, Arenas JM, Alia C, Narbon JJ. Evaluation of degradation of structural adhesive joints in functional automotive applications. Procedia Eng 2015;132:716–23. http://dx.doi.org/10.1016/j.proeng.2015.12.552.
[17] Korta J, Uhl T. Multi-material design optimization of a bus body structure. J KONES Powertrain Transp 2013;20(1):139–46.
[18] Marques EAS, da Silva LFM, Flaviani M. Testing and simulation of mixed adhesive joints for aerospace applications. Compos Part B Eng 2015;74:123–30. http://dx.doi.org/10.1016/j.compositesb.2015.01.005.
[19] Ascione F, Mancusi G, Spadea S, Lamberti M, Lebon F, Maurel-Pantel A. On the flexural behaviour of GFRP beams obtained by bonding simple panels: an experimental investigation. Compos Struct 2015;131:55–65. https://doi.org/10.1016/j.compstruct.2015.04.039.
[20] Lamberti M, Maurel-Pantel A, Ascione F, Lebon F. Influence of web/flange reinforcement on the GFRP bonded beams mechanical response: a comparison with experimental results and a numerical prediction. Compos Struct 2016;147:247–59. https://doi.org/10.1016/j.compstruct.2016.03.043.
[21] Kah P, Suoranta R, Martikainen J. Techniques for joining dissimilar materials: metals and polymers. Rev Adv Mater Sci 2014;36(2):152–64.
[22] Korta J, Mlyniec A, Uhl T. Experimental and numerical study on the effect of humidity-temperature cycling on structural multi-material adhesive joints. Compos Part B Eng 2015;79:621–30. http://dx.doi.org/10.1016/j.compositesb.2015.05.020.
[23] Agarwal A, Foster SJ, Hamed E. Testing of new adhesive and CFRP laminate for steel-CFRP joints under sustained loading and temperature cycles. Compos Part B Eng 2016;99:235–47. http://dx.doi.org/10.1016/j.compositesb.2016.06.039.
[24] Ghosh PK, Kumar K, Preeti P, Rajoria M, Misra N. Superior dissimilar adhesive joint of mild steel and aluminium using udm processed epoxy based tio2 nano-filler composite adhesive. Compos Part B Eng 2016;99:224–34. http://dx.doi.org/10.1016/j.compositesb.2016.06.014.
[25] Martinez MA, Chocron IS, Rodriguez J, Galvez VS, Sastre LA. Confined compression of elastic adhesives at high rates of strain. Int J Adhesion Adhesives 1998;18(6):375–83. http://dx.doi.org/10.1016/S0143-7496(98)00023-2.
[26] Banea MD, da Silva LFM, Campilho RDSG. The effect of adhesive thickness on the mechanical behavior of a structural polyurethane adhesive. J Adhesion 2015;91(5):331–46. http://dx.doi.org/10.1080/00218464.2014.903802.
[27] UNE-EN 11465:2009. Adhesives. Determination of tensile lap-shear strength of bonded assemblies. Madrid: AENOR; 2009. 11 p.
[28] Neto JABP, Campilho RDSG, da Silva LFM. Parametric study of adhesive joints with composites. Int J Adhesion Adhesives 2012;37:96–101. http://doi.org/10.1016/j.ijadhadh.2012.01.019.
[29] Encinas N, Oakley BR, Belcher MA, Blohowiak KY, Dillingham RG, Abenojar J, et al. Surface modification of aircraft used composites for adhesive bonding. Int J Adhesion Adhesives 2014;50:157–63. http://doi.org/10.1016/j.ijadhadh.2014.01.004.

PUBLICACIÓN 2

Composites Part B 165 (2019) 1–9

Contents lists available at ScienceDirect

Composites Part B

journal homepage: www.elsevier.com/locate/compositesb

Durability of steel-CFRP structural adhesive joints with polyurethane adhesives

Pedro Galvez*, Juana Abenojar, Miguel Angel Martinez

University Carlos III de Madrid, EPS Polytechnic School, Materials Science and Engineering and Chemical Engineering Department, Avda. de la Universidad, 30, 28911, Leganés, Spain

ARTICLE INFO

Keywords:
Polymer-matrix composites (PMCs)
Environmental degradation
Mechanical properties
Surface treatments
FRP-steel bonded joints

ABSTRACT

The use of reinforcing materials in steel structures is very widespread today because this combination is capable of bringing great improvements to this type of structures. In this work, a steel-CFRP (carbon fiber reinforced polymer) adhesive joint is proposed, trying to combine the good properties of both materials. Two structural polyurethane adhesives, one conventional and another hybrid, are selected to develop the joint due to the good properties of this material against external environmental agents and the high loads that are capable of resisting. The objective is to verify the suitability of this type of joints for structural applications in aggressive environments. For this purpose shear tests are carried out on specimens subjected to different exposure times in an aggressive environment, evaluating how their mechanical properties vary. Reliability studies are developed using a simplified model of the Weibull distribution, obtaining the distribution of failures of the joints. Microscopy techniques (Scanning Electron Microscope and optical microscope) are used to evaluate the failures of the studied specimens. The reliability of the joints under extreme aggressive conditions is verified in the results. Even having different behavior in the adhesives, both of them are able to maintain adequate strength after the degradation process.

1. Introduction

The use of joints of dissimilar materials in the industry has increased in recent years. An example of this trend is the use of fiber-reinforced polymers as reinforcement in structural engineering. Many authors are developing works related to the subject, Narmashiri et al. [1] study steel hollow pipe sections reinforced with CFRP subjected to transverse loads, and Zeng et al. [2] present an experimental study on the flexural behavior of full scale CFRP-strengthened H-section steel beams.

There are different techniques capable of join dissimilar materials: adhesive bonding, mechanical fastening and welding. Associated problems with conventional joints (stress concentration points, heat affected zones, fatigue and corrosion among others) require the development of new types of joints, being adhesive joints the best option actually. New technologies are currently being developed such as laser welding, ultrasonic welding and friction-stir welding. However, the use of these technologies in polymers materials is restricted only to thermoplastics [3].

In the last years, the use of adhesives is increasing. Manufacturers and designers of the aerospace, automotive, marine and building industries have found new possible uses. This has been possible thanks to the newly developed structural adhesives, allowing its use for high strength applications [4–6]. Among the benefits of using adhesives are: lower manufacturing costs, weight reduction, good resistance to static and dynamic loads, improved damage tolerance and quasi-homogeneous stress distribution. Pitta et al. [7] compared metal-metal and metal-composite adhesive bonded lap joints with metal-metal riveted lap joints, showing adhesive joints three times higher average strength than riveted joints.

There are different types of adhesives capable of being used in structural applications. Together with the already extended use of epoxy adhesives, polyurethane based adhesives are being used increasingly more. They were discovered in 1939 when the polyaddition polymerization reaction of polyisocyanates with functional hydroxyl or amine compounds was carried out. Nowadays, polyurethanes are being implemented in the industry in different ways: as coating thanks to the good properties against external agents [8], as binder in more efficient processes like brackish water desalination process [9], as sealant [10], as a foam in sandwich panels [11], as adhesive [12,13], and even in biomedical applications [14].

Chemistry of polyurethane adhesives has been extensively studied in the literature [15,16], showing great versatility and raising their use

* Corresponding author.
E-mail addresses: pgalvez@ing.uc3m.es (P. Galvez), abenojar@ing.uc3m.es (J. Abenojar), mamc@ing.uc3m.es (M.A. Martinez).

https://doi.org/10.1016/j.compositesb.2018.11.097
Received 4 September 2018; Received in revised form 6 November 2018; Accepted 25 November 2018
Available online 26 November 2018
1359-8368/

[17]. Recent studies have shown the capability of this material to be used in structural applications [18–21].

Works studying the effects of humidity and temperature on the mechanical properties of adhesive joints can be found in the literature, but in most cases using epoxy adhesives [22–24]. Viana et al. [25] developed a review about the temperature and humidity degradation of adhesive joints. The effect of harsh environment on shear and tensile strength of multi-material adhesive joints have been studied [26], as well as the influence of combined mechanical and environmental loads on the behavior of metal-composite adhesive joints [27]. Costa et al. [28] studied the effects of water on the fatigue behavior of aluminum adhesive joints. Heshmati et al. [29] study the effect of moisture in the mechanical properties of an epoxy adhesive, finding a direct relationship between moisture content and mechanical properties. This relationship is different from that found when it comes to polyurethane adhesives. Ageing mechanisms of polyurethane adhesives are studied in the literature [15], but works that study the mechanical behavior of polyurethane joints against temperature and humidity cannot be found. This paper seeks to address this lack.

Substrates are a fundamental part of the work with adhesives. Most metals have high surface energies, favoring the adhesion. However, in most cases, it is necessary to carry out surface treatments such as sanding (to obtain surface roughness), primer (to promote chemical bonding) or just cleaning, among others. Surface energy values in most polymers are low. Because of that, it is necessary to perform surface treatments capable to increase these values [30]. For adhesive joints, the polar value of the surface energy is the most important one. Using an atmospheric pressure plasma treatment (APPT), it is possible to increase it [31,32], as polar groups are incorporated on the material surface. Other treatments that can be carried out are: primer (to increase the surface energy and promote chemical bonding), chemical cleaning, peel ply, flaming and shot peening (among others). Roughness is noteworthy as one of the most important factors for the adhesive joints. Providing roughness to the surface (sanding in the steel or peel ply in the composite material), a better mechanical bonding can be obtained, by increasing contact surface [33].

This work is focused on the study of two different polyurethane structural adhesives. Tensile shear stress tests are made for different aging conditions in order to know the viability of the studied adhesive joints, using in each case the best surface treatment, obtaining always cohesive failure. For the steel substrate, the treatment recommended by the adhesive manufacturer is used. For the composite substrate, APPT is used.

2. Experimental procedures

2.1. Materials

The objective of this article is the development of steel-CFRP adhesive joints and the study of the behavior of these joints against a degradation process. Two different structural polyurethane adhesives were used for executing this work: Sikaflex® 252 and Sikaflex® 552AT. Both of them were supplied by Sika S.A.U. Spain. Sikaflex® 252 is a conventional single-component polyurethane adhesive. Sikaflex® 552AT is a hybrid single-component polyurethane adhesive with silane termination. The existence of silanes in the formulation of this hybrid adhesive allows bonding on surfaces without primer or more complex surface treatments. Both adhesives were cured at room temperature (25 °C and 50% relative humidity) for 15 days.

Two dissimilar materials were used as substrates: AISI 1012 carbon steel supplied by Carrocera Castrosua S.A. and carbon fiber reinforced polymer (CFRP) manufactured by pultrusion by Sika S.A.U. Spain, being its trade name Sika Carbodur® S-512. Dimensions for steel specimens were (in mm): length (L_S) = 100, thickness (T_S) = 1.6 and width (W_S) = 25. The dimensions of the CFRP specimens were (in mm): length (L_{CFRP}) = 100, thickness (T_{CFRP}) = 1.2 and width (W_{CFRP}) = 25.

2.2. Surface treatments

Sika® Primer 204N was used on the steel surface for Sikaflex® 252. Prior to the application of the primer, sanding with P180 sandpaper and solvent cleaning were carried out. For hybrid Sikaflex® 552AT it is not necessary to use primer on the steel because of the silane termination of this adhesive. Sanding with P180 sandpaper and solvent cleaning were also implemented for this adhesive. For CFRP substrate, APPT was carried out. The treatment consists of the application of ionized atmospheric air on the surface of the material through a torch. Surface energy values were increased, increasing wettability too, making possible the adhesion between the CFRP and the adhesive. The parameters used in the APPT were: 3 m/min of torch speed and 6 mm of torch-specimen distance.

2.3. Shear tests

Shear tests were carried out following UNE-EN 1465:2009 standard in a Microtest® universal testing machine, with test speed of 10 mm/min. Adhesive overlap (L_0) of 25 mm was selected instead of 12.5 mm as is indicated in the standard. The strength of joints developed with ductile adhesives (as those used in this work) increases with the increment of the overlap length, on the contrary that happens for brittle adhesives [34]. Thus, adhesive overlap of 25 mm is more suitable for joints with ductile adhesives. This study seeks to determine the ability of these adhesives to be used in structural applications in environments under humidity and temperature, subjected mainly to shear stress. In this test it is not possible to obtain pure shear stress, since other stresses such as peeling can also affect. So, shear stress (τ) is the predominant stress, calculated from a load, which actually is the average of the different existing loads. Fig. 1 shows the representation and the dimensions of the single-lap joints specimens used in this work. The dimensions were (in mm): adhesive thickness (t_A) = 2, adhesive width (W_{ADH}) = 25 and total specimen length (L_T) = 175. The excess adhesive was removed after the curing process. To obtain the desired adhesive dimensions, steel spacers were used.

2.4. Mechanical properties

To evaluate the degradation processes of the adhesive joints, stress-strain curves of each adhesive and condition are studied. From these curves, maximum shear stress (τ_{max}) in MPa, strain for maximum shear stress ($\delta_{\tau max}$) in %, and stiffness in MPa, are calculated. Curves were obtained from the results of the universal testing machine. In this way, from the values of load (F), adhesive overlap (L_0) and adhesive width (W_{ADH}), shear stress (τ) is calculated:

$$\tau = \frac{F}{L_0 \times W_{ADH}}$$

Strain [%] is determined by:

$$Strain = 100 \times \left(\frac{displacement}{L_0}\right)$$

Where displacement is the variation of position experienced by the clamp of the universal testing machine during the test, and L_0 is the adhesive overlap. Regarding stiffness is the slope of the curve between 0.2 MPa (τ_1) and 0.8 MPa (τ_2) in the shear stress – unit strain curves. Strain is represented in the graphs as a percentage; however, the slope is calculated from the values of unit strain for τ_1 (U_{S1}) and τ_2 (U_{S2}) according to:

$$Stiffness: \frac{\tau_2 - \tau_1}{U_{S2} - U_{S1}}$$

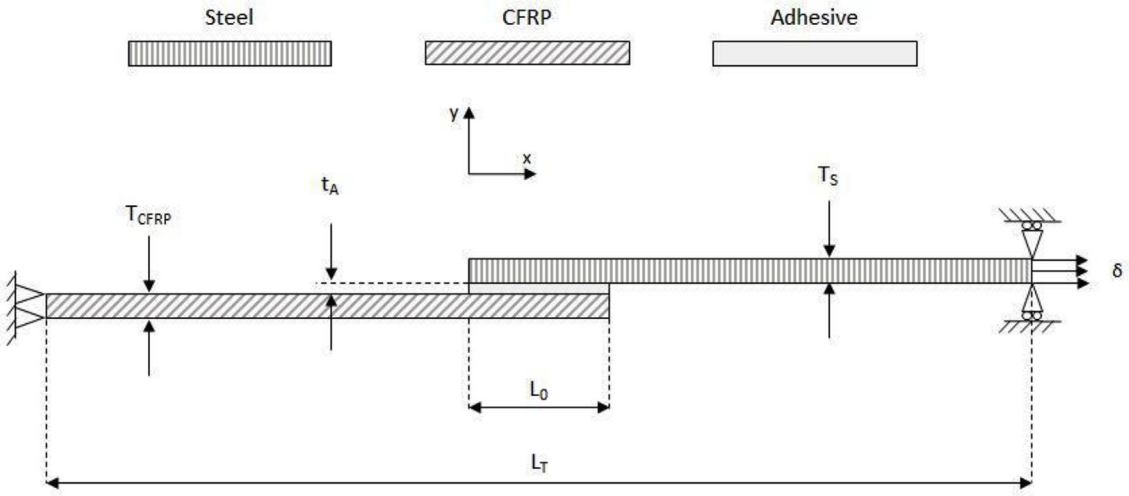

Fig. 1. Representation of the single-lap joint specimens used in this work.

2.5. Durability tests

Durability tests were developed to evaluate the ability of the adhesive joint to be used under humidity and temperature conditions. A climatic chamber (Fig. 2) was developed to carry out the study. A polypropylene closed box was used as specimen placement area. Through a special closing system made also of polypropylene, it was possible to obtain a complete sealing of the system. The chamber was designed to hold aqueous substances at the bottom. Water was used in this work. The presence of water made possible to obtain high values of relative humidity. The other factor to take into account is the temperature. The climatic chamber was introduced in a stove equipped with an air ventilation system (Digitronic TFT – JP Selecta S.A.) in order to obtain the desired temperature (70°C). The existence of water in a closed environment at 70°C allows obtaining a relative humidity close to 80%.

Temperature and relative humidity were monitored with a thermohigrometer (MSR 145 - MSR Electronics GmbH – Seuzach, Switzerland) throughout the experiment in order to determine the exact conditions inside the chamber. Three different conditions were used to evaluate the degradation process of the adhesive joint under conditions of humidity and temperature:

- Specimens without degradation.
- 100 h of degradation.
- 500 h of degradation.

Twelve specimens for each condition and adhesive were studied in order to have a specimen size enough to perform the statistical study correctly.

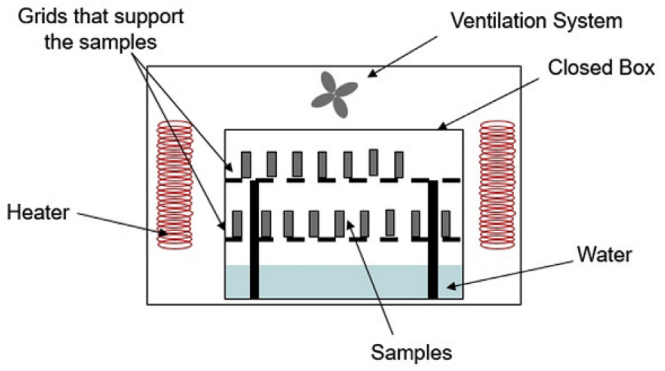

Fig. 2. Climatic chamber scheme.

2.6. Statistical studies

Statistical studies were carried out with the aim of determining the reliability of the developed adhesive joints before and after a degradation process in an aggressive environment. Any population of data obtained from laboratory tests should be analyzed to determine the suitability of the study. It is necessary to determine the appropriateness of all data, and find those values that can be considered anomalous to remove them (outliers), avoiding distortions in the final results of the reliability study. To discard the anomalous data, the Grubbs' test was used. This test can only be used in populations that follow a normal or Gaussian distribution, as it happened in the population that was studied in this work.

The adhesive joint proposed in this work can be used for structural applications. Any component designed to work in structural applications must be able to ensure correct operation throughout the useful life. To evaluate the reliability of the studied joints, Weibull model was used. The Weibull distribution can be used in the fields of mechanical, materials and chemical engineering. Weibull distribution allows studying what is the failure distribution of a particular component. This method does not determine which are the variables influencing on the failure rate, but it facilitates the identification and consideration of the failures. This methodology is useful for structural components in preventive maintenance programs. The minimum number of specimens needed to apply Weibull study is ten.

2.7. Thermal characterization

Differential scanning calorimetry (DSC) analyses (DSC 822e – Mettler Toledo GmbH – Greifensee, Switzerland) were carried out to understand the mechanisms of degradation of the adhesive after being subjected to conditions of humidity and temperature. The heating speed was 20°/min in a range with initial temperature of −60°C and final temperature of 200°C.

2.8. Characterization of the failure mode of the adhesive joint

The objective was to be able to determine conclusively the type of failure found in each condition and adhesive. Microscopy techniques may be necessary to determine the type of failure of the adhesive joint. Using these techniques, the surface can be studied and in many cases check the existence of a thin layer of adhesive therein, obtaining cohesive failure instead of adhesive failure as it seemed at first sight. To

Table 1
Mechanical values of adhesive joints made of Sikaflex® 252.

	0	100 h	500 h
Stiffness [MPa]	2.0 ± 0.3	3.4 ± 0.3	3.5 ± 0.3
τ_{max} [MPa]	1.1 ± 0.1	1.3 ± 0.1	1.2 ± 0.2
$\delta_{\tau max}$ [%]	72.3 ± 7.5	49.2 ± 5.4	47.0 ± 4.5
Type of failure	Cohesive	Cohesive	Cohesive

correctly characterize the failure mode of the adhesive joint, two different microscopy techniques were used: optical microscopy (Olympus GX71 - Olympus Corporation - Tokyo, Japan) and SEM microscopy (Teneo SEM - Thermo Fisher Scientific Inc. – Waltham, USA). Conventional photographic device is also used to take photos of broken specimens.

3. Results

Twelve specimens for each condition are tested. To plot the strain-stress curves of the performed tests, the most representative specimens for each condition are selected, seeking to simplify the information. To select the most representative specimens, Gaussian distribution curve is taken into account choosing the values closest to the arithmetic average. Cohesive failure is obtained in both adhesives for all studied conditions, as is explained in next sections.

3.1. Sikaflex® 252: degradation phenomena

As Table 1 shows, from 0 to 100 h of degradation, the adhesive undergoes a stiffening process. This is reflected in the stiffness, going from 2.0 ± 0.3 to 3.4 ± 0.3 MPa. In terms of τ_{max}, values go from 1.1 ± 0.1 to 1.3 ± 0.1 MPa. The increment of stiffness is very clear in the strain value for τ_{max} ($\delta_{\tau max}$), going from 72.3 ± 7.5% to 49.2 ± 5.4%. From 100 h to 500 h of degradation, no substantial changes were observed in the three studied values. As it is a polyurethane based adhesive, it cures in the presence of humidity. Changes in the mechanical properties of the adhesive are due to a post-curing process, which increases the degree of cross-linking in the polymer network, stiffening the polyurethane [35]. Differential Scanning Calorimetry (DSC) tests of Sikaflex® 252 show the existence of T_g in the studied range (from −60 °C to 200 °C - 20°/min). T_g is around −50 °C, so at room temperature (25 °C) and at degradation tests temperature (70 °C) the adhesive behaves elastically. In these conditions, the adhesive is not in a glassy state, but it is in a gummy state, being a typical circumstance of single-component polyurethanes. Tcharkhtchi et al. [35] study the effect of temperature on the mechanical properties of polyurethane, relating the loss of mechanical properties with the thermal degradation of the adhesive. The degradation phenomenon is associated with a reduction of the cross-linking density and the formation of linear molecules in the network, which can suffer plasticization. Since there is no decrease in the value of the mechanical properties of the adhesive after the exposure to extreme conditions during 500 h, it can be deduced that the adhesive has not undergone thermal degradation.

Stress-strain curves of three representative specimens for each degradation step are shown in Fig. 3. The curve of the tests without degradation shows lower slope than with degradation, for this reason the value of the stiffness increases with exposure to humidity and temperature. In terms of τ_{max}, the increase of this value is reflected in the curves corresponding to 100 h and 500 h.

3.2. Sikaflex® 552AT: degradation phenomena

As Table 2 shows, from 0 to 100 h of degradation, the adhesive loses stiffness, going from 8.9 ± 1.1 to 4.9 ± 1.3 MPa. In terms of τ_{max} values, these are going to remain constant, going from 1.6 ± 0.1 to 1.4 ± 0.2 MPa. This stiffness reduction is clear in the strain value for τ_{max} ($\delta_{\tau max}$), going from 22.2 ± 2.5% to 46.3 ± 14.8%. From 0 to 500 h of degradation, important changes in the values of the mechanical properties are observed.

Despite being a polyurethane based adhesive, in this case the presence of humidity and temperature will not cause a post-curing process. Nevertheless, the adhesive is less rigid and less resistant, so any changes in the polymer network have taken place. Exist two different ways of humidity absorption in epoxy [25] and polyurethane [36] adhesive joints: as free water, causing plasticization in the adhesive, and as bound water, producing swelling, plasticization and strength decrease in the adhesive. In Ref. [25], authors explain other mechanisms of degradation of the adhesive joint through the adhesive-substrate interface. The type of failure obtained, always cohesive, and the performed micrographs, allow us to deduce that one degradation mechanism in this case is due to the absorption of humidity by the adhesive. FTIR (Fourier Transform Infrared Spectroscopy) analyses are carried out in the CFRP substrate, showing that no water absorption has occurred during the time of exposure, discarding the degradation of the CFRP due to the moisture effect. Therefore, the variation of the mechanical properties of the joint is due to a degradation process in the adhesive, and not in the substrate.

Temperature is another mechanism of degradation of the adhesive joint, being the main mechanism in the case of polyurethanes. To study this phenomenon, DSC test were carried out (−60 °C–200 °C - 20°/min) in specimens without degradation and specimens submitted to 100 h of exposure to temperature and humidity. Bulk adhesive specimens are used. T_g was detected around −50 °C in both cases. Durability tests were carried out at 70 °C of temperature, so the softening process may be starting, as is shown in DMA test developed by other authors [37]. The degradation of the adhesive is evident at 500 h of exposure. Tcharkhtchi et al. [35] study this phenomenon, concluding that the degradation occurs due to the increment of critical molecular weight, and to the reduction of the cross-linking density associated to a chain scission in the polymer network. New linear molecules are set up, being able to have a plasticization effect, diminishing stress and stiffness values.

Stress-strain curves of three representative specimens for each degradation step are shown in Fig. 4. The curve of the tests without degradation shows higher slope than with degradation, for this reason the value of the stiffness decreases with exposure to humidity and temperature. In terms of τ_{max}, the decrease of this value is reflected in the curves corresponding to 100 h and 500 h. This is symptomatic of a plasticizing process. This phenomenon is produced by the presence of hydroxyl groups (−OH), which could form hydrogen bonds with water molecules [18].

3.3. Study of the reliability of the adhesive joints

Working with structural components, it is essential to know their reliability in order to be sure that they will be able to withstand the stress to which they will be subjected. In the case of durability studies, this factor is more important because different processes may appear in the adhesive joint, being necessary to quantify the risk of failure.

To quantify the risk of failure as a function of the time of exposure to humidity and temperature, a simplified Weibull model is used. This model seeks to compare the results of the tests under different exposure times. Therefore, as this is a qualitative analysis, it will not be necessary to develop more complex reliability models.

3.3.1. Sikaflex® 252

In Fig. 5, reliability curves of Sikaflex® 252 are shown. Shifting appears, coinciding with the increase in the value of stress found during the durability process. For the specimens without degradation, reliability starts to decrease from 750 kPa. From 1000 kPa of stress value,

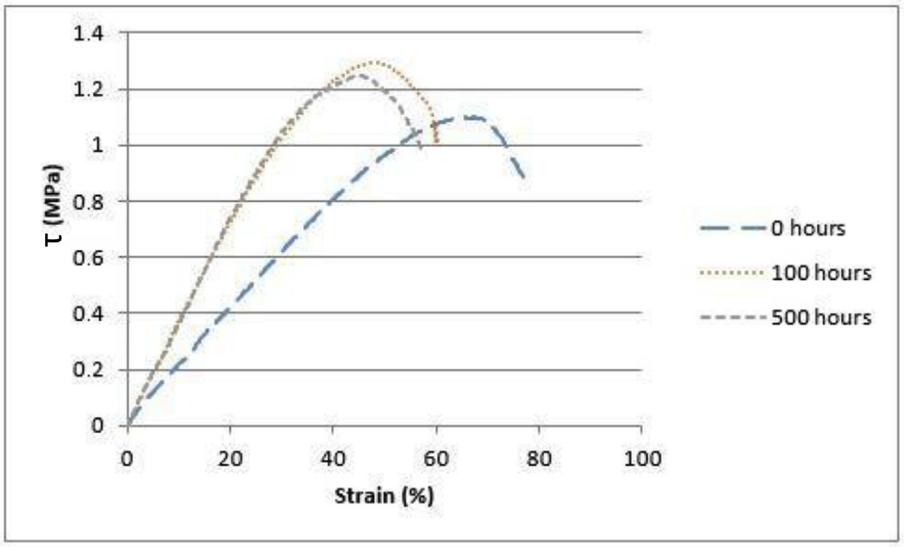

Fig. 3. Representative strain-stress curves of Sikaflex® 252 for each condition.

Table 2
Mechanical values of adhesive joints made of® 552AT.

	0	100 h	500 h
Stiffness [MPa]	8.9 ± 1.1	4.9 ± 1.3	5.0 ± 1.4
τ_{max} [MPa]	1.6 ± 0.1	1.4 ± 0.2	1.3 ± 0.1
$\delta_{\tau max}$ [%]	22.2 ± 2.5	46.3 ± 14.8	40.7 ± 9.7
Type of failure	Cohesive	Cohesive	Cohesive

when 70% of reliability is shown, the descent is greater. Finally, for values above 1300 kPa, the reliability is practically zero. The curves corresponding to 100 and 500 h of exposure are similar, showing a decrease in the reliability of the joints from values around 1000 kPa. With stress values higher than 1400 kPa, reliability is practically zero. This is consistent with the stress values obtained during the tests.

3.3.2. *Sikaflex® 552AT*

In Fig. 6 reliability curves of Sikaflex® 552AT are shown. Shifting, coinciding with the decrease in the value of stress found during the durability process, is observed. Specimens without degradation lose reliability from 1400 kPa. It is a curve with a clear vertical trend. This verticality shows a smaller dispersion of data, being positive in terms of reliability. From 1750 kPa reliability is lower than 20%. The curve relating to 100 h of exposure to humidity and temperature shows horizontal trend, ergo the variability of the data is greater, decreasing the reliability of the whole. From 1100 kPa, reliability is close to 90%, being less than 5% above 1700 kPa. For 500 h of exposure, degradation begins with stress values of 1100 kPa, as it happens for 100 h. Nevertheless, reliability descends at 1150 kPa quickly, being below 10% of reliability for values above 1400 kPa.

The verticality of the curve is a sign of reliability, the more vertical the curve, the smaller data dispersion is obtained. Fig. 5 shows how the verticality of the curve increases with the exposure time due to the post-curing of Sikaflex® 252. While in Fig. 6 the opposite happens, because in this case, Sikaflex® 552AT undergoes degradation and plasticization.

In the same way, the stiffening experienced by Sikaflex 252 correlates with greater reliability. While the plasticization experienced by Sikaflex 552AT correlates with adhesive degradation and worse reliability.

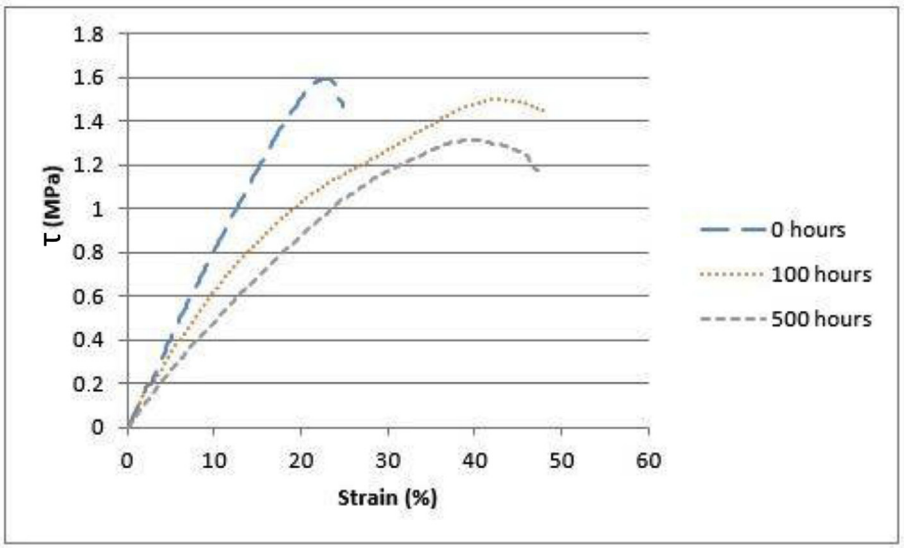

Fig. 4. Representative strain-stress curves of Sikaflex® 552AT for each condition.

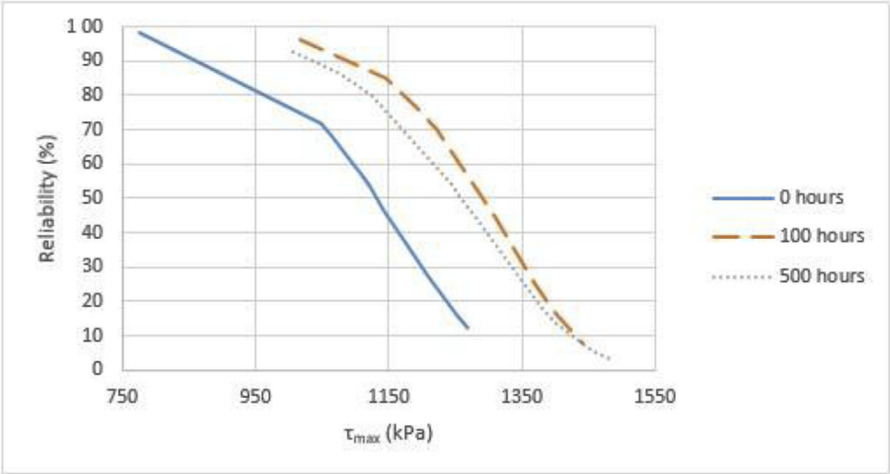

Fig. 5. Reliability curves of Sikaflex® 252.

3.4. Optical surface study

Micrographs of the adhesive joints are carried out to study the surfaces of the substrates after the tests. In this way, it has been possible to deduce the type of rupture achieved. In some cases, when the failure occurs close the substrate, an adhesive failure can be mistaken when the failure is cohesive. In other cases, it is possible to see the type of failure with the naked eye.

Fig. 7 shows the type of failure experienced for Sikaflex® 252 during the degradation process, being in all cases cohesive failure. The post-curing process that the adhesive undergoes does not cause apparent changes in the surface of the adhesive. Nevertheless, these changes are evident in the mechanical values, as it is shown in Table 1.

Fig. 8 shows the type of failure experienced for Sikaflex® 552AT during the degradation process. At 0 h of degradation, the failure is purely cohesive. For 100 h of degradation, the look of the failure changes, being apparently mixed. For 500 h of degradation, the failure becomes purely cohesive again, as well as for 0 h of degradation.

Fig. 9 shows the micrographs of both substrates for 100 h of degradation of Sikaflex® 552AT. In Fig. 9a) the surface of the carbon fiber reinforced polymer is shown. Traces of adhesive can be seen on it, which can lead us to think that at least in certain areas the failure is cohesive, although at first sight the appearances suggest an adhesive or mixed failure. In Fig. 9b) the surface of the steel is shown. In this case smaller amount of adhesive is visible on the surface, being less obvious that the failure is cohesive, finding areas of adhesive failure.

To be able to certify more correctly the type of failure, Scanning Electron Microscopy (SEM) is used achieving greater image increases. In Fig. 10, SEM micrographs of the substrates for 100 h of durability of Sikaflex® 552AT adhesive are shown. In Fig. 10a) the entire surface of CFRP covered by adhesive is observed, which leads to the conclusion that it is a cohesive failure. Fig. 10b) shows the adhesive adhered on the CFRP substrate. Epoxy resin of the CFRP substrate cannot be seen because is transparent, exposing the carbon fibers. The adhesive is capable of wetting almost the entire surface. In Fig. 10c), the adhesive almost covers all the surface of the steel substrate, except for small loopholes, showing cohesive failure. In Fig. 10d), the topography of the steel's surface is shown. Fig. 10c) and d) are the same image, but different detectors are used in the SEM microscope. Micrograph of Fig. 10c) is made with T1 detector (backscattered electrons) obtaining compositional contrast, being possible to differentiate the steel and the adhesive. Micrograph of Fig. 10d) is made with T2 detector (secondary electrons) getting the surface topography. In this case it is not possible to distinguish the adhesive and the steel. Fig. 10a) and b) are also obtained using T2 detector.

4. Conclusions

Each adhesive had different behavior against humidity and temperature. This is due to the difference in their composition. Sikaflex®

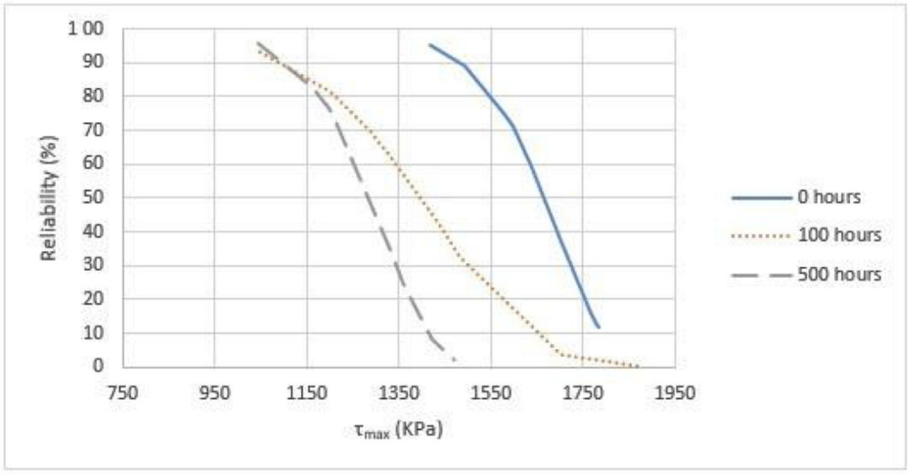

Fig. 6. Reliability curves of Sikaflex 552AT.

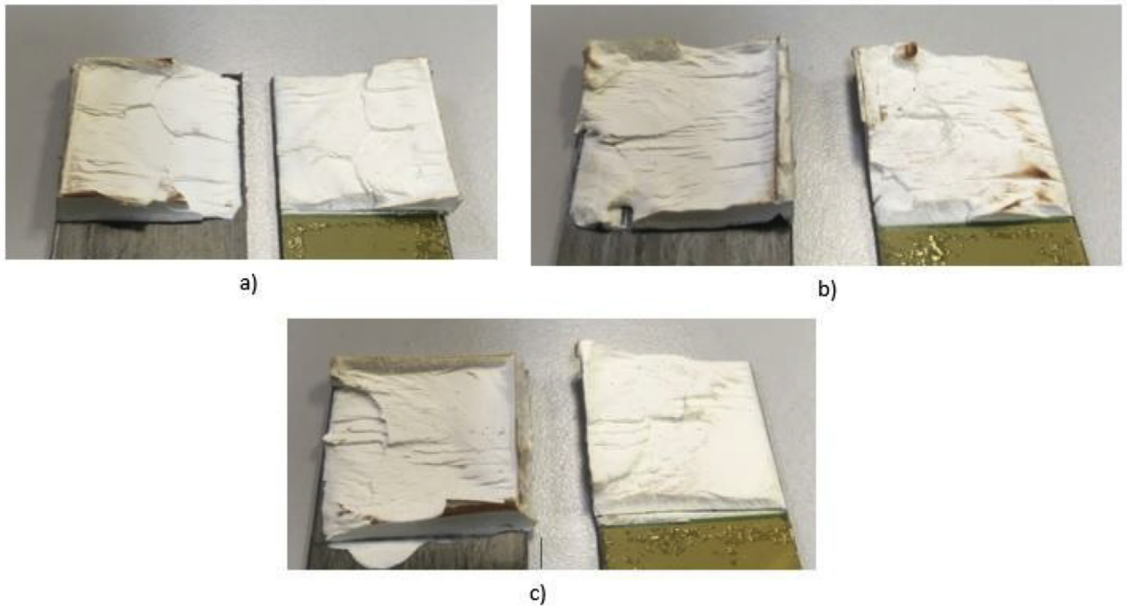

Fig. 7. Sikaflex® 252. a) Cohesive failure for 0 h of degradation. b) Cohesive failure for 100 h of degradation. c) Cohesive failure for 500 h of degradation.

252 is structural polyurethane adhesive, which cures by reaction with atmospheric humidity to form an elastomer. This adhesive shows better behavior against humidity and temperature as degradation conditions cause a post-curing process in it, changing its properties, increasing stiffness and maximum stress values. As for the type of failure, for Sikaflex® 252 is always cohesive. In terms of reliability, post-curing process allows to make the adhesive joint more reliable for higher stress values.

Sikaflex® 552AT cures by reaction with atmospheric humidity but it is a structural polyurethane adhesive with silane termination. This change in the formulation of the polymer makes the curing mechanism different from the Sikaflex® 252. Thus, for 0 h of degradation the adhesive has already reached all its properties. There is no post-curing process, and after 100 h of exposure to temperature and humidity, degradation is evident. In terms of mechanical properties, stiffness decreases like maximum stress values. The failure is cohesive too, but for 100 h of degradation may be doubts with the visual appearance of the failures. Thus, microscopy studies on the surfaces were carried out. These studies show the existence of a thin layer of adhesive on the surface of the substrate, proving that the failure is cohesive. In terms of reliability, the adhesive joint loses reliability over time in presence of humidity and temperature conditions. Even having different behavior, both adhesives are able to maintain adequate strength after the degradation process.

Conflicts of interest

The author(s) declared no potential conflicts of interest with respect to the research, authorship, and/or publication of this article.

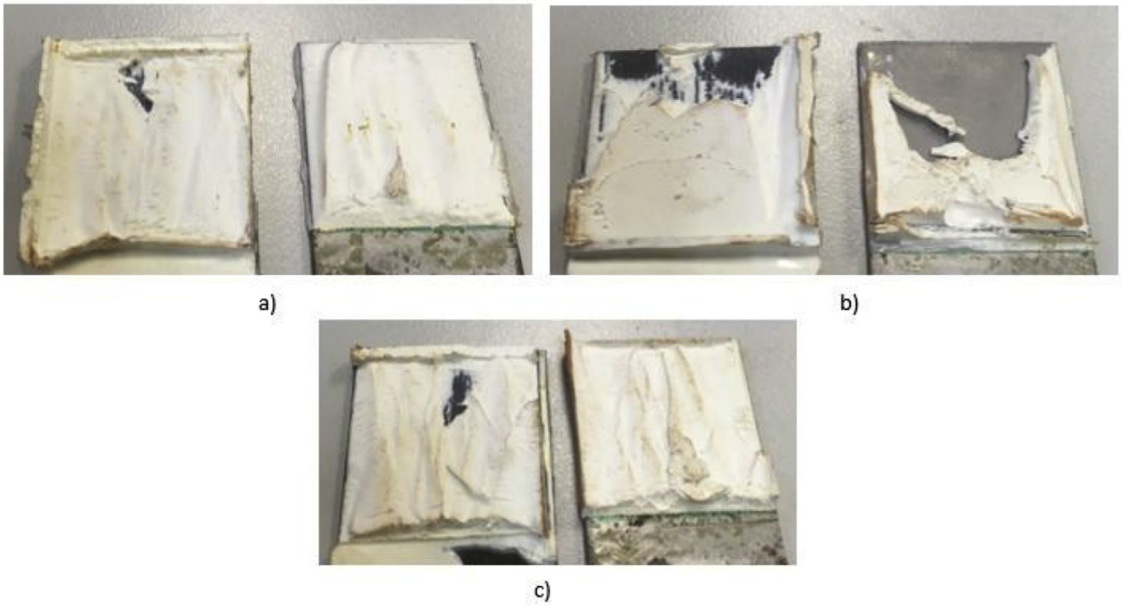

Fig. 8. Sikaflex® 552AT. a) Cohesive failure for 0 h of degradation. b) Apparently mixed failure for 100 h of degradation. c) Cohesive failure for 500 h of degradation.

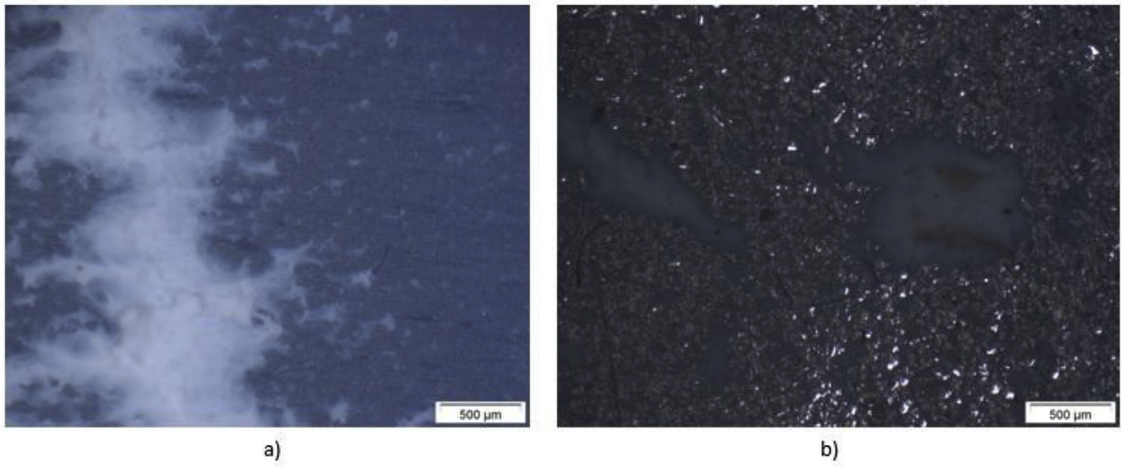

Fig. 9. Optical micrographs of Sikaflex® 552AT: a) Carbon fiber reinforced polymer surface. b) Steel surface.

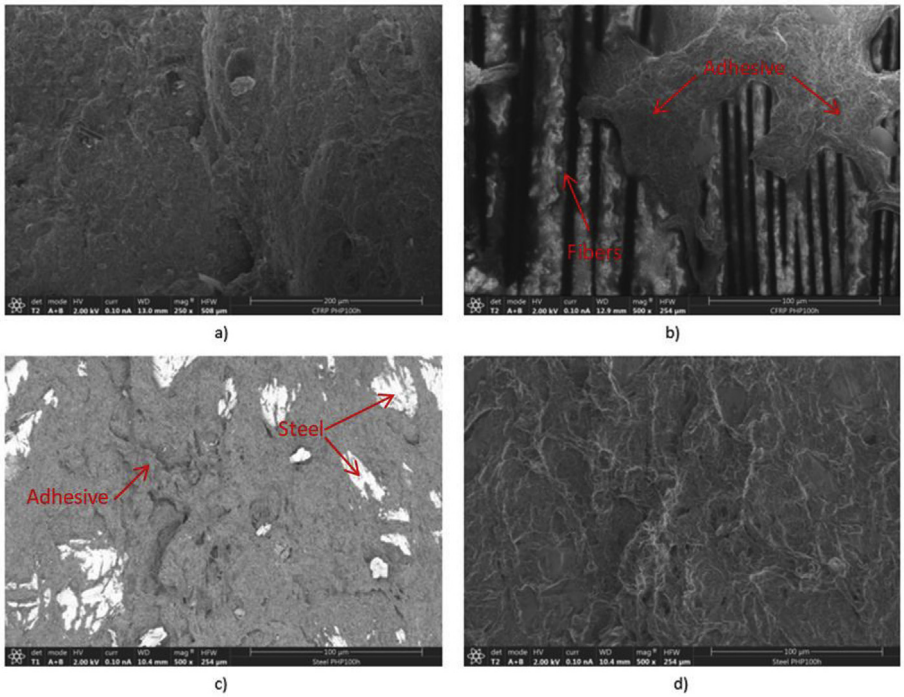

Fig. 10. SEM micrographs of Sikaflex® 552AT specimens for 100 h of aging: a) CFRP Surface (250x) b) CFRP Surface (500x) c) Steel surface (500x) d) Steel surface (500x).

Acknowledgements

This research was supported by Ministerio de Economia y Competitividad, Spain, under grants TRA2014-56471-C4-2-R. The authors gratefully acknowledge the collaboration of Castrosua S. A. for supplying the steel and Sika S.A.U. España for supplying the adhesives and the CFRP. IAAB (Alvaro Alonso Barba Technological Institute of Chemistry and Materials).

Appendix A. Supplementary data

Supplementary data to this article can be found online at https://doi.org/10.1016/j.compositesb.2018.11.097.

References

[1] Narmashiri K, Mehramiz G. Strengthening of steel hollow pipe sections subjected to transverse loads using CFRP. Struct Eng Mech 2016;60:163–73.
[2] Zeng J, Gao W, Liu F. Interfacial behavior and debonding failures of full-scale CFRP-strengthened H-section steel beams. Compos Struct 2018;201:540–52.
[3] Kah P, Suoranta R, Martikainen J, Magnus C. Techniques for joining dissimilar materials: metals and polymers. Rev Adv Mater Sci 2014;36:152–64.
[4] Higgins A. Adhesive bonding of aircraft structures. Int J Adhesion Adhes 2000;20:367–76.
[5] Banea MD, Rosioara M, Carbas RJC, da Silva LFM. Multi-material adhesive joints for automotive industry. Compos B Eng 2018;151:71–7.
[6] Banea MD, da Silva LFM. Adhesively bonded joints in composite materials: an overview. Proc IMechE 2009;223. Part L.
[7] Pitta S, Carles VM, Roure F, Crespo D, Rojas JI. On the static strength of aluminium and carbon fibre aircraft lap joint repairs. Compos Struct 2018;201:276–90.
[8] Chattopadhyay DK, Raju KVSN. Structural engineering of polyurethane coatings for high performance applications. Prog Polym Sci 2007;32:352–418.
[9] Fang CH, Liu PI, Chung LC, Shao H, Ho CH, Chen RS, Fan HT, Liang TM, Chang MC, Horng RY. A flexible and hydrophobic polyurethane elastomer used as binder for the activated carbon electrode in capacitive deionization. Desalination 2016;399:34–9.
[10] Chew MYL. Retention of movement capability of polyurethane sealants in the tropics. Construct Build Mater 2004;18:455–9.
[11] Chuda-Kowalska M, Garstecki A. Experimental study of anisotropic behavior of PU

foam used in sandwich panels. Steel Compos Struct 2016;20:43–56.
[12] Boutar Y, Naïmi S, Mezlini S, da Silva LFM, Ali MBS. Characterization of aluminium one-component polyurethane adhesive joints as a function of bond thickness for the automotive industry: fracture analysis and behavior. Eng Fract Mech 2017;177:45–60.
[13] Weiss J, Voigt M, Kunze C, Huacuja Sánchez JE, Possart W, Grundmeier G. Ageing mechanisms of polyurethane adhesive/steel interfaces. Int J Adhesion Adhes 2016;70:167–75.
[14] Zdrahala RJ, Zdrahala IJ. Biomedical Applications of Polyurethanes: a review of past promises, present realities, and a vibrant future. J Biomater Appl 1999;14:67–90.
[15] Cognard P. Handbook of adhesives and sealants. Elsevier Science; 2005.
[16] Matyjaszewski K, Möller M. Polymer science: a comprehensive reference. Elsevier BV; 2012.
[17] Strobech C. Polyurethane adhesives. Construct Build Mater 1990;4:214–7.
[18] Alia C, Arenas JM, Suarez JC, Pinilla P. Mechanical behavior of polyurethane adhesive joints used in laminated materials for marine structures. Ocean Eng 2016;113:64–74.
[19] Adam M, Lühring A, Popp M, Fecht S, Vallée T. Pre-applicable structural adhesives for timber engineering: glued-in G-FRP rods. Int J Adhesion Adhes 2016;67:121–7.
[20] Zain NM, Roslin EN, Ahmad S. Preliminary study on bio-based polyurethane adhesive/aluminum laminated composites for automotive applications. Int J Adhesion Adhes 2016;71:1–9.
[21] Galvez P, Quesada A, Martinez MA, Abenojar J, Boada MJL, Diaz V. Study of the behaviour of adhesive joints of steel with CFRP for its application in bus structures. Compos B Eng 2017;129:41–6.
[22] Heshmati M, Haghani R, Al-Emrani M. Environmental durability of adhesively bonded FRP/steel joints in civil engineering applications: state of the art. Compos B Eng 2015;81:259–75.
[23] Avendaño R, Carbas RJC, Marques EAS, da Silva LFM, Fernandes AA. Effect of temperature and strain rate on single lap joints with dissimilar lightweight adherends bonded with an acrylic adhesive. Compos Struct 2016;152:34–44.
[24] Chamochin R, Cano de Santayana M, Abenojar J, Pantoja M, Ballesteros Y, del Real JC. The effect of surface treatment on the behavior of toughened acrylic adhesive/GRP (epoxy) composite joints. J Adhes Sci Technol 2010;24:1903–16.
[25] Viana G, Costa M, Banea MD, da Silva LFM. A review on the temperature and moisture degradation of adhesive joints. Proc IMechE Part L: J. Mater. Des. Appl. 2016;0(0):1–14.
[26] Korta J, Mlyniec A, Uhl T. Experimental and numerical study on the effect of humidity-temperature cycling on structural multi-material adhesive joints. Compos B Eng 2015;79:621–30.
[27] Agarwal A, Foster SJ, Hamed E. Testing of new adhesive and CFRP laminate for Steel-CFRP joints under sustained loading and temperature cycles. Compos B Eng 2016;99:235–47.
[28] Costa M, Viana G, da Silva LFM, Campilho RDSG. Effect of humidity on the fatigue behaviour of adhesively bonded aluminium joints. Lat Am J Solid Struct 2017;14:174–87.
[29] Heshmati M, Haghani R, Al-Emrani M. Durability of bonded FRP-to-steel joints: effects of moisture, de-icing salt solution, temperature and FRP type. Compos B Eng 2017;119:153–67.
[30] Encinas N, Oakley BR, Belcher MA, Blohowiak KY, Dillingham RG, Abenojar J, Martínez MA. Surface modification of aircraft used composites for adhesive bonding. Int J Adhesion Adhes 2014;50:157–63.
[31] Encinas N, Lavat-Gil M, Dillingham RG, Abenojar J, Martínez MA. Cold plasma effect on short glass fibre reinforced composites adhesion properties. Int J Adhesion Adhes 2014;48:85–91.
[32] Abenojar J, Martínez MA, Encinas N, Velasco F. Modification of glass surfaces adhesion properties by atmospheric pressure plasma torch. Int J Adhesion Adhes 2013;44:1–8.
[33] del Real JC, Ballesteros Y, Chamochin R, Abenojar J, Molisani L. Influence of surface preparation on the fracture behavior of acrylic adhesive/CFRP composite joints. J Adhes 2011;87:366–81.
[34] Banea MD, da Silva LFM. Mechanical characterization of flexible adhesives. J Adhes 2009;85:261–85.
[35] Tcharkhtchi A, Farzaneh S, Abdallah-Elhirtsi S, Esmaeillou B, Nony F, Baron A. Thermal aging effect on mechanical properties of polyurethane. Int J Polym Anal Char 2014;19(7):571–84.
[36] Na J, Fan Y, Tan W, Guo S, Mu W. Mechanical behavior of polyurethane adhesive bonded joints as a function of temperature and humidity. J Adhes Sci Technol 2017;32:457–72.
[37] Razmara M, Saidpour SH, Arunchalam S. DMA Investigation on polyurethane (PUR). International conference on fascinating advancement in mechanical engineering. 2008. p. 11–3.

PUBLICACIÓN 3

Composites Part B 176 (2019) 107194

Contents lists available at ScienceDirect

Composites Part B

journal homepage: www.elsevier.com/locate/compositesb

Effect of moisture and temperature on the thermal and mechanical properties of a ductile epoxy adhesive for use in steel structures reinforced with CFRP

Pedro Galvez *, Juana Abenojar, Miguel Angel Martinez

University Carlos III de Madrid, EPS Polytechnic School, Materials Science and Engineering and Chemical Engineering Department, Avda. de la Universidad, 30, 28911, Leganés, Spain

ARTICLE INFO

Keywords:
Polymer-matrix composites (PMCs)
Mechanical properties
Thermal properties
Environmental degradation
FRP-Steel bonded joints

ABSTRACT

CFRP has proven to be a material capable of being used in many engineering applications, highlighting its good properties for reinforcement of steel structures. In this study, a new CFRP-steel adhesive joint is evaluated by using a structural and ductile epoxy adhesive to join the CFRP reinforcements to the steel structure. On the one hand, the epoxy adhesive has been thermally characterized by means of its kinetics of curing (Kissinger and Model Free Kinetics methods), finding behavior similar to other epoxy adhesives. On the other hand, different surface treatments are studied in order to achieve the best mechanical properties of the joint. In addition, the suitability of this kind of joints is assessed under durability conditions (60 °C and 99% relative humidity) and under thermal fatigue. Shear tests are realized on specimens subjected to different exposure times, studying the mechanisms that affect the degradation of the adhesive joint in each environment. Breaking surfaces were analyzed by Scanning Electron Microscopy (SEM) and by Energy-dispersive X-ray Spectroscopy. A simplified Weibull model is used to evaluate the reliability of the joints during both durability and thermal fatigue processes. The thermal and mechanical properties of the adhesive are determined, showing better behavior against thermal fatigue because moisture in the durability process accelerates degradation of the adhesive joint.

1. Introduction

The use of composite materials in industrial processes has grown exponentially in recent decades. The wide variety of composite materials currently available, together with their excellent properties [1] make their use possible in applications as diverse as aerospace [2,3], automotive [4,5], marine [6,7] and civil [8,9]. These materials have also proven to be particularly efficient as reinforcement in very different types of structures as they present high strength-weight ratio, good corrosion behavior, ability to be applied on old non-weldable metal elements, and good sustainability [10]. In this way, it is common to find concrete [11,12], steel [13,14] and cable structures [15] reinforced with composite materials. Focusing on CFRP strengthening of metallic structures, it is necessary to emphasize the use of this material for reinforcement of metallic bridges. Several interesting works have been developed in this area. Ghafoori et al. [16] present a design criterion developed for fatigue strengthening of a 120-year-old metallic railway bridge in Switzerland. They also present a prestressed un-bonded reinforcement (PUR) system developed to apply the strengthening. This method allows decreasing the time required for on-site strengthening procedures since unlike conventional prestressed CFRP reinforcement methods, preparation of the existing metallic bridge surface is not required. Hosseini et al. [17] study the strengthening of a 19th-century roadway metallic bridge using non-prestressed bonded and prestressed un-bonded CFRP plates. They demonstrate that the tensile stresses were reduced by approximately 15% and 44% in the bridge cross-girders after strengthening by the proposed non-prestressed bonded and prestressed un-bonded systems, respectively. Ghafoori et al. [18] present an application of prestressed carbon fiber reinforced polymer (CFRP) plates for the strengthening of metallic girders of 122 years old roadway bridge in Melbourne, Australia. They also use a wireless sensor network (WSN) for long-term structural monitoring of the retrofitted bridge girders. Results of short term and long term measurements show that the new system is very effective for flexural and fatigue strengthening of bridge girders.

Fiber reinforced polymer (FRP) materials should be joined to the main structure reliably and lastingly. There are different ways to carry

* Corresponding author.
E-mail addresses: pgalvez@ing.uc3m.es (P. Galvez), abenojar@ing.uc3m.es (J. Abenojar), mamc@ing.uc3m.es (M.A. Martinez).

https://doi.org/10.1016/j.compositesb.2019.107194
Received 12 March 2019; Received in revised form 4 July 2019; Accepted 12 July 2019
Available online 16 July 2019
1359-8368/

out this task. Oller et al. [19] use bolts to join the FRP sheets and the concrete beams, concluding that the FRP sheets are not effective if they are not anchored, as premature debonding takes place. D'Aniello et al. [10] explain the impossibility of welding or bolting/riveting new elements in many old structures due to the problems associated with these techniques. Traditional methods do not protect the structure against deterioration, caused mainly by corrosion and fatigue, besides adding considerable dead weight to the structure. Therefore, it is necessary to find other techniques capable of solving this problem, with adhesive bonding being the most promising of all.

Adhesives have been proved to be a suitable material for use in structural applications. Along these lines, it is possible to find adhesives in many different industrial fields. Galvez et al. [20] propose a new concept of CFRP (carbon fiber reinforced polymer) node adhesively bonded in steel structures of buses. Alia et al. [21] study the behavior of polyurethane-steel adhesive joints in marine structures. Adhesive suitability is proved after subjecting the adhesive joint to different aggressive conditions such as seawater or distilled water immersion. Marques et al. [22] test and simulate mixed adhesive joints for high temperature aerospace applications. They carry out experimental and numerical analyses, finding good agreement between both of them, validating the models for future optimization works. One of the promising fields for the use of adhesives is in civil engineering construction [23]. Similarly, Kumar et al. [24] carry out an excellent review on the use of adhesives in concrete and steel-concrete composite. This work shows that the use of structural adhesives is undoubtedly the most common and efficient technique to prevent structural degradation [25]. However, the use of this technique implies the appearance of several problems related to the different nature of both substrates and the fact that within the assembly of the joint the adhesive is definitely the weakest part [26].

As the adhesive is the critical aspect in the performance of steel profiles externally strengthened by CFRP, the behavior of the joint must be thoroughly investigated. In this way Martinelli et al. [27] investigated the bond behavior of prestressed CFRP plates adhesively bonded to steel substrate by means of numerical modeling and subsequent experimental validation. Bond behavior and debonding capacity of prestressed CFRP composites adhesively bonded to steel substrate were also studied by Hosseini et al. [28]. They demonstrated that during the prestress release the debonding failure of CFRP-steel joints is governed by a mixed-mode I/II (tensile/shear) fracture.

Working with structural elements makes it necessary to know their behavior in service conditions throughout their useful life [29]. A good way to evaluate the capability of these reinforcements is through durability tests. Heshmati et al. [30] conduct a comprehensive review about the environmental durability of adhesively bonded FRP/steel joints in civil engineering applications. They identify the individual and combined effects of moisture and temperature as the most critical environmental factors. Moisture can affect the resin and the adhesive causing swelling, plasticization, cracking and hydrolysis [31]. Soles et al. [32] demonstrate that there is a relationship between the adhesive surface topology and a high moisture absorption susceptibility, while Rider et al. [33] relate this high moisture absorption susceptibility with the polarity in resins. Sousa et al. [34] observe permanent effects in a structural adhesive, already being used in civil engineering applications, after hygrothermal and outdoor aging. Irreversible degradation mechanisms are experienced by the adhesive with moist environmental exposure, and as for temperature, higher exposure actively promotes diffusion. It is widely accepted that the adhesive, the resin matrix and the fiber/matrix interface are the most sensitive to thermal effect components in FRP/steel adhesive joints [30], and therefore they must be thoroughly studied.

Polyurethane and brittle epoxy adhesives are normally used for high-strength applications. This work is focused on the study of a ductile epoxy structural adhesive. This type of adhesive has never been used to join FRP reinforcements to steel structures. The aim of this work, then, is to study different surface treatments on both steel and CFRP substrates, looking for the best configuration. Tensile shear tests and thermal analyses are carried out after subjecting the specimens to different aggressive conditions. The capability of this kind of joints to be used in steel structures reinforced with CFRP is evaluated.

2. Experimental procedures

2.1. Materials

The aim of this publication is the development of steel-CFRP adhesive joints in order to evaluate their capability to be used in civil structures, taking into account feasible adverse environmental conditions. A ductile epoxy adhesive is selected in this work: Araldite® AW 4858/HW 4858 (Huntsman International LLC, The Woodlands, Texas, USA). This is a two-component structural epoxy adhesive with very high lap shear and peel strength. It can be used to bond different substrates such as composites, metals and thermoplastics. It has good moisture resistance and is extremely tough and resilient. The adhesive was cured at room conditions (25 °C and 35% relative humidity) for 7 days.

The proposed assembly is formed by a steel substrate (corresponding to the main structure), by an intermediate layer of adhesive, and by an external layer of composite material. For this reason, AISI 1012 carbon steel and carbon fiber reinforced polymer (CFRP) were selected as substrates. The AISI 1012 steel was supplied by Carrocera Castrosua S.A. (Santiago de Compostela, Spain), while the CFRP, whose trade name is Sika Carbodur® S-512, was manufactured by pultrusion by Sika S.A.U. (Alcobendas, Spain). Dimensions for the CFRP substrate were (in mm): width (W_{CFRP}) = 25, length (L_{CFRP}) = 100 and thickness (T_{CFRP}) = 1.2. Dimensions for the steel substrate were (in mm): width (W_s) = 25, length (L_s) = 100 and thickness (T_s) = 1.6.

2.2. Mechanical characterization

The mechanical properties of the adhesive were studied from dog-bone specimens for tensile tests. Although it is an epoxy adhesive, it is formulated to have a great capacity for deformation. Duncan et al. [35] explain that methods developed to characterize rubbers [36] have been normally used for adhesives. However, it is difficult to prepare good quality specimens because the viscosity of the adhesive causes pin-holing and gaps. Therefore, these authors propose the use of smaller specimens that require a lower quantity of adhesive and are easier to prepare (avoiding the appearance of gaps inside the adhesive). Nevertheless, in this work twelve adhesive specimens in mass were manufactured with the higher specimen size used by other authors to characterize adhesives [37].This was possible thanks to the use of the technique described in the French Standard NF T 76–142 [38] to produce 2 mm thickness plate specimens without internal porosities [39], and the subsequent machining of the specimens from the plate.

2.3. Thermal characterization

The cure kinetics of the adhesive was studied following the Kissinger model [40] and the model free kinetics (MFK) [41]. Previous works demonstrated the validity of both models for activation energy calculation. Abenojar et al. [42] calculated the activation energy of silica filled epoxy nano-composites using both methods. All thermal analyses were carried out in a DSC (Differential Scanning Calorimetry) device (DSC 822, Mettler Toledo, Greifensee, Switzerland). Adhesive samples of 8–10 mg of weight were analyzed. These samples were introduced into aluminum crucibles with 40 μL of capacity. The non-isothermal method from 0 to 200 °C at 5, 10 and 20°/min was selected to carry out the adhesive cure kinetics.

Kissinger argues that the activation energy is constant throughout the curing process, being calculated from Equation (1):

$$\ln\left(\frac{\beta}{T_p^2}\right) = -\frac{E_a}{RT_p} + C \quad (1)$$

where β is the heating rate (in °·min^{-1}), T_p is the temperature (in K) corresponding to the peak of the curing curve in the DSC diagrams, E_a is the activation energy (Jmol^{-1}), R is the gases constant, whose universal value is 8.314 J·mol^{-1}·K^{-1}, and C is the other constant. The STARe software (Mettler Toledo, Greifensee, Switzerland) was used to calculate the cure kinetics by MFK. To develop this method it is necessary to perform at least three scans at different heating rates. The main difference between this method and the Kissinger method is in terms of the activation energy, since for the MFK it is not constant. This activation energy is calculated as a function of the curing conversion degree, with the conversion degree obtained from the non-isothermal test. Finally, the curing times at different temperatures (25, 50, 75, 90 y 100 °C) were simulated as a function of the conversion degree.

The same DSC device was used to calculate the glass transition temperature of the adhesive for each stage and type of degradation, both for the thermal cycles and for durability. Tests were performed by the non-isothermal method from 0 to 200 °C at 20°/min ratio.

2.4. Surface treatments

Working with adhesives it is necessary to carry out the appropriate surface treatments that allow the best mechanical properties of the adhesive joint [43] to be obtained. In this work, this section is particularly relevant as it is an adhesive joint between two dissimilar materials, steel and CFRP. Four surface treatments were evaluated, looking for the best option for the proposed substrate-adhesive-substrate configuration. Surface treatment A consisted in solvent cleaning for CFRP. Sanding with P180 sandpaper and solvent cleaning were selected for steel. In surface treatments B, C and D the steel was treated in the same way every time. It was sanded with P180 sandpaper, subsequently cleaned, and finally pickled with ortho-phosphoric acid (85%) (OA treatment hereinafter). In surface treatment B, CFRP was only cleaned with solvent. The C surface treatment for CFRP consisted in solvent cleaning, atmospheric pressure plasma treatment (APPT) and the application of a primer layer. Finally, the CFRP surface was cleaned with solvent and treated with APPT in surface treatment D. In both the C and D treatments, 3 m/min of torch speed and 6 mm of torch-specimen distance were selected as APPT parameters. Sika® Primer 215 was selected for treatment C.

Five specimens of each surface treatment were studied. Treatment D turned out to be the best of all, and therefore it was the one selected to perform durability and aging tests.

2.5. Shear tests

Shear tests were realized following the standard UNE-EN 1465:2009. They were carried out in a universal testing machine (Microtest S.A., Madrid, Spain), see Fig. 1, with 1 mm/min rate and load cell of 20 kN. Although the standard indicates an adhesive overlap of 12.5 mm, in this work 25 mm was used. Banea and da Silva [44] demonstrated that in ductile adhesives, as the one selected in this work, the increment of the lap length is associated with an increment of the joint strength, the opposite of what happens in joints with brittle adhesives.

In this way, the capability of a ductile epoxy adhesive to be used in structural applications and, more specifically to join CFRP reinforcements to steel structures, is studied. Several types of tests can be used for this purpose, but nevertheless tensile shear test were selected since they are widely accepted and used to provide a measure of the mechanical properties of the adhesive joint [45]. Tensile shear test allows testing mainly shear stress, but other stresses like peeling can also appear. Alignment tabs were placed in the manufactured specimens to minimize this. Fig. 2 shows the single lap joint specimen configuration

Fig. 1. Shear tests on specimens.

utilized in this work. Specimen dimensions were (in mm): adhesive width (W_A) = 25, total specimen length (L_T) = 175 and adhesive thickness (t_A) = 0.2.

Maximum shear stress (τ_{max}), the strain reached for this stress ($\delta_{\tau max}$) and the joint stiffness were calculated. By using Equation (2), shear stress (τ) was calculated:

$$\tau = \frac{F}{S} \quad (2)$$

where F is the force obtained from the testing machine and S is the adhesive surface (L_0 x W_A). Strain ($\delta_{\tau max}$) was calculated from Equation (3):

$$\delta_{\tau max} = 100x\left(\frac{displacement}{L_0}\right) \quad (3)$$

with displacement being a value directly obtained from the testing machine and L_0 the adhesive overlap. In terms of joint stiffness, it was calculated from the slope of the elastic deformation zone in the stress-unit strain curves.

2.6. Durability tests

Durability tests were carried out in the adhesive joints. An in-house device was used as climatic chamber [29] to degrade the adhesive joints (Fig. 3). This device consisted of a polypropylene box with a large hole in the central part where the specimens were placed. In order to seal it hermetically, a special polypropylene closure system was utilized. Environmental conditions inside the chamber were monitored by a thermo-hygrometer (MSR 145, MSR Electronics GmbH, Seuzach, Switzerland). The chamber had a temperature of 60 °C and approximately 99% relative humidity. These conditions were obtained because the chamber was designed to hold liquid underneath it, with this liquid being a saturated solution of potassium sulfate (K_2SO_4). This salt at 60 °C causes a relative humidity greater than 95% [46]. The temperature was reached by putting the box into a stove (Digitronic TFT – JP Selecta S.

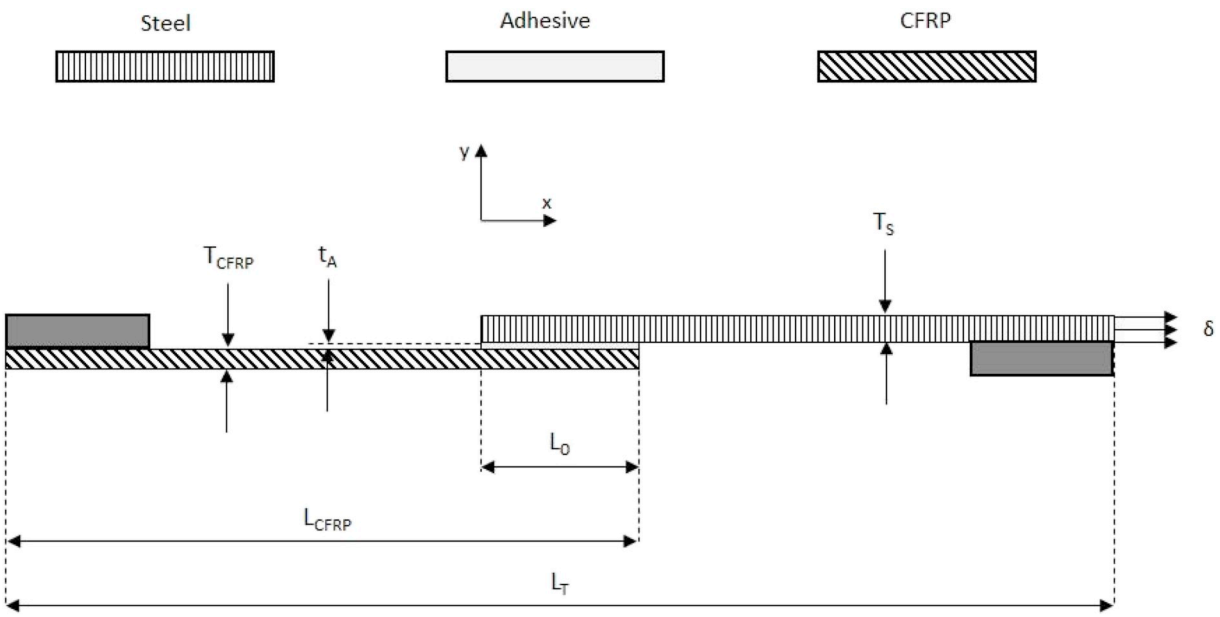

Fig. 2. Single lap joint specimen configuration.

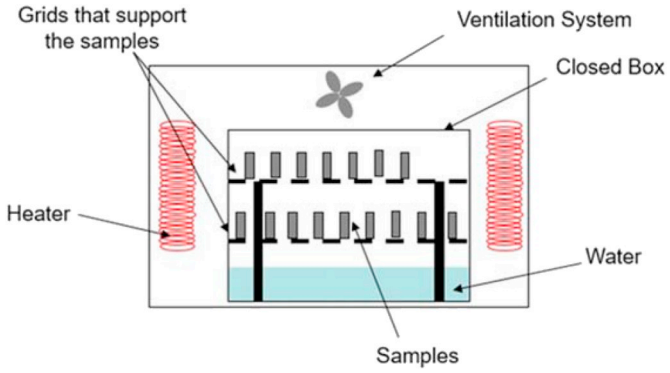

Fig. 3. Climatic chamber scheme.

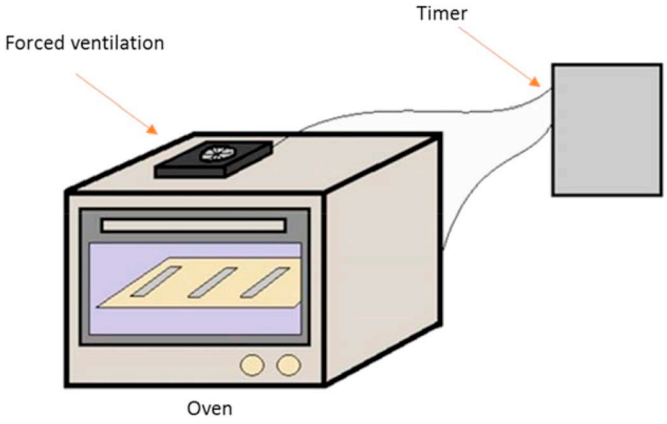

Fig. 4. Forced ventilation oven depiction.

A.). Five specimens were tested for each exposure time: 0 h, 2 h, 24 h, 168 h, 360 h and 768 h.

2.7. Thermal fatigue

In addition to the durability, thermal fatigue tests were carried out. For this purpose, an in-house electric forced ventilation oven [29] specially designed for this kind of experiments, and previously calibrated, was used (Fig. 4). Through this device it is possible to perform 30 min heating-cooling cycles, with temperatures of 20 °C minimum and 80 °C maximum. Five specimens were tested at 0, 48, 97, 240, 432, 912, 1776 and 2592 cycles.

2.8. Reliability study

Structural joints and any element designed to be used in structural applications must be studied statistically and in terms of reliability to determine their capabilities during the entire life cycle. All the obtained data were analyzed by means of the Grubbs test in order to discard outliers. In the same way, for the reliability study a simplified Weibull model was developed. Weibull distribution is a very effective tool to assess the capability of a structural element throughout its life cycle. Thanks to this study, it was possible to obtain a reliability percentage for any kind and time of exposure, providing an accurate idea of the joint capacity at each moment and condition.

2.9. FTIR-ATR

The effect of water absorption was studied by Fourier transform infrared spectroscopy – attenuated total reflectance (FTIR - ATR) in a Bruker Tensor 27 spectrometer (Bruker Optik GmbH, Ettlingen, Germany). Tests were carried out for a wavenumber (cm^{-1}) between 3100 and 3600 (cm^{-1}), which corresponds to O–H groups, since in the rest of the spectrum no variation was observed. Infrared spectra of the adhesive were obtained with ATR technique. In this technique, a diamond prism is used with an incident angle of IR radiation of 45°. Before the test, an in air background was realized to eliminate moisture and CO_2 influence in the air so that they would not affect the test results.

2.10. Characterization of the failure mode of the adhesive joint

When working with adhesives it is very important to characterize the failure mode of the joints. Micrographs were carried out with a Scanning Electron Microscope (SEM) (XL 30 SEM, Koninklijke Philips N.V., Amsterdam, Netherlands). The micrographs were made at 69 and 2000 magnifications in specimens without degradation, in specimens

subjected to 2592 thermal cycles and in specimens after 768 h of exposure to moisture and temperature. Energy-dispersive X-ray spectroscopy analysis (EDAX, Ametek Inc., Berwyn, Pennsylvania, U.S.) was also performed to determine semi-quantitatively the composition of the elements shown in the micrographs.

3. Results

3.1. Mechanical characterization

Mechanical properties of the adhesive are calculated from tensile tests with dog-bone specimens. Ten specimens are tested, obtaining the following results:

- Tensile strength (MPa): 33.02 ± 2.40.
- Strain (%): 8.54 ± 0.79.
- Young's Modulus (MPa): 475.50 ± 46.84.

It can be observed that despite being an epoxy adhesive, it has high strain and relatively low modulus in comparison with other usual epoxy adhesives.

3.2. Thermal properties

To study the thermal properties of the adhesive, DSC tests were carried out. The starting point of these tests is the calculation of the glass transition temperature (T_g) of the adhesive once it is cured and before being subjected to any type of degradation. This T_g in the midpoint is 68 °C. T_g is slightly higher than the degradation temperature (60 °C), so this is a correct temperature.

Additionally, the cure kinetics of the adhesive is studied by the Kissinger method and by Model Free Kinetics (MFK). Through the Kissinger equation (Equation (1)), the activation energy of the system (E_a), whose value is 49.35 kJ/mol, has been obtained, with this value being similar to the value obtained in other work with epoxy resins [47]. Focusing on Equation (1), it can be seen that it is an Arrhenius type equation, corresponding to the equation of a line. The independent variable corresponds to $1000/T_p$ with T_p being the temperature corresponding to the maximum of the curing curve in the DSC diagrams. T_p varies according to the heating rate of the test. To be able to plot the Kissinger line (Fig. 5), it is necessary to make at least three DSC tests at different heating rates. T_p values for 5, 10 and 20°·min^{-1} are: 92 ± 2 °C, 107 ± 2 °C and 122 ± 2 °C respectively. In all cases the enthalpy of the curing curve (ΔH_p) is 224 ± 1 J g^{-1}.

The dependent variable corresponds to $Ln(\beta/Tp^2)$. From β and T_p three points are obtained, and the Kissinger line can be plotted. The activation energy of the system (E_a) is obtained from the equation of the line, multiplying the slope by the gases constant R (8.314 J mol^{-1}K^{-1}). Error produced using this method is minimal as is seen in the value of R^2, which is very close to 1.

The Kissinger method is faster and simpler than the MFK since it assumes that the curing reaction is order 1 reaction. In a more complex curing system, more parameters are required and the activation energy changes according to the conversion degree during the curing process [47,48].Therefore, it may be necessary to find more precise models such as the MFK. In this model the activation energy varies during the curing reaction. Fig. 6 shows the activation energy as a function of the conversion degree. Being an epoxy resin, three well-differentiated phases are found within the curing process. In the first phase (up to 20% curing) n-order reaction takes place. In the central zone (between 20 and 70% curing) autocatalytic reaction is found, since oxirane rings begin to open, with OH groups being the auto-catalysts of the reaction [49]. N-order reaction appears again in the final phase (between 70 and 100% curing). N-order reactions require more energy because they are slower than the autocatalytic reaction, so slight increments appear at the beginning and at the end of the reaction, as can be seen in Fig. 6.

MFK allows simulating the time required to reach a certain percentage cure at a certain temperature. The values that are obtained in the simulation are shown in Table 1. The maximum studied time is 2 h. As can be seen in this table, it is possible to obtain 99% curing at different temperatures, needing 136.94 min at 50 °C and only 14.42 min at 100 °C. Below this temperature, at 25 °C, a cure percentage of 70% can be obtained in 198.62 min. Therefore, at low temperatures much more time is necessary to reach high curing percentages.

3.3. Surface treatment choice

In this section each surface treatment is evaluated. The objective is to select the best one to perform the durability process and the thermal cycles. Table 2 shows maximum shear stress (τ_{max}), strain ($\delta_{\tau max}$) and stiffness values for each of the four surface treatments studied in this work.

The results clearly show the importance of performing correct surface treatment. So option A, which in fact is not to perform any surface treatment, is by far the worst of all. In B and C the values of τ_{max}, strain and stiffness of the joint clearly increase compared to A. Treatment D is without a doubt the best of all. τ_{max} increases until values close to 20 MPa. This value is almost twice as much as the next highest value found in treatment C (10.33 ± 1.38). The increase in terms of $\delta_{\tau max}$ is also very clear, reaching values around 30 MPa. Finally, the stiffness value is also the highest (127.14 ± 1.68), although in this case it is practically the same as in treatment C.

Another aspect to highlight is that the type of failure in treatment A, treatment B and treatment C is adhesive failure. This kind of failure is negative; however, in treatment D mixed failure is obtained, with areas appearing with adhesive and cohesive failure over the steel surface. Values are high with relatively low standard deviations, and it is the best treatment without any doubt. Accordingly, it is the one selected.

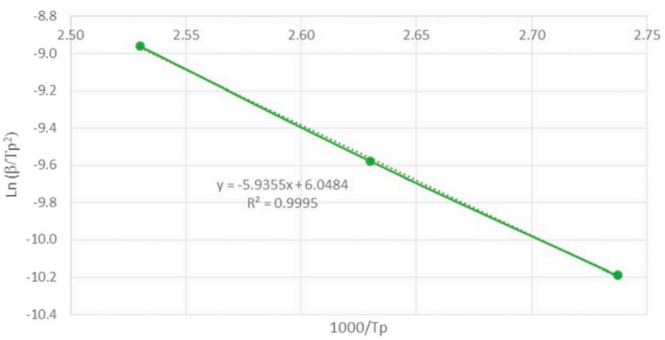

Fig. 5. Plot of the Kissinger line.

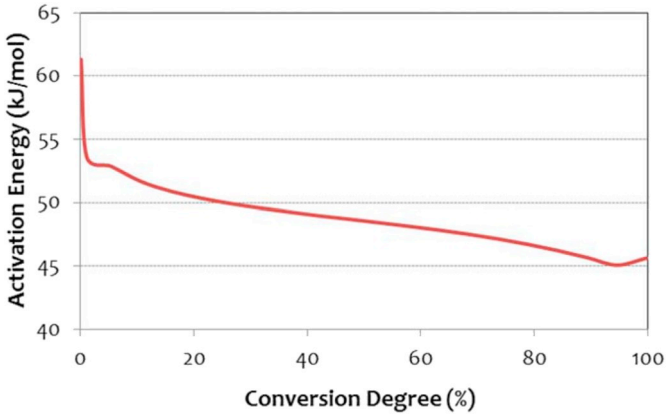

Fig. 6. Activation energy versus conversion degree in MFK.

Table 1
Simulation by MFK of the conversion degree as a function of the temperature.

Applied Kinetics: Conversion					
Temperature(°C)	25	50	75	90	100
Conversion Degree (%)	Time (min)-maximum 2 h				
10	46.68	9.19	2.3	1.1	0.69
20	70.76	14.65	3.8	1.85	1.18
30	93.53	19.83	5.26	2.59	1.66
40	116.21	25.11	6.76	3.36	2.17
50	140.76	30.91	8.44	4.22	2.74
60	167.51	37.41	10.36	5.22	3.41
70	198.62	45.22	12.73	6.47	4.25
80	–	55.59	15.98	8.22	5.43
90	–	72.57	21.45	11.19	7.46
99	–	136.94	40.98	21.52	14.42

Table 2
Mechanical values of the studied surface treatments.

	A	B	C	D
CFRP	–	–	APPT + Primer	APPT
Steel	–	OA treatment	OA treatment	OA treatment
Failure	Adhesive (Steel)	Adhesive (CFRP)	Adhesive (CFRP)	Mixed
τ_{max} (MPa)	0.25 ± 0.11	10.33 ± 1.38	6.56 ± 1.34	18.55 ± 1.77
$\delta_{\tau max}$ (%)	9.21 ± 1.05	12.67 ± 1.09	9.49 ± 0.95	29.51 ± 1.38
Stiffness (MPa)	3.47 ± 1.21	112.35 ± 2.74	125.82 ± 4.17	126.80 ± 3.79

3.4. Durability

3.4.1. Mechanical tests

The best surface treatment obtained in section 3.3 is selected to perform the test specimens for the durability process. Five specimens were manufactured and studied for each exposure time (0 h, 2 h, 24 h, 168 h, 360 h and 768 h). Fig. 7 shows the most representative stress-strain curves for each exposure time, while Table 3 shows average values of τ_{max}, $\delta_{\tau max}$ and stiffness as well for each exposure time. After 2 h of exposure, τ_{max} is almost constant, although a significant increment in the stiffness of the joint is observed. After 24 h of exposure to humidity and temperature, the degradation of the adhesive joint is evident. τ_{max}, $\delta_{\tau max}$ and stiffness decrease markedly. This degradation process continues up to 168 h. At this point it seems that the adhesive joint stabilizes and all the values remain constant until 360 h. After 768 h of exposure, the lowest values of both τ_{max} and $\delta_{\tau max}$ are observed, undoubtedly the moment of highest degradation of the joint. Fig. 7 clearly shows the entire degradation process, with the difference between the non-exposure specimen curve and the other ones being evident, especially the curve corresponding to 768 h of exposure.

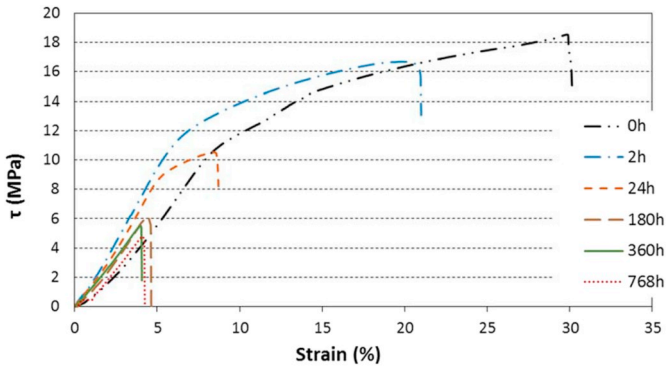

Fig. 7. Representative stress – strain curves of the durability process.

3.4.2. Degradation phenomena

Degradation phenomena of adhesive joints involve several factors that must be taken into account. In this case, both moisture and temperature have a main role, not only individually but also simultaneously. The individual effect of temperature and moisture in adhesive joints is well known. However, the combined effect of both factors depends on each adhesive.

Temperature is the main factor in the cross-linking increment of the polymer chains of the adhesive. This greater cross-linking is related to the increase of the adhesive joint stiffness [29]. Joints are stiffer after 2 h of exposure to moisture and temperature, staying almost constant throughout the durability process. This is because despite decreasing τ gradually, stiffness never recovers the values of specimens without degradation. Banea et al. [50] study the temperature effect (80 °C) in epoxy single lap adhesive joints. A 32% reduction in the strength of the adhesive joint in comparison to room conditions is found, with this decline being attributed to a loss of adhesive strength due to the temperature. In our case, this effect is combined with a moisture effect.

Adsorption and absorption processes can appear in the adhesive joints by moisture effect. In the adsorption process, moisture penetrates through the adhesive-adherent interface, causing joint deterioration and the subsequent decrease of the mechanical properties. In the absorption process, water penetrates into the adhesive. It can be absorbed by the polymer in two different ways [51]:

a) As free water, occupying free spaces of the polymer, resulting in material plasticization.
b) As bound water, forming single or multiple hydrogen bonds with the polymer chain, resulting in this case in swelling, plasticization and decreasing both strength and glass transition temperature.

Table 4 shows T_g values obtained for each exposure time. After 2 h, T_g decreases from 68 °C to 57 °C. This T_g reduction is related to swelling and especially to the adhesive plasticization.

In this work it can be considered that moisture has been absorbed mainly as bound water. When water penetrates into the adhesive, Type I bounds water are created. They act as a plasticizer and are responsible for T_g decreasing. These bounds disrupt Van der Waals initial forces between the polymer chains and the hydrogen bonds resulting in chain segment mobility increment [52]. After 24 h of exposure to moisture and temperature, T_g increases up to 71 °C. The increment continues gradually until reaching the maximum T_g at 79 °C after 320 h of exposure. This T_g is the same after 768 h of exposure. Secondary cross-linking appears between the main polymer chain and the water molecules, being responsible for the T_g increment. From this moment, Type II bounds water prevail, fundamentally affecting the Tg by promoting secondary cross-linking with hydrophilic groups such as hydroxyls and amines in the polymer network [53]. The amount of Type II bound water is greater with the increase of temperature and exposure time [54]. Fig. 8 shows infrared spectra for the band corresponding to the O–H groups (between 3100 and 3600 cm^{-1}), since it is the band where differences are observed throughout the process. Table 5 shows peak area values for each exposure time with respect to specimens without degradation (0 h). It is important to emphasize that this is not a quantitative analysis, but a qualitative analysis. Thus, it shows the difference (in percentage) in signal intensity for each exposure time specimen with respect to non-subjected specimen, whose peak area is 0%.

After 2 h under durability conditions, an 8% increment can be observed in the signal intensity. This peak is related to a primary phase of water absorption, with Type I bound water prevailing. This intensity drops to 5% after 24 h. This decline can be associated with changes in the polymer chain; Type I bound water loses prevalence and an increased amount of Type II bound water appears [54]. The peaks, and therefore the absorbance, increase gradually, until reaching the maximum value after 320 h of exposure (19%). At this moment, Type II bound water prevails, promoting secondary cross-linking with

Table 3
Mechanical values of the joint throughout the durability process.

Time (hour)	0	2	24	168	360	768
τ_{max} (MPa)	18.55 ± 1.77	18.13 ± 2.93	11.2 ± 1.21	6.53 ± 0.76	6.67 ± 0.84	4.65 ± 0.20
$\delta_{\tau max}$ (%)	29.51 ± 1.38	20.19 ± 2.96	9.77 ± 3.03	4.99 ± 0.39	4.87 ± 0.43	3.26 ± 0.51
Stiffness (MPa)	126.80 ± 3.79	181.8 ± 14.4	165.6 ± 10.1	139.4 ± 0.95	148.0 ± 5.70	152.45 ± 11.84

Table 4
T_g variation during the durability process.

Time (hours)	$T_g \pm 2$ (°C)
0	68
2	57
24	71
168	75
320	79
768	79

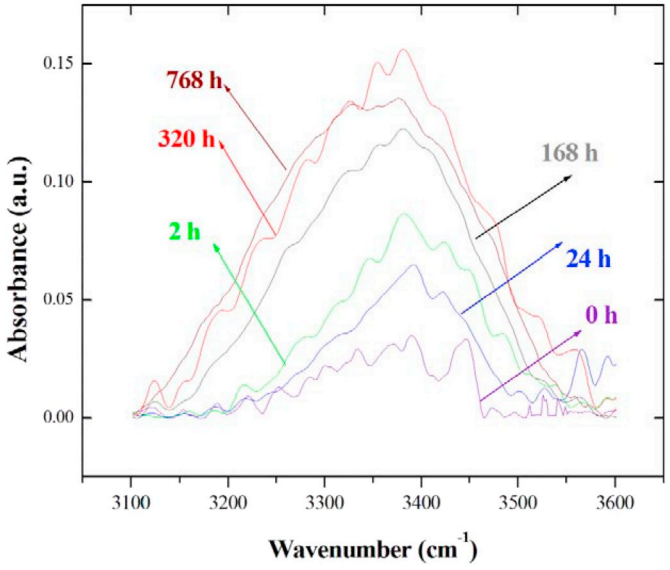

Fig. 8. Infrared spectra for the band corresponding to the O–H groups.

Table 5
Peak areas for each exposure time to moisture and temperature.

Time (hours)	Peak area (%)
0	0
2	8
24	5
168	17
320	19
768	14

hydrophilic groups such as O–H groups. Between 320 and 768 h, the signal intensity drops to 14%. After 320 h, the polymer reaches the saturation point and cannot absorb more water, starting a desorption process visible in the curve of 768 h. This desorption process is linked with the secondary cross-linking, which reduces the free volume of the polymer, and prevents the absorption process from continuing in time, since there is no space for water molecule penetration [55]. For this reason, both conditions are responsible for the degradation phenomena.

Fig. 9 shows SEM micrographs of non-exposure specimens and specimens after 768 h of durability. In non-exposure micrographs many areas with adhesive are observed, the darkest parts of the micrograph. These zones are analyzed by energy-dispersive X-ray spectroscopy certifying that it is indeed the adhesive; therefore the type of failure is mixed (areas with cohesive and adhesive failures). The micrograph for 768 h of durability does not show adhesive over the steel surface, with large corrosion areas appearing caused by the exposure to moisture and temperature. By means of energy-dispersive X-ray spectroscopy, the composition of these zones has been obtained resulting in iron oxide. It can then be assumed that together with the moisture absorption process in the adhesive, moisture also penetrates through the adhesive-adherent interface through an adsorption mechanism. Therefore, the failure at this time is purely adhesive.

The selected temperature to carry out the durability process causes a greater primary cross-linking of the polymer during the first hours. Subsequently it also causes degradation of the adhesive mechanical properties, and therefore degradation of the adhesive joint. Epoxy adhesives lose properties due to the moisture effect. These properties can be partly recovered by means of a drying process at room temperature and under controlled moisture [56]. However, in this work there is no drying process, and moisture accelerates the degradation of the adhesive. At the same time, moisture penetrates in the adhesive-adherent interface by means of an adsorption process, contributing to the degradation of the adhesive joint.

3.4.3. Reliability

Fig. 10 shows the reliability curves throughout the durability process, with the degradation suffered by the adhesive joints during each stage of the process being clearly visible. Shifting appears after 2 h of exposure to humidity and temperature. The curve of 0 h shows a reliability greater than 90% for τ_{max} close to 17 MPa. The curve of 2 h is very similar to the previous one; however, values higher than 90% reliability are reached for τ_{max} of approximately 15 MPa. After 24 h the curve moves towards the area of lower values of τ_{max}. Thus the curve of 24 h presents reliabilities greater than 90% for τ_{max} of 10 MPa. Reliability curves for 168 and 360 h are almost the same. At this point degradation is evident, and to reach a reliability of 90%, 6 MPa must not be exceeded. This value diminishes, and after 768 h of exposure, an approximate 90% reliability is obtained but only for τ_{max} less than 5 MPa.

3.5. Thermal fatigue

3.5.1. Mechanical tests

In the same way as in the durability section, the thermal fatigue process has been carried out by manufacturing the test specimens with the best surface treatments found in section 3.3. Five specimens are manufactured and studied for each number of cycles (0, 48, 97, 240, 432, 920, 1776 and 2592). Fig. 11 shows the most representative stress-strain curves and Table 6 shows average values of τ_{max}, $\delta_{\tau max}$ and stiffness for each number of cycles. τ_{max} undergoes a moderate decrease during the thermal fatigue process. Two drops of τ_{max} are observed during the process. The first one is at 97 cycles going from 18.55 ± 1.77 to 15.66 ± 1.11 MPa. The second one is at 1776 cycles when τ_{max} value of 13.25 ± 0.13 MPa is reached, which implies a decrease of 28.57% with respect to the non-exposure specimens.

Regarding $\delta_{\tau max}$ and stiffness, an obvious change after 48 cycles is observed. $\delta_{\tau max}$ decreases from 29.51 ± 1.38 to 20.42 ± 1.97% and stiffness increases from 126.80 ± 3.79 to 191.53 ± 6.70 MPa. The maximum stiffness value is obtained at 240 cycles (215.38 ± 12.42 MPa), with the strain being 14.50 ± 2.56%. After this point, both $\delta_{\tau max}$ and stiffness remain constant during all the process

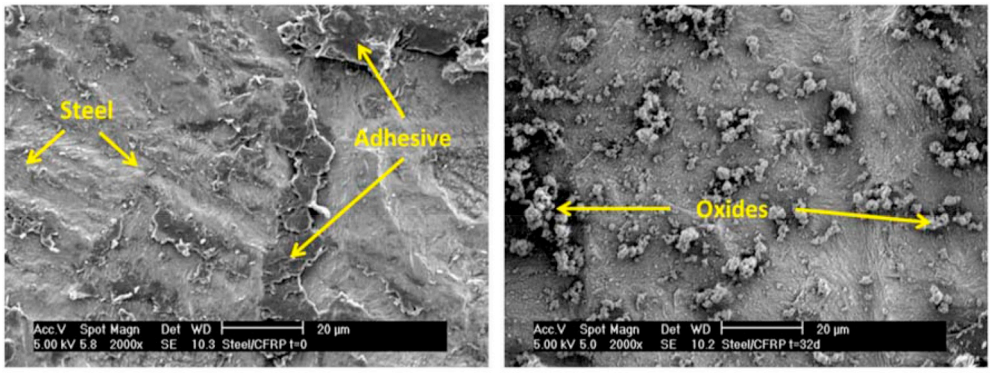

Fig. 9. a) SEM micrograph of specimen without degradation. b) SEM micrograph of specimen subjected to 768 h.

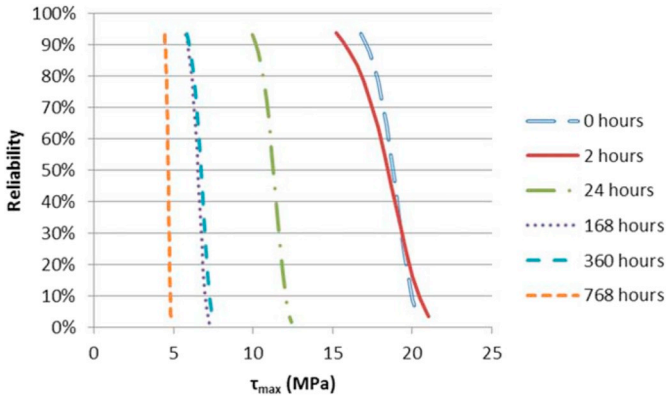

Fig. 10. Reliability curves during the durability process.

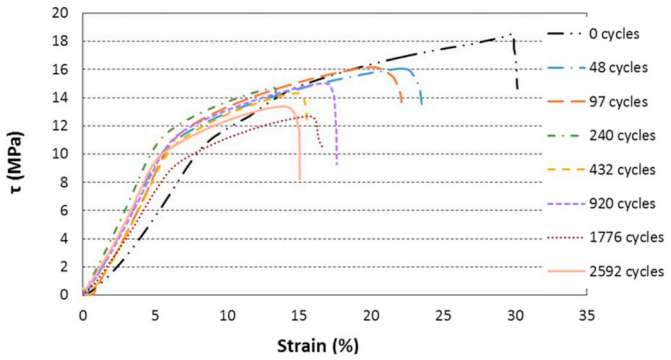

Fig. 11. Representative stress – strain curves of the thermal fatigue.

except at 1776 cycles when a small change in the stiffness value is observed. The degradation process is clear in Fig. 11, where representative stress-strain curves are shown. The differences between the non-exposure specimen curve and the ones under exposure are evident; especially with respect to the curve of the specimen subjected to 2592 cycles.

3.5.2. *Degradation phenomena*

Table 7 shows T_g variation and Fig. 12 shows DSC scans during the thermal fatigue process. The maximum temperature of the heating-cooling cycles is 80 °C, 12 °C above the T_g. After 48 cycles, T_g decreases to 60 °C as can be seen in Table 7. By subjecting the adhesive to temperatures higher than T_g, it will be in a rubbery state [55], not a glassy one, resulting in greater mobility of the polymer chains [57]. This greater mobility of the chains is associated with a decrease in the T_g [52] as occurs during the first 48 cycles.

At the same time as the mobility of the chains is increasing, the temperature increment is producing other changes in the adhesive. In thermoset polymers above the T_g chemical cross-links are induced, preventing the molecules from flowing, but providing enough mobility to the chains [58]. These links can make the adhesive stiffer, as is shown in Table 6.

During the first cycles, τ_{max} remains almost constant. After 432 cycles, T_g reaches 81 °C. It is evident that from 48 to 240 cycles the cross-linking degree continues to increase, in the same way that the stiffness (Table 6) of the joint has also increased. The cross-linking increment explains the T_g increase [59]. After 1776 cycles, T_g diminishes until 78 °C, recovering 81 °C after 2592 cycles. There are no research studies that can explain this T_g behavior due to thermal fatigue as is carried out in this work. This may be due to further deterioration in the polymer, and the polymer chains beginning to break. τ_{max} and the stiffness diminish at 1776 cycles, in the same way as it happens with the T_g, and therefore with the cross-linking, as explained above. T_g recovery after 2592 cycles can be explained with a new arrangement of the chains, with the subsequent stiffness, cross-linking and T_g increments. However, due to the already acquired degradation by the polymer, τ_{max} is not

Table 7
T_g variation during the thermal fatigue process.

Cycles	$T_g \pm 2$ (°C)
0	68
48	60
432	81
1776	78
2592	81

Table 6
Mechanical values of the joint throughout the thermal fatigue process.

Cycles	0	48	97	240	432	920	1776	2592
τ_{max} (MPa)	18.55 ± 1.77	16.75 ± 0.21	15.66 ± 1.11	15.43 ± 0.71	15.20 ± 0.56	15.33 ± 0.43	13.25 ± 0.13	13.14 ± 0.32
$\delta_{\tau max}$ (%)	29.51 ± 1.38	20.42 ± 1.97	17.09 ± 4.05	14.50 ± 2.56	15.24 ± 0.45	15.96 ± 0.86	15.43 ± 1.26	13.89 ± 1.66
Stiffness (MPa)	126.80 ± 3.79	191.53 ± 6.70	197.54 ± 7.91	215.38 ± 12.42	198.22 ± 10.23	196.97 ± 19.10	163.32 ± 17.17	195.31 ± 15.95

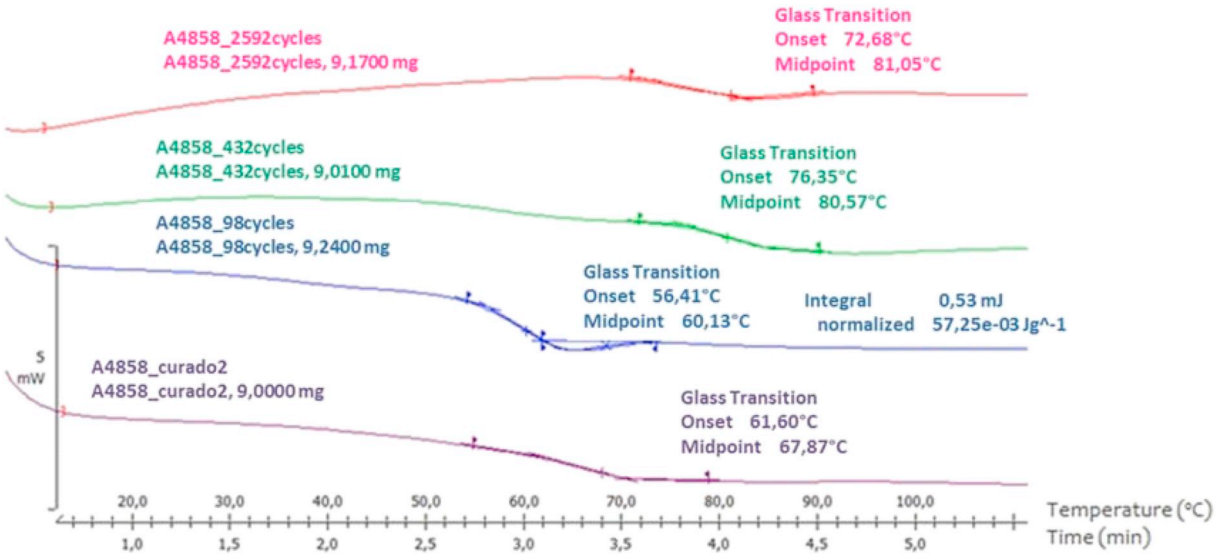

Fig. 12. Non-isothermal DSC curves for $20^{\circ}\cdot min^{-1}$ heating rate.

recovered.

Regarding τ_{max}, there is hardly any variation after 97 cycles. From 240 cycles, a change in tendency is observed. This change is related to a degradation process of the adhesive, causing a decrease in the adhesive strength, and therefore also of the adhesive joint [51]. τ_{max} values remain almost constant during the rest of the process; although in the last cycles another change of tendency is observed due to a greater degradation of the joint. No changes in the Infrared spectra are observed during the thermal fatigue process, so there is no absorbance variation, and therefore spectra are not attached.

As explained previously in section 3.3.2, in the micrograph of the specimen without degradation, large areas of adhesive are observed. After 48 cycles, the kind of failure changes as shown in Fig. 13, and delamination of the CFRP substrate, are observed in large areas of the adhesive joint. This type of failure is constant throughout the entire thermal fatigue process. Regarding the SEM micrograph for 2592 cycles, darker zones are analyzed by energy-dispersive X-ray spectroscopy, certifying that despite the long period of degradation they are still adhesive. Therefore zones with adhesive, cohesive and by substrate failures can be observed.

Delamination appears from the first exposure times (48 cycles) and only for thermal fatigue, since no evidence of this phenomenon is observed in durability specimens (Section 3.4). T_g of the adhesive for non-subjected specimens is 68 °C and T_g of the CFRP without degradation is around 100 °C, while the maximum cycle temperature is 80 °C. Thus, during the first cycles, the adhesive is working slightly above the T_g and the CFRP is working near its T_g. As explained before, during this phase greater mobility of the polymer chains is observed. At the same time the cross-linking degree gradually increases. Both adhesive and CFRP matrix are epoxy, and good compatibility is obtained. The greater mobility benefits the interactions between the chains of both the epoxy adhesive and the superficial resin layer. In the same way, the greater cross-linking makes the adhesive-resin interactions stronger. In certain areas these interactions are more resistant than the fiber-resin interlaminar interactions within the CFRP, causing delamination in the substrate. The CFRP is working during the entire thermal fatigue process below its T_g, and is not suffering significant degradation due to temperature.

3.5.3. *Reliability*

The degradation suffered by the joints during the thermal fatigue process is clearly shown in the reliability curves of Fig. 14. The curve for non-subjected specimens is the one that it is located at the right of the graph, showing more than 90% reliability for τ_{max} values above 18 MPa. Shifting appears after 48 cycles, when 90% reliability is reached for τ_{max} values close to 16 MPa. The curves continue shifting to the left in the following cycles, with the reliability curves for 97, 240, 432 and 920 cycles being almost the same. Around 90% reliability is reached for τ_{max} values of 15 MPa. Finally, the curves shift again to the left for 1776 and 2592 cycles. Both curves are practically the same, showing 90%

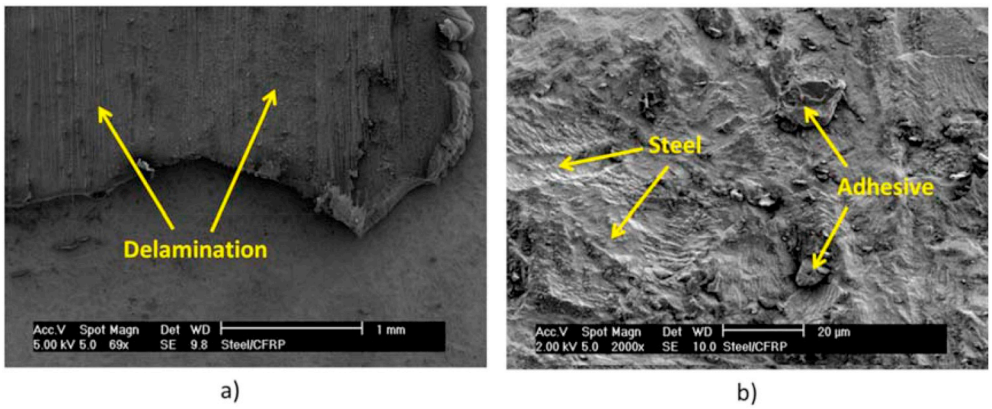

Fig. 13. SEM micrographs after 2592 thermal cycles. a) CFRP delamination. b) Steel surface.

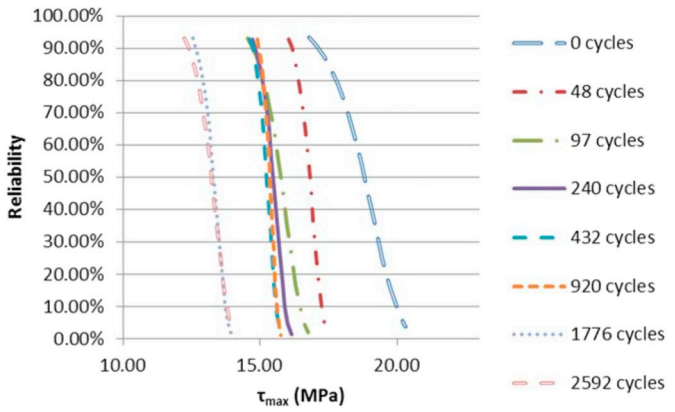

Fig. 14. Reliability curves during the thermal fatigue process.

reliability for τ_{max} values close to 13 MPa.

A good example of application of CFRP composites adhesively bonded to steel substrate is the work developed by Galvez et al. [20]. In this work the replacement of welded joints by adhesive joints in stress concentration nodes in bus structures is considered. The target value of the maximum shear stress is 0.42 MPa, much lower than the values obtained in this work (18.55 ± 1.77 MPa). Even after the joints are subjected to durability and thermal fatigue, the values are sufficient. Thereby after 768 h under durability conditions, maximum shear stress value is 4.65 ± 0.20 MPa, and after 2592 heat-aging cycles maximum shear stress value is 13.14 ± 0.32 MPa.

As a future research line, studies with CFRP-to-bonded joints in prestressed CFRP should be taken into account. Based on previous works, it could be said that long-term performance in prestressed systems shows good results. Täljsten et al. [60] compare the fatigue behavior of prestressed and non-prestressed adhesively bonded CFRP laminates for the strengthening of old metallic structures. Results show that it is possible to lengthen the fatigue life almost four times as long as a reference specimen with non-prestressed laminates. But in the case of prestressed laminates, crack growth was halted completely. Other authors have revealed that prestressed CFRP can prevent fatigue crack initiation by means of extensive laboratory tests [61] or even can arrest existing fatigue cracks [62] in critical hot-spots of metallic structures.

4. Conclusions

- The adhesive characterization shows higher ductility than conventional structural epoxy adhesives, although thermal properties are similar to other epoxy adhesives. The Kissinger method is faster and simpler than the MFK since it assumes that the curing reaction is order 1 reaction. Using MFK the kinetic of curing is simulated, showing that at higher temperature, less time is needed to obtain a 99% conversion degree.
- Both durability and thermal fatigue processes adversely affect the mechanical properties of the adhesive joint.
- Different mechanisms affect the integrity of the adhesive joint during the durability test. On the one hand, the temperature causes greater primary cross-linking of the polymer chains at the beginning, and a subsequent degradation of the adhesive joint. Moisture is absorbed mainly as bound water causing swelling and plasticization. Type I and Type II bound water are created, which are responsible for decreasing and increasing the adhesive T_g respectively. Moisture also penetrates by means of an adsorption process through the adhesive-substrate interface, accelerating the degradation process of the adhesive joint. Degradation is evident after 24 h of exposure, when τ_{max} drops by 40%.
- Thermal fatigue affects the integrity of the adhesive joint to a lesser extent than the durability process. During the first cycles, temperature increases the mobility of the chains, decreasing the value of the T_g. Longer exposure times increase the cross-linking and the T_g. Degradation is evident after 97 cycles, when τ_{max} drops by 15%.
- The durability process is more negative in terms of reliability than the thermal fatigue process.

Conflicts of interest

The author(s) declared no potential conflicts of interest with respect to the research, authorship, and/or publication of this article.

Acknowledgements

This work was supported by Interreg SUDOE, through KrEaTive Habitat project, grant number SOE1/P1/E0307. The authors gratefully acknowledge the collaboration of Castrosua S. A. for supplying the steel and Sika S.A.U. España for supplying the adhesives and the CFRP. IAAB (Álvaro Alonso Barba Institute of Chemistry and Materials Technology).

References

[1] Jones R. Mechanics of composite materials. CRC Press; 1998.
[2] Rana S, Fangueiro R, editors. Advanced composite materials for aerospace engineering. Woodhead Publishing; 2016.
[3] Mangalgiri PD. Composite materials for aerospace applications. Bull Mater Sci 1999;22:657–64.
[4] Machado JJM, Gamarra PMR, Marques EAS, da Silva LFM. Improvement in impact strength of composite joints for the automotive industry. Compos B Eng 2018;138:243–55.
[5] Ishikawa T, Amaoka K, Masubuchi Y, Yamamoto T, Yamanaka A, Arai M, Takahashi J. Overview of automotive structural composites technology developments in Japan. Compos Sci Technol 2018;155:221–46.
[6] Kapuria S, Das HN. Improving hydrodynamic efficiency of composite marine propellers in off-design conditions using shape memory alloy composite actuators. Ocean Eng 2018;168:185–203.
[7] Singh AAMM, Raj FM, Franco PA, Binoj JS. Evaluation of mechanical behavior of multifilament discarded fishnet/glass fiber and polyester composites for marine applications. Mar Struct 2018;58:361–6.
[8] Colangelo F, Russo P, Cimino F, Cioffi R, Farina I, Fraternali F, Feo L. Epoxy/glass fibres composites for civil applications: comparison between thermal and microwave crosslinking routes. Compos B Eng 2017;126:100–7.
[9] Ribeiro F, Sena-Cruz J, Branco FG, Júlio E. Hybrid effect and pseudo-ductile behaviour of unidirectional interlayer hybrid FRP composites for civil engineering applications. Constr Build Mater 2018;171:871–90.
[10] D'Aniello M, Portioli F, Landolfo R. Lap shear tests on hot-driven steel riveted connections strengthened by means of C-FRPs. Compos B Eng 2014;59:140–52.
[11] Javadian A, Wielopolski M, Smith IFC, Hebel DE. Bond-behavior study of newly developed bamboo-composite reinforcement in concrete. Constr Build Mater 2016;122:110–7.
[12] Justo J, París F. Experimental mechanical characterization of composite-concrete joints. Compos B Eng 2018;154:148–56.
[13] Teng JG, Yu T, Fernando D. Strengthening of steel structures with fiber-reinforced polymer composites. J Constr Steel Res 2012;78:131–43.
[14] Danilov AI. Some aspects of CFRP steel structures reinforcement in civil engineering. Procedia Eng. 2016;153:124–30.
[15] Liu Y, Zwingmann B, Schlaich M. Carbon fiber reinforced polymer for cable structures – a review. Polym. Basel 2015;7:2078–99.
[16] Ghafoori E, Motavalli M, Nussbaumer A, Herwig A, Prinz GS, Fontana M. Design criterion for fatigue strengthening of riveted beams in a 120-year-old railway metallic bridge using pre-stressed CFRP plates. Compos B Eng 2015;68:1–13.
[17] Hosseini A, Ghafoori E, Al-Mahaidi R, Zhao X, Motavalli M. Strengthening of a 19th-century roadway metallic bridge using nonprestressed bonded and prestressed unbonded CFRP plates. Constr Build Mater 2019;209:240–59.
[18] Ghafoori E, Hosseini A, Al-Mahaidi R, Zhao X, Motavalli M. Prestressed CFRP-strengthening and long-term wireless monitoring of an old roadway metallic bridge. Eng Struct 2018;176:585–605.
[19] Oller E, Pujol M, Marí A. Contribution of externally bonded FRP shear reinforcement to the shear strength of RC beams. Compos B Eng 2019;164:235–48.
[20] Galvez P, Quesada A, Martinez MA, Abenojar J, Boada MJL, Diaz V. Study of the behaviour of adhesive joints of steel with CFRP for its application in bus structures. Compos B Eng 2017;129:41–6.
[21] Alia C, Arenas JM, Suárez JC, Pinilla P. Mechanical behavior of polyurethane adhesive joints used in laminated materials for marine structures. Ocean Eng 2016;113:64–74.
[22] Marques EAS, da Silva LFM, Flaviani M. Testing and simulation of mixed adhesive joints for aerospace applications. Compos B Eng 2015;74:123–30.
[23] Mays GC. Structural applications of adhesives in civil engineering. Mater Sci Technol 1985;1:937–43.

[24] Kumar P, Patnaik A, Chaudhary S. A review on application of structural adhesives in concrete and steel–concrete composite and factors influencing the performance of composite connections. Int J Adhesion Adhes 2017;77:1–14.
[25] Shash AA. Repair of concrete beams – a case study. Constr Build Mater 2005;19:75–9.
[26] Hollaway LC, Cadei J. Progress in the technique of upgrading metallic structures with advanced polymer composites. Prog Struct Eng Mater 2002;4:131–48.
[27] Martinelli E, Hosseini A, Ghafoori E, Motavalli M. Behavior of prestressed CFRP plates bonded to steel substrate: numerical modeling and experimental validation. Compos Struct 2019;207:974–84.
[28] Hosseini A, Ghafoori E, Wellauer M, Marzaleh AS, Motavalli M. Short-term bond behavior and debonding capacity of prestressed CFRP composites to steel substrate. Eng Struct 2018;176:935–47.
[29] Galvez P, Abenojar J, Martinez MA. Durability of steel-CFRP structural adhesive joints with polyurethane adhesives. Compos B Eng 2019;165:1–9.
[30] Heshmati M, Haghani R, Al-Emrani M. Environmental durability of adhesively bonded FRP/steel joints in civil engineering applications: state of the art. Compos B Eng 2015;81:259–75.
[31] Böer P, Holliday L, Kang TH-K. Independent environmental effects on durability of fiber-reinforced polymer wraps in civil applications: a review. Constr Build Mater 2013;48:360–70.
[32] Soles CL, Chang FT, Gidley DW, Yee AF. Contributions of the nanovoid structure to the kinetics of moisture transport in epoxy resins. J Polym Sci, Part B: Polym Phys 2000;38:776–91.
[33] Rider AN, Brack N, Andres S, Pigram PJ. The influence of hydroxyl group concentration on epoxy–aluminium bond durability. J Adhes Sci Technol 2004;18:1123–52.
[34] Sousa JM, Correia JR, Cabral-Fonseca S. Some permanent effects of hygrothermal and outdoor ageing on a structural polyurethane adhesive used in civil engineering applications. Int J Adhesion Adhes 2018;84:406–19.
[35] Duncan B, Dean G. Measurements and models for design with modern adhesives. Int J Adhesion Adhes 2003;23:141–9.
[36] Treloar LRG. Stress-strain data for vulcanised rubber under various types of deformation. Trans Faraday Soc 1944;40:59–70.
[37] da Silva LFM, Rodrigues TNSS, Figueiredo MAV, de Moura MFSF, Chousal JAG. Effect of adhesive type and thickness on the lap shear strength. J Adhes 2006;82:1091–115.
[38] NF T 76-142. Méthode de préparation de plaques d'adhésifs structuraux pour la réalisation d'éprouvettes d'essai de caractérisation. 1988.
[39] da Silva LFM, Adams RD, Gibbs M. Manufacture of adhesive joints and bulk specimens with high-temperature adhesives. Int J Adhesion Adhes 2004;24:69–83.
[40] Kissinger HE. Reaction kinetics in differential thermal analysis. Anal Chem 1957;29:1702–6.
[41] Vyazovkin S, Wight CA. Isothermal and non-isothermal kinetics of thermally simulated reactions of solids. Int Rev Phys Chem 1998;17:407–33.
[42] Abenojar J, Tutor J, Ballesteros Y, del Real JC, Martínez MA. Erosion-wear, mechanical and thermal properties of silica filled epoxy nanocomposites. Compos B Eng 2017;120:42–53.
[43] Abenojar J, Martinez MA, Encinas N, Velasco F. Modification of glass surfaces adhesion properties by atmospheric pressure plasma torch. Int J Adhesion Adhes 2013;44:1–8.
[44] Banea MD, da Silva LFM. Mechanical characterization of flexible adhesives. J Adhes 2009;85:261–85.
[45] Grant LDR, Adams RD, da Silva LFM. Experimental and numerical analysis of single-lap joints for the automotive industry. Int J Adhesion Adhes 2009;29:405–13.
[46] Greenspan L. Humidity fixed points of binary saturated aqueous solutions. J. Res. Natl. Bur. Stand. A: Phys. Chem. 1977;81A:89–96.
[47] Burkanudeen A, Ramesh P. Novel latent epoxy curing agent for secondary insulation in electrical rotors and stators. IEEE Trans Dielectr Electr Insul 2012;19:1791–8.
[48] Barbosa AQ, da Silva LFM, Abenojar J, del Real JC, Paiva RMM, Öchsner A. Kinetic analysis and characterization of an epoxy/cork adhesive. Thermochim Acta 2015;604:52–60.
[49] Abenojar J, Encinas N, del Real JC, Martinez MA. Polymerization kinetics of boron carbide/epoxy composites. Thermochim Acta 2014;575:144–50.
[50] Banea MD, da Silva LFM. The effect of temperature on the mechanical properties of adhesives for the automotive industry. Proc. Inst. Mech. Eng. L J. Mater. Des. Appl. 2010;224:51–62.
[51] Viana G, Costa M, Banea MD, da Silva LFM. A review on the temperature and moisture degradation of adhesive joints. Proc. Inst. Mech. Eng. L J. Mater. Des. Appl. 2016;0(0):1–14.
[52] Zhou JM, Lucas JP. Hygrothermal effects of epoxy resin. Part II: variations of glass transition temperature. Polymer 1999;40:5513–22.
[53] De'Nève B, Shanahan MER. Water absorption by an epoxy resin and its effect on the mechanical properties and infra-red spectra. Polymer 1993;34:5099–105.
[54] Zhou JM, Lucas JP. Hygrothermal effects of epoxy resin. Part I: the nature of water in epoxy. Polymer 1999;40:5505–12.
[55] Abenojar J, Pantoja M, Martinez MA, del Real JC. Aging by moisture and/or temperature of epoxy/SiC composites: thermal and mechanical properties. J Compos Mater 2014;49:2963–75.
[56] Frigione M, Aiello MA, Naddeo C. Water effects on the bond strength of the concrete/concrete adhesive joints. Constr Build Mater 2006;20:957–70.
[57] Gao Y, Wu Y, Liu J, Zhang L. Effect of chain structure on the glass transition temperature and viscoelastic property of cis-1,4-polybutadiene via molecular simulation. J Polym Sci, Polym Phys 2017;55:1005–16.
[58] Hale A. Chapter 9: thermosets. In: Cheng SZD, editor. Handbook of thermal analysis and Calorimetry. Vol. 3: applications to polymers and plastics. Elsevier Science BV; 2002. p. 295–354.
[59] Abenojar J, Martinez MA, Velasco F, Pascual-Sánchez V, Martín-Martínez M. Effect of boron carbide filler on the curing and mechanical properties of an epoxy resin. J Adhes 2009;85:216–38.
[60] Täljsten B, Hansen CS, Schmidt JW. Strengthening of old metallic structures in fatigue with prestressed and non-prestressed CFRP laminates. Constr Build Mater 2009;23:1665–77.
[61] Ghafoori E, Motavalli M. A retrofit theory to prevent fatigue crack initiation in aging riveted bridges using carbon fiber-reinforced polymer materials. Polymers 2016;8:308.
[62] Hosseini A, Ghafoori E, Motavalli M, Nussbaumer A, Zhao X. Mode I fatigue crack arrest in tensile steel members using prestressed CFRP plates. Compos Struct 2017;178:119–34.

PUBLICACIÓN 7

International Journal of Adhesion and Adhesives 95 (2019) 102418

Contents lists available at ScienceDirect

International Journal of Adhesion and Adhesives

journal homepage: www.elsevier.com/locate/ijadhadh

Intensity of singular stress field (ISSF) variation as a function of the Young's modulus in single lap adhesive joints

Pedro Galvez[a,b], Nao-Aki Noda[a,*], Rei Takaki[a], Yoshikazu Sano[a], Tatsujiro Miyazaki[c], Juana Abenojar[b], Miguel Angel Martínez[b]

[a] Department of Mechanical Engineering, Kyushu Institute of Technology, 1-1 Sensui-cho Tobata-ku Kitakyushu-shi, Fukuoka, 804-8550, Japan
[b] Materials Science and Engineering and Chemical Engineering Department, University Carlos III de Madrid, Avenida de La Universidad 30, 28911, Leganes, Spain
[c] Department of Mechanical Systems Engineering, University of the Ryukyus, 1 Senbaru, Nishihara-cho Nakagami-gun, Okinawa, 903-0213, Japan

ARTICLE INFO

Keywords:
Intensity of singular stress field
Strength evaluation
Fracture mechanics
Finite element stress analysis

ABSTRACT

Employing mixed adhesive joints has been proven to be very useful. This type of joint leads to improved performance by increasing strength and decreasing stresses in critical areas of the joint. In the same way, the use of the Intensity of Singular Stress Field (ISSF) has been shown to be suitable for adhesive joint calculation, since the adhesive strength can be controlled by the ISSF at the interface end. Four finite element models have been created by combining two epoxy adhesives with different mechanical properties, and therefore with different Young's moduli. New mixed adhesive joints have been compared with respect to only-one adhesive joints in terms of the ISSF. The results show a clear improvement with one of the configurations of mixed adhesive joints. A significant decrease of 35.64% in the ISSF is obtained compared to the only-one adhesive configuration.

1. Introduction

The extensive development in the area of adhesives during recent decades has led to their use in a wide range of industries such as automotive, aerospace, construction, electronics, packaging and sports [1]. Adhesives provide several advantages over other traditional mechanical joints, among which we can highlight lower density and costs, homogeneous distribution of loads and ability to protect against corrosion among others. The increasingly widespread use of adhesives makes it necessary to develop and use techniques capable of accurately assessing their behaviour and ability. Finite element methods (FEM) have proven to be a very effective tool in the calculation of adhesive joints. Xará and Campilho [2] determine that the extended Finite Element Method, using different initiation criteria, is an accurate and appropriate tool for the strength prediction of single-L joints bonded with either brittle or ductile adhesives. Li et al. [3] and Noda et al. [4] find that adhesive strength can be controlled by the intensity of the singular stress field (ISSF) at the interface end, and also the strength of the lap joint can be given as $K_{\sigma c} = const$. Mintzas and Nowell [5] state that the strength of the adhesive bond can be expressed as $H_{cr} = const$. Thus logical and efficient ISSF methods can be applied to evaluate the adhesive strength, since it is proven that the ISSF may control it. Wang and Rose [6] developed a novel work which shows compact solutions for the corner singularity at the adhesive/adherent interface in a bonded lap joint. A numerical matched asymptotic expansion method is used to determine the stress intensity factors for the limiting case of rigid substrates. The suitability of the analytical solutions is proven as they are able to offer good results in terms of the singular stress fields at the adhesive/substrate corners with respect to the results obtained by finite elements using a fine mesh near the corner points. Goglio and Rossetto [7] demonstrate the relationship between the stress intensity factor and peak structural stresses in the adhesive at the overlap ends. They propose a procedure to estimate the stress intensity factor without the need for a detailed finite element analysis of the joints. The equations of the problem are solved by a valid numerical procedure. The suitability of the procedure is evaluated for single lap joints by combining different values of joint parameters, establishing the type of stress that should be considered to obtain the correct definition of the stress intensity factor.

UNE-EN 1465 and JIS K6850 are the Spanish and Japanese standards that detail how to calculate the adhesive strength in lap joints. Nevertheless, the specimen configuration significantly affects the lap joint strength, and therefore this strength cannot be expressed as $\tau_{ave} = const$, as pointed out by Li et al. [3]. Ideally, single lap joint tests are intended to be conducted under pure shear loading, but in fact the existence of other loads is well known in the literature, which have

* Corresponding author.
E-mail address: noda.naoaki844@mail.kyutech.jp (N.-A. Noda).

https://doi.org/10.1016/j.ijadhadh.2019.102418
Received 20 March 2019; Accepted 8 June 2019
Available online 06 August 2019
0143-7496/

Nomenclature

Symbols

E	Young's Modulus
$K_{\sigma c}$	Critical ISSF
υ	Poisson's Ratio
σ_{ys}	Steel yield strength
σ_{fs}	Steel tensile strength
ε_{fs}	Steel elongation at break
σ_{fa}	Adhesive tensile strength
ε_{fa}	Adhesive elongation at break
G	Shear modulus
T_A	Adhesive thickness
L_0	Adhesive overlap
W_A	Single lap joint specimen width
T_S	Steel substrate thickness
L_S	Steel substrate length
L_T	Specimen length
L_{0A1}	Adhesive 1 overlap
L_{0A2}	Adhesive 2 overlap
K_σ, K_τ	ISSF
r	Radial distance away from the singular point
$f_{\theta\theta}(\theta, \lambda_k)$, $f_{r\theta}(\theta, \lambda_k)$	Non-dimensional functions of angle θ and λ_k
α, β	Dundurs´ material parameters
θ	Angle from the interface corner
λ	Singular index
σ_y, τ_{xy}	Tension and shear stress component near the crack tip
σ_0	Tension at both ends of single lap joint
τ_{ave}	Average shear stress at fracture
$\sigma^*_{y0,FEM}$, $\tau^*_{xy0,FEM}$	FEM stresses at the interface corner of the reference problem
$\sigma_{y0,FEM}$, $\tau_{xy0,FEM}$	FEM stresses at the interface corner of the unknown problem

Abbreviations

FEM	Finite elements method
ISSF	Intensity of Singular Stress Field
RWCIM	Reciprocal work contour integral method

produced other efforts such as peeling [8]. Maximum peeling stress is located within the adhesive bond near the adhesive-adherent interface at the corner edge, as is demonstrated by Martinez et al. [9]. Li et al. [10] find that ISSF at the interface corner is related with the peeling force, and in the same way the peeling force directly depends on the adhesive stiffness and the adhesive thickness. The stiffness effect on the ISSF is discussed, focusing on how to minimize the ISSF in single lap joint specimens by means of the combination of one higher Young's modulus and one lower Young's modulus epoxy adhesives. Incorporating different adhesives (with different mechanical properties) into the bond-line can improve the stress distribution and can also reduce these stresses. The literature shows other works with mixed adhesive joints such as the joints proposed in this present study. Chiminelli et al. [11] observe that by using the mixing adhesive approach to create new mixed adhesive joints, the ultimate load can be increased by 70% with respect to the base adhesives assemblies. Breto et al. [12] have studied the singularity impact by means of two independent methodologies to select the intermediate material between adhesive bands in mixed adhesive joints. Fitton et al. [13] show the effect of variable modulus bond-lines in single lap joints, concluding that these kinds of joints are able to reduce stress concentration, increase the strength of the joint, reduce the experimental scatter and even change the mode of failure. Da Silva et al. [14] compare mixed adhesive joints with joints only manufactured with a brittle adhesive, obtaining higher joint strength for mixed adhesive joints. The best adhesive joint combination in the present work is composed of one ductile adhesive at the ends of the overlap, and one brittle adhesive in the central area. Carbas et al. [15] have created an induction heating method to manufacture adhesively bonded functionally graded joints obtaining a performance improvement close to 70%.

Despite the fact that there are several related studies, as has been seen, none of them have studied the effect of Young's modulus in non-mixed and mixed adhesive joints in terms of the Intensity of Singular Stress Field (ISSF). Four single lap joint models are developed in this work, combining two epoxy adhesives with different mechanical properties, studying the behaviour in terms of the ISSF of each model.

2. Specimen design

2.1. Materials

In this work structural AISI 4140 alloy steel was selected for both substrates. The main mechanical properties of this steel are: Young´s modulus (E_s) of 210 GPa, yield strength (σ_{ys}) of 415 MPa, tensile strength (σ_{fs}) of 655 MPa, elongation at break (ε_{fs}) of 25.70% and Poisson´s ratio (υ_s) of 0.3. Two structural epoxy adhesives (SikaPower®-1511 and SikaPower®-1548) were considered. Table 1 shows the mechanical properties of the adhesives, highlighting the difference in the values of the Young's modulus. Being a purely theoretical study, manufacturer mechanical properties of the AISI 4140 alloy steel and the adhesives were used to perform the simulation.

Table 1
Manufacturer mechanical properties of SikaPower®-1511 and SikaPower®-1548.

Property	SikaPower®-1511	SikaPower®-1548
Young´s modulus, E_a [GPa]	3.3	1.0
Poisson´s ratio, υ_a	0.367	0.396
Tensile strength, σ_{fa} [MPa]	45.0	30.0
Elongation at break, ε_{fa} [%]	3	9
Shear Modulus, G [GPa]	1.21	0.36

2.2. Specimen geometry

Single lap joint configuration was selected to calculate ISSF. Two different configurations of single lap joint were used. The first one was with a completely homogeneous adhesive layer, using a unique adhesive. The second one used two adhesives, one adhesive for the corners, and another adhesive for the central area. An image and the dimensions of both single lap joint configurations can be seen in Fig. 1. The chosen dimension for the Single Lap Joint specimens were (in mm): adhesive thickness (T_A) = 0.2, adhesive overlap (L_0) = 25, adhesive and steel width (W_A) = 25, steel thickness (T_S) = 25, steel length (L_S) = 100, specimen length (L_T) = 175, adhesive 1 overlap (L_{0A1}) = 15, adhesive 2 overlap (L_{0A2}) = 5. Da Silva et al. [16] demonstrated that adhesive thickness of 0.2 mm is the most suitable value in terms of the lap shear strength of epoxy adhesives. In Ref. [3], the effect of adherent steel thickness T_s on the ISSF was investigated under the same tensile load. It was then found that the ISSF decreases with increasing T_s and becomes constant when $T_s \geq 25$ mm. This is because the bend deformation of the single lap joint becomes smaller under $T_s \geq 25$ mm. For this reason, 25 mm of steel substrate thickness was chosen to carry out this work.

Four models were studied combining the properties of both SikaPower®-1511 and SikaPower®-1548 adhesives. In Model 1 and

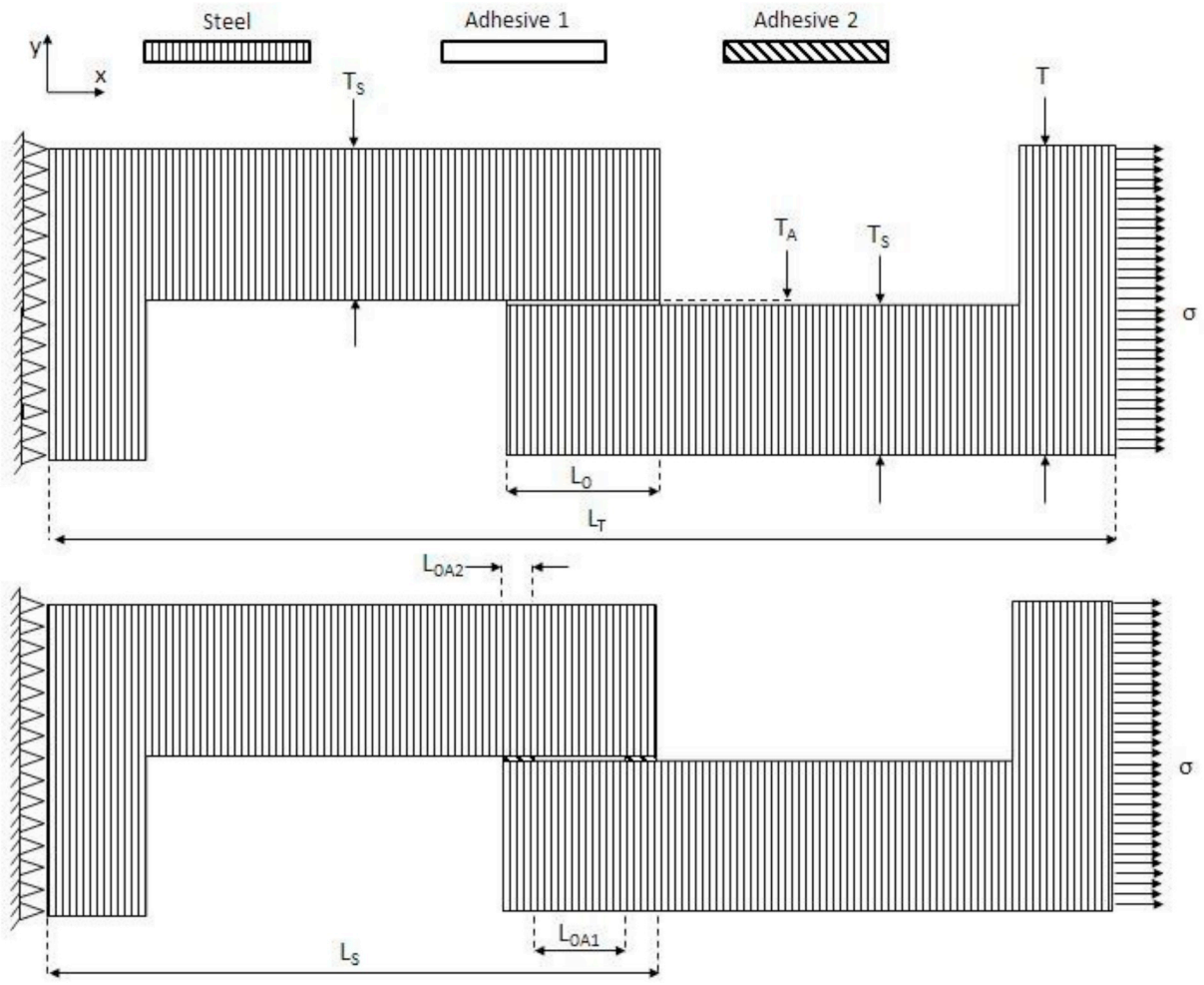

Fig. 1. Depiction of studied single lap joint configurations.

Model 2, homogeneous layers of the SikaPower®-1511 and SikaPower®-1548 were used respectively. In Model 3 and Model 4 both adhesives were combined. SikaPower®-1548 was used in the corners and SikaPower®-1511 in the center in Model 3, while in Model 4 the opposite was done. Adhesive configurations of the models are shown in Fig. 2.

3. Calculation of ISSF

Intensity of the singular stress field (ISSF) was used to evaluate the effect of the Young's Modulus in single lap joints. The ISSF method is described in this section. Zhang et al. [17,18] showed the ability of mesh-independent techniques to calculate the ISSF. α and β are the parameters of Dundurs [19], which are defined by the shear modulus G_m and by the Poisson's ratio υ_m, with m = a for the adhesive and m = s for the substrate. α and β were calculated from Eq (1) and Eq (2):

$$\alpha = \frac{G_a(k_s+1) - G_s(k_a+1)}{G_a(k_s+1) + G_s(k_a+1)} \tag{1}$$

$$\beta = \frac{G_a(k_s-1) - G_s(k_a-1)}{G_a(k_s+1) + G_s(k_a+1)} \tag{2}$$

k_m was calculated from Eq (3):

$$k_m = \begin{cases} \frac{3-\upsilon_m}{1+\upsilon_m} \\ 3-4\upsilon_m \end{cases} \tag{3}$$

where $^{3-\upsilon_m}/_{1+\upsilon_m}$ is relative to the plane stress and $3-4\upsilon_m$is relative to the plane strain. In this work, the effect of the Young's Modulus was discussed in terms of the ISSF. Noda et al. [20] affirm that this is possible since in 2D modelling, the adhesive strength can be expressed as a constant value of the ISSF. Singular index (λ) characterizes the singular stress field in lap joints, and was calculated from eigenequation (Eq (4)), which was derived by Bogy [21], proving two real roots for the majority of material combinations [3,4]:

$$4sin^2(\pi\lambda)\left\{sin^2\left(\frac{\pi\lambda}{2}\right)-\lambda^2\right\}\beta^2 + 4\lambda^2sin^2(\pi\lambda)\alpha\beta + \left\{sin^2\left(\frac{\pi\lambda}{2}\right)-\lambda^2\right\}\alpha^2 - 4\lambda^2sin^2(\pi\lambda)\beta - 2\left\{\lambda^2cos(2\pi\lambda) + sin^2\left(\frac{\pi\lambda}{2}\right)cos(\pi\lambda) + \frac{1}{2}sin^2(\pi\lambda)\right\}\alpha + sin^2\left(\frac{3\pi}{2}\lambda\right) - \lambda^2 = 0 \tag{4}$$

Regarding the boundary conditions (Fig. 3), fixed tensile stress

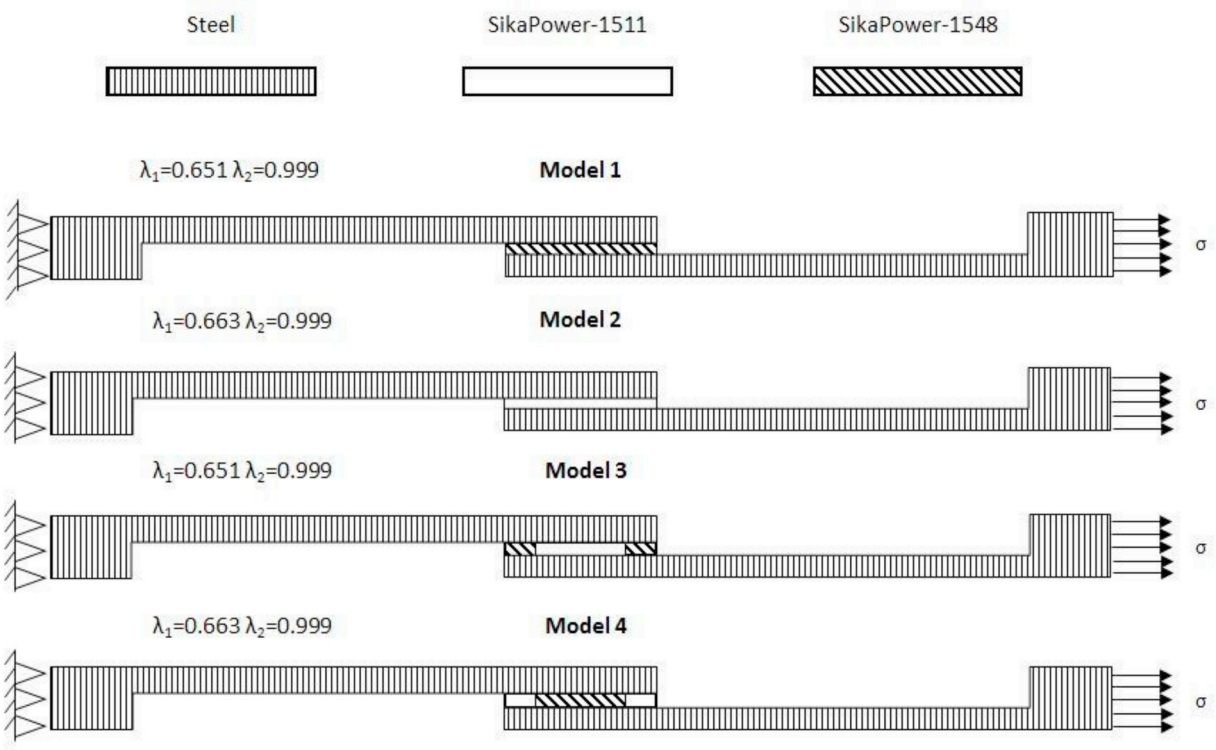

Fig. 2. Adhesive configurations of the studied models.

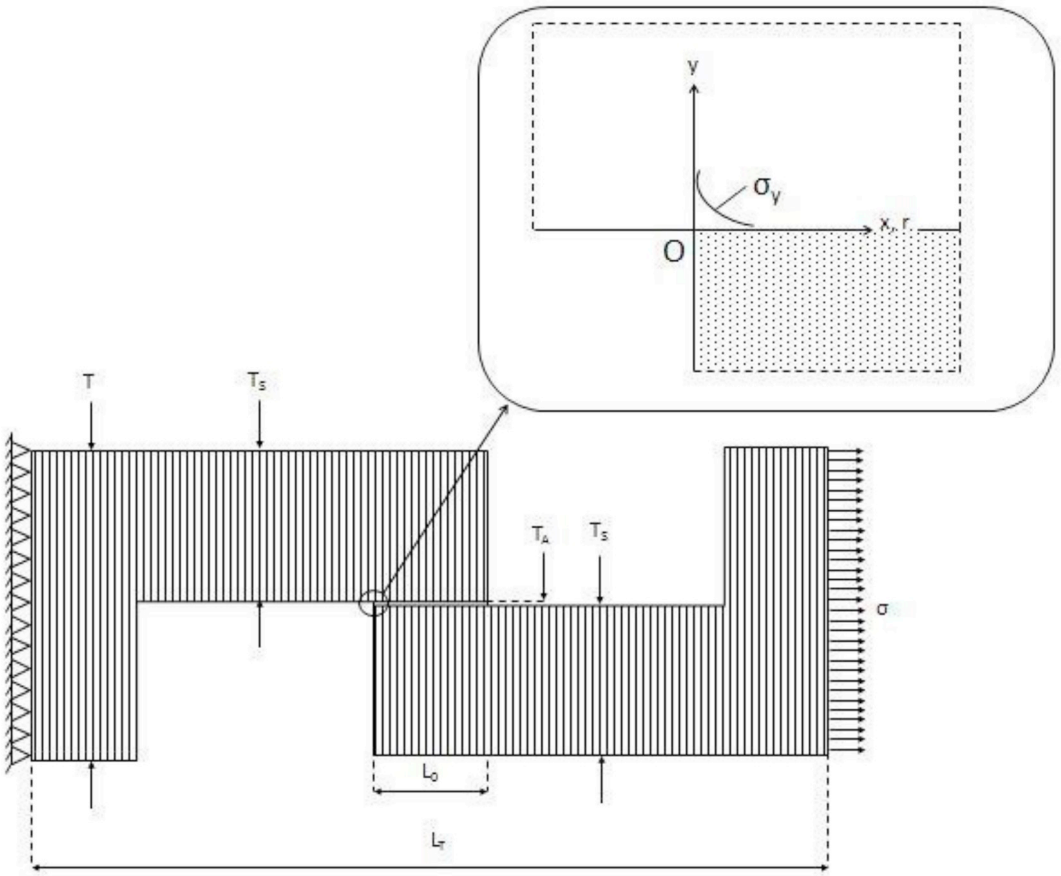

Fig. 3. Boundary conditions: σ = 1 MPa, P/W = 50.2 N/mm, T_A = 0.2 mm, T_S = 25 mm, T = 50.2 mm, W = 25 mm, L_T = 175 mm, L_0 = 25 mm.

$\sigma = 1\ MPa$ was selected. This tensile stress corresponds to a load parameter (P/W) of 50.2 N/mm. The load parameter was calculated from Eq (5):

$$\frac{P}{W} = \sigma T. \tag{5}$$

where P is the load, W is the specimen width (25 mm), σ is the tensile stress (1 MPa) and T is the total thickness of the specimen (50.2 mm). Total thickness was calculated from $T = (2T_s) + T_A$, with T_S being the substrate thickness and T_A the adhesive thickness. σ = 1 MPa was selected in all models to perform the simulation under the same conditions.

By setting σ = 1 MPa as the boundary condition reliable qualitative analysis can be ensured. Analogous models (those with the same materials combination in the edge corner) can be properly compared.

Continuing with the theoretical framework, the stresses σ_y and τ_{xy} that are located around the interface end can be expressed as follows:

$$\sigma_y = \frac{K_{\sigma,\lambda_1}}{r^{1-\lambda_1}} + \frac{K_{\sigma,\lambda_2}}{r^{1-\lambda_2}} \cong \frac{K_{\sigma,\lambda_1}}{r^{1-\lambda_1}}\left(1 + C_\sigma r^{\lambda_2-\lambda_1}\right)$$

$$\tau_{xy} = \frac{K_{\tau,\lambda_1}}{r^{1-\lambda_1}} + \frac{K_{\tau,\lambda_2}}{r^{1-\lambda_2}} \cong \frac{K_{\tau,\lambda_1}}{r^{1-\lambda_1}}\left(1 + C_\tau r^{\lambda_2-\lambda_1}\right). \tag{6}$$

where r is the radial distance away from the corner singular point O. In previous studies [17,18,20,22], the strength of butt joints was also expressed as a constant value independent of the adhesive thickness, although the boundary is straight instead of notch shaped. Therefore, in previous studies [3,4], the term ISSF (Intensity of Singular Stress Field) has been used instead of notch stress intensity factors defined for notches [23]. In Eq (6), $K_{\sigma,\lambda 1}$ and $K_{\sigma,\lambda 2}$ are the values of the ISSF. C_σ and C_τ are two ratios which are almost constant except for extreme geometries of adhesive [20], and were calculated following Eq (7). In Ref. [4], the adhesive strength of the single lap joints can be expressed as a constant value of ISSF except in the case of very short adhesive overlap length. If $\lambda_2 \approx 1$ the effect of $K_{\sigma,\lambda_2}/r^{1-\lambda_2}$ and $K_{\tau,\lambda_2}/r^{1-\lambda_2}$ becomes very small in Eq (6). Thus ISSFs are commanded only by $K_{\sigma,\lambda 1}$ and $K_{\tau,\lambda 1}$, with both values being the expression of ISSF parameters, as explained in previous studies [4].

Table 2
Material properties of SikaPower®-1548 and AISI 4140, material combination of Model 1 and Model 3.

Material	E (GPa)	υ	α	β	λ_1	λ_2
AISI 4140	210.0	0.3	−0.990	−0.170	0.651	0.999
SikaPower®1548	1.0	0.396				

Table 3
Material properties of SikaPower®-1511 and AISI 4140, material combination of Model 2 and Model 4.

Material	E (GPa)	υ	α	β	λ_1	λ_2
AISI 4140	210.0	0.3	−0.968	−0.202	0.663	0.999
SikaPower®1511	3.3	0.367				

$$C_\sigma = \frac{K_{\sigma,\lambda_2}}{K_{\sigma,\lambda_1}}$$

$$C_\tau = \frac{K_{\tau,\lambda_2}}{K_{\tau,\lambda_1}} \tag{7}$$

In the present study the value of ISSF was calculated in four different models (Fig. 2). Material combination in the edge corner must be the same to be able to compare two models. Therefore, Model 1 could be compared with Model 3, and Model 2 could be compared with Model 4, since in both cases the combination of materials in the corner singular point was the same. Fig. 4 shows the material combination of Model 1 – Model 3 and Model 2 – Model 4 in the corner singular point O. In Refs. [3,4], the adhesive strength of the lap joint is expressed as a constant value of the ISSF (K_σ) independent of the adhesive geometry. Accordingly, the strength of Model 1 and Model 3 can be compared in terms of ISSF since they have the same singular stress field with the same singular index λ ($\lambda_1 = 0.651$, $\lambda_2 = 0.999$ as is shown in Fig. 2

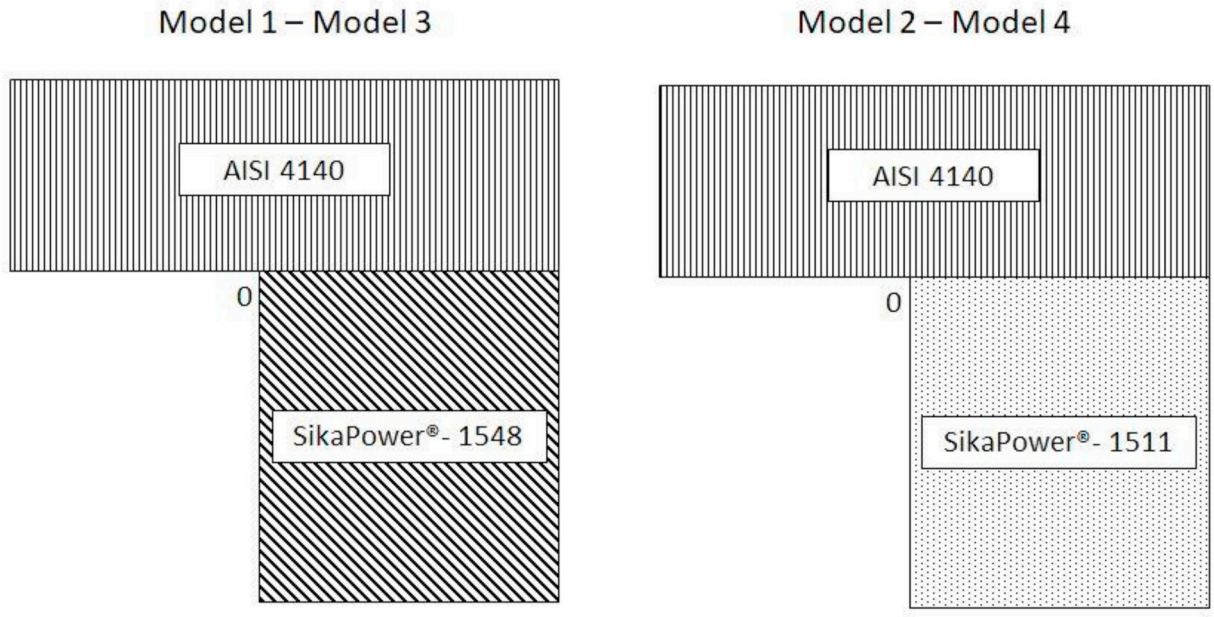

Fig. 4. Material combination in Model 1 – Model 3 and Model 2 – Model 4.

and Table 2). In a similar way, the strength of Model 2 and Model 4 can be compared in terms of the ISSF since they have the same singular stress field with the same singular index λ ($\lambda_1 = 0.663$, $\lambda_2 = 0.999$ as is shown in Fig. 2 and Table 3).

$K^*_{\sigma,\lambda 1}$ and $K^*_{\tau,\lambda 1}$ are the reference solutions, while the unknown solutions were designated $K_{\sigma,\lambda 1}$ and $K_{\tau,\lambda 1}$. The stress distribution obtained by means of the finite elements method (FEM) are designated $\sigma^*_{y0,FEM}$ and $\tau^*_{y0,FEM}$ for the reference solutions and $\sigma_{y0,FEM}$ and $\tau_{y0,FEM}$ for the unknown solutions. Therefore, from Eq (6) the ratios $K_{\sigma,\lambda 1}/K^*_{\sigma,\lambda 1}$ and $\sigma_{y0,FEM}/\sigma^*_{y0,FEM}$ can be indicated as is shown in Eq (8):

$$\frac{K_{\sigma,\lambda_1}}{K^*_{\sigma,\lambda_1}} = \frac{\sigma_{y0,FEM}}{\sigma^*_{y0,FEM}} \tag{8}$$

Eq (8) is valid if the reference value is known, and as long as the same mesh pattern has been applied in the FEM models in both reference and unknown solutions. Analogously, the same kind of equation can be used to calculate $K_{\tau,\lambda 1}$ (Eq (9)):

$$\frac{K_{\tau,\lambda_1}}{K^*_{\tau,\lambda_1}} = \frac{\tau_{xy0,FEM}}{\tau^*_{xy0,FEM}} \tag{9}$$

In this work, the ISSF values for Models 1 and 2 were selected as reference values. Since no study exists in the literature with this combination of materials, specimen configuration and boundary conditions, both reference values were calculated by means of the Reciprocal Work Contour Integral Method (RWCIM) [4,24], whose details are shown in Appendix A.

Stresses σ_θ and $\tau_{r\theta}$ in the r direction around interface corner O in Fig. 3 can be expressed as:

$$\sigma_\theta = \frac{K_1}{r^{1-\lambda_1}} f_{\theta\theta}(\theta, \lambda_1) + \frac{K_2}{r^{1-\lambda_2}} f_{\theta\theta}(\theta, \lambda_2)$$

$$\tau_{r\theta} = \frac{K_1}{r^{1-\lambda_1}} f_{r\theta}(\theta, \lambda_1) + \frac{K_2}{r^{1-\lambda_2}} f_{r\theta}(\theta, \lambda_2) \tag{10}$$

where r is the radial distance away from the corner singular point O. K_k (k = 1,2) has real values; $f_{\theta\theta}(\theta,\lambda_k)$ and $f_{r\theta}(\theta,\lambda_k)$ are non-dimensional functions of angle θ and λ_k. There are three boundaries in a bi-material open wedge such as the one shown in Fig. 3, two traction-free edges (at angles θ = -π/2 and θ = π) and one in the interface (θ = 0). If the focus is on the interface stress, four parameters control the intensity of singular stress fields (ISSFs):

$$K_1 f_{\theta\theta}(\theta, \lambda_1)|(\theta = 0) = K_{\sigma,\lambda_1}. \quad K_2 f_{\theta\theta}(\theta, \lambda_2)|(\theta = 0) = K_{\sigma,\lambda_2}$$

$$K_1 f_{r\theta}(\theta, \lambda_1)|(\theta = 0) = K_{\tau,\lambda_1} \quad K_2 f_{r\theta}(\theta, \lambda_2)|(\theta = 0) = K_{\tau,\lambda_2} \tag{11}$$

These parameters ($K_{\sigma,\lambda 1}$, $K_{\sigma,\lambda 1}$, $K_{\tau,\lambda 1}$, $K_{\tau,\lambda 2}$) are controlled from K_1 and K_2, so the singular stress field is also controlled by the two real parameters. The integral path for RWCIM is shown in Fig. 5. The plane strain condition was selected to carry out the linear elastic analyses in MSC Marc software. Depiction of the selected mesh pattern to perform these analyses is shown in Fig. 6. Eight-node elements were utilized around the interface corner edge, while for other regions away from the interface corner edge, four-node elements were selected. Minimum mesh size (e_{min}) was: 1.882E-6 mm ($1/3^{12}$ mm).

4. Calculation of the reference solution

Singular stress distribution on the interface near the edge corner for Model 1 by means of the RWCIM is shown in Fig. 7. From σ_y equation ($\sigma_y = \frac{1.32}{r^{0.3494}} - \frac{0.08631}{r^{0.00000806}}$), $K^*_{\sigma,\lambda 1} = 1.32$ [MPa·mm$^{1-\lambda 1}$] and $K^*_{\sigma,\lambda 2} = -0.086$ [MPa·mm$^{1-\lambda 2}$] are obtained. While from τ_{xy} equation ($\tau_{xy} = -\frac{0.5211}{r^{0.3494}} - \frac{0.0001407}{r^{0.00000806}}$), $K^*_{\tau,\lambda 1} = -0.521$ [MPa·mm$^{1-\lambda 1}$] and $K^*_{\tau,\lambda 2} = -0.0001407$ [MPa·mm$^{1-\lambda 2}$] are obtained. In the same way, $\lambda_1 = 0.651$ and $\lambda_2 = 0.999$. Finite elements stress distributions are $\sigma^*_{y0,FEM} = 238.835$ [MPa] and $\tau^*_{xy0,FEM} = -97.637$ [MPa]. Material properties for SikaPower®-1548 and AISI 4140 are summarized in Table 2.

Singular stress distribution on the interface near the edge corner for Model 2 using RWCIM is shown in Fig. 8. From σ_y equation ($\sigma_y = \frac{2.030}{r^{0.3366}} - \frac{0.3029}{r^{0.00009136}}$), $K^*_{\sigma,\lambda 1} = 2.030$ [MPa·mm$^{1-\lambda 1}$] and $K^*_{\sigma,\lambda 2} = -0.303$ [MPa·mm$^{1-\lambda 2}$] are obtained. While from τ_{xy} equation ($\tau_{xy} = -\frac{0.7534}{r^{0.3366}} - \frac{0.001572}{r^{0.00009136}}$), $K^*_{\tau,\lambda 1} = -0.753$ [MPa·mm$^{1-\lambda 1}$] and $K^*_{\tau,\lambda 2} = -0.001572$ [MPa·mm$^{1-\lambda 2}$] are obtained, with λ values being: $\lambda_1 = 0.663$ and $\lambda_2 = 0.999$. At the same time, the finite elements stress distributions are: $\sigma^*_{y0,FEM} = 291.581$ [MPa] and $\tau^*_{xy0,FEM} = -118.176$ [MPa]. Material properties of SikaPower®-1511 adhesive and AISI 4140 adherent are summarized in Table 3.

5. Calculation of the unknown solution

After calculating the reference value of ISSF for Models 1 and 2, Eq (8) and Eq (9) can be used. As explained above, the results for Model 1 are the reference solutions to calculate Model 3. In the same way, the results of Model 2 are the reference solutions to calculate Model 4. From Eq (8) and Eq (9) unknown values of Model 3 and Model 4 are calculated. $K^*_{\sigma,\lambda 1}$ and $K^*_{\tau,\lambda 1}$ are the reference solutions of ISSF, while the unknown solutions have been designated as $K_{\sigma,\lambda 1}$ and $K_{\tau,\lambda 1}$. The stress distribution obtained by means of finite element method (FEM) is designated as $\sigma^*_{y0,FEM}$ and $\tau^*_{xy0,FEM}$ for the reference solution, and $\sigma_{y0,FEM}$ and $\tau_{xy0,FEM}$ for the unknown solution.

The ISSF results for Model 3 are: $K_{\sigma,\lambda 1} = 0.850$ [MPa·mm$^{1-\lambda 1}$] and $K_{\tau,\lambda 1} = -0.335$ [MPa·mm$^{1-\lambda 1}$]. Stress distributions by FEM are: $\sigma_{y0,FEM} = 153.713$ [MPa] and $\tau_{xy0,FEM} = -62.842$ [MPa]. While ISSF results for Model 4 are: $K_{\sigma,\lambda 1} = 2.626$ [MPa·mm$^{1-\lambda 1}$] and $K_{\tau,\lambda 1} = -0.974$ [MPa·mm$^{1-\lambda 1}$]. Stress distributions by FEM are: $\sigma_{y0,FEM} = 377.115$ [MPa] and $\tau_{xy0,FEM} = -152.835$ [MPa].

Zhang et al. [17,18] have demonstrated the effectiveness of the mesh-independent technique to calculate ISSF. In this way, adhesive strength can be shown as a constant value of critical ISSF ($K_{\sigma c}$ = const.) [4,21,25]. Thus, the value of the ratios $\sigma_{y0,FEM}/\sigma^*_{y0,FEM}$ and $\tau_{xy0,FEM}/\tau^*_{xy0,FEM}$ are constant and independent of the mesh size. Table 4 shows FEM stress distributions and stress ratios obtained by different mesh sizes for Model 1 and Model 3. Table 5 shows FEM stress distributions and stress ratios obtained by different mesh sizes for Model 2 and Model 4. Ratios in both cases are constant, therefore the independence of the mesh is proven and the work is validated.

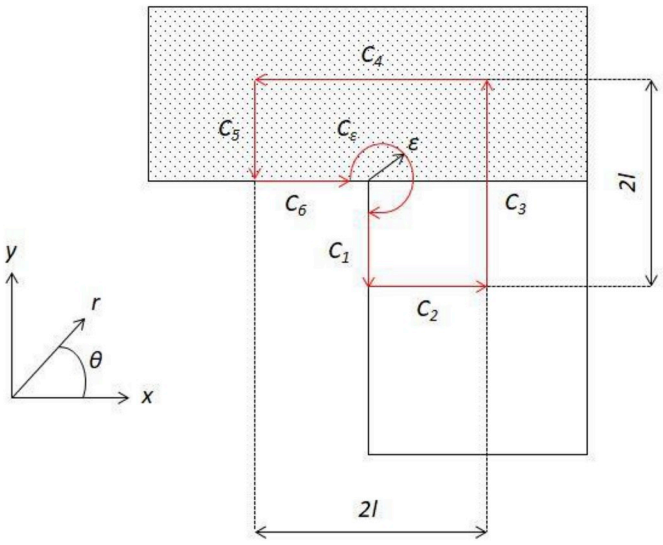

Fig. 5. Integral path C for RWCIM (C=$C_1 + C_2 + C_3 + C_4 + C_5 + C_6 + C_\varepsilon$).

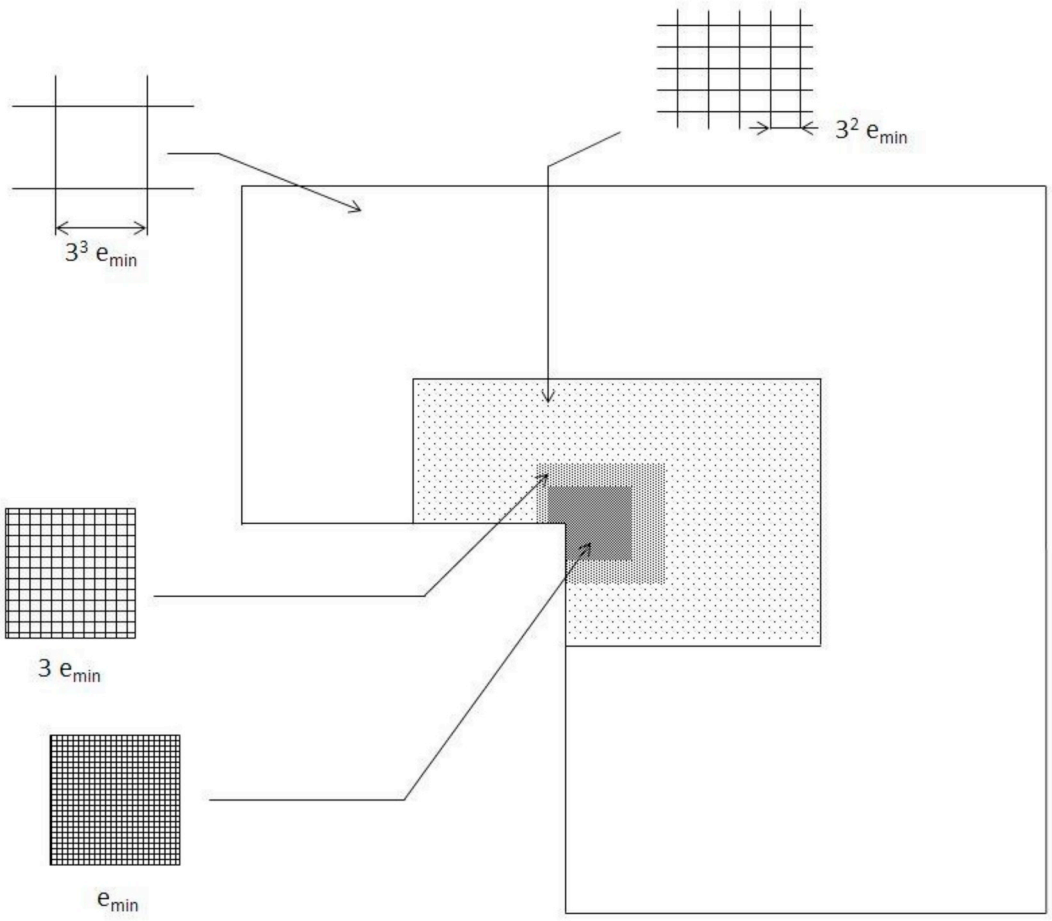

Fig. 6. Mesh pattern near the interface edge corner.

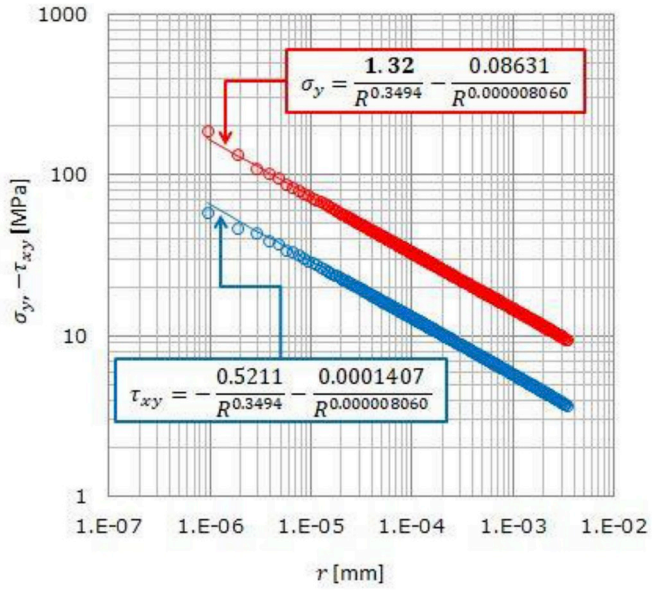

Fig. 7. Singular stress distribution on the interface near the edge corner for Model 1.

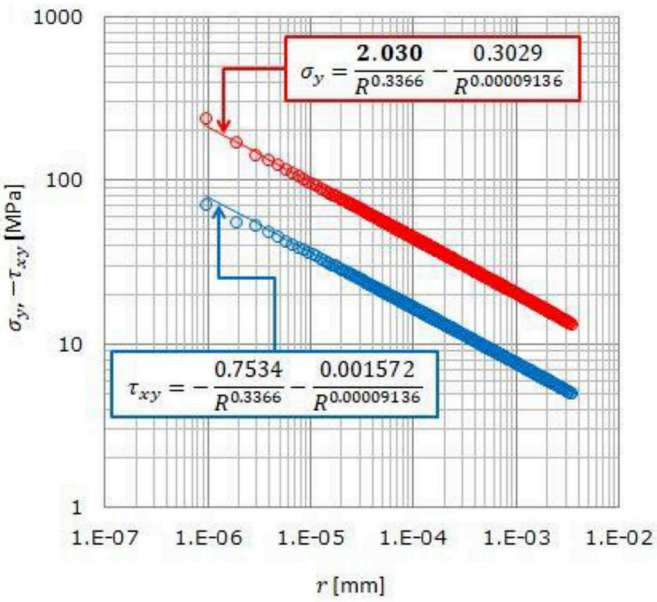

Fig. 8. Singular stress distribution on the interface near the edge corner for Model 2.

Table 4
FEM stress distributions obtained by different mesh sizes for Model 1 and Model 3.

$e_{min} = 1/3^{12}$ mm			$e_{min} = 1/3^{11}$ mm		
r	$\sigma_{y,FEM}$ (MPa)	$\sigma_{y,FEM}/\sigma^*_{y,FEM}$	r	$\sigma_{y,FEM}$ (MPa)	$\sigma_{y,FEM}/\sigma^*_{y,FEM}$
0	153.713	0.644	0	104.695	0.644
e_{min}	121.868	0.644	e_{min}	82.993	0.643
$2e_{min}$	85.741	0.643	$2e_{min}$	58.382	0.643
$3e_{min}$	70.185	0.643	$3e_{min}$	47.786	0.643
$4e_{min}$	66.776	0.643	$4e_{min}$	45.464	0.643
$5e_{min}$	61.477	0.643	$5e_{min}$	41.855	0.643

Table 5
FEM stress distributions obtained by different mesh sizes for Model 2 and Model 4.

$e_{min} = 1/3^{12}$ mm			$e_{min} = 1/3^{11}$ mm		
r	$\sigma_{y,FEM}$ (MPa)	$\sigma_{y,FEM}/\sigma^*_{y,FEM}$	r	$\sigma_{y,FEM}$ (MPa)	$\sigma_{y,FEM}/\sigma^*_{y,FEM}$
0	377.115	1.293	0	260.462	1.293
e_{min}	311.634	1.293	e_{min}	215.188	1.294
$2e_{min}$	224.026	1.294	$2e_{min}$	154.660	1.294
$3e_{min}$	185.257	1.294	$3e_{min}$	127.880	1.294
$4e_{min}$	175.21	1.294	$4e_{min}$	120.941	1.294
$5e_{min}$	162.349	1.294	$5e_{min}$	112.057	1.294

Table 6
ISSF values of Model 1 (reference solution) and Model 3.

	Model 1		Model 3
$K^*_{\sigma,\lambda 1}$ [MPa·mm$^{1-\lambda 1}$]	1.320	$K_{\sigma,\lambda 1}$ [MPa·mm$^{1-\lambda 1}$]	0.850
$\sigma^*_{y0,FEM}$ [MPa]	238.835	$\sigma_{y0,FEM}$ [MPa]	153.713
$K^*_{\tau,\lambda 1}$ [MPa·mm$^{1-\lambda 1}$]	−0.521	$K_{\tau,\lambda 1}$ [MPa·mm$^{1-\lambda 1}$]	−0.335
$\tau^*_{xy0,FEM}$ [MPa]	−97.637	$\tau_{xy0,FEM}$ [MPa]	−62.842

Table 7
ISSF values of Model 2 (reference solution) and Model 4.

	Model 2		Model 4
$K^*_{\sigma,\lambda 1}$ [MPa·mm$^{1-\lambda 1}$]	2.030	$K_{\sigma,\lambda 1}$ [MPa·mm$^{1-\lambda 1}$]	2.626
$\sigma^*_{y0,FEM}$ [MPa]	291.581	$\sigma_{y0,FEM}$ [MPa]	377.115
$K^*_{\tau,\lambda 1}$ [MPa·mm$^{1-\lambda 1}$]	−0.753	$K_{\tau,\lambda 1}$ [MPa·mm$^{1-\lambda 1}$]	−0.974
$\tau^*_{xy0,FEM}$ [MPa]	−118.176	$\tau_{xy0,FEM}$ [MPa]	−152.835

6. Comparison of the models

As observed in Table 6, Model 3 (Fig. 4) improves the behaviour of the adhesive joint in terms of ISSF. All critical values ($K_{\sigma,\lambda 1}$, $K_{\tau,\lambda 1}$, $\sigma_{y0,FEM}$, $\tau_{xy0,FEM}$) have been reduced by 35.64% compared to Model 1. Only one adhesive has been used in Model 1, the lower Young's modulus one. While in Model 3, two adhesives are used, lower Young's modulus adhesive in the corner and higher Young's modulus adhesive in the central area of the joint. The results show that the lower Young's modulus adhesive works better in the corner as long as the central area of the joint is more rigid.

Table 7 shows the results of Model 2 and Model 4. The opposite happens in the comparison of Model 1 and Model 3. All critical values ($K_{\sigma,\lambda 1}$, $K_{\tau,\lambda 1}$, $\sigma_{y0,FEM}$, $\tau_{xy0,FEM}$) have been increased by 29.33% in Model 4 compared with Model 2. If only one adhesive is used, and this adhesive has enough Young's modulus, the result is better than if the same adhesive is used in the corners, and one adhesive with lower Young's modulus is used in the central area.

7. Conclusions

- The effect of Young's Modulus in terms of the ISSF is studied from the results obtained in the different models. Two models can be compared if the material combination in the edge corner is the same. In this way, Model 1 is compared with Model 3, while Model 2 is compared with Model 4.
- Model 3 shows a decrease of 35.64% of ISSF value compared with Model 1. The lower Young's modulus adhesive works better in the corner as long as the central area is covered by a higher Young's modulus adhesive.
- Model 4 shows an increase of 29.33% of the ISSF value compared with the reference Model 2. The combination of the higher Young's modulus adhesive in the corner and the lower Young's modulus adhesive in the central area performs worse than applying a homogeneous layer of the higher Young's modulus adhesive only.
- The reciprocal work contour integral method (RWCIM) is a valid method to calculate the intensity of singular stress field (ISSF). However, it is a very complex method, and errors may occur during the calculation process. Reference values are calculated following RWCIM, with the reference models being Model 1 and Model 2.
- Calculating ISSF from the reference value and the stress ratio is just as accurate as using RWCIM (reciprocal work contour integral method). But it is necessary to know the reference value to be able to use it. In the same way, it is necessary to use the same mesh pattern, the same boundary conditions, and the same specimen configuration both in the reference and unknown solution. Model 3 and Model 4 are calculated by this method.

Conflicts of interest

The author(s) declare having no potential conflicts of interest with respect to the research, authorship, and/or publication of this article.

Acknowledgements

This research was supported by University Carlos III de Madrid under grants for researcher mobility, by the Alvaro Alonso Barba Technological Institute of Chemistry and Materials (IAAB), and by the Ministerio de Economía y Competitividad, Spain, under grants TRA2014-56471-C4-2-R.

Appendix A. Calculation of the reference solution by mean of Reciprocal Work Contour Integral Method (RWCIM)

The ISSF value of the unknown solution ($K_{\sigma,\lambda 1}$) can be easily calculated from the FEM stress ratio with Eq (8). However, in this case the reference solution is also unknown ($K^*_{\sigma,\lambda 1}$), since there is no other study in the literature with the same material combination, specimen configuration and boundary conditions. Therefore, it is necessary to use RWCIM to calculate the reference value. This method is based on Betti's reciprocal theorem. By mean of Williams´ eigenfunction expansion method, displacement and stress in the vicinity of the interface corner edge can be expressed as [25]:

$$\sigma_{ij} = \sum_{k=1}^{\infty} K_k f_{ij}(\theta, \lambda_k) r^{\lambda_k - 1} \tag{A.1}$$

$$u_i = \sum_{k=1}^{\infty} K_k g_i(\theta, \lambda_k) r^{\lambda_k} \tag{A.2}$$

where K_k is obtained by RWCIM, f_{ij} and g_i are the eigenfunctions which depend on λ_k and θ angle. Eq (A.3) is obtained from Betti's reciprocal theorem [25]:

$$\oint_C (\sigma_{ij} u_i^* - \sigma_{ij}^* u_i) \boldsymbol{n}_j ds = 0 \tag{A.3}$$

where the normal vector of the boundary C is $\mathbf{n}_j$. σ^*_{ij} and u^*_i are the complementary stress and displacement. They satisfy the same equilibrium and constitutive relations as σ_{ij} and u_i, respectively. Both stress (σ^*_{ij}) and displacement (u^*_i) are expressed as is shown in Eq (A.4) and Eq (A.5) respectively [25]:

$$\sigma_{ij}^* = \sum_{k=1}^{\infty} K_k^* f_{ij}(\theta, \lambda_k^*) r^{\lambda_k^* - 1} = \sum_{k=1}^{\infty} K_k^* f_{ij}(\theta, -\lambda_k) r^{-\lambda_k - 1} \tag{A.4}$$

$$u_i^* = \sum_{k=1}^{\infty} K_k^* g_i(\theta, \lambda_k^*) r^{\lambda_k^*} = \sum_{k=1}^{\infty} K_k^* g_i(\theta, -\lambda_k) r^{-\lambda_k} \tag{A.5}$$

Integral path C ($C_1 + C_2 + C_3 + C_4 + C_5 + C_6 + C_\varepsilon$) is shown in Fig. 5. C_1 and C_6 lines are located along the stress free surface, and therefore, the integrals along these lines are zero. This assumes a change in Eq (A.3), which can now be written as:

$$\int_{-\pi/2}^{\pi} (\sigma_{ij} u_i^* - \sigma_{ij}^* u_i) \varepsilon \boldsymbol{n}_j d\theta = \int_{C'} (\sigma_{ij} u_i^* - \sigma_{ij}^* u_i) \boldsymbol{n}_j ds \tag{A.6}$$

Not taking into account C_1 and C_6 makes $C' = C_2 + C_3 + C_4 + C_5$. σ_{ij} and u_i be located on the left side of the equation as shown in Eq (A.1) and Eq (A.2). While σ_{ij} and u_i located on the right side of the equation are the stress and displacement calculated by means of FEM ($\sigma_{ij,FEM}$ and $u_{i,FEM}$). σ^*_{ij} and u^*_i are given by Eq (A.4) and Eq (A.5). When $\varepsilon \to 0$, the integral on the left side of the equation becomes constant. The following equation is used as K^*_k [25]:

$$1/K_k^* = \int_{-\pi/2}^{\pi} \left[f_{ij}(\theta, \lambda_k) g_i^*(\theta, \lambda_k^*) - f_{ij}^*(\theta, \lambda_k^*) g_i(\theta, \lambda_k) \right] \boldsymbol{n}_j d\theta \tag{A.7}$$

ISSF K_k is obtained from the following equation:

$$K_k = \int_{C'} (\sigma_{ij,FEM} u_{ik}^* - \sigma_{ijk}^* u_{i,FEM}) \boldsymbol{n}_j ds \tag{A.8}$$

where $\sigma_{iik}^* = K_k^* f_{ii}(\theta, \lambda_k^*) r^{\lambda_k^* - 1}$ and $u_{ik}^* = K_k^* g_i(\theta, \lambda_k^*) r^{\lambda_k^*}$. RWCIM is a valid method to calculate the ISSF. However, it is also a very complex method and requires a large number of calculations (such as operations with matrix and numerical integration). Therefore, it is not a very practical method. The proposed method in section 5 to calculate the ISSF (from a reference solution of the ISSF) is just as accurate as the RWCIM, but is more convenient and practical. In this method it is only necessary to focus on the results obtained by FEM at the corner point without risking calculation errors.

References

[1] Banea MD, Da Silva LFM. Adhesively bonded joints in composite materials: an overview. Proc Inst Mech Eng L J Mater Des Appl 2009;223:1–18.
[2] Xará JTS, Campilho RDSG. Strength estimation of hybrid single-L bonded joints by the extended finite element method. Compos Struct 2018;183:397–406.
[3] Li R, Noda NA, Takaki R, Sano Y, Takase Y, Miyazaki T. Most suitable evaluation method for adhesive strength to minimize bend effect in lap joints in terms of the intensity of singular stress field. Int J Adhesion Adhes 2018;86:45–58.
[4] Noda NA, Li R, Miyazaki T, Takaki R, Sano Y. Convenient adhesive strength evaluation method in terms of the intensity of singular stress field. Int J Comput Methods 2018;15(1). 1850085 01-30.
[5] Mintzas A, Nowell D. Validation of an Hcr-based fracture initiation criterion for adhesively bonded joints. Eng Fract Mech 2012;80:13–27.
[6] Wang CH, Rose LRF. Compact solutions for the corner singularity in bonded lap joints. Int J Adhesion Adhes 2000;20:145–54.
[7] Goglio L, Rossetto M. Evaluation of the singular stresses in adhesive joints. J Adhes Sci Technol 2009;23:1441–57.
[8] Galvez P, Abenojar J, Martinez MA. Durability of steel-CFRP structural adhesive joints with polyurethane adhesives. Compos B Eng 2019;165:1–9.
[9] Martinez MA, Velasco F, Abenojar J, Pantoja M, Del Real JC. Analytical solution to calculate the stress distribution in pin-and-collar samples bonded with anaerobic adhesives (following ISO 10123 standard). Int J Adhesion Adhes 2008;28. 405-10.
[10] Li G, Lee-Sullivan P, Thring RW. Nonlinear finite element analysis of stress and strain distributions across the adhesive thickness in composite single-lap joints. Compos Struct 1999;46:395–403.
[11] Chiminelli A, Breto R, Izquierdo S, Bergamasco L, Duvivier E, Lizaranzu M. Analysis of mixed adhesive joints considering the compaction process. Int J Adhesion Adhes 2017;76:3–10.
[12] Breto R, Chiminelli A, Lizaranzu M, Rodríguez R. Study of the singular term in mixed adhesive joints. Int J Adhesion Adhes 2017;76:11–6.
[13] Fitton MD, Broughton JG. Variable modulus adhesives: an approach to optimized joint performance. Int J Adhesion Adhes 2005;25. 329-36.
[14] da Silva LFM, Lopes MJCQ. Joint strength optimization by the mixed-adhesive technique. Int J Adhesion Adhes 2009;29. 509-14.
[15] Carbas RJC, da Silva LFM, Critchlow GW. Adhesively bonded functionally graded joints by induction heating. Int J Adhesion Adhes 2014;48. 110-18.
[16] da Silva LFM, Rodrigues TNSS, Figueiredo MAV, de Moura MFSF, Chousal JAG. Effect of adhesive type and thickness on the lap shear strength. J Adhes 2006;82. 1091-115.
[17] Zhang Y, Noda NA, Takaishi K, Lan X. Effect of adhesive thickness on the intensity of singular stress at the adhesive dissimilar joint. J Solid Mech Mater Eng 2010;4(10). 1467-79.
[18] Zhang Y, Noda NA, Wu PZ, Duan ML. A mesh-independent technique to evaluate stress singularities in adhesive joints. Int J Adhesion Adhes 2015;57. 105-17.
[19] Dundurs J. Discussion: ´´edge-bonded dissimilar orthogonal elastic wedges under normal and shear loading´´. Trans ASME J Appl Mech 1969;36. 650-2.
[20] Noda NA, Miyazaki T, Li R, Uchikoba T, Sano Y. Debonding strength evaluation in terms of the intensity of singular stress at the interface corner with and without fictitious crack. Int J Adhesion Adhes 2015;61:46–64.
[21] Bogy DB. Two edge-bonded elastic wedges of different materials and wedge angles under surface tractions. Trans ASME J Appl Mech 1971;38. 377-86.
[22] Noda NA, Ren F, Takaki R, Wang Z, Oda K, Miyazaki T, Sano Y. Intensity of singular stress field over the entire bond line thickness range useful for evaluating the adhesive strength for plate and cylinder butt joints. Int J Adhesion Adhes 2018;85. 234-50.
[23] Noda NA, Takase Y. Generalized stress intensity factors of V-shaped notch in a round bar under torsion, tension, and bending. Eng Fract Mech 2003;70. 1447-66.
[24] Carpenter WC. Insensitivity of the reciprocal work contour integral method to higher order eigenvectors. Int J Fract 1995;73:93–108.
[25] Mintzas A, Nowell D. Validation of an Hcr – based fracture initiation criterion for adhesively bonded joints. Eng Fract Mech 2012;80:13–27.

CONTENIDO PUBLICADO FUERA DEL JOURNAL CITATION REPORTS (JCR)

PUBLICACIÓN 5

Fracture toughness in Mode I (G_{IC}) for ductile adhesives

2017 J. Phys.: Conf. Ser. 843 012008

(http://iopscience.iop.org/1742-6596/843/1/012008)

IOP Conf. Series: Journal of Physics: Conf. Series **843** (2017) 012008 doi:10.1088/1742-6596/843/1/012008

Fracture toughness in Mode I (G_{IC}) for ductile adhesives

P Gálvez[1], RJC Carbas[2], RDSG Campilho[3], J Abenojar[1], MA Martínez[1] and LFM da Silva[2]

[1] Department of Material Science and Engineering, Universidad Carlos III de Madrid, Avenida de la Universidad 30, 28911, Leganés, Spain.

[2] Departamento de Engenharia Mecânica, Faculdade de Engenharia da Universidade do Porto, Portugal.

[3] Departamento de Engenharia Mecânica, Instituto Superior de Engenharia do Porto, Instituto Politécnico do Porto, Portugal.

pgalvez@ing.uc3m.es

Abstract. Works carried out in this publication belong to a project that seeks the replacement of welded joints by adhesive joints at stress concentration nodes in bus structures. Fracture toughness in Mode I (G_{IC}) has been measured for two different ductile adhesives, SikaTack Drive and SikaForce 7720. SikaTack Drive is a single-component polyurethane adhesive with high viscoelasticity (more than 100%), whose main use is the car-glass joining and SikaForce 7720 is double-component structural polyurethane adhesive. Experimental works have been carried out from the test called Double Cantilever Beam (DCB), using two steel beams as adherents and an adhesive thickness according to the problem posed in the Project, of 2 and 3 mm for SikaForce 7720 and SikaTack Drive, respectively. Three different methods have been used for measuring the fracture toughness in mode I (G_{IC}) from the values obtained in the experimental DCB procedure for each adhesive: Corrected Beam Theory (CBT), Compliance Calibration Method (CCM) and Compliance Based Beam Method (CBBM). Four DCB specimens have been tested for each adhesive. Dispersion of each G_{IC} calculation method for each adhesive has been studied. Likewise variations between the three different methods have been also studied for each adhesive.

1. Introduction

In recent years, the use of adhesives for structural applications [1] is growing due to the benefits and solutions that this technology is capable of providing to different industries. Among the potential beneficiaries of adhesive technology are Aerospace and Automotive Industries.

Using adhesives enable improving the performance obtained with traditional joints, allowing the joint of dissimilar materials, reducing the structure weight and manufacturing costs, improving the resistance to dynamic and static loads, reaching quasi homogeneous stress distribution and better damage tolerance [2].

Actually, traditional joining techniques (welding, rivets, screws…) continue being used mostly, but problems related to these joints make necessary to develop other joining technologies. It is necessary to know all the characteristics of any material designed for be used in structural applications, so that it is possible to predict its behavior for the raised solicitations. Finite element software are increasingly

widespread in adhesive joints, being able to simulate the behavior of the joint. To obtain a correct operation of the program it is necessary to know precisely all the properties of the involved materials in the adhesive joint. Thus, mechanical characterization of adhesive is mandatory prior to its use.

Fracture resistance values of structural adhesives can be calculated with different tests, widely studied in the literature [3,4,5]. In this work, Double Cantilever Beam (DCB) test have been carried out in order to obtain the Fracture Toughness in mode I (G_{IC}) value of two ductile polyurethane adhesives, SikaTack Drive and Sika Force 7720.

Most common methodologies for analysis of G_{IC} are based on linear elastic fracture mechanics (LEFM), including Compliance Calibration Method (CCM) and Corrected Beam Theory (CBT), but recently developed method such Compliance-Based Beam Method (CBBM) is based on the crack equivalent concept, depending only on the specimen`s compliance during the test [6]. DCB test allows obtaining the resistance to crack initiation and propagation, being able to calculate the R-curve (Resistance Curve), plotting G_{IC} versus crack length [7].

1.1. DCB Data Analysis

To avoid the accumulation of data, in this work only the formulas are exposed, being able to find more complete information in [6] and [8]:

-Compliance Calibration Method (CCM):

$$G_{IC} = \frac{P^2}{2b}\frac{dC}{da}$$

P is the load and b the specimen width. The compliance (C) is calculated by $C = \frac{\delta}{P}$ being δ the specimen displacement. $C = f(a)$ curves are adjusted by cubic polynomials ($C = C_3a^3 + C_2a^2 + C_1a + C_0$).

-Corrected Beam Theory (CBT):

$$G_{IC} = \frac{3P\delta}{2b(a + |\Delta|)}$$

Corrected Beam Theory (CBT) is based on elementary beam theory including the effects of crack tip rotation and deflection, being Δ crack length correction for crack tip rotation and deflection. For calculating Δ, a linear regression analysis of $(C)^{1/3}$ versus a data is carried out.

-Compliance-Based Beam Method (CBBM) [8,9]:

$$G_{IC} = \frac{6P^2}{b^2h}\left(\frac{2a_{eq}^2}{h^2E_f} + \frac{1}{5G}\right)$$

This method, based on the crack equivalent concept, depends only on the compliance of the specimen during the test. a_{eq} is the equivalent crack length, estimated from the experimental compliance. $a_{eq} = a + |\Delta| + \Delta a_{FPZ}$, being a real crack length, Δ the root rotation correction for the initial crack length and Δa_{FPZ} the correction because the fracture process zone (FPZ) is considered. h is the specimen height; E_f is a corrected flexural modulus, which takes into account some phenomena that may affect the $P - \delta$ curves, such as the stiffness variability between different specimens; and G is the substrate´s shear modulus.

2. Experimental Procedure

2.1. *Double Cantilever Beam Test (DCB)*

Different materials can be used as substrate for developing DCB Test, normally metals such as Steel and Aluminum, but it is possible find other works carried out with substrates made of unidirectional fiber-composite materials [10]. Two steel substrates have been used in this work for manufacturing each specimen. So that each pair of substrates are bonded together with the adhesive. A cohesive failure is essential to calculate correctly the fracture toughness of the studied adhesives.

Tests are carried out at room conditions on a universal testing machine through an opening process by pin loading at the beam-ends, with 1mm/min of test velocity. Tensile testing machine reproduces for each test the curves of applied load versus displacement (P-δ curves). The crack propagation is measured over the length of the adhesive with a calibrated ruler using a digital photography system, taking photos every five seconds until the process is finalized (Figure 1).

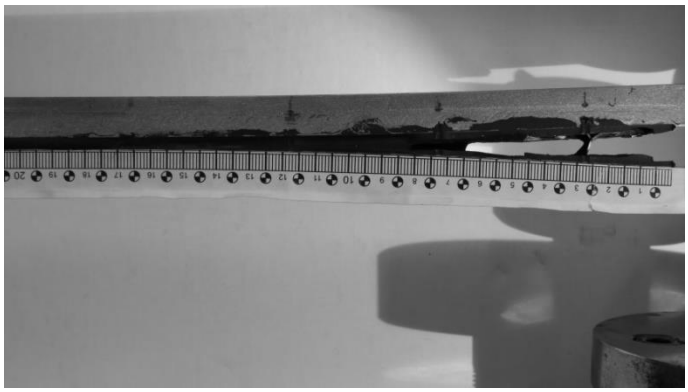

Figure 1. Crack propagation measured over the adhesive length.

2.2. *Test Geometry*

The test specimen sketch is shown in Figure 2, being F_c the applied force, whose values are obtained from the collected data during the test developed by the tensile testing machine. d= substrate thickness, being a constant value of 12.5mm. a=crack length, result of the sum of initial crack length and measured length values. w_{med}=substrate width, being a constant value of 25mm. The thickness of the adhesive layer is different on both adhesives, being 3 mm for Sikatack Drive and 2 mm for SikaForce 7720.

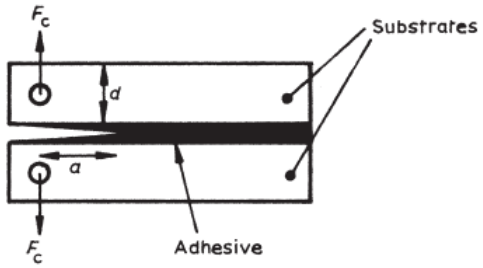

Figure 2. Measurements of DCB Specimen used [3].

2.3. Materials

Two different polyurethane structural adhesives supplied by Sika ® are used for the development of this work. One single-component adhesive with high viscoelasticity (more than 100%) whose trade name is SikaTack Drive. And other double-component ductile adhesive, called SikaForce 7720.

3. Results

From the DCB tests, $P-\delta$ curves were obtained for both adhesives. Representative curves of the studied adhesives are shown in Figure 3. As shown in the figure, the double-component adhesive (SikaForce 7720) presents less elongation at break due to its lower elastoplasticity. In the case of SikaTack, a greater elongation for higher values of rupture is obtained. In terms of elastic-plastic bahavior, it is important to remark that the most ductile adhesive, SikaTack Drive, is able to continue deforming for a longer time before reaching the minimum breaking value.

Figures 4 and 5 show representative curves of Resistance (R-Curve) of both adhesives. G_{IC} values are obtained from these graphs. The horizontal part of the curves represents G_{IC} values, so that, after a first peak of maximum G_{IC} value, this value stabilizes. This stabilization zone shows a set of similar values, where the sought value is obtained. G_{IC} values for both adhesives are shown in Table 1.

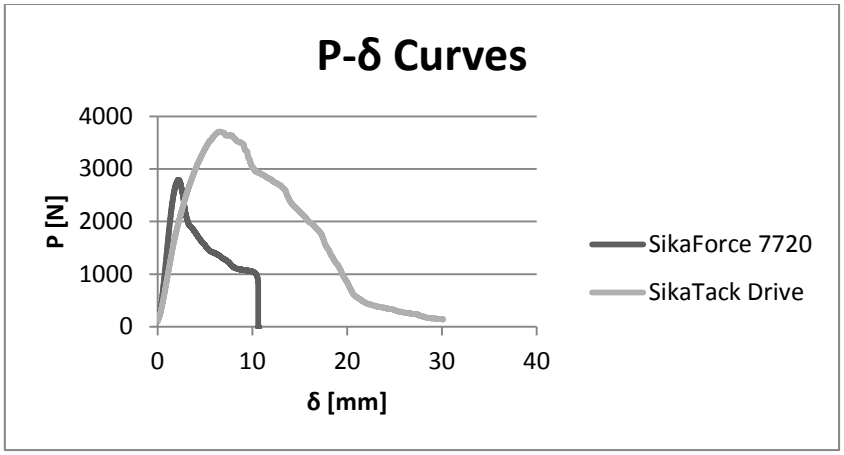

Figure 3. P-δ curves for SikaForce 7720 and SikaTack Drive. As the graph shows, SikaTack Drive is more ductile than SikaForce 7720, being also greater the maximum breaking value.

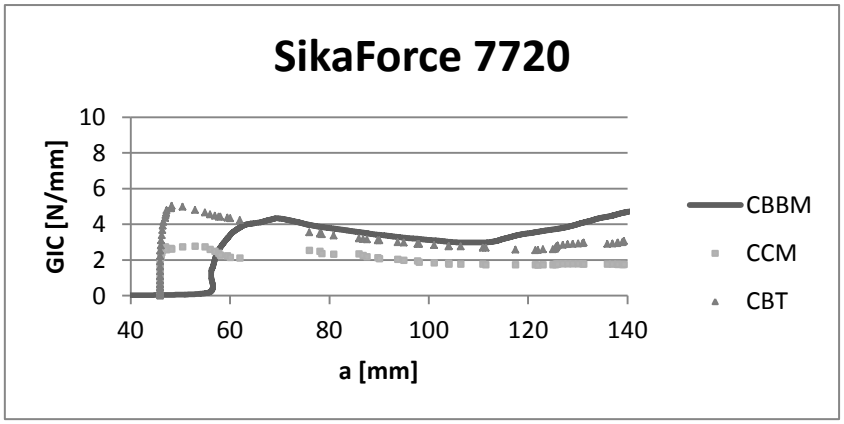

Figure 4. Representative Resistance Curve (R-Curve) for SikaForce 7720.

As Figure 4 shown (SikaForce 7720), CBBM and CBT curves are similar, being the curve for CCM similar but with lower G_{IC} values. Figure 5 (SikaTack Drive) shows similar curves for CBBM and CCM models, being different the CBT curve. CBBM model depends only on the compliance of the specimen during the test, with G_{IC} not being affected by errors due to the crack propagation measuring over the length of the adhesive with a calibrated ruler.

The CBT model includes a crack length correction for crack tip rotation and deflection (Δ). So better behavior is obtained in CBT model for Sikaforce 7720 than for SikaTack Drive. In the case of CCM model, the opposite happens. Better elastic-plastic behavior of SikaTack Drive allows better adjustment of $C = f(a)$ curves by cubic polynomials ($C = C_3a^3 + C_2a^2 + C_1a + C_0$).

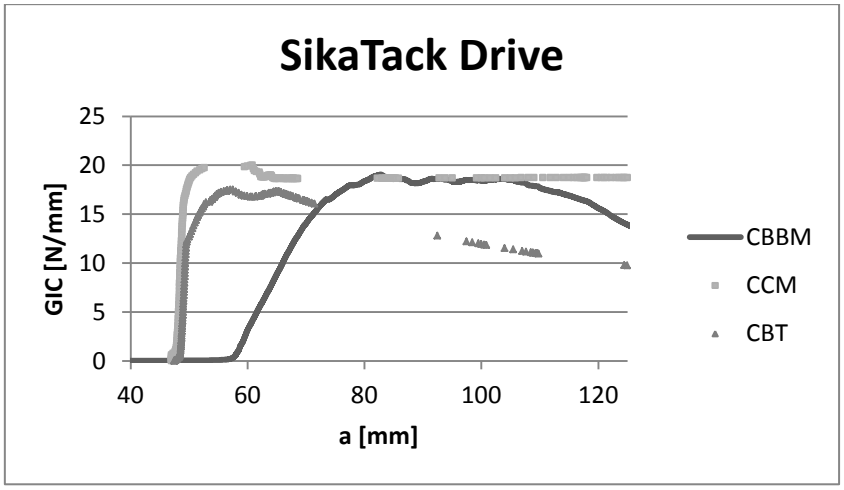

Figure 5. Representative Resistance Curve (R-Curve) for SikaTack Drive.

Table 1. G_{IC} values (in N/mm) for both studied adhesives with the three employed models.

	SikaTack Drive	SikaForce 7720
CBBM (N/mm)	20.63±1.56	3.83±0.72
CCM (N/mm)	18.35±1.40	2.18±0.28
CBT (N/mm)	17.45±2.77	3.24±0.86

4. Conclusions

Recent works have demonstrated the validity of using CBBM model in adhesives, being probably the most reliable method to obtain G_{IC}. This is due to the difficulty of measuring experimentally crack growth with an optical system, which is aggravated by high elastic-plastic behavior of both studied adhesives. The CBBM is only based on the crack equivalent concept, depending only on the compliance of the specimen during the test.

The CBT model shows better results for SikaForce 7720 and CCM model shows better results for SikaTack Drive. This is due to the different properties of each adhesive, together with the different adjustment of each model.

5. References

[1] Higgins A 2000 Adhesive bonding of aircraft structures *International Journal of Adhesion and Adhesives* **20** 367-76
[2] Banea M D and da Silva L F M 2009 Adhesively bonded joints in composite materials: an overview *Proceedings of the Institution of Mechanical Engineers, Part L: Journal of materials design and applications* **223**
[3] Kinloch A J 1987 Fracture mechanics of adhesive joints *Adhesion and Adhesives* chapter 7 pp 264-338
[4] Blackman B R K 2011 Fracture Tests *Handbook of Adhesion Technology* pp 474-501
[5] Lee R J, Butler J R, Yates T and Davidson R 1997 Test methods for adhesive fracture properties *MTS adhesives project 2 failure modes and criteria* Report No. 5 Annex 1
[6] Banea M D, da Silva L F M and Campilho R D S G 2012 Effect of temperature on tensile strength and mode I fracture toughness of a high temperature epoxy adhesive *Journal of adhesion science and technology* **26** 939-53
[7] Lamut M, Turk R and Torkar M 2008 Determination of the adhesive fracture energy G_C of structural adhesives using DCB and peel tests *RMZ-Materials and Geoenvironment* **55** 476-89
[8] de Moura M F S F, Campilho R D S G and Gonçalves J P M 2008 Crack equivalent concept applied to the fracture characterization of bonded joints under pure mode I loading *Composites science and technology* **68** 2224-30
[9] de Moura M F S F, Gonçalves J P M, Chousal J A G and Campilho R D S G 2008 *International Journal of adhesion and Adhesives* **28** 419-26
[10] Blackman B, Dear J P, Kinloch A J and Osiyemi S 1991 The calculation of adhesive fracture energies from double-cantilever beam test specimens *Journal of materials science letters* **10** 253-56

Acknowledgments
Spanish Ministry of Education and Science through the Project TRA2014-56471-C4-2-R, Institute of Materials Alvaro Alonso Barba (IAAB) and Sika®.

CONTENIDO PENDIENTE DE PUBLICACIÓN EN EL JOURNAL CITATION REPORTS (JCR)

PUBLICACIÓN 4

Manuscript Details

Manuscript number	COST_2019_2060
Title	Effect of moisture and temperature on thermal and mechanical properties of structural polyurethane adhesive joints
Article type	Full Length Article

Abstract

The aim of this study was to evaluate the effect of humidity and temperature in the mechanical and thermal properties of two polyurethane adhesives joints. Single and double component adhesives were selected, in order to compare their different properties to join dissimilar materials (steel and carbon fiber composite). By means of two devices specially developed for the study, durability and heat-aging tests were performed. The ability of the adhesives to cope with temperature (72°C) and humidity (82%), and facing temperature variations (from 26°C to 72°C) was studied. Shear tests and Shore D hardness measurements were carried out after the specimens were subjected to different exposure times and adverse environments. Joint reliability was studied by means of a simplified Weibull model. Besides, differential scanning calorimetry and infrared spectroscopy were made to understand the changes produced in the adhesives. Different behaviors were found for each adhesive, but they showed good characteristics to be used in structural applications under adverse environments.

Keywords	Polymer-matrix composites (PMCs); Environmental degradation; Mechanical properties; Thermal properties; FRP-steel bonded joints.

Corresponding Author	Pedro Galvez
Corresponding Author's Institution	Universidad Carlos III de Madrid
Order of Authors	Pedro Galvez, Sara Lopez de Armentia, Juana Abenojar, Miguel Martinez

Suggested reviewers	Eduardo Marques, Juan del Real, Nao-Aki Noda

Submission Files Included in this PDF

File Name [File Type]

Cover Letter.docx [Cover Letter]

Galvez_Manuscript_Compos Struct.docx [Manuscript File]

To view all the submission files, including those not included in the PDF, click on the manuscript title on your EVISE Homepage, then click 'Download zip file'.

7th June 2019

Dear Editor:

Enclosed is a paper, entitled “Effect of moisture and temperature on thermal and mechanical properties of structural polyurethane adhesive joints", please accept it as a candidate for publication in Composite Structures.

Authors:

1. Pedro Galvez Villarino

   Materials Science and Engineering and Chemical Engineering Department, University Carlos III de Madrid. Avda. de la Universidad, 30. 28911, Leganes, Madrid, Spain.

   E-mail: pgalvez@ing.uc3m.es

2. Sara Lopez de Armentia Hernandez

   Materials Science and Engineering and Chemical Engineering Department, University Carlos III de Madrid. Avda. de la Universidad, 30. 28911, Leganes, Madrid, Spain.

   E-mail: slopezar@pa.uc3m.es

3. Juana Abenojar Buendia

   Materials Science and Engineering and Chemical Engineering Department, University Carlos III de Madrid. Avda. de la Universidad, 30. 28911, Leganes, Madrid, Spain.

   E-mail: abenojar@ing.uc3m.es

4. Miguel Angel Martinez Casanova

   Materials Science and Engineering and Chemical Engineering Department, University Carlos III de Madrid. Avda. de la Universidad, 30. 28911, Leganes, Madrid, Spain.

   E-mail: mamc@ing.uc3m.es

This work is focused on the study of the behavior of two polyurethane adhesives under aggressive conditions. The ability of both adhesives for their use in structural applications is evaluated from the changes detected in their mechanical and thermal properties.

We strongly believe the contribution of this study warrants its publication in Composite Structures.

The paper is our original unpublished work and it is not submitted to any other journal for reviewing.

Sincerely,

D. Pedro Galvez Villarino
Materials Science and Engineering and Chemical Engineering Department
Carlos III University
Avda. de la Universidad 30.
28911 Leganés. Madrid. SPAIN
Tlf: (+34) 91 624 88 62
e-mail: pgalvez@ing.uc3m.es

Effect of moisture and temperature on thermal and mechanical properties of structural polyurethane adhesive joints

Pedro Galvez[1,*], Sara Lopez de Armentia[2], Juana Abenojar[3] and Miguel Angel Martinez[4]

Materials Science and Engineering and Chemical Engineering Department, University Carlos III de Madrid, Leganes, Spain.

pgalvez@ing.uc3m.es[1], slopezar@pa.uc3m.es[2], abenojar@ing.uc3m.es[3], mamc@ing.uc3m.es[4]

Abstract

The aim of this study was to evaluate the effect of humidity and temperature in the mechanical and thermal properties of two polyurethane adhesives joints. Single and double component adhesives were selected, in order to compare their different properties to join dissimilar materials (steel and carbon fiber composite). By means of two devices specially developed for the study, durability and heat-aging tests were performed. The ability of the adhesives to cope with temperature (72°C) and humidity (82%), and facing temperature variations (from 26°C to 72°C) was studied. Shear tests and Shore D hardness measurements were carried out after the specimens were subjected to different exposure times and adverse environments. Joint reliability was studied by means of a simplified Weibull model. Besides, differential scanning calorimetry and infrared spectroscopy were made to understand the changes produced in the adhesives. Different behaviors were found for each adhesive, but they showed good characteristics to be used in structural applications under adverse environments.

Keywords: Polymer-matrix composites (PMCs), Environmental degradation, Mechanical properties, Thermal properties, FRP-steel bonded joints

1. Introduction

Technological progress is only possible with the development of new processes and materials. Many studies are based on obtaining composite materials with different properties to be used in diverse industries. For example, graphene-based composites are a clear example of newly developed composite materials [1], being possible to find this type of materials in applications such as electronic transistor [2] or batteries [3]. In terms of sustainability, eco-friendly composite materials are being incorporated into industrial processes largely. In this way, Delogu et al. [4] considered the use of innovative composites in electric vehicles, and Enciso et al. [5] carried out studies with natural fibers in polymeric matrix, with good resistance and durability. Besides, this trend is found in the latest models of big companies such as Airbus or Boeing, which use more than 50% of composite materials in their structure. Kalanchiam et al. [6] and Mangalgiri [7] explain the advantages of composite materials in aircraft structures highlighting the aircraft performance improvement thanks to the structure weight reduction. The use of these composite materials in industrial processes is leading to the development of new hybrid structures [8], which are very widespread in recent years. Thus, it is possible to take advantage of the properties that both materials can bring to the joint [9,10]. This implies the existence of new technological challenges and the need to develop new adhesives capable of joining materials of different nature such as metals and composites.

There are several ways to join dissimilar materials [11], summarized in three main processes: mechanical, chemical and thermal. Adhesives can achieve this function since they allow the easy joint among two dissimilar materials, even at very low temperatures [12]. Compared with traditional bonds, adhesive bonding presents some advantages. Loads are distributed more homogeneously and they can be used for high strength applications thanks to

their high resistance to both static and dynamic loads [13]. Besides, they are low-density polymers, which allow the weight to be reduced. As a consequence of all these advantages, it will be possible to reduce energy consumption and repair costs. Previous works [14] combine the good properties of both composite materials and adhesives in the development of a new concept of node for bus structures.

The great advances in the field of polymers, and more specifically in adhesives, allow their use in applications as diverse as aircraft structures [15], aerospace [16,17] and automotive industry [18], marine [19], building [20], biomedical [21], and photovoltaic applications [22] among others.

Any material must be carefully tested before being implemented. Environmental factors, such as heat or humidity, adversely affect any element adhesively bonded [23,24], being able to cause catastrophic failures, even at values much lower than the limit of the material. Under thermal cycling, the deterioration is greater in adhesive joints due to the residual stresses between the adhesive and the adherents [25]. The different thermal expansion properties of the adhesive and the adherents, and the shrinkage of the adhesive due to the curing generate these stresses [26]. In the same way, other authors as Sousa et al. [27] observe considerable reduction of joint strength due to thermal cycles on adhesively bonded joints between pultruded GFRP adherends. Under conditions of temperature and moisture, combined with the residual stresses, the joint failure may occur due to the degradation of the adhesive-adherent interface [28]. Three major consequences into the adhesive have been usually observed due to the exposition [29]: curing, temperature degradation and adhesive drying. Sometimes, and for a short time of exposure, a post-curing phenomenon occurs, improving the adhesive capability [30], but finally

the properties begin to descend [31]. In other cases, and under sufficiently high temperatures, the degradation of the adhesive joint takes place even for short exposure times [32].

A suitable way to reach better behavior against environmentally adverse conditions is through the improvement of the adhesive joint performance by developing the appropriate surface treatments [33-35]. Achieve complete cleaning on the surfaces can become complicated in real fields, but it is necessary to develop at least the minimum surface treatment that allows obtaining the required adhesion strength [36]. The ideal performance of the adhesive joint is obtained by means of cohesive failure. Recent works study the effect of surface treatments on the durability of adhesive joints [37]. Atmospheric pressure plasma treatment has proven to be very effective in adhesive bonding with composite materials [38], increasing the surface energy of the polymer, promoting the adhesion. Nevertheless, many factors affect the strength of single lap joints, and other surface treatments could be necessary depending on the conditions of use and the substrate properties [39].

In this paper, the behavior of two polyurethane structural adhesives against two adverse environments is studied and compared. The degradation process of each adhesive joint in each environment is obtained, determining the suitability of these adhesives to be used in structural applications under this type of conditions. In particular, these adhesives will be applied in the structure of a bus. Therefore, an adverse environment is one in which the bus will not work normally but may be exposed in a circumstantial manner.

2. Experimental Procedure

2.1. Materials

Carbon fiber reinforced polymer (CFRP) and AISI 1012 carbon steel were selected as substrates. Carbon fiber fabric (GG 600T – MEL Composites – Barcelona, Spain), and epoxy resin (SR 8500 – Sicomin Epoxy Systems – Châteauneuf-les-Martigues, France) with the hardener (SD8601 – Sicomin Epoxy Systems – Châteauneuf-les-Martigues, France) were used. CFRP specimens were manufactured by hand lay-up process. While Carrocera Castrosua S.A. provided steel specimens. CFRP specimens had the following dimensions (in mm): width (W_{CFRP}) = 25, thickness (T_{CFRP}) = 4.2 and length (L_{CFRP}) = 100. While steel specimens dimensions were (in mm): width (W_S) = 25, thickness (T_S) = 1.6 and length (L_S) = 100.

Two adhesives supplied by Sika S.A.U. Spain were selected for carrying out the work: Sikaforce® 7720 and Sikatack® Drive. Sikaforce® 7720 is double-component thermoset structural polyurethane adhesive (PUR) [40]. It is able to be used with both polymers and metals, and as it is a double component adhesive, the curing is produced by chemical reaction of the two components. The chemical base of the component A are polyols, while for the component B are isocyanate derivatives. Both components are mixed with a mixing ratio of 100:25 in volume, resulting in a viscous liquid of approximately 1.50 g/cm^3 of density. Higher temperatures speed up the curing process, while low temperatures have the opposite effect, slowing the curing mechanism.

Sikatack® Drive is a single component thermoplastic polyurethane elastomer (TPU) [40] adhesive. This adhesive is mainly used in the automotive industry for joining the windshield to the body of the automobiles. It cures by reaction with atmospheric humidity. Temperature also affects since the absolute water content in the air depends on the air temperature, decreasing with the cold, slowing down the curing reaction. Being single-component polyurethane, polyols and isocyanates are already mixed. The density of the adhesive is 1.25 g/cm^3, thus for the same

volume of adhesive, the single-component adhesive has lower mass than the double component polyurethane adhesive. To assure full cure of the adhesives, specimens of both adhesives were cured for 480 hours at room temperature (50% relative humidity and 25°C).

2.2. Surface Treatments

To assure cohesive break in the studied adhesive joints different surface treatments were needed. In the joint bonded with Sikaforce® 7720, CFRP surface treatment consisted in solvent cleaning plus atmospheric pressure plasma treatment (APPT). The optimized parameters of the APPT were 6 mm of torch-specimen distance and 3 m/min of torch speed. While on the steel surface, the surface treatment consisted in sanding with P180 sandpaper, solvent cleaning and pickling with ortho-phosphoric acid (85%).

In the joint bonded with Sikatack® Drive, CFRP surface treatment consisted in: solvent cleaning followed by APPT with the same parameters used before, and finally Sika® Primer 215. While on the steel surface, the surface treatment consisted in sanding with P180 sandpaper, solvent cleaning and Sika® Primer 204N. Table 1 shows surface treatments and mechanical properties of Sikaforce® 7720 and Sikatack® Drive: maximum tensile strength (σ_{max}), Modulus of elasticity (E) and elongation at break (δ).

-INSERT TABLE 1-

2.3. Durability Tests

Durability tests were carried out in a climatic chamber. This device consists of a polypropylene sealed box equipped with a hermetic closing system with water inside it. Samples were placed without being in contact with the liquid. The objective of the test is not only to know

the behavior of the joint against the humidity but also discover how it works under high values of ambient temperature. Therefore, the climatic chamber was installed into a stove (Digitronic TFT – JP Selecta S.A.).

Environmental conditions were recorder throughout the experiment using a thermohigrometer (MSR 145 – MSR Electronics GmbH – Seuzach, Switzerland). Thus, it was possible to know the conditions to which the specimens were subjected into the chamber. The exact conditions were 82% of relative humidity and 72°C of temperature. To evaluate the degradation of the adhesive joint, tests were carried out on specimens exposed to five different times of degradation: 2 hours, 24 hours, 168 hours, 360 hours and 768 hours. For each exposure time, ten specimens were tested.

2.4. Heat-aging Cycles

Heat-aging cycles were carried out in an oven modified by the authors. The device consists on an electrical oven equipped with a refrigeration system. Each cycle is programmed to last 1800 seconds using a timer, and it is composed by a heating phase and a cooling phase. The maximum temperature during the heating phase is 72°C, and the minimum temperature after the cooling process is 26°C. The samples were tested at different cycles: 100, 250, 528, 1004 and 2936. Ten specimens were tested for each number of cycles and adhesive. 120 specimens were checked altogether.

In both durability and heat-aging cycles, 72°C were selected as maximum temperature. By selecting this temperature, according to the supplier, the two adhesives worked above their respective T_g for non-degraded specimens. In addition, Sikatack® Drive worked above the melting temperature of the crystalline domains of its hard segments.

2.5. Dimensional variation

Dimensional changes can occur in the adhesive during the curing process. These changes can affect the joint negatively, by the appearance of crevices in the adhesive bond. These crevices are areas with high risk of corrosion, since one of the substrates was steel subjected to conditions of high humidity (82% R.H.) and temperature (72°C). The corrosion can be due to both, the entry of water in the crevice and the creation of differential aeration cells. Adhesives are suitable for working in components with complex shapes, but this type of structure is the most commonly subjected to corrosion problems [41,42]. For this reason it is important to determine the dimensional variation that can occur during the curing process.

In order to determine the dimensional variation, the adhesives during their curing process were subjected to an analysis. They were dispensed and flush in a mold and a touch probe (RMP600, Renishaw, UK) was placed and calibrated on the uncured adhesive surface. The mold dimensions were (in mm): 12x12x36. To avoid the probe to stick with the adhesive, a polytetrafluoroethylene (PTFE) plate was positioned between the adhesive and the touch probe, as can be seen in Figure 1. After 720 hours of curing at room temperature, the displacement of the touch probe was measured.

-INSERT FIGURE 1-

2.6. Mechanical characterization

To evaluate the capacity of the selected adhesives, shear test was carried out. For the realization of these tests, universal testing machine (Microtest EM2/200/FR – Microtest S.A. – Madrid, Spain) was used according to UNE-EN 1465:2009 with test speed of 2 mm/min. Tests were carried out in specimens subjected to all the studied exposure times. The dimensions of the

specimens were (in mm): total specimen length (L_T) = 175, adhesive thickness (T_{AD}) = 2, and adhesive overlap (L_0) = 25. The excess of adhesive was removed after the curing process, and previously of the degradation process. Two alignment tabs were used during the tests to minimize the bending effect. Single lap joint configuration was selected for this work, as it is shown in Figure 2.

-INSERT FIGURE 2-

To evaluate the degradation processes of the adhesive joints, stress-strain curves of each adhesive and condition were studied and compared with non-subjected specimens. From these curves, maximum shear stress (τ_{max}), strain for maximum shear stress ($\delta\tau_{max}$) and stiffness values were acquired. Curves were obtained from the results of the universal testing machine. In this way, from the values of load (F), adhesive overlap (L_0) and adhesive width (W_{ADH}), shear stress (τ) is calculated:

$$\tau = \frac{F}{L_0 \cdot W_{ADH}}$$

Strain [%] is determined by:

$$Strain = \left(\frac{displacement}{L_0}\right) \cdot 100$$

Where displacement is the variation of position experienced by the clamp of the universal testing machine during the test, and L_0 is the adhesive overlap. Regarding stiffness, it is represented by the slope of the curve between 2 MPa (τ_1) and 4 MPa (τ_2) in the shear stress – unit strain curves. Strain is represented in the graphs as a percentage; however, the slope is calculated from the values of unit strain for τ_1 (U_{S1}) and τ_2 (U_{S2}) according to:

$$Stiffness: \frac{\tau_2 - \tau_1}{U_{S2} - U_{S1}}$$

Shore D hardness was measured (according to ASTM D2240) in both Sikaforce® 7720 and Sikatack® Drive during the degradation processes. Bulk adhesive specimens were manufactured for this purpose. They were subjected to the same conditions as the shear test specimens. Ten measurements were made for each environment and degradation time using a Shore hardness tester by Zwick-Roell (Ulm, Germany).

2.7. Reliability

Structural components should be studied exhaustively in order to ensure a correct operation during the whole life cycle. There are different statistical models to know the reliability of critical elements in engineering designs [43], highlighting: normal, lognormal, exponential and Weibull distributions.

Simplified Weibull model was selected for performing this work. Nowadays, the use of Weibull distribution is very widespread in the industry, especially in technologically leading sectors such as the aerospace [44] or automotive [45]. With the Weibull distribution it is not possible to know the causes of the failure. However, it is possible to calculate the risk of failure of a structural component as a function of variables like time or stress, as it was done in this work.

2.8 Chemical characterization

The adhesives were characterized after different degradation conditions by differential scanning calorimetry (DSC) and Fourier-transform infrared spectroscopy (FTIR).

DSC 822 differential scanning calorimeter by Mettler Toledo GmbH (Greifensee, Switzerland) was used. Since polyurethanes have glass transition temperatures at low temperatures, in this work scans from -80 to 250°C with 10°/min rate for the Sikatack® Drive and from -20 to 250°C with 20°/min rate for the Sikaforce® 7720 have been used. Samples around 9 mg were tested in aluminum crucibles of 40 µl under nitrogen atmosphere. Glass transition temperature (T_g) was obtained for each exposure time in both environments and they were compared with T_g of adhesives without aging.

A Bruker Tensor 27 (Bruker Optik GmbH, Madrid, Spain) spectrometer was used to obtain the IR spectra of the samples after and before durability tests. The attenuated total multiple reflection technique (ATR) was used to analyze the chemical modifications produced to about 5–10 µm of the sample depth. A diamond prism was used and the incident angle of the IR radiation was 45°. Forty scans with a resolution of 4 cm^{-1} between 600 and 4000 cm^{-1} were obtained and averaged. Mass specimens were used to perform the spectra.

Sikatack® Drive is single-component elastomeric polyurethane that cures mainly due to moisture effect. This type of adhesive usually has two distinct areas in their thermal properties: soft segment and hard segment. Soft segment is formed by partially amorphous zones, being representative T_g that oscillate between -60 and -20°C and in some cases could be possible to find a small melting peak corresponding to the crystalline part. Hard segment is formed by crystalline zones characteristic of thermoplastic polymers. It is normal to find in this segment a melting peak in the DSC. It is also possible to find eminently amorphous hard segments. Then both T_g and T_m can be found. Sometimes in TPU (thermoplastic polyurethane elastomer) only one T_g is obtained at low temperatures. This happens because there is no separation phase between soft and hard zones. Separation phase and crystalline formation can be inhibited by the

presence of chemical cross-links [46]. Greater amount of tiols produces T_g increment and less mobility in the chains. Double-component polyurethanes as Sikaforce® 7720 are thermoset polymers (PUR). This kind of polymer shows only one T_g. Meaning of T_g in polyurethanes is very different from the meaning of the T_g in epoxies. In polyurethanes as Sikaforce® 7720, at room temperature they are viscoelastic materials, and they become more rigid with the temperature increment. In polyurethanes as Sikatack® Drive the stiffness is determined by the condition (type and temperature range) of the hard segment.

3. Results

3.1 Dimensional variation

After 720 hours of curing, changes in the dimensions of both Sikatack® Drive and Sikaforce® 7720 are not found, since the dimensional variation in both adhesives is less than 1μm (0.01%). This means that these adhesives present high dimensional stability and when cured, they do not expand or contract. This is a key element in the prevention of crevice appearing.

3.2 Characterization of adhesives

3.2.1. Differential scanning calorimetry (DSC)

To understand the changes that happen on the adhesives, in this point DSC and FTIR of adhesives before aging are shown. Figure 3 shows the DSC of Sikaforce 7720 (PUR), it corresponds to the heating at 20 º/min. High rate is selected in order to see small changes, which are invisible at lower rate. This adhesive shows a T_g around 32 ºC (depending on the rate) and a small melting peak around 85 ºC. This peak can be due to small crystalline part, because thermoset is not totally amorphous, or due to additives.

Figure 4 shows the DSC of Sikatack® Drive (TPU) at 20 º/min. This adhesive has two segments (soft and hard). It is possible to see a T_g at low temperature (-40ºC) and a T_m at 60ºC. Both of them correspond to the soft segment. Besides, there is a small T_g at 105 ºC and a small and wide melting area (from 130 to 180 ºC) with a peak at 150 ºC, characteristic of the hard segment. This peak is due to the melting of the crystalline domains of the hard segment, and can overlap with the T_g relative to these segments [47]. The second heating shows that the melting peaks of both, PUR and the soft segment in TPU, are related to the small crystalline part, since they do not disappear.

-INSERT FIGURE 3-

-INSERT FIGURE 4-

3.2.2. Fourier-transform infrared spectroscopy (FTIR)

Figure 5 and Figure 6 show infrared spectra of Sikaforce® 7720 and Sikatack® Drive, respectively before being subjected to any type of degradation. Both spectra have been normalized from the peak relative to the methyl groups located between 2800 cm^{-1} and 3000 cm^{-1}.

-INSERT FIGURE 5-

Most representative peaks for Sikaforce® 7720 correspond to carbon-hydrogen bonds (out-of-plane δ aromatic ring) at 705 cm^{-1}, carbon-hydrogen bonds (aromatic cycles) at 860 cm^{-1}, carbon-hydrogen bonds (aromatic cycles) between 1074 cm^{-1} and 1080 cm^{-1}, carbon-carbon bonds (alkyl) at 1229 cm^{-1}, carbon-carbon double bonds (aromatic cycles) at 1440 cm^{-1}, carbon-oxygen double bonds (urethane) between 1720 cm^{-1} and 1730 cm^{-1}, carbon-nitrogen-oxygen

double bonds (C=N=O asymmetric stretch vibration) at 2340 cm^{-1}, and carbon-hydrogen bonds between 2800 cm^{-1} and 3000 cm^{-1}.

-INSERT FIGURE 6-

Most representative peaks for Sikatack® Drive correspond to carbon-hydrogen bonds (aromatic cycles) between 1074 cm^{-1} and 1080 cm^{-1}, carbon-carbon double bonds (aromatic cycles) at 1265 cm^{-1}, carbon-oxygen bonds at 1367 cm^{-1}, carbon-carbon double bonds (aromatic cycles) at 1440 cm^{-1}, carbon-oxygen double bonds (urethane) between 1720 cm^{-1} and 1730 cm^{-1}, and carbon-hydrogen bonds between 2800 cm^{-1} and 3000 cm^{-1}.

3.3. Durability Tests

Stress-strain curves allow knowing the mechanical properties of the materials or even of an adhesive joint as it is proposed in this work. Thus, it is possible to know the behavior of the joint and the degradation of the adhesive for each exposure time. Figure 7 shows representative stress-strain curves and Table 2 shows values of maximum stress (τ_{max}), maximum strain (δ_{max}), stiffness and hardness (SHD) of Sikaforce® 7720 and Sikatack® Drive during the degradation process under conditions of temperature and humidity.

-INSERT FIGURE 7-

-INSERT TABLE 2-

3.3.1. Sikaforce® 7720

As Figure 7 (up) and Table 2 show, there is hardly any variation between the unexposed specimens and the specimens exposed two hours to the adverse environment. After 24 hours, strain value remains constant, while the values of maximum stress and stiffness increase. This

trend is maintained up to 168 hours of exposure, when maximum value of stress is obtained (8.55±0.37 MPa), observing in the same way the decrease in the value of strain. After 360 hours of exposure, the maximum value of stiffness is obtained (105.38±3.69 MPa). The loss of properties in the adhesive is evident after the degradation process at 768 hours of exposure, when the lowest value of maximum stress is obtained (6.07±0.55 MPa). Cohesive failure (through the adhesive) is observed from 0 to 360 hours of exposure, while the failure becomes adhesive (through the interface adhesive-steel) after 768 hours of exposure.

The behavior of the adhesive up to 168 hours of exposure is typical of a post-curing process, showing an improvement in the properties until post-curing is completed. This effect is positive up to 360 hours of exposure, when the mechanical properties begin to decrease. Polyurethane cures with moisture, and temperature causes an increase in the cross-linking of the polymer chains [48]. These two phenomena are associated with an increase in the maximum stress and in the stiffness values of the adhesive joint. After 360 hours of exposure, the degradation of the joint is evident. Viana et al. [28] found that a fundamental factor in the degradation of the adhesive is the captured water as bound water, which create single or multiple hydrogen bonds with the polymer chain. The fundamental consequence of this process is the decrease of the maximum stress values, obtaining, in the same way, plasticization and swelling of the adhesive. However, since it is a polyurethane adhesive, temperature is the most important factor in the degradation process. Tcharkhtchi et al. [48] relate the degradation by effect of temperature in polyurethanes with an increment of the critical molecular weight, and with the formation of linear molecules in the network due to the chain scission, resulting in a lower cross-linking density.

In specimens subjected to 768 hours of exposure, adhesive failure is observed through the steel interface. This is due to the previous degradation suffered by the adhesive and to an adsorption process. Water can penetrate through the adhesive-substrate interface in an adsorption phenomenon, weakening the adhesion forces between the adhesive and the substrate.

Hardness values of Sikaforce® 7720 during the durability process are shown in Table 2. From 0 to 24 hours of exposure hardness values are almost constant at 60±1 (as it happens with τ). After 168 and 360 hours, hardness increases to their highest values reaching 64±1 and 63±1, respectively. Finally, after 768 hours the lowest hardness value is obtained (52±2).

Results show an obvious correlation between the trend followed by hardness and τ values. Polymer undergoes changes during the durability process, making it harder in the middle of the process, to later lose that hardness due to degradation.

3.3.2. Sikatack® Drive

In the case of this adhesive, post-curing process is not observed. Adhesive degradation is seen practically from the beginning of exposure to humidity and temperature, as it is observed in Figure 7 down and Table 2. After 168 hours of exposure, the degradation is evident, decreasing the maximum stress value from 4.17±0.15 MPa (in specimens without exposure) until 3.29±0.25 MPa. Among 168 and 768 hours of exposure, a significant change in the properties of the joint is not observed, obtaining 2.92±0.18 MPa of maximum stress in specimens with 768 hours of exposure.

Cohesive failure is observed until 24 hours of exposure, when mixed failure appears. The degradation process of the adhesive takes place from early stages of degradation, as it is observed in the values of the mechanical properties (Table 2). This adhesive shows different

behavior respecting the other adhesive against the combination of temperature and humidity. Mechanical properties improvement is not observed, on the contrary that happens in the same adhesive with heat-aging cycles (as is explained later). Therefore, it is possible to conclude that humidity is the main factor in the degradation process of the Sikatack® Drive.

Thus, during the first 24 hours an absorption phenomenon is taken place. Water is absorbed by the adhesive as bound water, creating new hydrogen bonds in the polymer chain. This phenomenon can provoke adhesive plasticization, decreasing in the same way the strength. As the failure is cohesive, it is clear that until this moment there is no adsorption phenomenon. This trend changes after 24 hours of exposure. Water also penetrates through an adsorption process in the steel surface, causing adhesive failure in some parts of the specimen. This is very clear in the specimens exposed during 768 hours, showing greater percentage of adhesive failure.

Hardness values of Sikatack® Drive during the durability process are shown in Table 2. From 0 to 24 hours of exposure hardness values keep almost constant, standing around 18 SHD. After 168 hours of exposure hardness decrease to around 15 SHD, being constant until the end of the degradation process. Trend of hardness values is consistent with the changes experienced by τ throughout the degradation process. At the beginning, the polymer is not degraded and hardness values do not vary. However, after 168 hours of exposure there is an evident decrease in the value of both τ and hardness, and therefore the polymer begins to degrade.

3.3.3. Optical Study

In order to evaluate the type of failure obtained during the tests, photographs of each specimen are taken after being tested. The most representative image has been selected for each case.

Figure 8a and 8b show representative specimens for durability test of Sikaforce® 7720. Cohesive failure is observed in specimens without exposure in the same way that happens in specimens subjected to 2, 24, 168 and 360 hours of exposure (Figure 8a). Nevertheless, specimens subjected to 768 hours of exposure show adhesive failure through the interface between the steel and the adhesive (Figure 8b).

Figure 8c and 8d show representative specimens for durability test of Sikatack® Drive. Cohesive failure is observed until 360 hours of exposure (Figure 8c), when the failure becomes mixed. From this moment, it is possible to observe large areas of the steel substrate with adhesive failure (Figure 8d). This trend is very clear in specimens subjected to 768 hours of exposure.

-INSERT FIGURE 8-

3.4. Heat-aging Cycles

-INSERT FIGURE 9-

-INSERT TABLE 3-

3.4.1. Sikaforce® 7720

The behavior of the adhesive (Figure 9 up) is similar than the behavior found in durability tests (Figure 7 up). Table 3 shows values of maximum stress (τ_{max}), maximum strain (δ_{max}), stiffness and hardness (SHD) of Sikaforce® 7720 and Sikatack® Drive during the heat-aging cycles.

Among 0 and 100 cycles no obvious changes appear in the mechanical properties of the adhesive, being constant the values of stress, maximum strain and stiffness, as it is shown in

Table 3. From 250 cycles, an increase in the values of stress (6.83±0.03 MPa) and stiffness (76.52±1.71) is observed. This trend continues until 1004 cycles, reaching stress of 7.31±0.21 MPa and stiffness of 87.38±13.04 MPa. This behavior is again characteristic of a post-curing process, which causes an increase in the cross-linking density of the polymer, varying the mechanical properties of the material [48]. After 1968 cycles, degradation of the adhesive is observed with a decrease in the value of the τ_{max} (6.49±1.00 MPa). This circumstance is basically due to the increment of critical molecular weight, and to the reduction of cross-linking density correlated to the chain scission in the network. Linear molecules formed in the network may undergo plasticization, decreasing both Young's modulus and tensile strength values [48]. Post-curing and degradation processes are evident in Figure 9 up, where stress-strain curves are shown. However, this degradation is not catastrophic and the adhesive maintains its properties.

Hardness values of Sikaforce® 7720 during heat-aging cycles are shown in Table 3. From 0 to 100 cycles hardness values are almost constant at around 59±1. After 250 and 528 cycles, hardness increases to their highest values reaching 65±1 and 70±1 respectively. From this moment hardness value drops until 61±2 for 1968 cycles.

Correlation between the trend followed by hardness and τ values is shown again. Polymer undergoes changes during the thermal fatigue, becoming harder until reaching 528 cycles to later lose that hardness due to degradation.

3.4.2. Sikatack® Drive

Figure 9 down shows Sikatack® Drive stress-strain curves during the heat-aging cycles. The behavior of the adhesive is different in comparison with the durability tests (Figure 7 down). The adhesive is not degraded from the first exposure times, and a post-curing process is observed.

Among 0 and 250 cycles, changes in the mechanical properties of the adhesive are observed. An increase in the values of maximum stress (from 4.17±0.15 MPa to 5.14±0.35 MPa) and stiffness (from 15.92±2.48 to 21.84±2.94 MPa) is found, as it is shown in Table 3. From 528 cycles, a decrease in τ_{max} (4.28±0.53 MPa) and stiffness (16.09±0.87 MPa) is observed regarding to the maximum values of the process. This trend continues until 1968 cycles, when the degradation of the adhesive is evident (3.58±0.26 MPa for τ and 16.03±0.22 MPa for stiffness). In this case, two phenomena are taking place: post-curing up to 250 cycles, and degradation of the adhesive from 528 to 1968 cycles. These phenomena are due to the effect of temperature, in the same way that is explained in the previous section for Sikaforce® 7720. Akderya et al. [49] study the effect of thermal fatigue in epoxy adhesive single lap joints, finding similar behavior in terms of maximum load carrying capacity. In this particular case epoxy and polyurethane adhesives can be compared.

Hardness values of Sikatack® Drive during heat-aging cycles are shown in Table 3. These values hardly change during the process, being practically constant until reaching 1004 cycles. After 1968 cycles, a small change of this trend is observed, reaching hardness lowest value (17±1 SHD). Analogy between τ and hardness trend is observed again, since in both cases the minimum value is obtained at 1968 cycles, which is the point of greatest degradation of the adhesive joint.

3.4.3. Optical Study

Figure 10a and 10b show representative specimen for heat-aging cycles of Sikaforce® 7720. Cohesive failure is observed both in the specimens without degradation and in the specimens subjected to heat-aging cycles.

Figure 10c and 10d shows representative specimens for heat-aging cycles of Sikatack® Drive. Cohesive failure is observed until 528 cycles, when adhesive zones appear on the steel surface, leaving visible the primer. An increase in the area of the adhesive failure zones is observed with the increase of the number of cycles.

-INSERT FIGURE 10-

3.5. Reliability

In order to give a measure of the risk of failure as a function of the exposure time to the proposed conditions, a simplified Weibull model is used. Reliability studies are carried out from the results obtained in the mechanical tests, being able to effectively assess the effect of both exposure time and environment conditions in terms of reliability of the adhesive joint.

3.5.1. Sikaforce® 7720

Figure 11 shows reliability curves of Sikaforce® 7720 during the durability process. Curves of the specimens without degradation and subjected to two hours under durability conditions are almost the same, just as it happens with their mechanical properties as can be seen in Table 2, showing 90% of reliability for values of τ_{max} close to 6 MPa. Shifting appears from 24 hours of exposure, coinciding with the post-curing process of the adhesive, and 95% of reliability is found for τ_{max} around 7 MPa. The best results are observed for 168 hours of exposure, when 95% of reliability is obtained for τ_{max} values above 8 MPa. Shifting appears again after 360 hours of exposure, but this time in the opposite direction, showing a change in the trend associated with the degradation process of the adhesive. Reliability of 95% is found for values under 8 MPa. Degradation is evident in the curve of 768 hours of exposure, whose τ_{max} for

95% of reliability is around 5.5 MPa. Last curve has the smallest slope of all, showing a greater dispersion of the data. This is logical, since it is the curve with longer exposure times.

-INSERT FIGURE 11-

Figure 12 shows reliability curves of Sikaforce® 7720 during the heat-aging process. The behavior is similar than for durability. In this way, curves of 0 cycles and 100 cycles are almost the same. During the first 100 cycles, no evident changes are observed in the mechanical properties of the adhesive, as it is shown in Table 3. 90% of reliability is observed for values of τ_{max} greater than 6 MPa. Shifting appears after 250 cycles, being the post-curing process evident. Reliability greater than 95% is obtained for values of τ_{max} close to 7 MPa. This curve shows the smallest data dispersion, being the curve with the highest slope of the whole graph. In the curve of 528 cycles the end of the post-curing process can be seen. 95% of reliability is observed for τ_{max} above 7.5 MPa. After 528 cycles the degradation process takes place, being clear in the curve of 1004 cycles. Shifting appears in the decreasing direction of τ_{max}. 95% of reliability for values close to 8.5 MPa can be observed. After 1968 cycles the degradation is evident as can be seen in the reliability curve. The slope is clearly horizontal compared to the other curves, showing a large dispersion of data. Reliability drops; getting 95% of reliability for τ_{max} values around 5.5 MPa.

-INSERT FIGURE 12-

3.5.2. Sikatack® Drive

Figure 13 shows reliability curves of Sikatack® Drive during the durability process. In this case, the degradation process begins from the first times of exposure. τ_{max} above 4 MPa is

observed in the curve without degradation for 95% of reliability, being the highest value of the graph. Shifting appears in the decreasing direction of τ_{max}, according to the degradation process of the adhesive, from the first exposure times. Curves of 2 and 24 hours are similar, as it happens with the results obtained in the mechanical tests (Table 2). τ_{max} close to 4 MPa for 95% of reliability is observed in both cases. Curves of 168 and 360 hours are also similar regarding the value of τ_{max} for 95% of reliability. Mechanical values in both cases are also similar (Table 2). Finally, after 768 hours of exposure, the worst reliability values are observed. Reliability below 20% is shown for τ_{max} of 3 MPa.

-INSERT FIGURE 13-

Figure 14 shows reliability curves of Sikatack® Drive during the heat-aging process. The behavior is different than for durability, and in this case a post-curing process can be observed. In this way, for 0 cycles and 100 cycles, reliability greater than 90% is shown at 4 MPa of τ_{max}. Both curves are similar, in the same way that their mechanical properties, as can be seen in Table 3. Shifting appears in the increasing direction of τ_{max} at 250 cycles. Higher than 90% of reliability for 5 MPa of τ_{max} is observed, being the best curve of the entire graph. From 250 cycles the degradation process takes place, appearing shifting in the decreasing direction of τ_{max}. At 528 cycles reliability is zero for τ_{max} close to 5 MPa, and in the case of 1004 cycles this occurs at values below 4.5 MPa. Finally, after 1968 cycles, the worst reliability values are observed, since the reliability is zero for values lower than 4 MPa of τ_{max}.

-INSERT FIGURE 14-

3.6. Chemical characterization

3.6.1. Differential Scanning Calorimetry (DSC)

3.6.1.1. Sikaforce® 7720

Before the degradation process T_g is 29.74°C. This value increases with the exposure time (both heat-aging cycles and durability) in line with the increment in the mechanical properties of the adhesive joint (Table 4). These increases are related to an increment of the cross-linking inside the polymer [48]. Other authors such as Garrett et al. [50] explain that during the T_g increment, the cross-linking and the ordering of the chains increases too, resulting in a greater crystallinity and restricting the mobility of the amorphous domains in the polymer. In this case, an increment of crystallinity is not found since its ΔH keeps the initial value (-0.2 $J \cdot mol^{-1}$).

The greater cross-linking is mainly due to the post-curing experienced by the adhesive during the durability process and the heat-aging cycles. Chains lose mobility and the polymer becomes more rigid. Table 4 shows thermal properties of Sikaforce® 7720 during the durability tests. From 0 to 24 hours of exposure no variations are observed. After 168 hours of exposure this trend changes, increasing the value of the T_g up to 37.09°C. This temperature remains constant after 360 hours of exposure (35.78°C). However, after 768 hours of exposure, and when the degradation is evident in the adhesive (taking into account the mechanical values), T_g decreases until 28.50°C.

Regarding heat-aging cycles, similar behavior is observed. Table 5 shows thermal properties of Sikaforce 7720® during the heat-aging cycles. In this way, from 0 to 528 cycles of exposure no changes in T_g values are observed. After 1004 cycles of exposure, the value of the T_g increases up to 33.20°C. This is consistent with the results of the mechanical values, and with the processes that take place within the polymer chains. Cross-linking increases due to a post-

curing process (as previously explained), increasing the mechanical properties and the T_g. After 1968 cycles, adhesive degradation is evident, and both T_g (28.45°C) and mechanical properties decrease significantly.

3.6.1.2. Sikatack® Drive

This adhesive shows a T_g due to the soft segments at -43.42°C in specimens that are not subjected to degradation. During the durability tests T_g increases rapidly from 2 hours of exposure (-34.67°C). This trend continues throughout the process until reaching the maximum value after 768 hours (-22.42°C).

Despite having similar behavior to Sikaforce® 7720 regarding to the T_g, mechanical properties of Sikatack® Drive descend from the first exposure times. As it is explained before, cross-linking increment of the polymer chains causes the increase of the T_g value. However, during the durability process, there are several factors that can affect the integrity of the adhesive joint. In this case, the adhesive joint suffers a phenomenon of adsorption. The humidity of the environment penetrates through the adhesive-substrate interface, worsening the properties of the joint. This is clear thanks to the study of the types of failure found during the durability process. From short exposure times (24 hours) large areas with adhesive failure are observed on the specimens' surface (Figure 8). The longer the exposure time, the more surface with adhesive failure is observed. These changes are only observed on Tg of soft segment, there are not any change on the hard segment.

Regarding heat-aging cycles, T_g values remain practically constant throughout the process. The most relevant change is observed at 250 cycles, when T_g rises to -39.60°C. This increment is related to a greater cross-linking of the polymer, and also with τ (5.14±0.35 MPa)

and stiffness (21.84±2.94 MPa) increase. On the other hand, T_g drops to -44.51°C after 1968 cycles. At this point, changes in the polymer chain are produced again and cross-linking decreases. Polymer is degraded, and τ decrease (3.58±0.26 MPa) is very clear. Heat-aging process does not produce noticeable modifications in T_g values, which could indicate that this type of degradation does not affect significantly the phase separation between the hard and soft segments in the polyurethane bulk [51].

3.6.2. Fourier-Transform Infrared Spectroscopy (FTIR)

Changes are not observed in the infrared spectra in either of the two adhesives during the degradation processes. Both adhesives do not show differences on peak around 3000-3100 cm^{-1}, corresponding to OH group, although changes are evident in the mechanical properties and in the DSC. This may be due to low water uptake that it is not detected by infrared spectroscopy.

4. Conclusions

The aim of this paper was to evaluate and compare the behavior of two different adhesives (one single-component and other double-component polyurethanes) subjected to adverse environmental conditions.

Despite being two polyurethane based adhesives, the differences in their chemical composition make their behavior different against the studied conditions. Sikaforce® is a double-component adhesive, which requires the polyols of component A and the isocyanates of component B to be mixed in order to trigger the polymerization reaction and the curing of the adhesive. This difference in the formulation makes it more appropriate to be able to afterwards develop all its mechanical properties, thanks to the presence of humidity and temperature. The adhesive does not reach the maximum value of its mechanical properties only with the mixture

of the components, being necessary the exposure to humidity (82% R.H.) and temperature (72°C).

Therefore, during the first stages of exposure to moisture, it will favor the post-curing of the adhesive. While the temperature increases the cross-linking of the polymer chains. After long exposure times, the polymer begins its degradation process.

The single-component adhesive has both polyols and isocyanates directly in its composition. It needs the presence of humidity to achieve curing. However, once the curing is completed, the presence of moisture is harmful. The adhesive absorbs water, creating new hydrogen bridges into the polymer chain.

Sikatack® Drive shows a phenomenon of adsorption from 24 hours of exposure, while Sikaforce 7720® shows a phenomenon of adsorption from 768 hours. The water penetrates, in both cases, by the interface between the adhesive and the substrate. This phenomenon is much more evident in the double-component adhesive, since the failure observed is completely adhesive, while the single-component adhesive shows mixed failure. Regarding the mechanical properties, although the single-component adhesive begins the degradation process from few times of exposure, its degradation is gradual. On the contrary that happens in the double-component adhesive, whose degradation is more pronounced.

The effect of the heat-aging cycles is similar in both adhesives, as a post-curing process takes place in both cases. Both polymers increase the cross-linking of their chains, with the consequent variation in terms of the mechanical properties. The degradation is evident in both adhesives after 1968 cycles, when chain excision in the polymer network happen, reducing the cross-linking density, and increasing the critical molecular weight. New more linear molecules

are formed in the network, and they undergo plasticization, decreasing Young's modulus and tensile strength values.

Acknowledgements

Spanish ministry of Economía y Competitividad under grants TRA2014-56471-C4-2-R. Instituto Tecnológico de Química y Materiales Álvaro Alonso Barba (IAAB).

Conflict of interests

The author(s) declared no potential conflicts of interest with respect to the research, authorship, and/or publication of this article.

5. References

[1] Mohan VB, Lau K, Hui D, Bhattacharyya. Graphene-based materials and their composites: A review on production, applications and product limitations. Compos Part B – Eng 2018; 142: 200-20.

[2] Eda G, Chhowalla M. Graphene-based composite thin films for electronics. Nano Lett 2009; 9: 814-8.

[3] Luo B, Zhi L. Design and construction of three dimensional graphene-based composites for lithium ion battery applications. Energy Environ Sci 2015; 8: 456-77.

[4] Delogu M, Zanchi L, Dattilo CA, Pierini M. Innovative composites and hybrid materials for electric vehicles lightweight design in a sustainability perspective. Mater Today Commun 2017; 13: 192-209.

[5] Enciso B, Abenojar J, Martinez MA. Influence of plasma treatment on the adhesion between a polymeric matrix and natural fibres. Cellulose 2017; 24: 1791-1801.

[6] Kalanchiam M, Chinnasamy M. Advantages of Composite Materials in Aircraft Structures. IJAME 2012; 6: No. 11.

[7] Mangalgiri PD. Composite materials for aerospace applications. Bull Mater Sci 1999; 22: 657-64.

[8] Rizzo F, Pinto F, Meo M. Development of multifunctional hybrid metal/carbon composite structures. Compos Struct 2019; 222: 110907.

[9] Sakundarini N, Taha Z, Abdul-Rashid SH, Ghazila RAR. Optimal multi-material selection for lightweight design of automotive body assembly incorporating recyclability. Mater Design 2013; 50: 846-57.

[10] Wargnier H, Kromm FX, Danis M, Brechet Y. Proposal for a multi-material design procedure. Mater Design 2014; 56: 44-9.

[11] Martinsen K, Hu SJ, Carlson BE. Joining of dissimilar materials. Cirp Ann-Manuf Techn 2015; 64: 679-99.

[12] Anes V, Pedro R, Henriques E, Freitas M, Reis L. Bonded joints of dissimilar adherends at very low temperatures – An adhesive selection approach. Theor Appl Fract Mec 2016; 85: 99-112.

[13] L.F.M.da Silva, R.D.S.G.Campilho, Design of adhesively-bonded composite joints, in: Fatigue and Fracture of Adhesively-Bonded Composite Joints (Part two), 2015, Pages 43-71, Woodhead Publishing Series in Composites Science, Elsevier Ltd, Cambridge, UK.

[14] Galvez P, Quesada A, Martinez MA, Abenojar J, Boada MJL, Diaz V. Study of the behaviour of adhesive joints of steel with CFRP for its application in bus structures. Compos Part B – Eng 2017; 129: 41-6.

[15] Hart-Smith, L.J. Adhesively bonded joints in aircraft structures. In Handbook of Adhesion Technology, 1st ed.; da Silva, L.F.M., Öchsner, A., Adams, R.D., Eds.; Springer-Verlag: Berlin Heidelberg, 2011; Vol. 2, pp 1103-47.

[16] Marques EAS, Da Silva LFM, Flaviani M. Testing and simulation of mixed adhesive joints for aerospace applications. Compos Part B – Eng 2015; 74: 123-30.

[17] Quan D, Urdániz JL, Rouge C, Ivanković A. The enhancement of adhesively-bonded aerospace-grade composite joints using steel fibres. Compos Struct 2018; 198: 11-18.

[18] Hu P, Han X, Li WD, Li L, Shao Q. Research on the static strength performance of adhesive single lap joints subjected to extreme temperature environment for automotive industry. Int J Adhes Adhes 2013; 41: 119-26.

[19] Davies P, Evrard G. Accelerated ageing of polyurethanes for marine applications. Polym Degrad Stabil 2007; 92: 1455-64.

[20] Fufa SM, Labonnote N, Frank S, Rüther P, Jelle BP. Durability evaluation of adhesive tapes for building applications. Constr Build Mater 2018; 161: 528-38.

[21] Gomes TD, Caridade SG, Sousa MP, Azevedo S, Kandur MY, Öner ET, Alves NM, Mano JF. Adhesive free-standing multilayer films containing sulfated levan for biomedical applications. Acta Biomater 2018; 69: 183-95.

[22] Bauermann LP, Fokuhl E, Stecklum S, Philipp D, Geipel T, Kraft A, Eitner U, Fischer T, Breitenbücher D. Qualification of conductive adhesives for photovoltaic application – accelerated ageing tests. Energy Procedia 2017; 124: 554-9.

[23] Kinloch, A.J. Adhesion and adhesives: science and technology; Springer: Netherlands, 1987.

[24] Batuwitage C, Fawzia S, Thambiratnam D, Al-Mahaidi R. Durability of CFRP strengthened steel plate double-strap joints in accelerated corrosion environments. Compos Struct 2017; 160: 1287-98.

[25] Humfeld GR, Dillard DA. Residual stress development in adhesive joints subjected to thermal cycling. J Adhes 1998; 65: 277-306.

[26] da Silva LFM, Adams RD. Stress-free temperature in a mixed-adhesive joint. J Adhesion Sci Technol 2006; 20: 1705-26.

[27] Sousa JM, Correia JR, Firmo JP, Cabral-Fonseca S, Gonilha J. Effects of thermal cycles on adhesively bonded joints between pultruded GFRP adherends. Compos Struct 2018; 202: 518-29.

[28] Viana G, Costa M, Banea MD, da Silva LFM. A review on the temperature and moisture degradation of adhesive joints. Proc IMechE Part L: J Materials: Design and Applications 2016; 0(0): 1-14.

[29] Hu P, Han X, Li WD, Li L, Shao Q. Research on the static strength performance of adhesive single lap joints subjected to extreme temperature environment for automotive industry. Int J Adhes Adhes 2013; 41: 119-26.

[30] Akderya T, Çevik M, Sayman O. Influence of thermal ageing on tensile performance of E-glass fibre/epoxy composite joints bonded with a diverse set of adhesives. J Adhes 2018. DOI: 10.1080/00218464.2018.1480371.

[31] Li W, Pang B, Han X, Tang L, Zhao K, Hu P. Predicting the strength of adhesively bonded T-joints under cyclic temperature using a cohesive zone model. J Adhes 2015; 92: 892-907.

[32] Taskin NU, Sahin A. Effect of aging time at high temperature on the shear strength of adhesively bonded aluminum composite foam joints. J Adhes 2018; 95: 308-24.

[33] Sorrentino L, Polinini W, Bellini C, Parodo G. Surface treatment of CFRP: influence on single lap joint performances. Int J Adhes Adhes 2018; 85: 225-33.

[34] Gonzalez-Canche NG, Flores-Johnson EA, Cortes P, Carrillo JG. Evaluation of surface treatments on 5052-H32 aluminum alloy for enhancing the interfacial adhesion of thermoplastic-based fiber metal laminates. Int J Adhes Adhes 2018; 82: 90-9.

[35] Su Y, de Rooij M, Grouve W, Akkerman R. The effect of titanium surface treatment on the interfacial strength of titanium – Thermoplastic composite joints. Int J Adhes Adhes 2017; 72: 98-108.

[36] Kwon DS, Yoon SH, Hwang HY. Effects of residual oils on the adhesion characteristics of metal-CFRP adhesive joints. Compos Struct 2019; 207: 240-54.

[37] Mandolfino C, Lertora E, Gambaro C, Pizzorni M. Durability of polyamide bonded joints: influence of surface pre-treatment. Int J Adhes Adhes 2018; 86: 123-30.

[38] Encinas N, Lavat-Gil M, Dillingham RG, Abenojar J, Martinez MA. Cold plasma effect on short glass fibre reinforced composites adhesion properties. Int J Adhes Adhes 2014; 48: 85-91.

[39] Boutar Y, Naïmi S, Mezlini S, Ali MBS. Effect of surface treatment on the shear strength of aluminium adhesive single-lap joints for automotive applications. Int J Adhes Adhes 2016; 67: 38-43.

[40] Kaiser G, Schmölzer S, Straber C, Pohland S, Turan S. Handbook DSC Differential Scanning Calorimetry; NETZSCH-Gerätebau GmbH: Germany, 2015.

[41] Monrrabal G, Ramírez-Barat B, Bautista A, Velasco F, Cano E. Non-destructive electrochemical testing for stainless-steel components with complex geometry using innovative gel electrolytes. Metals-Basel 2018; 8: 500.

[42] Monrrabal G, Guzmán S, Hamilton IE, Bautista A, Velasco F. Design of gel electrolytes for electrochemical studies on metal surfaces with complex geometry. Electrochim Acta 2016; 220: 20-8.

[43] Haldar A, Mahadevan S. Probability, Reliability and Statistical Methods in Engineering Design; John Wiley & Sons Inc: United States, 2000.

[44] Zhongda Y, Junxiang D, Dawei W. Reliability estimation of aero-engine based on mixed Weibull distribution model. IOP Conf Ser: Earth Environ Sci 2018; 113: 012073.

[45] Attardi L, Guida M, Pulcini G. A mixed-Weibull regression model for the analysis of automotive warranty data. Reliab Eng Syst Safe 2005; 87: 265-73.

[46] Chiou BS, Schoen PE. Effects of crosslinking on thermal and mechanical properties of polyurethanes. J Appl Polym Sci 2002; 83: 212-23.

[47] Pérez-Limiñana MA, Arán-Aís F, Torró-Palau AM, Orgilés-Barceló C, Martín-Martínez JM. Influence of the hard-to-soft segment ratio on the adhesion of water-borne polyurethane adhesive. J Adhesion Sci Technol 2007; 21: 755-73.

[48] Tcharkhtchi A, Farzaneh S, Abdallah-Elhirtsi S, Esmaeillou B, Nony F, Baron A. Thermal aging effect on mechanical properties of polyurethane. Int J Polym Anal Ch 2014; 19(7): 571-84.

[49] Akderya T, Sayman O, Kemiklioğlu U, Arap O. A comparative study on effects of thermal fatigue caused by thermal-oil cycling on tensile properties of single lap composite joints bonded with different kinds of adhesives. J Adhes 2018. DOI: 10.1080/00218464.2018.1440213.

[50] Garrett JT, Xu R, Cho J, Runt J. Phase separation of diamine chain-extended poly(urethane) copolymers: FTIR spectroscopy and phase transitions. Polymer 2003; 44: 2711-19.

[51] Pérez-Limiñana MA, Arán-Aís F, Orgilés-Barceló C. Waterborne polyurethane adhesives based on gelatine-stabilized AgNPs with improved antimicrobial properties. J Adhes 2014; 90: 860-76.

Figures

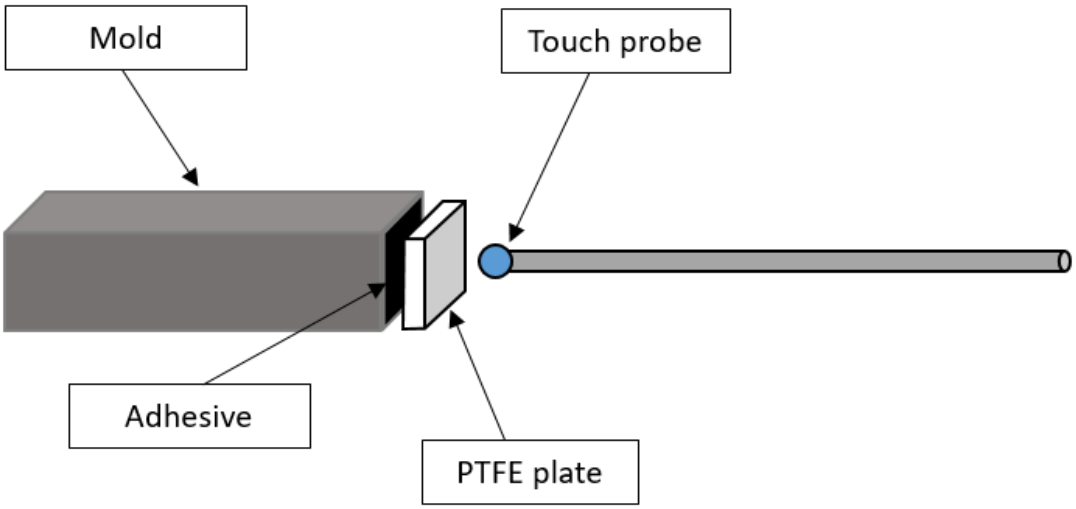

Figure 1. Scheme of the dimensional variation test.

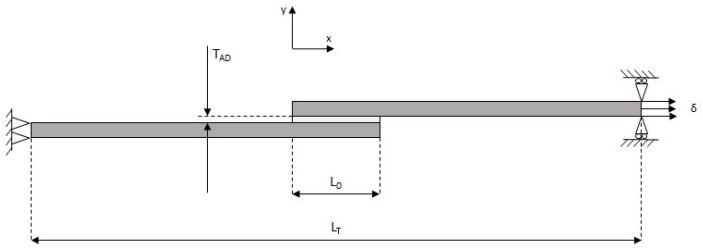

Figure 2. Single lap joint specimen representation.

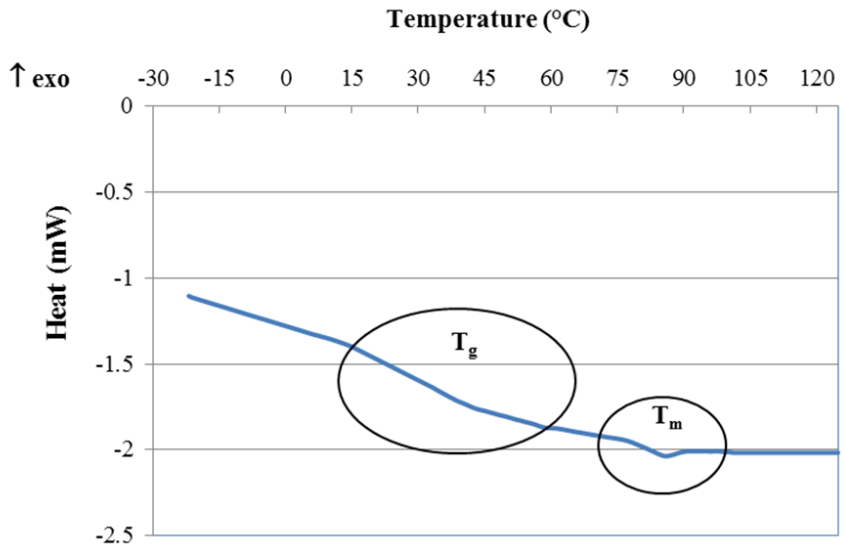

Figure 3. DSC of Sikaforce® 7720 (PUR).

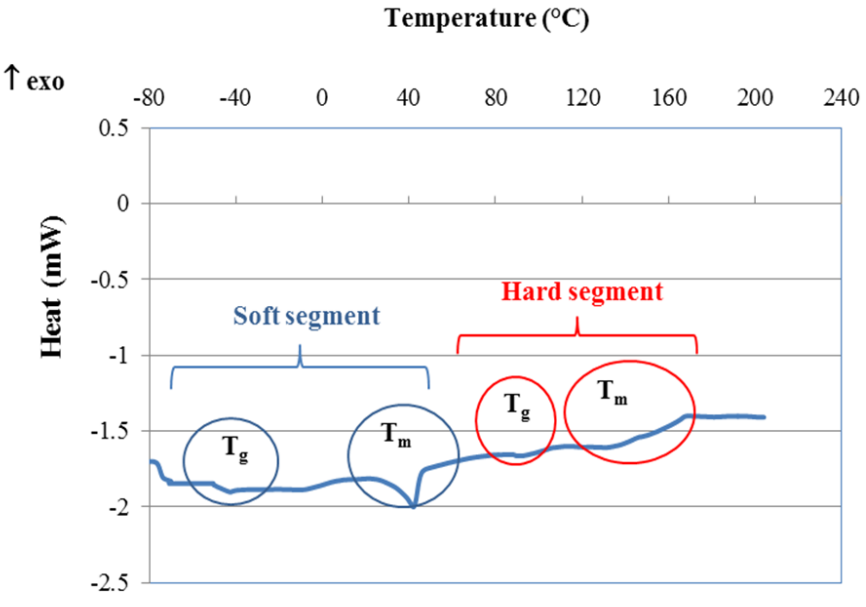

Figure 4. DSC of Sikatack® Drive (TPU).

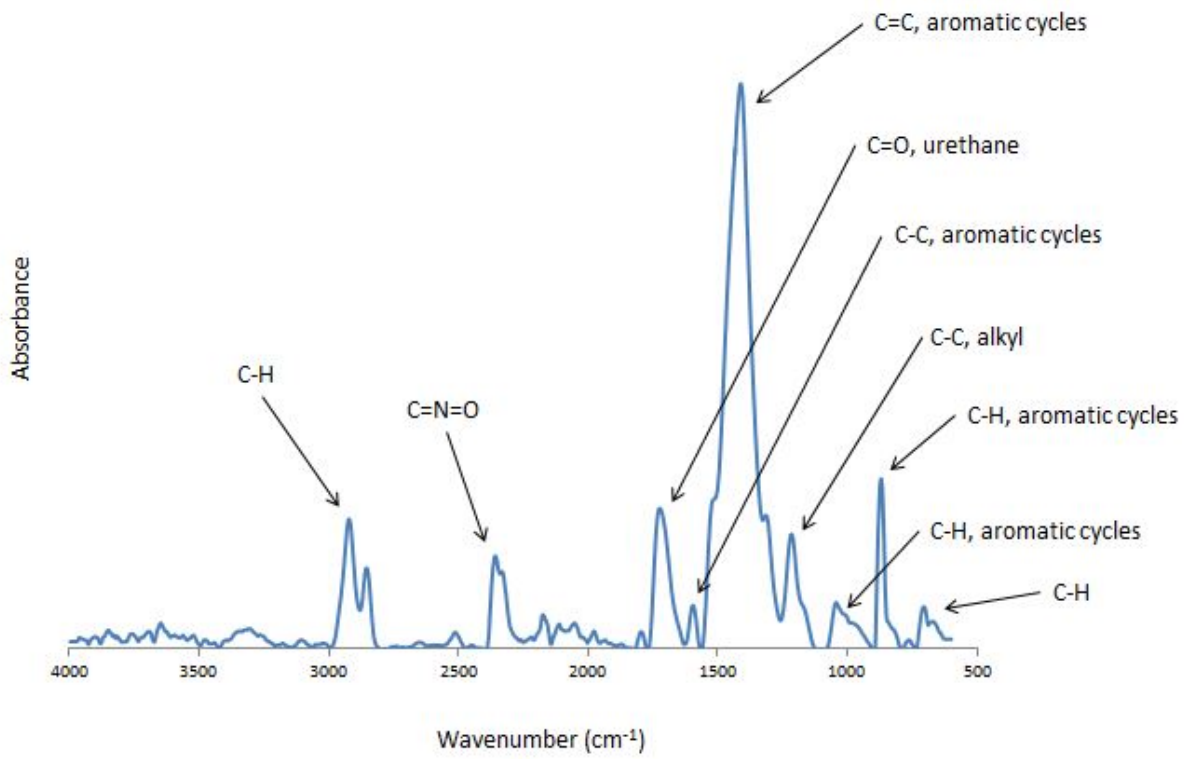

Figure 5. Infrared spectra of Sikaforce® 7720 before being subjected to any type of degradation.

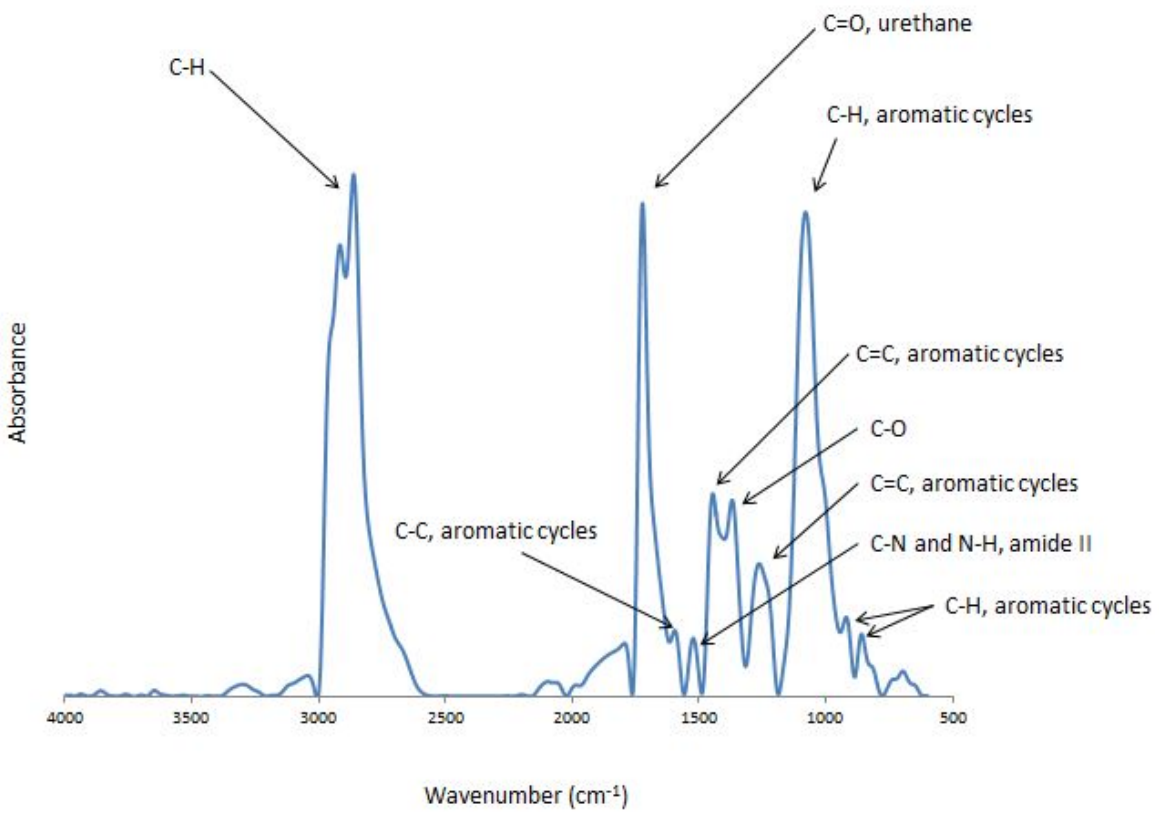

Figure 6. Infrared spectra of Sikatack® Drive before being subjected to any type of degradation.

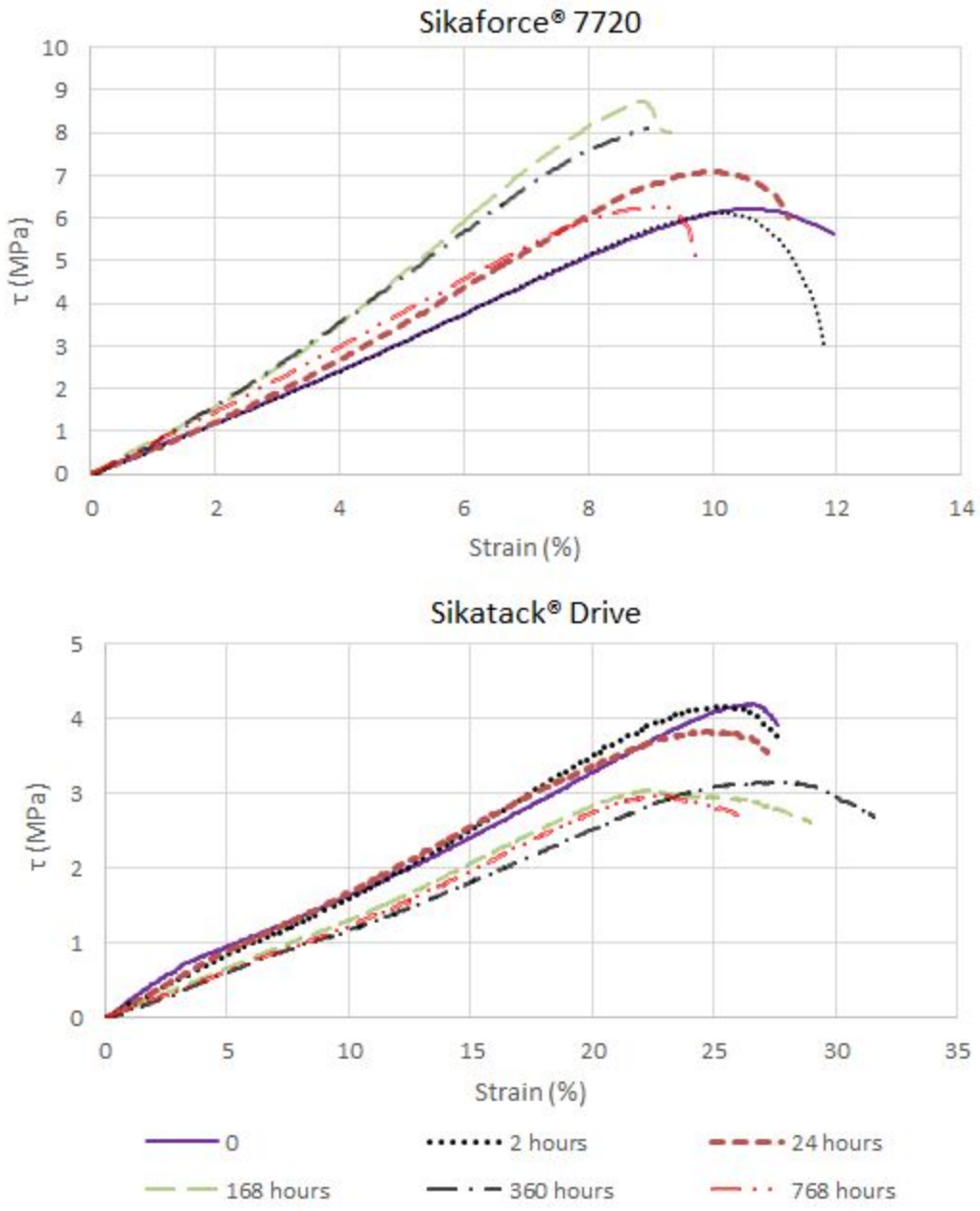

Figure 7. Representative stress-strain curves of Sikaforce® 7720 (up) and Sikatack® Drive (down) during the durability tests.

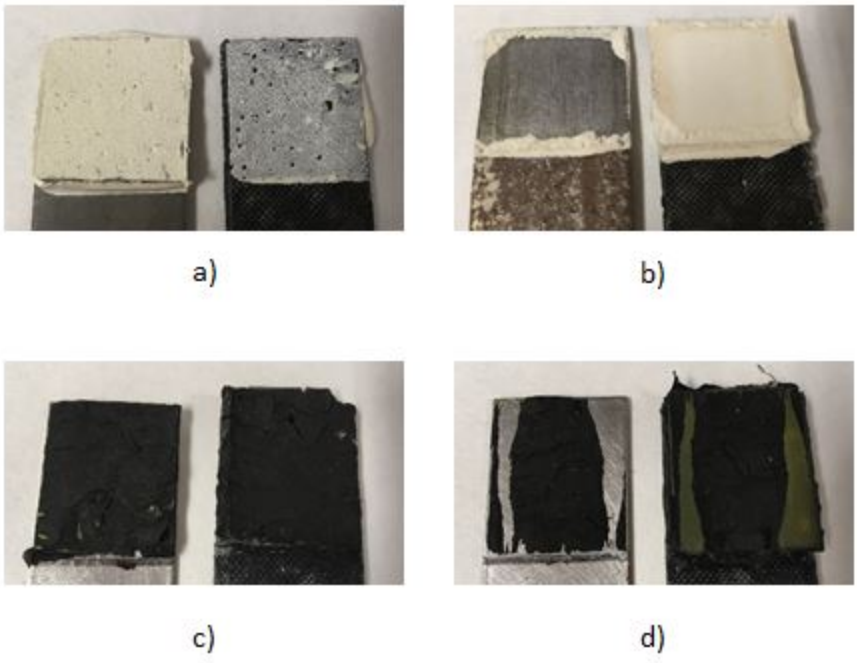

Figure 8. Durability process. Representative cohesive failure a) and adhesive failure b) for the Sikaforce® 7720. Representative cohesive failure c) and mixed failure d) for the Sikatack® Drive.

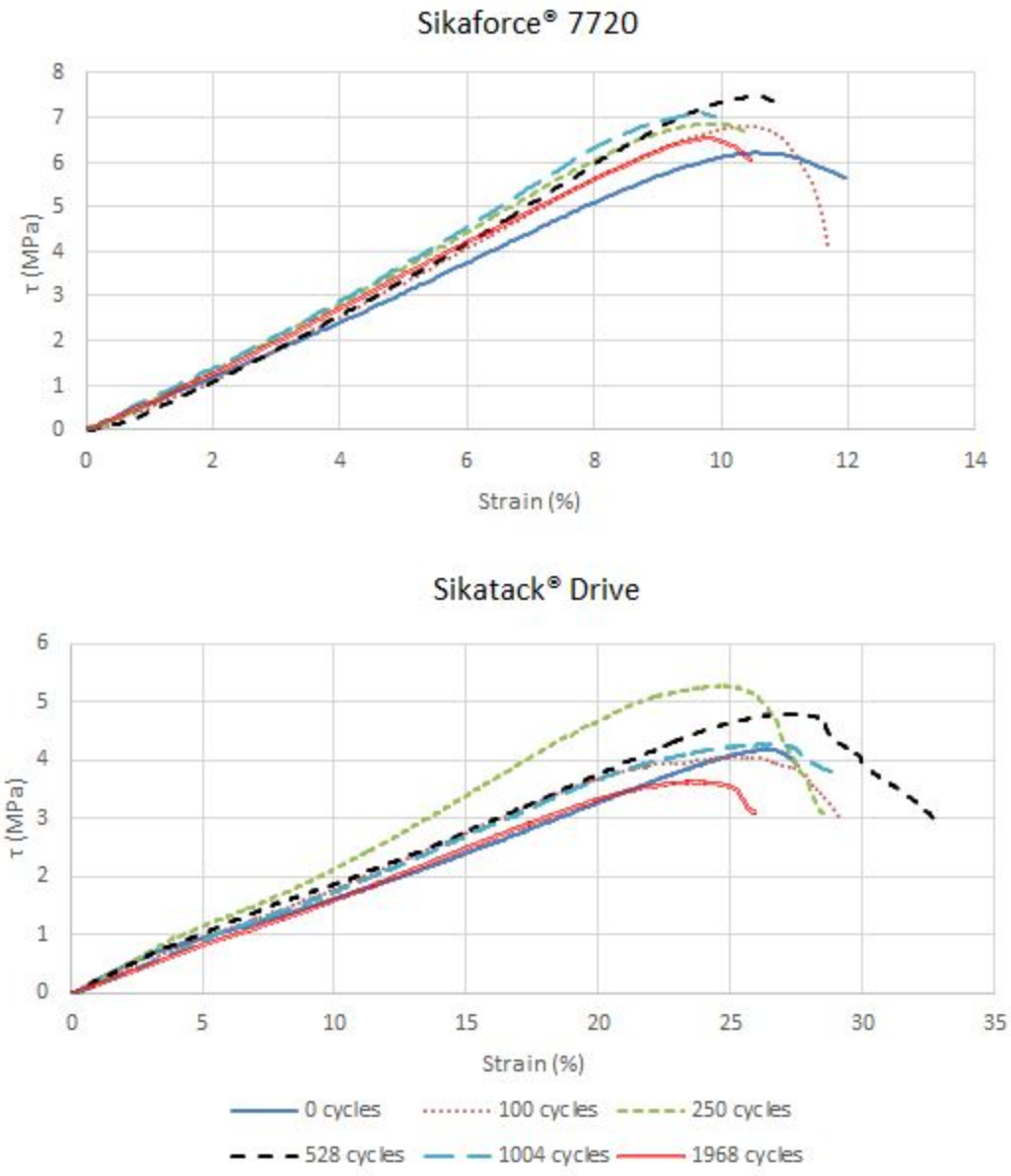

Figure 9. Representative stress-strain curves of Sikaforce® 7720 (up) and Sikatack® Drive (down) during the heat-aging cycles.

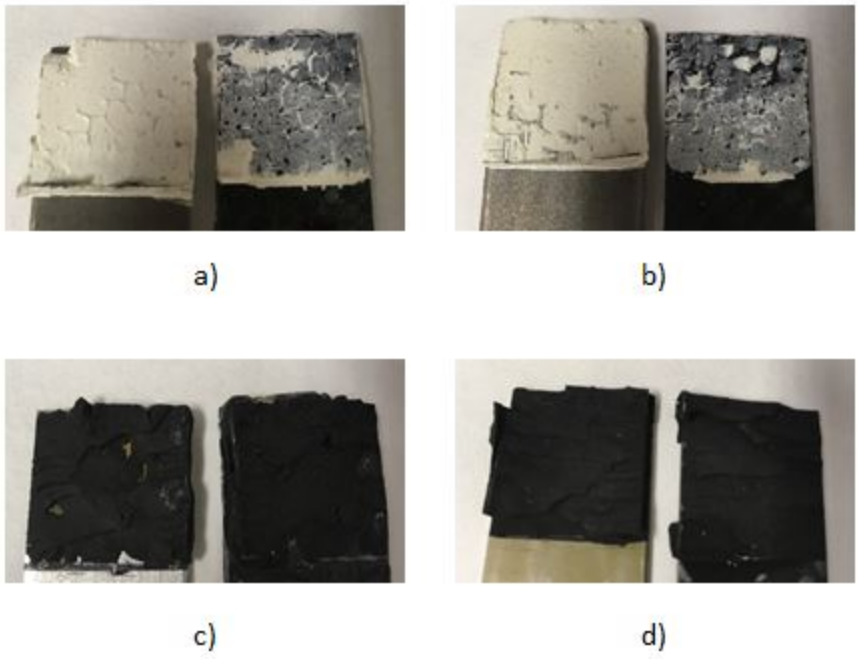

Figure 10. Heat-aging cycles. Representative cohesive failure (a and b) for Sikaforce® 7720. Representative cohesive failure (c and d) for Sikatack® Drive.

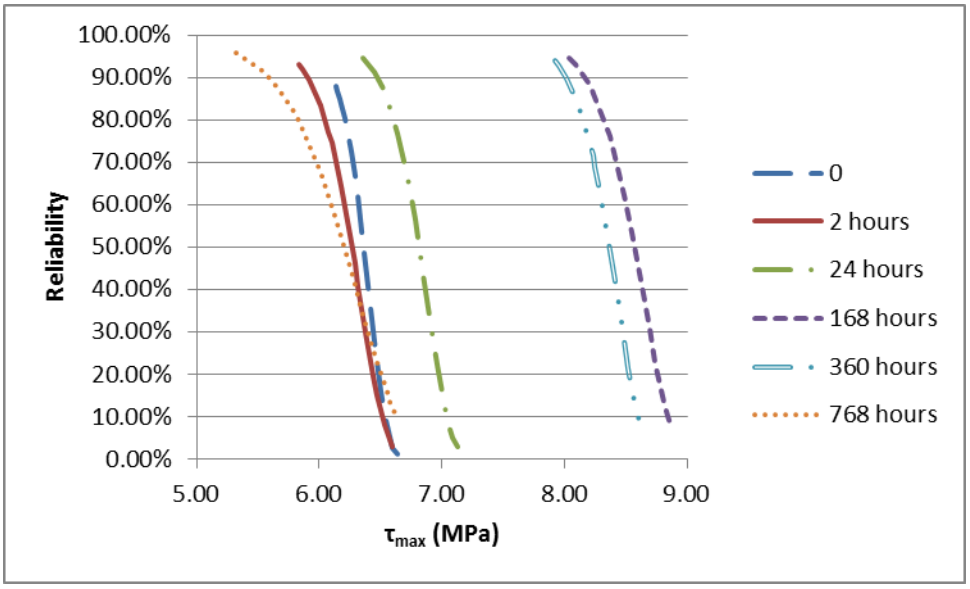

Figure 11. Reliability curves of Sikaforce® 7720 during the durability process.

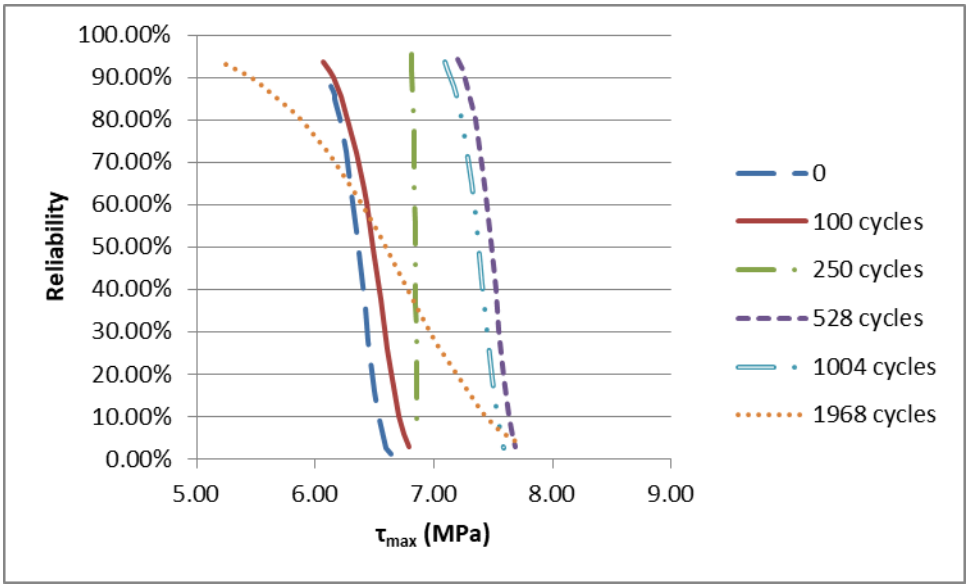

Figure 12. Reliability curves of Sikaforce® 7720 during the heat-aging process.

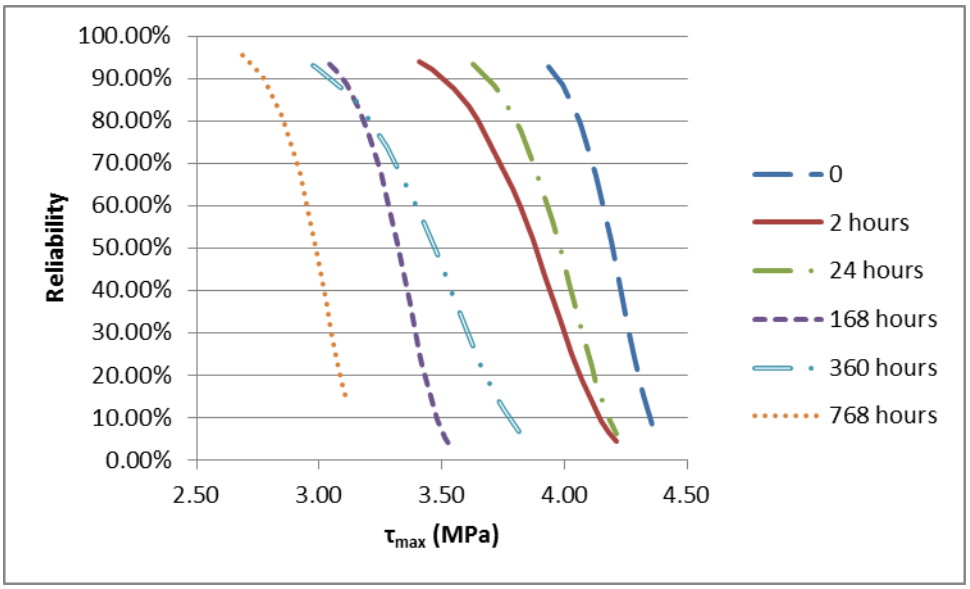

Figure 13. Reliability curves of Sikatack® Drive during the durability process.

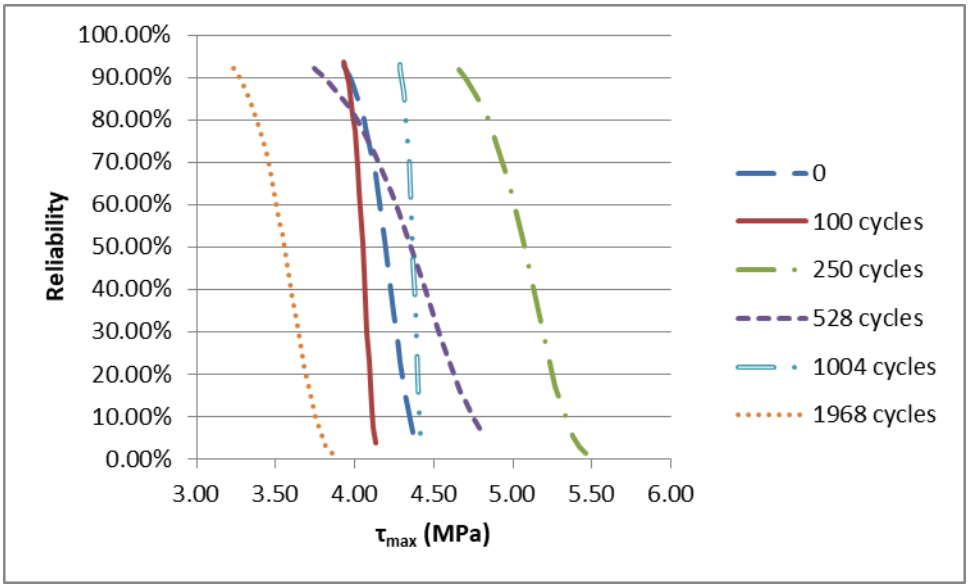

Figure 14. Reliability curves of Sikatack® Drive during the heat-aging process.

Tables

Table 1. Surface treatments and properties of Sikaforce® 7720 and Sikatack® Drive.

Adhesive	Type	σ_{max} (MPa)	E (MPa)	δ (%)	CFRP treatment	Steel treatment
Sikaforce® 7720	Double-component	8.57 ± 0.98	31.62 ± 4.23	31.08 ± 5.02	Cleaning + APPT	Sanding + Cleaning + Pickling
Sikatack® Drive	Single-component	4.04 ± 0.36	2.67 ± 0.13	140.29 ± 13.20	Cleaning + APPT	Sanding + Cleaning + Primer

Table 2. Mechanical values of Sikaforce® 7720 and Sikatack® Drive during the durability tests.

	Time	0	2 hours	24 hours	168 hours	360 hours	768 hours
Sikaforce® 7720	**τ (MPa)**	6.33±0.23	6.18±0.32	6.85±0.35	8.55±0.37	8.29±0.29	6.07±0.55
	δ_{max} (%)	10.95±0.86	10.64±0.65	9.74±0.49	8.85±0.29	8.69±0.92	8.97±0.30
	Stiffness (MPa)	64.63±2.04	66.13±0.92	79.44±1.53	97.33±4.86	105.38±3.69	77.49±9.05
	SHD	60±1	60±1	61±2	64±1	63±1	52±2
Sikatack® Drive	**τ (MPa)**	4.17±0.15	3.93±0.37	3.89±0.24	3.29±0.25	3.32±0.38	2.92±0.18
	δ_{max} (%)	25.10±2.70	25.26±0.35	25.50±0.65	23.41±1.01	22.73±3.33	26.02±2.66
	Stiffness (MPa)	15.92±2.48	16.07±0.50	15.49±0.67	14.54±0.29	15.20±2.45	12.69±1.10
	SHD	19±1	18±1	18±1	15±1	16±1	15±1

Table 3. Mechanical values of Sikaforce® 7720 and Sikatack® Drive during the heat-aging cycles.

	Cycles	0	100	250	528	1004	1968
Sikaforce® 7720	**τ (MPa)**	6.33±0.23	6.43±0.29	6.83±0.03	7.45±0.20	7.31±0.21	6.49±1.00
	δ_{max} (%)	10.95±0.86	10.94±0.59	10.07±0.12	10.63±0.19	9.49±1.09	8.83±1.41
	Stiffness (MPa)	64.63±2.04	67.87±5.61	76.52±1.71	79.10±1.09	87.38±13.04	82.97±6.75
	SHD	60±1	59±1	65±1	70±1	65±1	61±2
Sikatack® Drive	**τ (MPa)**	4.17±0.15	4.04±0.08	5.14±0.35	4.28±0.53	4.36±0.07	3.58±0.26
	δ_{max} (%)	25.10±2.70	25.58±0.53	23.01±1.34	25.68±1.22	25.59±0.68	23.03±0.97
	Stiffness (MPa)	15.92±2.48	16.11±0.96	21.84±2.94	16.09±0.87	16.27±0.73	16.03±0.22
	SHD	19±1	18±1	19±1	19±2	19±1	17±1

Table 4. Thermal properties of Sikaforce® 7720 and Sikatack® Drive during the durability tests.

	Time	0	2 hours	24 hours	168 hours	360 hours	768 hours
Sikaforce® 7720	**T_g (°C) ± 2**	29.74	30.21	29.65	37.09	35.78	28.50
Sikatack® Drive	**T_g (°C) ± 2**	-43.42	-34.67	-31.47	-30.61	-27.83	-22.42

Table 5. Thermal properties of Sikaforce® 7720 and Sikatack® Drive during the heat-aging cycles.

	Cycles	**0**	**100**	**250**	**528**	**1004**	**1968**
Sikaforce® 7720	**T_g (°C) ± 2**	29.74	30.05	29.37	30.25	33.20	28.45
Sikatack® Drive	**T_g (°C) ± 2**	-43.42	-42.50	-39.60	-43.54	-42.05	-44.51

PUBLICACIÓN 6

Designing, manufacturing and testing of a new 3D steel-CFRP node bonded by adhesives for its use in bus structures

Journal:	*Journal of Materials Science & Technology*
Manuscript ID	Draft
Manuscript Type:	Research Article
Date Submitted by the Author:	n/a
Complete List of Authors:	Quesada, Alejandro; Universidad Carlos III de Madrid Escuela Politécnica Superior, GAlvez, Pedro; Universidad Carlos III de Madrid Escuela Politécnica Superior Boada, Maria Jesus; Universidad Carlos III de Madrid Escuela Politécnica Superior Martinez, Miguel Angel Garcia-Pozuelo, Daniel; Universidad Carlos III de Madrid Escuela Politécnica Superior Abenojar, Juana
Keywords:	Steel-CFRP joints, MFO algorithm, FEM model, Multimaterial, Structural adhesives, Mechanical testing
Speciality:	Adhesion, Composites, Failure Mechanisms, Finite Element Modeling, Steel

Designing, manufacturing and testing of a new 3D steel-CFRP node bonded by adhesives for its use in bus structures

Abstract

Composite materials are a reliable and appropriate alternative to metal structures and elements. These materials can reduce costs and weight by maintaining high values of strength and security. On the other hand, the use of adhesives in industrial processes has increased in the recent years. This is possible due to the development of structural adhesives. Current bus steel structures have great fatigue problems due to their stiffness, resulting in unwanted breaks at certain stress concentration nodes. In this work, a 3D steel-CFRP node bonded by adhesives has been designed and manufactured. Firstly a predesign has been performed using optimization techniques by means of Finite Elements Method calculations. Secondly the new prototype has been mechanically tested by mean of four-point flexural test. The results show the capacity of the new CFRP node to be used in bus structures. The test results validate the FEM models with a deviation in the strength value of 8 %.

Keywords

Steel-CFRP joints, MFO algorithm, FEM model, Multimaterial, Structural adhesives, Mechanical testing.

Introduction

Composite materials are a reliable and appropriate alternative to metal structures and elements. These materials can reduce costs and weight by maintaining high values of strength and security. Through the use of different matrices and reinforcements it is possible to develop new materials capable of adapting to the needs raised at each moment. Nowadays these types of material are used in all industrial areas. From highly technological aerospace industry, with the clear example of the Boeing 787 Dreamliner which structure consists of more than 50% composite materials, to less technological shoe industry.

Focusing on the aerospace industry, epoxy resin is the most used matrix. However, different reinforcements are used depending on the application, highlighting carbon, glass, kevlar and boron fibers [1]. These materials are located in different sections of the aircraft as primary structure component (its integrity is critical for the aircraft), control components (as ailerons or spoilers), external components (as fairings or radomes) and internal components (as floors or doors). Conventional carbon fiber reinforced polymer matrix composites are prone to suffer from stress concentration, being necessary the development of new composite materials such as MMC (Metal Matrix Composite), PMC (Polymer Matrix Composite), and CMC (Ceramic Matrix Composite) with more balanced properties by fiber selection [2]. Sufang et al. [3] give an overview of the state of the art in the design, preparation and properties of carbon fiber reinforced UHTC (Ultra-High Temperature Ceramic) composites for ultra-high temperature aerospace application. Barile et al. [4] develop two different composites by combining the same fibers with two types of resins and two manufacturing

processes. They verify that elastic properties are affected by the type of resin while the compressive behavior is differently affected by the manufacturing process.

In recent years, the use of adhesives in industrial processes has increased. This is possible due to the development of structural adhesives. Adhesives provide great advantages over other forms of join, being the most outstanding: creation of a continuous bond, corrosion prevention (sealed joint), stress distribution over a joint area, vibration reduction, invisibility of joints within assembly, mass minimization in an assembly, no substrate deformation and minimizations of components in an assembly [5].In [6] Choi et al. face the problem of joining dissimilar materials by conventional welding techniques.

Nowadays structural adhesives are used in many industries [7] as diverse as aerospace, automotive, railway, marine, civil construction or electrical. Elmarakbi et al. [8] studied the adhesive bonding of the prepared 3-Phase hierarchical graphene-based epoxy nanocomposite laminates for automotive applications. Banea et al. [9] study multi-material adhesive joints for automotive industry, showing benefits as design flexibility and ability to join dissimilar and/or new materials. Huang et al. [10] propose a new waterproof seal layer using polyurethane adhesive to prevent water from infiltrating into the subgrade bed under the slab track of high-speed railway. Speth et al. [11] show greater use of adhesives and composite materials in the marine industry in recent years, finding a new design challenge in the use of bonded joints between composite and steel structures. A logical method for the design and certification of adhesively-bonded composite to steel joints for the marine industry is described. Adhesive joints are becoming increasingly important also in the civil industry, entailing

several challenges related to the joint durability. Galvez et al. [12] study the effect of moisture and temperature in the mechanical and thermal properties of steel-CFRP adhesive joints using polyurethane adhesives for their application as reinforcement in structural engineering. New developments in adhesives with conductive capabilities make possible their use in electrical and electronic applications. Two examples are new graphene and carbon nanotube reinforced epoxy adhesives created by Han et al. [13]. This kind of adhesive show better mechanical and conductive properties than non-reinforced adhesives and are able to be used in electronic applications.

Current bus structures have great fatigue problems due to their stiffness, resulting in unwanted breaks at certain stress concentration nodes [14]. Nowadays the most used material in the manufacture of bus structures is the high strength steel, since it provides good mechanical properties at a reasonable price. Bus structures are formed by hollow rectangular cross sections beams joined to each other by welding. Main reasons given by the manufacturers for using welded joints are the cost, and the fact that welding is a fast and sturdy process. In the same way there are hardly any dimensional changes and it is not necessary to use filling material [15]. On the other hand, heat affected zones appear during the welding process, decreasing the joint strength [16]. Premature failures can appear due to corrosion, and dynamic loads can trigger a fatigue process that favors the appearance of cracks [17,18]. This problem can be avoided by introducing a new CFRP joint concept which makes a specific zone of the structure be more flexible. In [14], the adhesive was characterized by means of experimental tests and the positive effect of the joint in the behavior of the coach structure was proved with calculations over a complete bus FEM model.

In this work, the node has been designed and manufactured. Structural polyurethane adhesive has been used to join the node to steel beams equal to those used in the bus structure. Firstly a predesign has been performed using optimization techniques by means of Finite Elements Method calculations. The optimal CFRP thickness and the optimal adhesive Young Modulus were obtained as predesign results. Secondly the capacity of the new prototype has been tested by mean of four-point flexural test.

Numerical Study

Steel-CFRP adhesive structural joint FEM model

In previous works [14], a complete FEM model of bus superstructure was developed to select the most stressed joint in the original bus steel body frame in a torsion load state test because this kind of tests makes the bus body frame to be more stressful in normal service conditions [19]. This FEM model was experimentally validated through a real bus structure (fig 1). The selected node exhibits complex three-dimensional stress state.

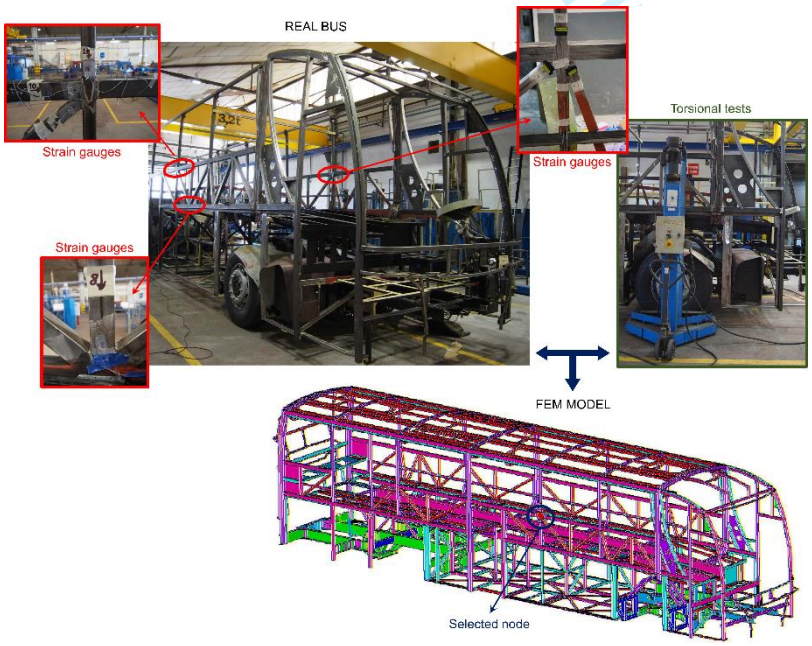

Figure 1. Bus body frame FEM model and validating tests

For this study, a parametric FEM model of a steel-CFRP adhesive structural joint has been developed using ANSYS Mechanical ADPL in order to calculate the bending stiffness and the stress state within the CFRP part and feed the optimization algorithm. Once the capability of the original design was proved to overcome the normal service conditions of the bus superstructure, the optimization was carried out over a flexion load state, characteristic of an extraordinary situation of the bus.

The node core consists of five arms carbon-epoxy FRP part dimensioned to be inserted in the steel structure. The part is joined to the steel beams through the structural adhesive as shown in Figure 2.

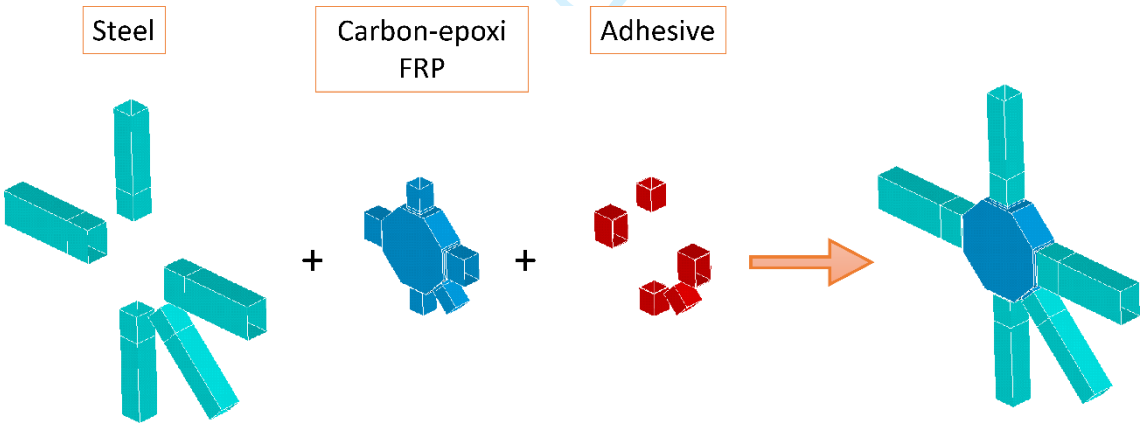

Figure 2. Scheme of the steel-CFRP adhesive structural joint

The model combines shell elements for the CFRP part and the steel beams and solid elements for the adhesive volumes. The solid elements are joined to the shell ones by

sharing a layer of nodes. In addition to the adhesive interaction, a surface-to-surface contact condition has been defined between steel and CFRP faces.

The model has the following main characteristics:

- CFRP part:
  - Number of nodes: 13635.
  - Number of degrees of freedom per node: 6 (ux, uy, uz, rotx, roty, rotz).
- Steel beams:
  - Number of nodes: 26780.
  - Number of degrees of freedom per node: 6 (ux, uy, uz, rotx, roty, rotz).
- Structural adhesive:
  - Number of nodes: 10980.
  - Number of degrees of freedom per node: 3 (ux, uy, uz).

To simulate the behavior of the used materials different material models have been considered [20]. Linear elastic model has been defined to model the steel and adhesive parts, while linear orthotropic model has been selected to simulate the CFRP part. The material models properties are summarized in Table 1. The properties of the adhesive are obtained from [14]. The properties of the carbon-epoxy FRP have been characterized through tensile, compression and in-plane shear tests assuming a balanced $0^0/90^0$ fabric [19]. Steel beams properties have been provided by the bus manufacturer.

Table1. Material properties

Material	Property	Value
Steel	Young modulus	E_S = 210 GPa
	Poisson´s ratio	ν_S = 0.29
	Yield strength	S_S = 400 MPa
Adhesive	Young modulus	E_{adh} = [2 - 5] and [70 - 90] MPa
	Poisson´s ratio	ν_{adh} = 0.45
	Shear strength	τ_{max} = 4.4 MPa
Carbon-epoxi FRP	Young modulus	$E_{11} = E_{22}$ = 61.8 GPa
	Tangent Modulus	G_{12} = 4.63 GPa
		$G_{13} = G_{23}$ = 3 GPa
	Poisson´s ratio	ν_{12} = 0.07
	Limit stresses	$S_{11T} = S_{22T}$ = 884.7 MPa
		$S_{11C} = S_{22C}$ = -417.1 MPa
		S_{12} = 79.3 MPa

Otherwise, the capacity of reticular structures to resist loads is determined more by the strength and the stiffness of its joints than by the properties of the beams themselves. The bending test of the vertical pillar joints connected the waist rail are a recurrent way to check the capability of the bus structure [21], [22], [23]. Considering that the steel-CFRP adhesive structural joint is assumed to bound one side vertical pillar with the waist rail of the bus body frame, it is necessary to analyze its behavior under bending loads. The implemented loading state consists of applying a lateral displacement of 20 mm on the top of the vertical pillar while fixing the ends of the other four arms of the joint as shown in Figure 3. The results obtained from the FEM model are the reaction loads in the vertical pillar and the complete stress condition in the critical node of the CFRP part. As indicated in Introduction, the thickness of the CFRP part and the Young modulus of the adhesive have been found to be of influence

in the joint manufacturing costs and stiffness. For this reason, both have been selected as optimization parameters for the parametric FEM model definition.

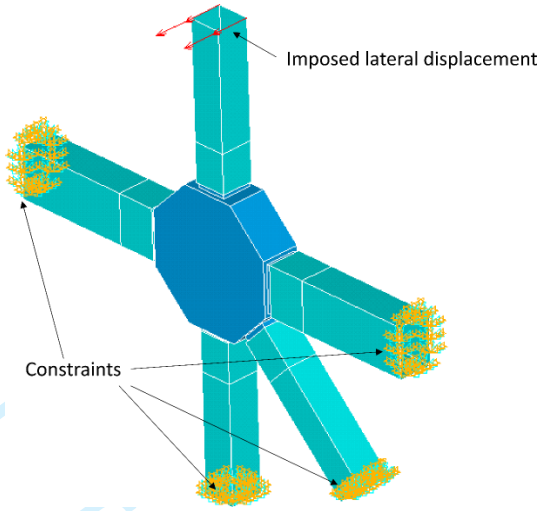

Figure 3. Boundary conditions of the FEM model

Moth-flame optimization algorithm

The Moth-flame Optimization (MFO) is a metaheuristic algorithm proposed by Mirjalili [24] and inspired from the natural behavior of moths. Moths fly following the moon light using transverse orientation, which allows them to travel long distances in a straight way. Nevertheless, when moths see an artificial light (flame), they fly around it following a spiral path due to the moon is much farther than the light. This fact causes that the moth converges towards the light.

Taking into account the behavior of moths of converging towards artificial lights, the steps of the algorithm based on MFO are (see Figure 4):

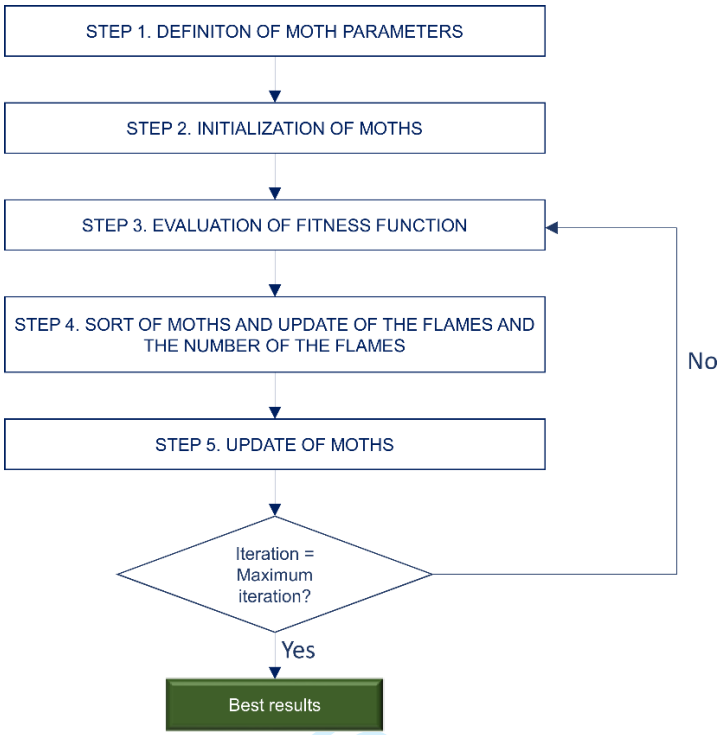

Figure 4. Steps of the MFO algorithm

- STEP 1. The MFO parameters are defined: number of moths and flames (possible solutions), *D* , number of search design variables (dimension), *N*, fitness function, lower and upper bounds, and iterations.
- STEP 2. A population of moths, $M = \{M_1, M_2, \dots, M_N\}$, is randomly initialized in the search space bounded by *N* and *D*. Each *jth* variable of the *ith* individual of the population, $M_i = \left(m_{i,1}, m_{i,2}, \dots, m_{i,D}\right)^T$, is initialized as:

$$m_{i,j} = \left(m_j{}^{ub} - m_j{}^{lb}\right) rand() + m_j{}^{lb} \qquad (1)$$

where $m_{i,j} \in M_i$ with *j = (1, 2, … , D)* and $m_j{}^{lb}$ and $m_j{}^{ub}$ are the lower and upper bounds, respectively, of the *jth* variable.

- STEP 3. The fitness function (or objective function) is evaluated for each moth and stored in $\overrightarrow{OM} = \{OM_1, OM_2, \dots, OM_N\}$.
- STEP 4. The best positions of the moths obtained so far are saved in flames: $F = \{F_1, F_2, \dots, F_N\}$. The flames are sorted based on their fitness values. The dimensions of *M* and *F* are equal. The fitness values of flames are stored in $\overrightarrow{FM} = \{FM_1, FM_2, \dots, FM_N\}$.
- STEP 5. The position of each moth is updated around its corresponding flame using equation (2):

$$M_i = S(M_i, F_k)\ k = (1, 2, \dots, N) \quad (2)$$

where M_i is the *ith* moth, F_k is the *kth* flame, $F_k = \left(F_{k,1}, F_{k,2}, \dots, F_{k,D}\right)^T$ and *S* is the logarithmic spiral function used to update the moths:

$$S(M_i, F_k) = D_i \cdot e^{bt} \cdot cos(2\pi t) + F_k \quad (3)$$

where D_i is the distance between the *ith* moth and the *kth* flame and it is calculated as follows:

$$D_i = |F_k - M_i| \quad (4)$$

b is a constant which defines the shape of the logarithmic spiral and *t* is a random value between - 1 and 1 which represents how close the moth should be to the flame (*t=-1* is the closest position to the flame and *t=1* is the farthest position to the flame).

Instead of updating the position of moths with respect to *N* different positions in the search space, the number of flames, *Q*, is decreased in each iteration to deal with the exploration versus exploitation trade-off:

$$Q = round\left(N - l \cdot \frac{N-1}{l_{max}}\right) \quad (5)$$

where l is the current number of iteration and l_{max} is the maximum number of iterations. This means that moths update their position respect to the best flame at the end of the iteration process.

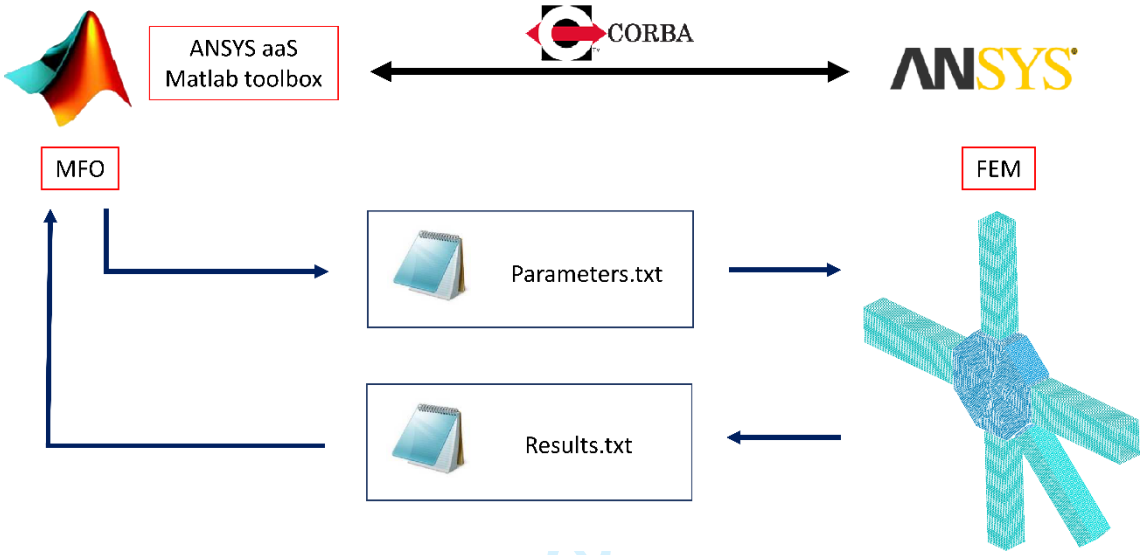

Figure 5. Communication between Matlab and ANSYS

Optimization Results and Discussion

To carry out the optimization process with the steel-CFRP adhesive structural joint FEM model, a modified source code of MFO written in Matlab [25] has been used. The communication between Matlab and ANSYS has been done through the ANSYS aaS Matlab toolbox (Figure 5). This special toolbox enables a command library, helping the users to achieve the connection and to execute ANSYS instructions with its own

programming language. The following commands have been used in order to create the communication code in MATLAB:

- *initialize_orb*: to instantiate Object Request Broker (ORB) in Matlab.
- *load_ansys_aas*: to initialize ANSYS aaS Toolbox.
- *actmapdlserver*: to initialize connection to Mechanical APDL.
- *executeCommandToString()*: to send commands to the FEA software. ANSYS language must be written between quotes.
- *terminate*: to finish the software connection.

For data and results interchange, ANSYS and Matlab generate two auxiliary text files, where the model parameters and variables are stored.

The objective of the problem is to minimize the composite volume (manufacturing cost) and maximize its bending stiffness. These properties hardly depend on the thickness of the CFRP part, t, and the Young modulus of the adhesive, E_{adh}, so that these are going to be considered as the decision variables of the process. There is one constraint considered concerning the stress values in the CFRP. Tsai-wu failure criterion has been applied because it is adequate for composite materials under multiaxial stresses. The Tsai-Wu safety factor has been evaluated to the most stressed node in the CFRP.

The optimization problem is defined as follows:

Find:

$$x = [x_1, x_2] = [t, E_{adh}]$$

Minimize:

$$f(x) = \frac{A \cdot x_1}{V_0} + \frac{k_0}{k(x_1, x_2)}$$

Subject to:

$$F_1 \cdot \sigma_x + F_2 \cdot \sigma_y + F_{11} \cdot {\sigma_x}^2 + F_{22} \cdot {\sigma_y}^2 + F_{66} \cdot {\tau_{xy}}^2 + 2 \cdot F_{12} \cdot \sigma_x \cdot \sigma_y \leq 1.0$$

Variable range:

$$2mm \leq x_1 \leq 8mm,$$

$$2MPa \leq x_2 \leq 5MPa \text{ or } 71MPa \leq x_2 \leq 90MPa$$

where *A* is the area covered by CFRP fabrics, V_0 is the CFRP reference volume, k_0 is the reference bending stiffness, *k* is the bending stiffness which is calculated dividing the reaction force by the imposed displacement in the vertical pillar. F_1, F_2, F_{11}, F_{22}, F_{66} and F_{12} are the Tsai-Wu coefficients obtained from the following expressions:

$$F_1 = \frac{1}{S_{11T}} - \frac{1}{S_{11C}},\ F_2 = \frac{1}{S_{22T}} - \frac{1}{S_{22C}},\ F_{11} = \frac{1}{S_{11T} \cdot S_{11C}},\ F_{22} = \frac{1}{S_{22T} \cdot S_{22C}},\ F_{66} = \frac{1}{S_{12}}$$

F_{12} cannot be experimentally determined through uniaxial load tests. Some approaches have been suggested by different authors [26]. In this work, for preliminary design, F_{12} is assumed to be *0* [27]. The reference values K_0 and V_0 have been used in order to get normalized and dimensionless terms for the fitness function.

The two parameters have been let to vary in limited intervals:

- It seemed reasonable to let the composite thickness vary from 2 mm to 8 mm. Higher values carry out assembly problems with other parts of the structure, while lower composite thickness could be difficult to manufacture.
- Commercial polyurethane adhesives can be found with elasticity modulus from 2 MPa to 5 MPa and from 70 MPa to 90 MPa (with a different formulation).

Table 2 shows the best result obtained using different number of search agents and iterations. Simulations have been repeated in order to check the consistency of the algorithm.

Table 2. Best results obtained for different number of search agents and iterations

Nº Test	Nº search Agents	Nº Iterations	Optimum values for parameters t (mm)	Optimum values for parameters E_{adh} (MPa)	Best score
1	80	50	6.87	4.50	1.832228
2	80	50	6.91	4.56	1.832118
3	40	150	7.01	4.72	1.832494
4	40	150	6.91	4.56	1.832072
5	80	26	6.96	4.63	1.832553
6	80	26	6.89	4.54	1.832126
average	-	-	6.92±0.05	4.68±0.08	-

Nº Test	Optimum volume (10^{-4} m^3)	Optimum bending stiffness (N/mm)	Tsai-Wu failure Index
1	7.52	239	0.999
2	7.57	242	0.999
3	7.68	248	0.999
4	7.56	242	0.999
5	7.62	245	0.999
6	7.55	241	0.999
average	7.50±0.06	243±3	-

With the average design values (*t = 6.92 mm* and E_{adh} *= 4.68 MPa*) a bending stiffness of *243 N/mm* results with a Tsai-Wu failure index of 0.999, which means that the design is in the stress limit with the imposed displacement of 20 mm at the end of the steel beam. The imposed load at the end of the beam, *F,* is obtained from the FEM model and has a value of *4.84 kN* and this force results in a bending moment in the junction:

$$M = 4.84\ kN \cdot 0.2\ m = 0.968\ kNm \quad (6)$$

Experimental procedure

Materials

New node had been manufactured using carbon fiber reinforced polymer from A-Stage. Epoxy resin (SR 8500 – Sicomin Epoxy Systems – Châteauneuf-les-Martigues, France) with hardener (SD8601 – Sicomin Epoxy Systems – Châteauneuf-les-Martigues, France) was selected as matrix. Carbon fiber fabric (GG 600T – MEL Composites – Barcelona, Spain) was used as reinforcement. AISI 1012 carbon steel beams supplied by Carrocera Castrosua S.A. were used to manufacture complete node prototypes. These beams are exactly the same as those used by the bus manufacturer.

Different ductile adhesives were studied to evaluate the suitability of each of them for the raised problem. Single-component polyurethane adhesive (Sikatack® Drive) was selected due to its high strength and good behavior against environmentally adverse conditions. This adhesive is designed to join the windshield with the car body. It shows hyper-elastic behavior that makes it ideal for the application proposed in this work.

Surface treatment

Working with adhesives it is necessary to ensure cohesive failure. In this work two dissimilar materials (steel and CFRP) were bonded, which adds more difficulty to the process.

Two different surface treatments were carried out to guarantee the correct adhesion of the adhesive on both substrates. The treatment selected for the steel surface was: sanding with P180 sandpaper, solvent cleaning and Sika® Primer 204N. While the treatment for the CFRP surface was: solvent cleaning, APPT (6 mm of torch-specimen distance and 3 m/min of torch speed) and Sika® Primer 215.

Manufacturing process

Nowadays there are different ways to manufacture composite materials pieces: hand lay-up, spray lay-up, resin transfer molding, compression molding, injection molding, vacuum assisted method, autoclave processing, pultrusion and filament winding [28]. In this project it was decided to work with the resin and the carbon fibers separately, beginning the manufacturing of the node from A-Stage, instead of using prepregs (B-Stage). Prepregs allow a greater ease in the manufacture of complex pieces of CFRP (carbon fiber reinforced polymer), however also have a number of very important limitations: early expiration, need to be stored in the freezer at low temperatures and especially the cost. By using the resin and the fibers separately from A-Stage costs could be reduced, materials were stored at room temperature in the lab and same resin and fibers could be used by the partners of this project. Once the starting point in the manufacturing of the node was decided, hand lay-up process to manufacture the node was selected.

The complex design of the new CFRP node results in many manufacturing problems. To solve this problem a PLA node was manufactured by 3D printing. This PLA node was used as a core for the final node of CFRP. In this way, the PLA core was covered layer by layer by hand lay-up process. Six layers of carbon fiber fabric were used in the manufacture of the node, to approximately match with the 6.92 mm thickness found as a result of the optimization calculations. Use a PLA core was a problem since the epoxy resin has poor compatibility with this material. Therefore, it was necessary to perform an atmospheric pressure plasma treatment on the surface of the core. The parameters used in the plasma were: 6 mm of torch-specimen distance and 3 m/min of torch speed. Activating the PLA surface, resin-core compatibility is increased. Figure 6 shows node manufacturing by hand lay-up process.

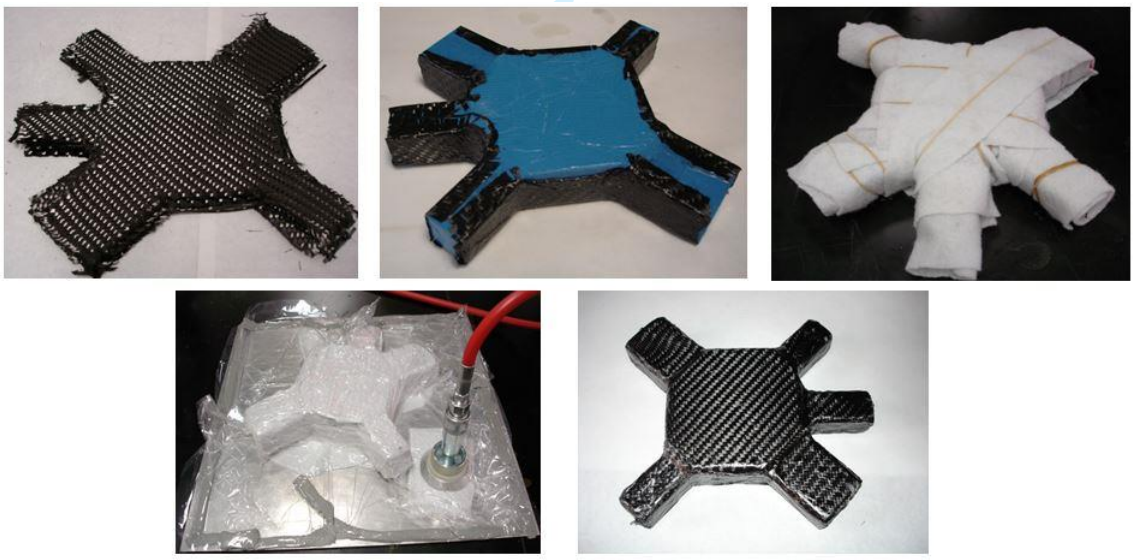

Figure 6. Node manufacturing by hand lay-up process.

The final prototype was the result of joining the CFRP node by means of adhesives to the two 170 mm long and 40x40x4 mm square hollow ssection steel beams (Figure 7). In previous works [14], the ideal adhesive configuration was calculated. CFRP node had

been manufactured to allow a clearance of 2 mm between steel beam and CFRP node surfaces. Therefore, the adhesive thickness was 2 mm, occupying this empty space. In order to know the behavior of the whole set (CFRP node, adhesive and steel beams) three prototypes were manufactured and tested.

Figure 7. Final prototype (CFRP node + adhesive + steel beams).

Four-point flexural test

Four-point flexural tests were carried out in a universal testing machine with a load cell of 200 kN. The behavior of the prototypes against deformation speed of 55 mm per minute was evaluated. Test configuration is shown in Figure 8, with loading pins distance of 240 mm and supporting pins distance of 400 mm. A real test image with the extensometric instrumentation to validate the models can be seen in Figure 9. This test allows reproducing more adverse conditions than the service conditions of the bus reproduced previously with the complete FEM model. From the results of these tests, force-displacement curves, maximum force, displacement for maximum force, and absorbed energy are calculated.

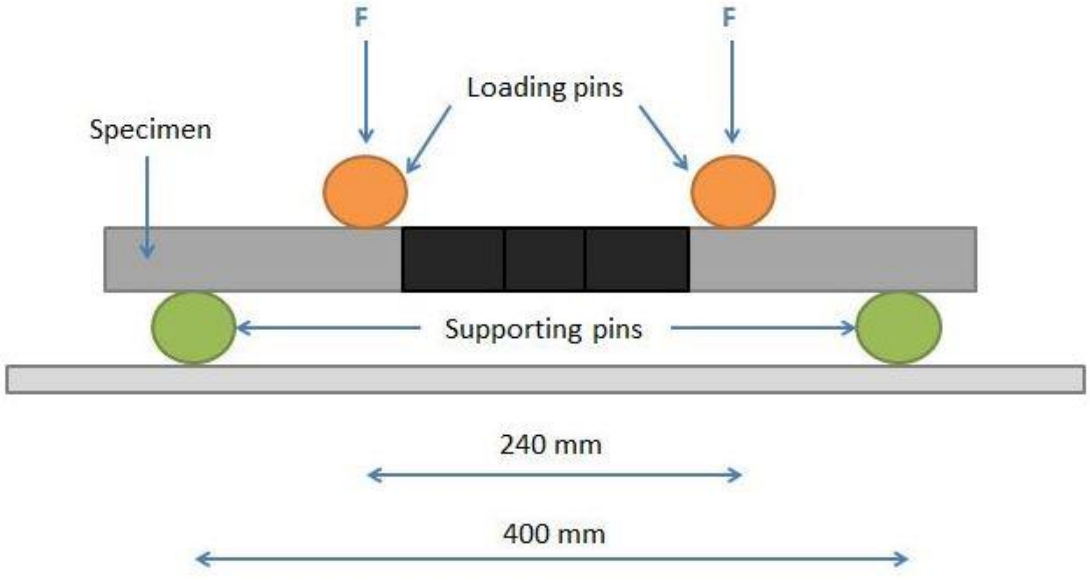

Figure 8. Four-point flexural test configuration.

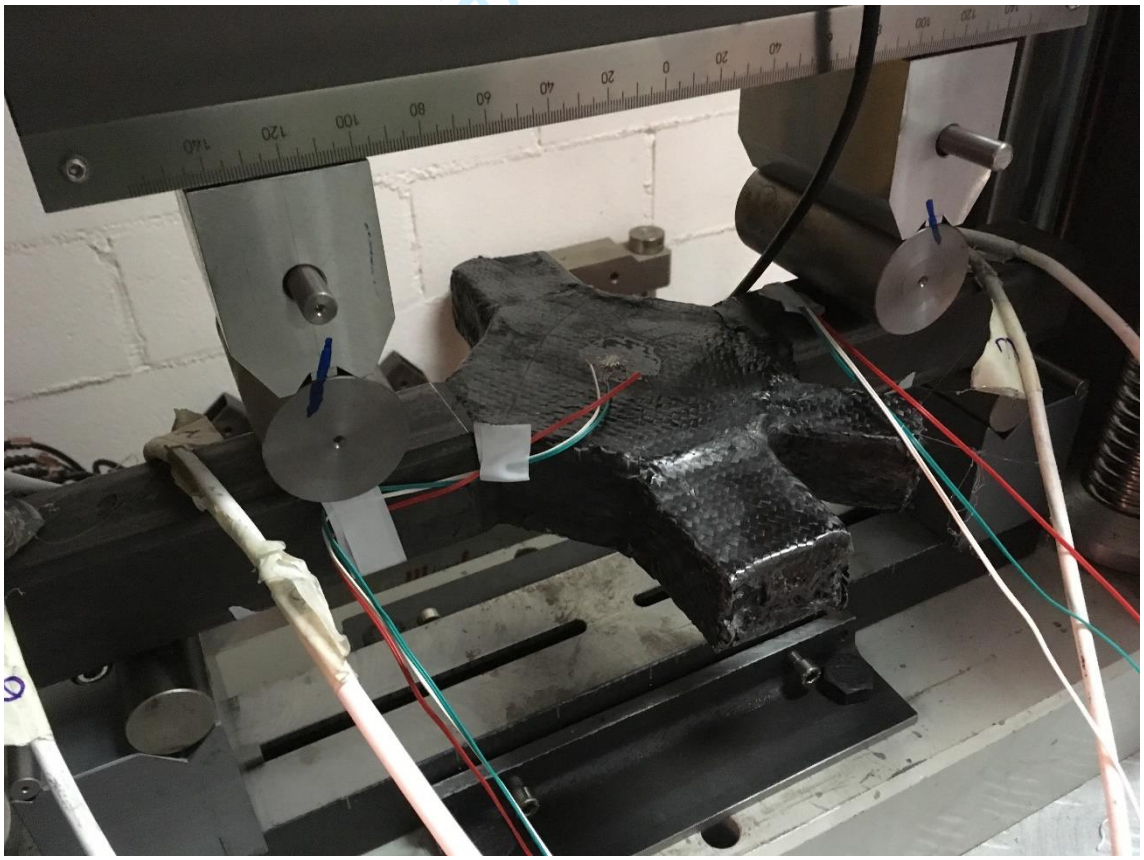

Figure 9. Test instrumentation and disposition.

Results

New node concept has already been introduced in previous works [14]. Figure 10 shows the current representation of the steel node and its location in the bus.

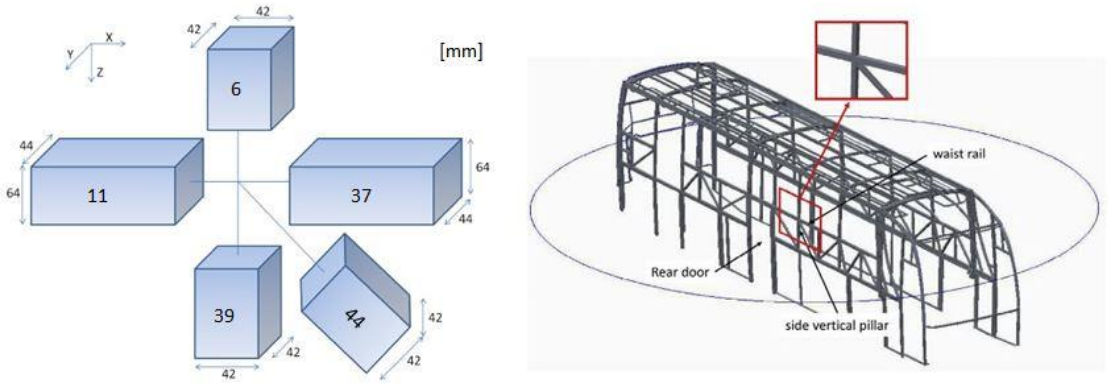

Figure 10. Representation and localization of current steel node.

Four-point flexural test

The CFRP node obtains 26.17±1.03 kN with a displacement of 13.32±3.18 mm. It means a moment in the junction of 1.05±0.04 kNm. Figure 11 shows force-displacement curves of the CFRP nodes. Maximum force and displacement values are very similar even though the shape of the curves are not very similar among them.

The maximum bending moment found in the tests match adequately with the values obtained in the FEM simulations, since a deviation of 8 % in the failure load with respect to the simulation results.

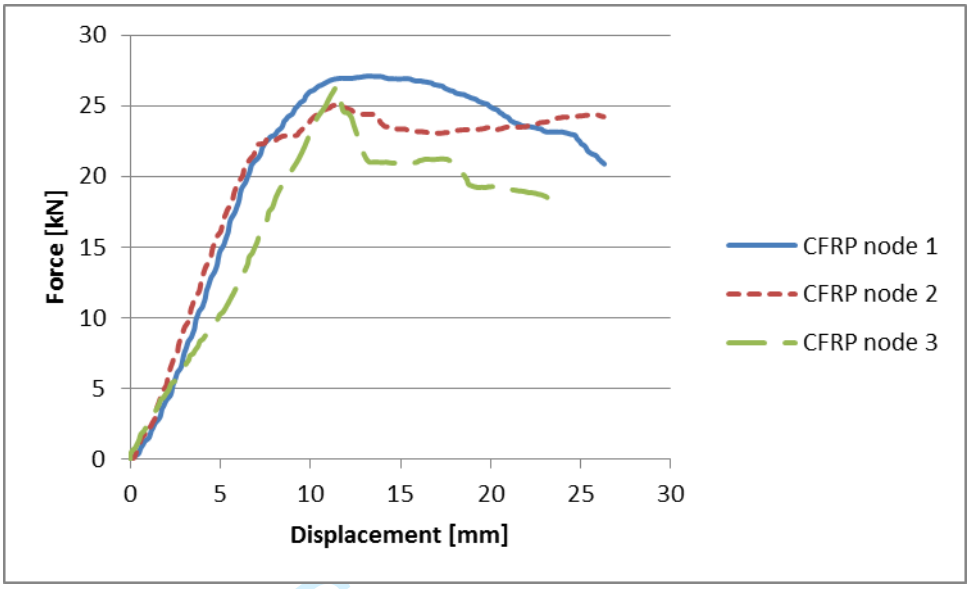

Figure 11. Force-displacement curves of the CFRP nodes.

Failure analysis

It is essential to thoroughly study the types of failure both in the adhesive and the CFRP node. Therefore, once four-point bending tests were completed, most affected areas of the new prototype were studied. Regarding the adhesive, cohesive failure has been obtained in all the tests as it is shown in Figure 12.

Figure 12. Cohesive failure in the adhesive.

The node fails by breaking in both webs of the beam section. Failure modes found in the CFRP node are shown in Figure 13. Web fracture is observed in Figure 13a, showing a clean break of the material. In Figure 13b delamination between fiber layers and material deformation are observed. Delamination is clear as separation of the fiber layers due to a failure of the matrix is observed. Regarding the deformation zone, the piece rotates without breaking or delaminating, but the transformation is permanent, reaching the plastic deformation zone of the material.

In every beam under bending loading maximum tension stress appear in the upper flange and maximum compression stress in the lower flange, while webs are mainly under shear stress. The result of the test shows that flanges are strong enough to avoid failure by normal stress, but webs are not strong enough to avoid failure by shear stress.

New design effort is needed to strengthen the webs by increasing the CFRP thickness or by modifying the CFRP fabrics placing and orientation.

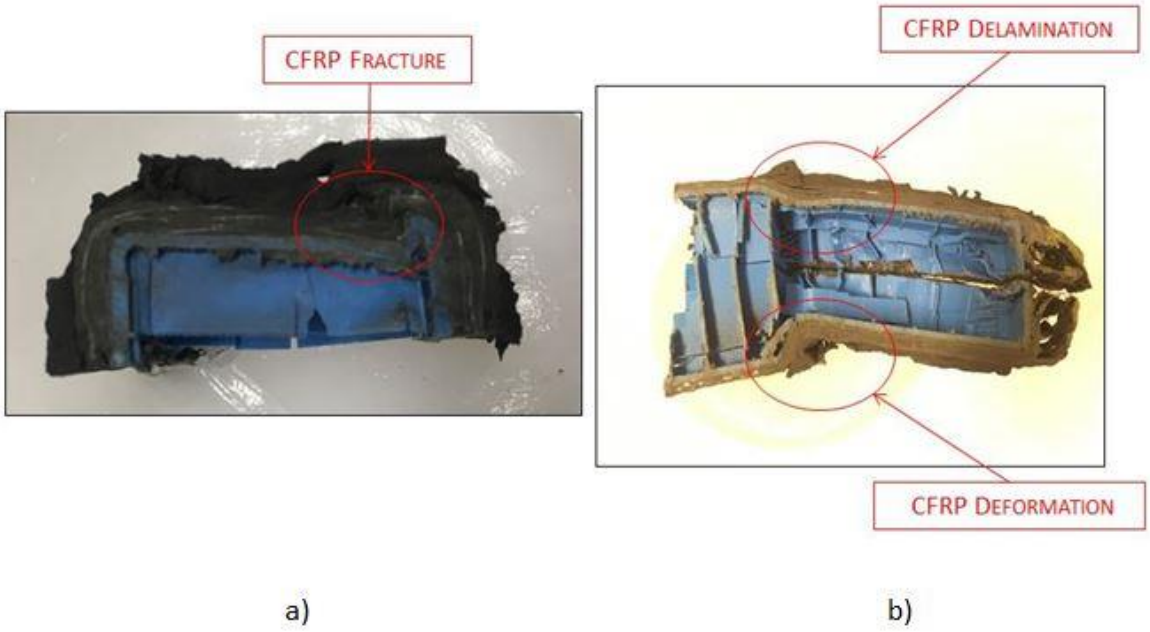

Figure 13. Break types of the CFRP node.

Conclusions and future works

The MFO algorithm has been successfully applied to the mechanical pre-design of a new steel-CFRP adhesive structural joint. The composite thickness and the adhesive Young modulus have been defined as design variables, and the algorithm has found an optimum solution maximizing the component stiffness while minimizing the composite volume of the piece. It is also important to note that the algorithm has been modified to deal with variables whose range is divided into two regions. The response of the system to changes in the design variables has been calculated in a FEM model of the joint. The communication between the FEM solver and the software that implements the optimization algorithm has been automated by the ANSYS aaS Matlab toolbox.

Regarding the tests, the maximum strength results are sufficient for the structure to work in normal bus service conditions according to the requirements of the joint, but the analysis of the breaking mode points to improve the CFRP piece design in the direction to get a tension failure of the flange instead of a shear failure of the web. The failure is cohesive in the adhesive joint. In the CFRP node, areas with material fracture, interlaminar delamination and plastic deformation are observed. The test results validate the FEM models with a deviation in the strength value of 8 %

For future works a new node design should be performed, increasing the CFRP thickness in the webs of the section and studying the best disposure of the fiber directions to avoid the shear failure of the piece against bending loads.

Acknoeledgements

This research was supported by Ministerio de Economia y Competitividad, Spain, under grants TRA2014-56471-C4-1-R and TRA2014-56471-C4-2-R. The authors gratefully acknowledge the collaboration of Castrosua S. A. who provided with the CAD information and let making tests over a manufacturing specimen and Sika S.A.U. España for supplying the adhesives. Authors also thank Miguel Esteban for assistance with the simulations.

[1] D. Gay, S.V. Hoa, S.W. Tsai. Composite Materials, Design and Applications CRC Press LLC Boca Raton (2003).

[2] X. Zhang, Y. Chen, J. Hu. Recent advances in the development of aerospace materials. Prog Aerosp Sci 97 (2018) 22-34.

[3] S. Tang, C. Hu. Design, Preparation and Properties of Carbon Fiber Reinforced Ultra-High Temperature Ceramic Composites for Aerospace Applications: A Review. Journal of Materials Science & Technology 33, (2017) 117-130.

[4] C. Barile, C. Casavola, F. De Cillis. Mechanical comparison of new composite materials for aerospace applications. Compos Part B-Eng 162 (2019) 122-128.

[5] K. Martinsen, S.J. Hu, B.E. Carlson. Joining of dissimilar materials. CIRP Ann-Manuf Techn 64 (2015) 679-699.

[6] C.Y. Choi, D.C. Kim, D.G. Nam, Y.D. Kim, Y.D. Park. A Hybrid Joining Technology for Aluminum/Zinc Coated Steels in Vehicles. Journal of Materials Science & Technology 26 (2010) 858-864.

[7] L.F.M. da Silva, A. Öchsner, R. Adams eds. Handbook of Adhesion Technology. Springer-Verlag Berlin Heidelberg (2011).

[8] A. Elmarakbi, P. Karagiannidis, A. Ciappa, F. Innocente, F. Galise, B. Martorana, F. Bertocchi, F. Cristiano, E. Villaro Ábalos, J. Gómez. 3-Phase hierarchical graphene-based epoxy nanocomposite laminates for automotive applications. Journal of Materials Science & Technology 35 (2019) 2169-2177.

[9] M.D. Banea, M. Rosioara, R.J.C. Carbas, L.F.M. da Silva. Multi-material adhesive joints for automotive industry. Compos Part B-Eng 151 (2018) 71-77.

[10] J. Huang, Q. Su, Y. Cheng, B. Liu, T. Liu. Improved performance of the subgrade bed under the slab track of high-speed railway using polyurethane adhesive. Constr Build Mater 208 (2019) 710-722.

[11] D.R. Speth, Y.P. Yang, G.W. Ritter. Qualification of adhesives for marine composite-to-steel applications. Int J Adhes Adhes 30 (2010) 55-62.

[12] P. Galvez, J. Abenojar, M.A. Martinez. Durability of steel-CFRP structural adhesive joints with polyurethane adhesives. Compos Part B-Eng 165 (2019) 1-9.

[13] S. Han, Q. Meng, S. Araby, T. Liu, M. Demiral. Mechanical and electrical properties of graphene and carbon nanotube reinforced epoxy adhesives: Experimental and numerical analysis. Compos Part A-Appl (2019) 116-126.

[14] P. Galvez, A. Quesada, M.A. Martinez, J. Abenojar, M.J.L. Boada, V. Diaz. Study of the behaviour of adhesive joints of steel with CFRP for its application in bus structures. Compos Part B-Eng 129 (2017) 41-46.

[15] I.Dost, S.A. Khan, M. Aziz. Mechanical evaluation of joining methodologies in multi material car body. Int J Adv Eng Technol 5(1) (2012) 259-268.

[16] T. Sakiyama, G. Murayama, Y. Naito,.K. Saita, Y. Miyazaki, H. Oikawa, T. Nose. Dissimilar metal joining technologies for steel sheet and aluminum alloy sheet in auto body. Nippon Steel Tech Rep 103 (2013) 91-98.

[17] C.M. Branco, J. A. Ferreira. Fatigue analysis of bus structures. In: Proceedings of the european conference on fracture, ECF5 (1984) 643-658.

[18] J.A.Perez, F. Badea, D. Arribas. Experimental characterization of the strain concentration factor in welded junctions of rectangular tube beam using digital image correlation. Procedia - Soc Behav Sci 160 (2014) 440-448.

[19] A. Quesada, M.J. Lopez-Boada, A. Chiminelli, R. Breto, M.A. Martinez, P. Galvez, D. Garcia-Pozuelo, E. Olmeda, V. Diaz A new joint of FRP design for a bus structure. In: Proceedings on the 7th International Conference on Mechanics and Materials in Design (2017).

[20] M.A. Wahab The mechanics of adhesives in composite and metal joints. DEStech Publications (2014).

[21] D. Croccolo, M.D. Agostinis, N. Vincenzi Structural analysis of an articulated urban bus chassis via FEM: a methodology applied to a case study. Strojniki vestnik -Journal of Mechanical Engineering 57 (2011) 799-809.

[22] T. Vichiensamuth, M. Pimsarn, K. Takahashi, T. Tantanawat. A Simplified Model of a Reinforced Square Hollow Section (SHS) T-Joint for Stress Evaluation in Bus Superstructures. IOP Conference Series: Materials Science and Engineering 46 (2013) 012034.

[23] H.C. Hong, H.W. Huang. Effects of Cont Rail Joint Type on Bus Rollover Crashworthiness. Advances in Manufacturing Science and Engineering V. Trans Tech Publications 945 (2014) 165-161.

[24]S. Mirjalili. Moth-flame optimization algorithm: A novel nature-inspired heuristic paradigm. Knowledge-Based Systems 89 (2015) 228-249.

[25] S. Mirjalili. Like moths to a flame (2017) URL http://www.alimirjalili.com/MFO.htm

[26]S. Li, E. Sitnikova, Y. Liang, A.S. Kaddour The tsai-wu failure criterion rationalised in the context of UD composites. Composites Part A: Applied Science and Manufacturing 102 (2017) 207-217.

[27] R. Narayanaswami, H.M. Adelman Evaluation of the tensor polynomial and Hoffman strength theories for composite materials. Journal of Composite Materials 11 (1977) 366-377.

[28] K. Balasubramanian, M.T.H. Sultan, N. Rajeswari. Manufacturing techniques of composites for aerospace applications. In: Sustainable Composites for Aerospace Applications. Woodhead Publishing (2018) 55-67.

Chapter 5:

CONCLUSIONS

Index

Chapter 5:

CONCLUSIONS

5.1 CONCLUSIONS

In the same way as it was done in the objectives, conclusions have been divided into three main parts:

5.1.1 TO SOLVE THE EXISTING MECHANICAL FATIGUE PROBLEMS IN WELDED BUS STEEL SUPERSTRUCTURES BY USING ADHESIVE JOINTS AND COMPOSITE MATERIALS

It can be affirmed that it is possible to use adhesive joints in the nodes of the bus superstructure where stress concentration occurs, and thus reduce the fatigue problems associated with these structures:

-The proposed adhesive joint shows values far superior to the stresses that it must bear, an order of magnitude higher than the most unfavorable service condition posed.

-The new raised adhesive joint allows obtaining greater elasticity at the reference node, decreasing the relative rigidity of the surroundings and minimizing mechanical fatigue.

-By replacing welded joints by new CFRP components, it is possible to decrease the weight of the structure, allowing greater efficiency by reducing fuel consumption.

Regarding durability of steel-CFRP structural adhesive joints with conventional and hybrid polyurethane adhesives:

-Each adhesive have different behavior against humidity and temperature. This is due to the difference in their composition.

-Conventional polyurethane adhesive is structural adhesive, which cures by reaction with atmospheric humidity to form an elastomer. This adhesive shows better behavior against humidity and temperature as degradation conditions cause a post-curing process in it, changing its properties, increasing stiffness and maximum stress values.

-Hybrid polyurethane adhesive cures by reaction with atmospheric humidity but it is a structural adhesive with silane termination. This change in the formulation of the polymer makes the curing mechanism different from the conventional one. Thus, for 0 h of degradation the adhesive has already reached all its properties. There is no post-curing process, and after 100 h of exposure to temperature and humidity, degradation is evident. In terms of mechanical properties, stiffness decreases like maximum stress values. In terms of reliability, the adhesive joint loses reliability over time in presence of humidity and temperature conditions.

-Even having different behavior, both adhesives are able to maintain adequate strength after the degradation process.

Regarding the effect of moisture and temperature on thermal and mechanical properties of structural polyurethane adhesive joints (single-component and double-component adhesives):

-The effect of two different adhesives (one single-component and other double-component polyurethanes) subjected to adverse environmental conditions is evaluated.

-Despite being two polyurethane based adhesives, the differences in their chemical composition make their behavior different against the studied conditions.

-Double component adhesive does not reach the maximum value of its mechanical properties only with the mixture of the components, being necessary the exposure to humidity (82% R.H.) and temperature (72°C). Therefore, during the first stages of exposure to moisture, it will favor the post-curing of the adhesive. While the temperature increases the cross-linking of the polymer chains. After long exposure times (768 hours), the polymer begins its degradation process.

-Single component adhesive needs the presence of humidity to achieve curing. However, once the curing is completed, the presence of moisture is harmful. The adhesive absorbs water, creating new hydrogen bridges into the polymer chain.

-Single component adhesive shows a phenomenon of adsorption from 24 hours of exposure, while double component adhesive shows a phenomenon of adsorption from 768 hours. The water penetrates, in both cases, by the interface between the adhesive and the substrate. This phenomenon is much more evident in the double-component adhesive, since the failure observed is completely adhesive, while the single-component adhesive

shows mixed failure. Regarding the mechanical properties, although the single-component adhesive begins the degradation process from few times of exposure, its degradation is gradual. On the contrary that happens in the double-component adhesive, whose degradation is more pronounced.

-The effect of the heat-aging cycles is similar in both adhesives, as a post-curing process takes place in both cases. Both polymers increase the cross-linking of their chains, with the consequent variation in terms of the mechanical properties. The degradation is evident in both adhesives after 1968 cycles, when chain excision in the polymer network happen, reducing the cross-linking density, and increasing the critical molecular weight. New more linear molecules are formed in the network, and they undergo plasticization, decreasing Young's modulus and tensile strength values.

Regarding designing, manufacturing and testing of a new CFRP node bonded by adhesives for its use in bus superstructures:

-The results show the capacity of the new CFRP node to be used in bus superstructures.

- Manufacturing method is very widespread so the CFRP node implementation would be viable on an industrial scale.

-The maximum strength results are sufficient to work in service conditions according to the requirements of the joint. But the analysis of the breaking mode requires improving the CFRP piece design to get a tension failure of the flange instead a shear failure of the web.

-The use of new CFRP node together with adhesives improves the fatigue behavior of the assembly and makes it more efficient.

-The test results validate the FEM models developed by the Mechanical Engineering Department of Universidad Carlos III de Madrid with a deviation in the strength value of 8%.

-The failure is cohesive in the adhesive joint. In the CFRP node, areas with material fracture, interlaminar delamination and plastic deformation are observed.

Regarding the adhesives characterizations:

-Ultimate tensile strength, breaking strength, maximum elongation and Young´s Modulus are calculated for all the studied adhesives.

-Fracture toughness in mode I (GIC) is also calculated for the most suitable adhesives for the raised problem in bus superstructures.

-Most common methodologies for analysis of GIC are based on linear elastic fracture mechanics (LEFM), including Compliance Calibration Method (CCM) and Corrected Beam Theory (CBT), but recently developed method such Compliance-Based Beam Method (CBBM) is based on the crack equivalent concept, depending only on the specimen`s compliance during the test.

-Recent works have demonstrated the validity of using CBBM model in adhesives, being probably the most reliable method to obtain GIC. This is due to the difficulty of measuring experimentally crack growth with an optical system, which is aggravated by high elastic-plastic behavior of both studied adhesives. The CBBM is only based on the crack equivalent concept, depending only on the compliance of the specimen during the test.

5.1.2 TO SOLVE PROBLEMS CAUSED BY MECHANICAL FATIGUE IN CIVIL STEEL STRUCTURES BY USING ADHESIVES AND COMPOSITE MATERIALS

-By using a new type of ductile epoxy adhesive it is possible to obtain more flexible joints and therefore with better fatigue behavior.

-Regarding thermal characterization, thermal properties are similar to other epoxy adhesives. The Kissinger method is faster and simpler than the MFK, since it assumes that the curing reaction is order 1 reaction. Using MFK the activation energy of the process is calculated as a function of the conversion degree and the isothermal curing kinetics can be simulated starting from non-isothermal curing; showing that at higher temperature, less time is needed to obtain a 99% of conversion degree.

-Both durability and thermal fatigue processes adversely affect the mechanical properties of the adhesive joint.

-Different mechanisms affect the integrity of the adhesive joint during the durability test. On the one hand, the temperature causes greater primary cross-linking of the polymer

chains at the beginning, and a subsequent degradation of the adhesive joint. Moisture is absorbed mainly as bound water causing swelling and plasticization. Type I and Type II bound water are created, which are responsible for decreasing and increasing the adhesive Tg respectively. Moisture also penetrates by means of an adsorption process through the adhesive substrate interface, accelerating the degradation process of the adhesive joint. Degradation is evident after 24 h of exposure, when τmax drops by 40%.

-Thermal fatigue affects the integrity of the adhesive joint to a lesser extent than the durability process. During the first cycles, temperature increases the mobility of the chains, decreasing the value of the Tg. Longer exposure times increase the cross-linking and the Tg. Degradation is evident after 97 cycles, when τmax drops by15%.

-The durability process is more negative in terms of reliability than the thermal fatigue process.

5.1.3 TO GUARANTEE NEW JOINT RESISTANCE AGAINST THE EFFORTS UNDER THE ADHESIVE JOINT WILL BE SUBJECTED BY MEANS OF FINITE ELEMENT ANALYSIS, STUDYING THE SINGULARITIES BASED ON THE INTENSITY OF SINGULAR STRESS FIELD (ISSF)

-The effect of Young's Modulus in terms of the ISSF is studied from the results obtained in the different models. Two models can be compared if the material combination in the edge corner is the same.

-The lower Young's modulus adhesive works better in the corner as long as the central area is covered by a higher Young's modulus adhesive.

-The combination of the higher Young's modulus adhesive in the corner and the lower Young's modulus adhesive in the central area performs worse than applying a homogeneous layer of the higher Young's modulus adhesive only.

-The reciprocal work contour integral method (RWCIM) is a valid method to calculate the intensity of singular stress field (ISSF). However, it is a very complex method, and errors may occur during the calculation process.

- Calculating ISSF from the reference value and the stress ratio is just as accurate as using RWCIM (reciprocal work contour integral method). But it is necessary to know the reference value to be able to use it. In the same way, it is necessary to use the same mesh pattern, the same

boundary conditions, and the same specimen configuration both in the reference and unknown solution.

5.2 CONCLUSIONES

Del mismo modo que en los objetivos, las conclusiones han sido divididas en tres partes principales:

5.2.1 RESOLVER LOS PROBLEMAS DE FATIGA MECÁNICA EXISTENTES EN SUPERESTRUCTURAS DE ACERO (SOLDADAS) DE AUTOBÚS MEDIANTE EL USO DE UNIONES ADHESIVAS Y MATERIALES COMPUESTOS

Es posible usar uniones adhesivas en los nodos de la superestructura de autobús donde la concentración de tensiones ocurre, y por lo tanto reducir los problemas de fatiga asociados a estas estructuras:

-La unión adhesiva propuesta muestra valores de resistencia muy superiores a los esfuerzos que debe soportar: un orden de magnitud mayor que la condición de servicio más desfavorable planteada.

-La nueva unión adhesiva planteada permite obtener mayor elasticidad en el nodo de referencia, disminuyendo la rigidez relativa del entorno y minimizando la fatiga mecánica.

-Reemplazando las uniones soldadas por nuevos elementos de CFRP es posible disminuir el peso de la estructura, aumentando la eficiencia mediante la reducción del consumo de combustible.

Respecto a la durabilidad de uniones adhesivas estructurales acero-CFRP con un adhesivo de poliuretano convencional y otro híbrido:

-Cada adhesivo tiene un comportamiento diferente frente a la humedad y la temperatura. Esto es debido a las diferencias en su composición.

-El adhesivo de poliuretano convencional es un adhesivo estructural que cura por reacción con la humedad atmosférica para formar un elastómero. Este adhesivo muestra mejor comportamiento frente a la humedad y la temperatura ya que las condiciones de

degradación le inducen un proceso de post-curado, cambiando sus propiedades, e incrementando la rigidez y los valores de esfuerzo máximo.

-El adhesivo de poliuretano híbrido cura por reacción con la humedad atmosférica pero es un adhesivo estructural con terminación silano. Este cambio en la formulación del polímero hace que el mecanismo de curado sea diferente que en el adhesivo de poliuretano convencional. En consecuencia, las probetas sin degradar ya han alcanzado todas sus propiedades. No existe un proceso de post-curado, y después de 100 horas de exposición a temperatura y humedad, la degradación es evidente. En términos de propiedades mecánicas, la rigidez decrece como los valores máximos de esfuerzo. Respecto a la fiabilidad, la unión adhesiva pierde fiabilidad con el paso del tiempo cuando es expuesta a condiciones de humedad y temperatura.

-Incluso teniendo diferente comportamiento, ambos adhesivos son capaces de mantener una adecuada resistencia después del proceso de degradación.

Respecto al efecto de la humedad y la temperatura en las propiedades térmicas y mecánicas de uniones adhesivas con adhesivos de poliuretano estructurales (mono-componente y bi-componente):

-El efecto de someter a condiciones adversas a dos adhesivos diferentes (poliuretano mono-componente y bi-componente) fue evaluado.

-A pesar de ser dos adhesivos de poliuretano, las diferencias en su composición química hacen que su comportamiento sea distinto frente a las condiciones estudiadas.

-El adhesivo bi-componente no alcanza el valor máximo de sus propiedades mecánicas solo con la mezcla de sus componentes, siendo necesario la exposición a humedad (82% de humedad relativa) y temperatura (72°C). Por lo tanto, durante las primeras etapas de exposición a humedad, se favorecerá el post-curado del adhesivo. Mientras que la temperatura incrementa el entrecruzamiento de las cadenas del polímero. Después de largos tiempo de exposición (768 horas), comienza la degradación del polímero.

-El adhesivo mono-componente necesita la presencia de humedad para curar. Sin embargo, una vez el curado se ha completado, la presencia de humedad es perjudicial. El adhesivo absorbe agua, creando nuevos puentes de hidrógeno dentro de las cadenas del polímero.

-El adhesivo mono-componente muestra un fenómeno de adsorción desde las 24 horas de exposición, mientras que el adhesivo bi-componente muestra el mismo fenómeno de adsorción desde las 768 horas. El agua penetra, en ambos casos, a través de la intercara entre el adhesivo y el sustrato. Este fenómeno es mucho más evidente en el adhesivo bi-componente, ya que la rotura observada es completamente adhesiva, mientras que el adhesivo mono-componente muestra fallo mixto. Respecto a las propiedades mecánicas, a pesar de que el adhesivo mono-componente comienza el proceso de degradación desde poco tiempo de exposición, su degradación es gradual. Al contrario de lo que ocurre en el adhesivo bi-componente, cuya degradación es más pronunciada.

-El efecto de los ciclos de envejecimiento térmico es similar en ambos adhesivos, al tener lugar un post-curado en ambos casos. Los dos polímeros incrementan el entrecruzamiento de sus cadenas, con la consecuente variación de sus propiedades mecánicas. La degradación es evidente en ambos adhesivos después de 1968 ciclos, cuando tiene lugar la escisión de la cadena en la red del polímero, reduciendo la densidad de entrecruzamiento, e incrementando el peso molecular crítico. Se forman nuevas moléculas más lineales en la red, experimentando plastificación, disminuyendo los valores de módulo de Young y resistencia.

Respecto al diseño, fabricación y ensayo de un nuevo nodo de CFRP unido mediante adhesivos para su uso en superestructuras de autobús:

-Los resultados muestran la capacidad del nuevo nodo para ser utilizado en superestructuras de autobús.

-El método de fabricación está muy extendido, por lo que la implementación del nodo de CFRP es viable a escala industrial.

-Los resultados de resistencia máxima son suficientes para trabajar en condiciones de servicio de acuerdo a las solicitaciones de la unión. Pero el análisis del modo de fallo requiere mejorar el diseño de la pieza de CFRP, y así evitar que la fractura se produzca en los brazos del nodo.

-El uso de un nuevo nodo de CFRP junto con adhesivos mejora el comportamiento a fatiga de todo el conjunto y hace que sea más eficiente.

-Los resultados de los ensayos validan los modelos de elementos finitos desarrollados por el Departamento de Ingeniería Mecánica de la Universidad Carlos III de Madrid con una desviación del valor de resistencia del 8%.

-El fallo es cohesivo en la unión adhesiva. En el nodo de CFRP se observan zonas con fractura del material, con delaminación de las capas de fibra y con deformación plástica.

Respecto a la caracterización de los adhesivos:

-La resistencia a tracción, la resistencia a rotura, la elongación máxima y el módulo de Young son calculados para todos los adhesivos estudiados.

-La tenacidad a fractura en modo I (GIC) también es calculada en los adhesivos más adecuados para el problema planteado en superestructuras de autobús.

-Las metodologías más comunes para el análisis del GIC están basadas en la mecánica de fractura elástica-lineal (LEFM- linear elastic fracture mechanics), incluyendo Compliance Calibration Method (CCM) y Corrected Beam Theory (CBT). Pero otros métodos más recientes como el Compliance-Based Beam Method (CBBM) están basados en el concepto de grieta equivalente, que depende solo de las variables fuerza y desplazamiento obtenidas durante el ensayo.

-Trabajos recientes han demostrado la validez del CBBM en adhesivos, siendo probablemente el método más fiable para obtener el GIC. Esto es debido a la dificultad de medir experimentalmente el crecimiento de grieta con un sistema óptico, lo cual se ve agravado por el comportamiento elasto-plástico de los adhesivos estudiados. El CBBM está basado en el concepto de grieta equivalente, y sólo depende de las variables fuerza y desplazamiento obtenidas durante el ensayo.

5.2.2 RESOLVER PROBLEMAS CAUSADOS POR FATIGA MECÁNICA EN ESTRUCTURAS CIVILES DE ACERO USANDO ADHESIVOS Y MATERIALES COMPUESTOS

-Usando un nuevo tipo de adhesivo epoxi elástico es posible obtener uniones más flexibles y por lo tanto con mejor comportamiento a fatiga.

-Respecto a la caracterización térmica, las propiedades térmicas son similares a las de otros adhesivos epoxi. El método de Kissinger es más rápido y sencillo que el MFK, ya

que asume que la reacción de curado es de orden 1. Usando el MFK se calcula la energía de activación del proceso en función del grado de conversión y se puede simular la cinética de curado isotérmica partiendo de curados no-isotérmicos, mostrando que a mayores temperaturas es necesario menos tiempo para obtener un 99% de grado de conversión.

-Tanto el proceso de durabilidad como el de fatiga térmica afectan adversamente a las propiedades mecánicas de la unión adhesiva.

-La integridad de la unión adhesiva se verá afectada por diferentes mecanismos durante el ensayo de durabilidad. Por otro lado, la temperatura causa un mayor entrecruzamiento primario de las cadenas del polímero al principio, y una posterior degradación de la unión adhesiva. La humedad es absorbida principalmente como agua ligada (bound water) causando hinchamiento y plastificación. Se crea agua ligada de Tipo I y de Tipo II, que es responsable del descenso e incremento de la Tg del adhesivo respectivamente. La humedad también penetra por medio de un proceso de adsorción a través de la intercara entre el adhesivo y el sustrato, acelerando el proceso de degradación de la unión adhesiva. La degradación es evidente después de 24 horas de exposición, cuando τ_{max} cae un 40%.

-La fatiga mecánica afecta a la integridad de la unión adhesiva en menor medida que el proceso de durabilidad. Durante los primeros ciclos la temperatura incrementa la mobilidad de las cadenas, disminuyendo el valor de la Tg. Mayores tiempos de exposición incrementan el entrecruzamiento y la Tg. La degradación es evidente después de 97 ciclos, cuando τ_{max} cae un 15%.

-El proceso de durabilidad es más negativo en términos de fiabilidad que la fatiga térmica.

5.2.3 GARANTIZAR LA RESISTENCIA DE LAS NUEVAS UNIONES FRENTE A LOS ESFUERZOS A LOS QUE ESTARÁ SOMETIDA POR MEDIO DE ANÁLISIS DE ELEMENTOS FINITOS, ESTUDIANDO LAS SINGULARIDADES MEDIANTE EL INTENSITY OF SINGULAR STRESS FIELD (ISSF)

-El efecto del módulo de Young en términos del ISSF es estudiado a partir de los resultados obtenidos en los diferentes modelos. Dos modelos pueden ser comparados si la combinación de material en la esquina adhesivo-substrato es la misma.

-El adhesivo con menor módulo de Young trabaja mejor en las esquinas siempre y cuando la zona central sea cubierta por un adhesivo con mayor módulo de Young.

-La combinación del adhesivo con mayor módulo de Young en las esquinas y el adhesivo con menor módulo de Young en la zona central funciona peor que aplicar una capa homogénea del adhesivo con mayor módulo de Young únicamente.

- Reciprocal Work Contour Integral Method (RWCIM) es un método válido para calcular el ISSF. Sin embargo, es un método muy complejo, y pueden ocurrir errores durante el proceso de cálculo.

-Calcular el valor de ISSF a partir del valor de referencia y de la relación de tensiones es tan preciso como usar el RWCIM. Pero es necesario conocer este valor de referencia para poder usarlo. Del mismo modo es necesario utilizar el mismo tamaño de malla, las mismas condiciones de contorno, y la misma configuración de probeta tanto en la solución de referencia como en la solución desconocida. .

Capítulo 6:

LÍNEAS DE TRABAJO FUTURAS

Capítulo 6:

LÍNEAS DE TRABAJO FUTURAS

La realización de esta Tesis Doctoral ha permitido la obtención de nuevas uniones adhesivas acero-CFRP capaces de reemplazar a las actuales uniones soldadas en estructuras metálicas. Estas nuevas uniones son capaces de aportar elasticidad a la estructura, mejorando su comportamiento a fatiga, con unos valores de resistencia muy superiores a los requerimientos del sistema.

De esta forma ha sido posible abrir una línea de investigación prometedora en el campo de los adhesivos, y su uso en estructuras multimaterial junto con materiales compuestos. Las líneas de trabajo futuras, al igual que el resto de la Tesis Doctoral se dividen en tres partes fundamentales:

1. Resolver los problemas de fatiga mecánica existentes en superestructuras de acero (soldadas) de autobús mediante el uso de uniones adhesivas y materiales compuestos:

-Optimizar el nodo de CFRP para igualar sus valores de resistencia a los existentes en los actuales nodos de acero.

-Estudiar el comportamiento del nuevo nodo frente al vuelvo y frente a impacto.

2. Resolver problemas causados por fatiga mecánica en estructuras civiles de acero usando adhesivos y materiales compuestos.

-Estudiar otros adhesivos elásticos similares que presenten un mejor comportamiento ante condiciones medioambientales extremas.

-Estudiar el uso de otras configuraciones de refuerzo formadas por piezas de CFRP pretensadas.

3. Garantizar la resistencia de las nuevas uniones frente a los esfuerzos a los que estará sometida por medio de análisis de elementos finitos, estudiando las singularidades mediante el Intensity of Singular Stress Field (ISSF):

-Optimizar los modelos de elementos finitos para encontrar la mejor configuración posible en las uniones adhesivas planteadas.

-Contrastar y comparar a través de ensayos experimentales los resultados obtenidos en el estudio de singularidades.